# INVESTIGATING THE ROLE OF *SLFN14* MUTATIONS IN INHERITED THROMBOCYTOPENIA AND HAEMATOPOIESIS

Rachel J. Stapley

A thesis submitted to the University of Birmingham for the degree of

DOCTOR OF PHILOSOPHY


UNIVERSITY OF BIRMINGHAM

British Heart Foundation

Institute of Cardiovascular Sciences

College of Medical and Dental Sciences

University of Birmingham

May 2021

## Abstract

Schlafen 14 (SLFN14) has recently been identified as an endoribonuclease responsible for cleaving RNA to regulate and inhibit protein synthesis. Early studies revealed members of the *SLFN* family are capable of altering lineage commitment during T-cell differentiation, using cell cycle arrest as a means of translational control. *SLFN14* mutations have been previously reported as causing inherited macrothrombocytopenia and bleeding in patients. The aim of this thesis was to uncover potential mechanisms for how *SLFN14* and its mutations contribute to inherited thrombocytopenia and altered haematopoiesis. A novel CRISPR knock-in mouse of *SLFN14*-K208N and platelet specific knock-out mouse using the PF4Cre loxP system were used to better understand the involvement of *SLFN14* in haematopoiesis and platelet function. Gross haematological analysis, *in vitro* and *in vivo* studies of platelet and erythrocyte function, as well as analysis of spleen and bone marrow progenitors were used. Homozygous mice for the K208N mutation do not survive to weaning age due to severe anaemia. Heterozygotes exhibit microcytic erythrocytosis, haemolytic anaemia, splenomegaly and abnormal thrombus formation examined by intravital microscopy although *in vitro* platelet function and morphology remain unchanged. RT-PCR of transcription factor *GATA1* in *SLFN14*-K208N mice revealed significant reduction in *GATA1* mRNA from whole bone marrow suggesting the SLFN14 endoribonuclease is active in haematopoiesis. In addition, *SLFN14 PF4Cre* mice show macrothrombocytopenia with reduced proportion of megakaryocytes in the bone marrow although platelet function was retained. This suggests *SLFN14* is a key regulator in mammalian haematopoiesis and a species-specific mediator in platelet and erythrocyte production and function.

## Publications arising from this thesis

**Stapley RJ**, Smith CW, Haining EJ, Bacon A, Lax S, Pisareva VP, Pisarev AV, Watson SP, Khan AO, Morgan NV; Heterozygous mutation *SLFN14 K208N* in mice mediates species-specific differences in platelet and erythroid lineage commitment. *Blood Advances*. 2021;5(2):377-390. (Stapley et al., 2021)

Khan, AO, **Stapley, RJ**, Pike, JA, et al; the UK GAPP Study Group. Novel gene variants in patients with platelet-based bleeding using combined exome sequencing and RNAseq murine expression data. *J Thromb Haemost.* 2021;19(1):262-268 (Khan et al., 2021)

Khan AO, Slater A, Maclachlan A, Nicolson PLR, Pike JA, Reyat JS, Yule J, **Stapley R**, Rayes J, Thomas SG, Morgan NV. Post-translational polymodification of β1-tubulin regulates motor protein localisation in platelet production and function. *Haematologica*. 2020 Dec 17; Online ahead of print. (Khan et al., 2020a)

Almazni, I*, **Stapley, RJ***, Khan, AO, Morgan, NV. A comprehensive bioinformatic analysis of 126 patients with an inherited platelet disorder to identify both sequence and copy number genetic variants. *Human Mutation*. 2020 Nov;41(11):1848-1865. (Almazni et al., 2020)

**Stapley RJ**, Pisareva VP, Pisarev AV, Morgan NV. *SLFN14* gene mutations associated with bleeding. *Platelets*. 2020;31(3):407-410. (Stapley et al., 2020)

Almazni I, **Stapley R**, Morgan NV. Inherited Thrombocytopenia: Update on Genes and Genetic Variants Which may be Associated With Bleeding. *Frontiers in Cardiovascular Medicine*. 2019;6(80). (Almazni et al., 2019)

* Contributed equally

## Acknowledgements

Firstly thank you to Dr Neil Morgan, for giving me the opportunity to do my PhD in your lab. Your help and guidance throughout my project has been invaluable and you have always had confidence in me and pushed me to achieve my best. You have been such a positive influence and mentor to me over the past 3 years and hopefully long may our successes continue! Thank you for encouraging me to keep going and being so understanding when things haven't worked (or when I've decided to change genotyping methods for the 'n'th time…). I would also like to thank my second supervisor Prof Steve Watson. I am incredibly lucky to have joined and worked in a lab which is so established and I have to thank this collaboration for that.

Thank you to Lizzie for helping me when I first started in the lab. Thank you for introducing, training and providing me with the right tools (literally!) to do the mouse work and being so kind in helping me find my feet. Also thank you to Sian who helped set up this project, mouse licence and with all the initial patient phenotyping. My project really wouldn't have existed nor had such potential if it wasn't for your hard work.

I have been extremely lucky to work with some amazing people over the past three years. Abs, your eye for detail and constant encouragement to 'tell a story' has helped me to stay focused on the science throughout. When I have at times totally lost confidence in myself you have been there with a reasoning head for which I cannot thank you enough. Chris, your 'not so subtle' judging has made me think twice about every result I ever generated, but I guess that's what has helped me think 'what next' and write this thesis. Natalie J you really helped me through the whole COVID phase when times were tough and it seemed like the world would never be normal again! You are the most organised person to work alongside and I REALLY miss that. Julie, thank you for being my cheerleader and looking out for me over the past few years. I really admire you as a female scientist and if one day I'm as good as you, I

know I've made it. Lourdes, Ying and Beata you often don't get the recognition you deserve for your hard work but thank you so much for all your patience, advice and help throughout my time in the lab. Thank you to Natalie P, Steve T and everyone in the lab who helped me with all my mouse samples before the first COVID lockdown. That really was a mad few days and it was your help and team spirit which made that possible.

Thank you to the BMSU at the University of Birmingham. Without the mice my project and this thesis would not exist so a big shout out goes to you. In particular to Karen, Claire, Alison, Diane, Saiqa and Emma for being so friendly and helpful.

Thank you to the British Heart Foundation for my funding. You hold a special place in my heart for many reasons but without this funding I would not have been able to do this work or been so well supported throughout.

My family... Mummy, Daddy and Elizabeth, you are the best. Without your love and support I would not be where I am today. Thank you for understanding when I was in a bad mood from failed experiments and late nights at the lab. Thank you for supporting me even though we haven't been able to see each other much over the past year, I'm very much looking forward to more family time soon. I feel your love with me always – I hope that champagne is in the fridge! Carole and Vernon, the best "in-laws" I could wish for. Thank you for your encouragement and faith in me, I cannot wait for more family holidays and trips to see you soon.

Rikki, where do I even begin?! Thank you for the late night lab pick-ups, my morning coffee, looking after me and just generally loving me. You're the best. If you do end up reading this thesis it may be proof I haven't just done the same experiment for years and I even managed to get some of them to work…despite the moaning and tears. I love you so much.

Finally, to my Gramps. The one person who had more confidence in me than anybody in this entire world and certainly more than I will ever have in myself. You told me to "do it and do it

bloody well” and I suppose by writing this, I have done it and I can’t quite believe it! I know you’ve been watching down on me and have given me your strength to continue. I hope I have done you proud and know that I will keep going. I see the robin and know you’re there. This is for you xx

**Table of Contents**

**List of Figures**

**Chapter 1**



**Chapter 3**



**Chapter 4**

**Chapter 5**

**Chapter 6**



**Chapter 7**

# List of Tables

# Chapter 1

General Introduction

# Chapter 1 – General Introduction

## 1.1 Overview of haematopoiesis

Haematopoiesis is the process of blood cell production primarily in the bone marrow. Haematopoietic stem cells (HSCs) can differentiate into various progenitors and downstream mature blood cells which circulate in the blood. These terminally differentiated cells have various properties including oxygen transport, thrombus or clot formation and fighting infection. Reduction in the number of these cells, or alterations in their function can cause diseases which in the most severe cases can be fatal. The initial point of differentiation begins with the HSC which has multipotent potential. Each 'branch' of the haematopoietic tree stems from the HSC and contains a series of progenitor cells, specifically differentiated and programmed to produce one, or in some cases multiple different cell types. This is determined by specific transcription factors and cytokines which allow cells to become more lineage restricted with each stage. The two main lineages are lymphoid and myeloid. The Common Lymphoid Progenitor (CLP) further differentiates to produce T lymphocytes, B lymphocytes and natural killer (NK) cells which together comprise the complex adaptive immune system. The myeloid lineage originates from the Common myeloid Progenitor (CMP) which further differentiates into Megakaryocyte Erythroid Progenitors (MEPs) for the production of platelets and erythrocytes or myeloblasts for the production of granular leukocytes forming the innate immune system (Figure 1.1).

This hierarchical view of stem cell differentiation in recent years has been contested in the field (Velten et al., 2017). Following the advancement of single cell profiling and identification of self-renewal properties of intermediate progenitors this process is now seen as more of a continuum, with a less 'step-wise' organisation pattern. Intermediate progenitors have less self-renewal properties than HSCs and are defined as committed to their particular lineage. Renewal and differentiation is tightly orchestrated at the transcript level and in some

instances has been proposed certain progenitors may possess bias toward certain cell fates particularly in disease.

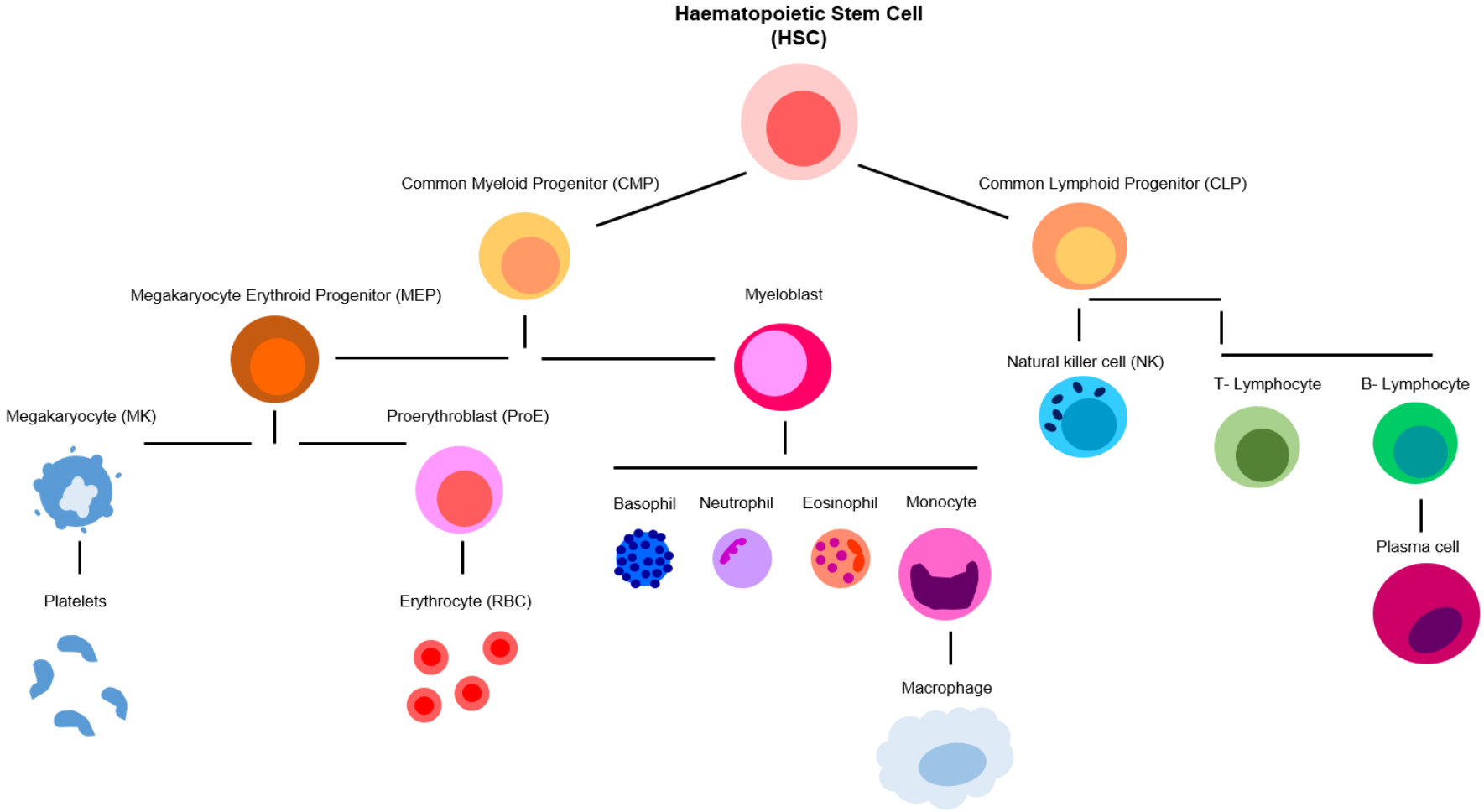


**Figure 1.1: Overview of haematopoiesis.** Haematopoietic stem cells (HSC) form the origin of all blood cells. They are multipotent and capable of producing cell types in multiple lineages. From here, the tree branches into lymphoid (to produce cells of the adaptive immune system) and myeloid lineages (to produce platelets and erythrocytes).

## 1.2 Platelets

### 1.2.1 Megakaryopoiesis and platelet production

MKs are formed from HSCs produced in the bone marrow and are specialised to produce blood cells (Figure 1.1) although in early development they are also found in the yolk sac, foetal liver and spleen (Machlus et al., 2014). HSCs give rise to multipotent progenitor cells in the myeloid lineage termed MEPs. These cells differentiate into either MKs or erythroid progenitors based on their receptor profile and exposure to transcription regulators angling lineage biases. MKs account for approximately 1% of all myeloid cells and are a rare cell type making them both difficult to identify *in situ* and study (Ogawa, 1993). Once MKs differentiate further, their self-renewal capacity becomes limited and undergo maturation. During differentiation, MKs undergo endomitosis, a cycle of DNA replication devoid of cytokinesis (cytoplasmic division) and karyokinesis (nuclear division) (Lordier et al., 2008). This results in generation of a polylobulated nucleus (polyploidy) (Ogawa, 1993) and proceeded by generation of a demarcation membrane system (DMS) and granule biogenesis (Behnke, 1968, Ambrosio et al., 2012). Proteins including vWF and fibrinogen are packaged into granules through endocytosis and MKs are equipped with all necessary components ready for pro-platelet release. Proplatelet extensions into sinusoidal blood vessels and the shear force of blood catalyses platelet release into the circulation (Machlus et al., 2014). Dysregulation of these processes can lead to a variety of platelet function disorders and/or result in altered platelet number significantly impairing haemostasis. (Figure 1.2)

### 1.2.2 Transcription factors: Megakaryopoiesis

Transcription factors (TFs) bind to the DNA of promoter or enhancer regions of specific genes directly involved in differentiation of MKs. These are important to initiate gene expression and developmental changes in the MK which lead to the production of viable, normal functioning platelets. GATA-1, FOG-1, Fli-1, NF-E2 and RUNX-1 are the main

identified transcription factors in humans and mice (Patel et al., 2005, Geddis, 2010). GATA-1 acts in the early and mid-stages of thrombopoiesis controlling cell replication, cytoplasmic maturation and development of platelet organelles alongside it's cofactor FOG-1 (Shivdasani, 2001) (Figure 1.2) Fli-1 and transcription factor NF-E2 are active during the latter stages of megakaryocyte maturation, where mice deficient in both of these genes lack circulating platelets, reduced α-granules and disorganised internal membranes, indicating megakaryocyte maturation arrest (Zang et al., 2016). RUNX-1 forms a complex with Fli-1 subsequently silencing non-muscle myosin heavy chain IIB (MYH10) to increase cell ploidy and regulate megakaryocyte maturation (Antony-Debré et al., 2012). Novel genetic technologies have allowed identification of mutations within the named transcription factors impacting platelet biogenesis and have helped in the diagnosis of congenital thrombocytopenia and bleeding disorders (Almazni et al., 2021, Deutsch and Tomer, 2006).

### 1.2.3 Cytokines: Megakaryopoiesis

Thrombopoietin (TPO) is the predominant cytokine which stimulates maturation of MKs and can be used to monitor platelet production (Kaushansky, 2005, Patel et al., 2005, Kaushansky, 2009, Zeigler et al., 1994). TPO is produced in the liver and acts by binding to the cellular homologue myeloproliferative leukaemia virus oncogene (Mpl) (Kaushansky et al., 1995, Ng et al., 2014). Interestingly it has been shown in MpI knockout mouse models there is a significant reduction in the number of MKs and platelets but also reduced cell counts in other lineages, indicative that TPO and c-Mpl play important roles early in haematopoiesis (Gurney et al., 1994, Carver-Moore et al., 1996). Additionally, injecting recombinant protein into mice increased the circulating platelet count substantially over a seven day period, strongly suggesting TPO is essential for the production of platelets (Lok et al., 1994). This greatly aided first *in vitro* studies of MKs and platelets whereby $CD34^+$ cells isolated from whole blood could be differentiated in culture with the addition of TPO (Choi et al., 1995). Upon formation of the TPO-c-Mpl construct, cytoplasmic tyrosine kinase, Janus

Kinase 2 (JAK2) is activated. The cytoplasmic tails of c-Mpl receptor become closer in proximity, as do the JAK2 molecules and are activated by trans-autophosphorlyation (Geddis, 2010). JAK2 activation then initiates cellular cascade reactions in signal transducer and activator of transcription (STAT), mitogen-activated protein kinase (MAPK) and phosphoinositol-3 kinase (PI3K) pathways; all promoting megakaryocyte differentiation and proliferation (Geddis, 2010).

In addition to TPO, stem cell factor (SCF) also plays an important role in maintaining steady state megakaryopoiesis. SCF is expressed in both membrane and soluble forms, binding to the transmembrane c-Kit receptor expressed on HSCs (Zsebo et al., 1990, Flanagan and Leder, 1990, Williams et al., 1990). Downstream c-Kit signalling on $CD34^+$ cells promotes steady haematopoiesis and megakaryopoiesis *in* vitro (Lennartsson and Rönnstrand, 2012).

Megakaryopoiesis is a tightly regulated process and can up/down-regulate in response to bleeding or thrombosis. These changes are largely governed by TPO cytokine and its respective receptors, c-Mpl to maintain optimum circulating levels of platelets (Figure 1.2).

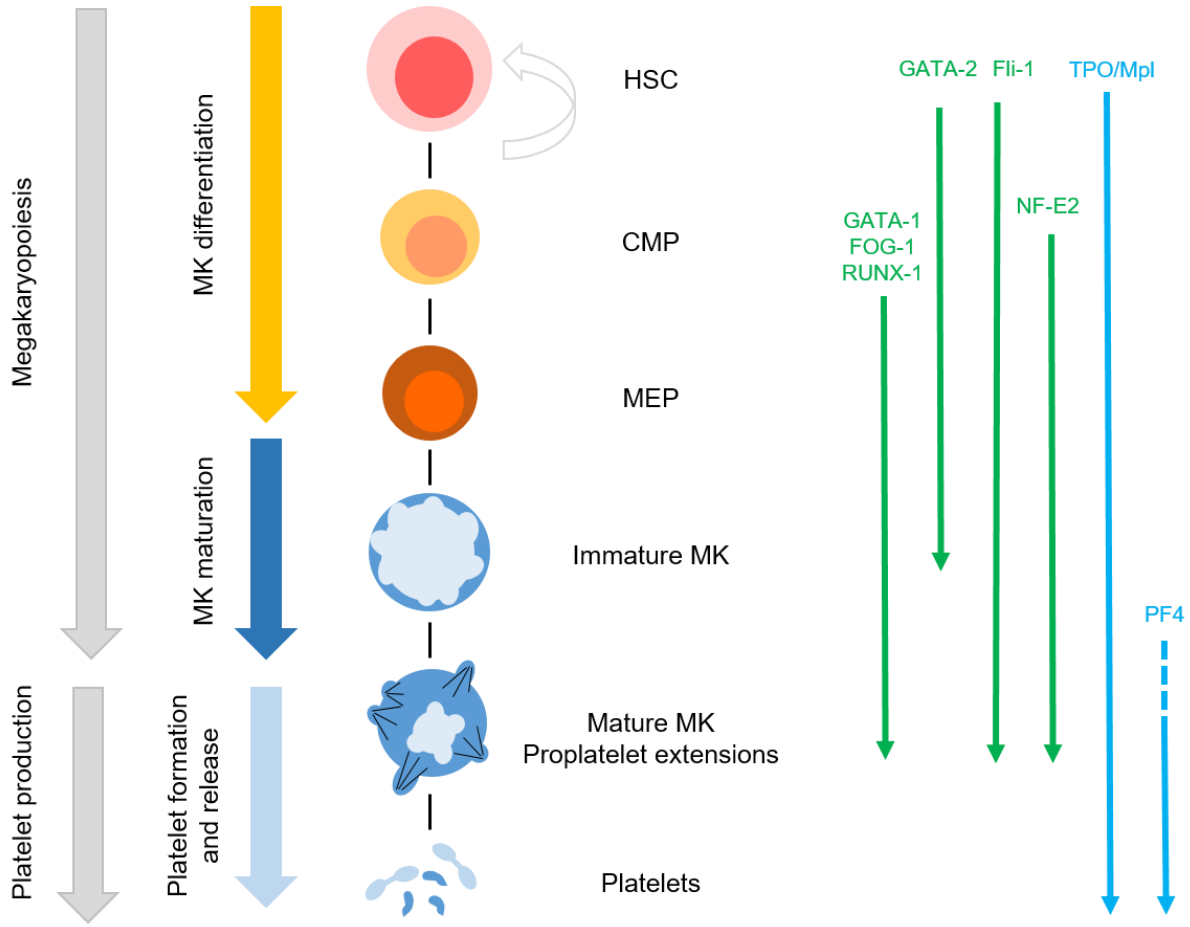


**Figure 1.2: MK differentiation and platelet formation.** HSCs differentiate into myeloid committed CMPs with self-renewal capacity and further into MEPs. Here, MKs proliferate and undergo endomitosis to become polyploid immature MKs with increase cellular content. Further maturation involves generation of the MK cytoskeleton and granule biogenesis. Once MKs are fully matured they produce pseudopodia extensions governed by the DMS which marks the initiation of proplatelet formation. This extends and forms branches forming proplatelet extensions which are subsequently released as barbell structures (light blue) from the MK by shear stress which then mature into mature circulating platelets (darker blue). MK differentiation, maturation and platelet formation is orchestrated by a series of transcription regulators (right hand side - green) and cytokines (right hand side – blue). Their involvement in this process varies and is highlighted by arrows of progression.

### 1.2.4 Platelet structure and function

Platelets are small anucleate cells (approximately 2µm in diameter) of discoid shape maintained by microtubules and microfilaments in the cytoskeleton. In a resting state, endothelial cells suppress adhesion of pro-coagulant cells and proteins preventing unnecessary clot formation (Watson, 2009). However, when the endothelial wall is damaged, exposed collagen encourages adhesion of platelets by binding to vWF through membrane bound glycoprotein GPIb-IX-V. At high shear rates, this initiates platelet arrest at the site of injury, intracellular signalling to cause shape change and recruitment of neighbouring platelets to stabilise the platelet plug (Reininger, 2008). In conditions of low shear, platelets adhere to collagen by directly binding with GPVI and GPIIb/IIIa (integrin αIIbβ3). GPVI is involved in the early stages of platelet activation; binding to collagen causing tyrosine phosphorylation of the FcRγ chain and downstream activation of the immunoreceptor tyrosine-based action motif (ITAM) pathway for platelet activation (Jandrot-Perrus et al., 2000). The principal role of integrin αIIbβ3 is to bind to fibrinogen, forming inter-platelet connections and thrombus formation (Jandrot-Perrus et al., 2000). Integrins stabilise the plug formation in high shear conditions, securing the thrombus at the site of damage.

When a thrombus is formed, and platelets are activated, granules within the platelets secrete molecules to recruit further platelets. Platelets contain several types of granules which release their contents upon platelet activation and stimulate additional platelet recruitment in thrombus formation. Dense (δ) granules secrete many molecules, the most abundant of which is ADP, acting on P2Y1 and P2Y12 receptors triggering further shape changes, granule secretion and activation of integrin $\alpha_{IIb}\beta_3$ (Hou et al., 2015). Thromboxane synthase ($TXA_2$) is generated from arachidonic acid (AA) through the cyclooxygenase pathway (COX1) and adheres to the thromboxane $A_2$ receptor ($TXA_2$) (Hou et al., 2015). C-type lectin-like receptor 2 (CLEC-2) binds to its ligand podoplanin, initiating platelet activation through tyrosine phospohorylation similar to GPVI (Boulaftali et al., 2014). These secretion events

occur as secondary messengers to amplify activation and inside-out signalling, recruiting additional platelets for aggregation.

Alpha (α) granules secrete fibrinogen and vWF to propagate aggregation at the site of injury and traffic GPVI receptors to the membrane surface. P-selectin, also released by α granules, migrates to the membrane and gathers circulatory monocytes, neutrophils and leukocytes, initiating the inflammatory response (Golebiewska and Poole, 2015).

Upon activation, platelets can express toll-like receptors (TLRs) which have been well characterised in neutrophils, macrophages and dendritic cells in response to pathogens (Janeway and Medzhitov, 2002). These TLRs are thought to play critical roles in the platelet mediated immune response and TLR-9 has been shown to localise at the platelet membrane surface, separate from other granule released markers of activation such as P-selectin (Thon et al., 2012). Although T-granules do not appear as isolated granule population as seen in δ and α granules, they play a critical secondary role in platelet recruitment and thrombus formation and platelet-leukocyte interactions (Thon et al., 2012). In addition, platelets contain peroxisome proliferator-activated receptors (PPARs) which play a major role in modulating platelets in inflammation and attenuating platelet activation (Spinelli et al., 2008).

After the release of granule contents, the coagulation cascade begins. Circulating thrombin is activated and acts on protease activated receptors 1 and 4, (Marconi et al.) (PAR3 and PAR4 are present in mice) which are Gq receptor proteins acting within a positive feedback loop to stimulate cytoskeletal changes for platelet activation (Zarpellon et al., 2017). Thrombin aids the conversion of circulating fibrinogen to its insoluble form fibrin and the coagulation cascade. Fibrin molecules form strengthened polymers which results in a stable fibrous network connecting neighbouring platelets and a secure thrombus at the site of injury. (Figure 1.3, Figure 1.4).

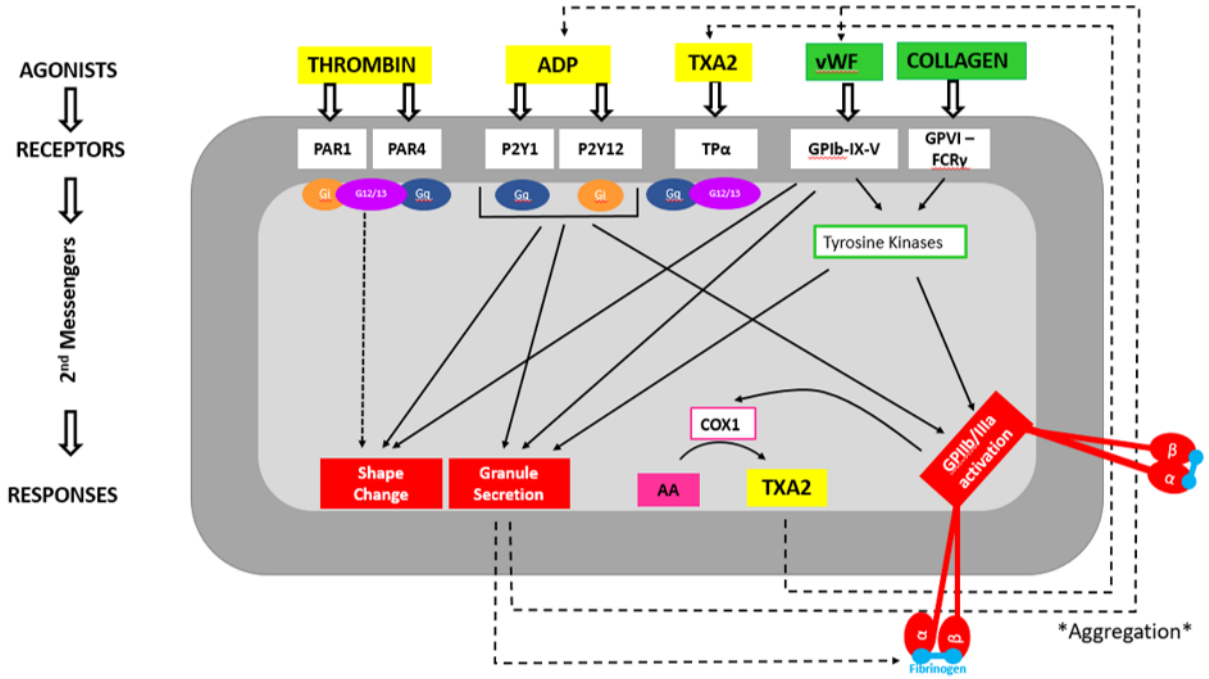


**Figure 1.3: Platelet activation and haemostatic signalling pathways.** Platelet agonist's thrombin, ADP and $TXA_2$ signal through G-protein coupled receptors (G-PCRs). This leads to cytoskeletal rearrangement, secretion of granule content and integrin activation. In this way, thrombin is a powerful agonist which initiates platelet activation and ADP and $TXA_2$ act as positive feedback mechanisms in maintaining platelet activation (dotted lines). GPVI signalling is initiated by the binding of collagen to dimerised GPVI receptors and vWF signals using the same tyrosine phosphorylation signalling pattern. Together this initiates platelet shape change, degranulation and integrin activation to bind fibrinogen strengthening platelet-platelet interactions.

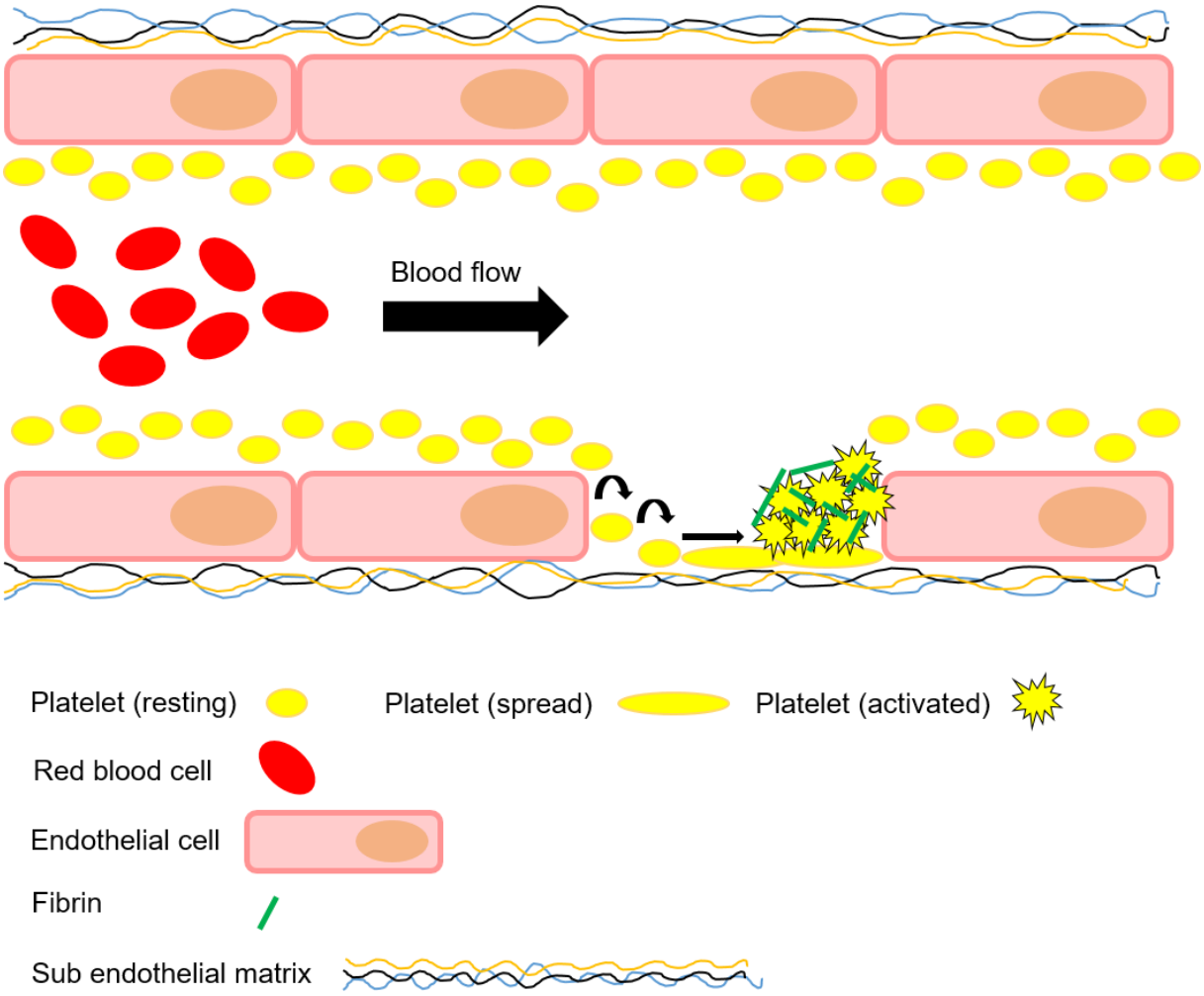


**Figure 1.4: Platelets in thrombus formation.** The primary role of platelets is in haemostasis, to reduce blood loss through bleeding and prevent damage to the sub endothelial matrix. Platelets are marginalised towards the vessel walls under their resting state. Upon vessel injury, platelets adhere to the exposed sub-endothelial matrix and begin to activate binding to vWF on exposed collagen. Platelets roll along the surface in a bid to slow down and enhance low affinity binding of GPVI to collagen at the site of injury. As platelets spread, GPVI signalling causes further platelet activation. Platelets degranulate, and recruit others to the growing thrombus due to ADP released from α-granules and $TXA_2$. Platelets aggregate by activated integrin αIIbβ3 and fibrinogen released from granules. Thrombin, activates more platelets and generates fibrin from fibrinogen to stabilise the thrombus. Thrombus retraction occurs by cytoskeletal tension and integrin outside-in signalling. This secures the thrombus at the injured vessel wall. Eventually the clot breaks down by fibrinolysis, releasing activated platelets for macrophage mediated clearance.

## 1.3 Erythrocytes

### 1.3.1 Erythropoiesis and red blood cell production

Erythropoiesis describes the process of differentiation and maturation of erythroid progenitors through to erythrocytes (red blood cells). This begins at the MEP which has propensity to develop into either MKs or erythroid progenitors. Typically, erythropoiesis begins in the yolk sac where the first erythrocytes form, critical for survival of the embryo (Tavassoli, 1991). This is then followed by definitive erythropoiesis occurring in foetal liver in embryos and postnatal bone marrow. Erythropoiesis occurs in three stages whereby MEPs differentiate into the earliest erythroid specific progenitors, burst forming unit (BFU-E) and subsequently colony forming unit erythroid progenitors (CFU-E). The second stage is the production of nucleated erythroid precursors, namely the Proerythroblast (ProE) which undergoes a series of cell division and morphological changes as it differentiates towards the reticulocyte (immature erythrocyte) (Chen et al., 2009). The third stage is where erythroblasts expel their nuclear content and notably reduce in size forming reticulocytes and subsequently erythrocytes (Mei et al., 2021). Reticulocytes are immature and possess different cytoskeletal membrane compared to more mature reticulocytes and erythrocytes. The most well-known characteristic is their innate ability to lose CD71 expression with maturation, notably one of the best ways to separate reticulocytes based on age in flow cytometry assays (Chen et al., 2009, Malleret et al., 2013). Residual erythroblast RNA is also present in newest reticulocytes therefore staining with RNA dyes gives enables haematologists to investigate immature reticulocyte fraction (IRF) indicative of erythrocyte turnover (Wollmann et al., 2014, Davis et al., 1995). Mature reticulocytes circulate in the blood stream for approximately one day before maturing into erythrocytes (Chasis et al., 1989). (Figure 1.5).

### 1.3.2 Transcription factors: Erythropoiesis

Alone, or as part of transcriptional complexes, the fine tuning of erythropoiesis is maintained by a cohort of TFs specific to the formation, proliferation and differentiation of multipotent cells of self-renewal capacity, to mature erythrocytes with various functions (Figure 1.5)

Putative oncogene *Spi-1* (PU.1), Fli-1 and GATA-2 all act in primitive erythropoiesis on BFU-E and CFU-E. Here they collectively act to increase proliferation of early erythroid precursors for further differentiation. Fli-1 only acts during early stages of erythropoiesis and in previous studies, over expression of Fli-1 results in inhibition of erythroid differentiation and in fact impairs the cell's ability to respond to critical erythroid inducers (Athanasiou et al., 2000). GATA-2 expression is present in primitive erythroid cells as well as early ProEs before GATA switching occurs, and in the presence of co-factor FOG, GATA-2 is repressed in definitive erythropoiesis and GATA1 takes over (Tsang et al., 1997). Erythroid Kruppel-like factor (EKLF) and Basic Kruppel-like factor (BKLF) both function to induce β-globin gene expression in mature erythroblasts (Miller and Bieker, 1993). Finally, Signal transducer and activator of transcription (Stat5) promotes survival of late erythroid progenitors and mature cells in the circulation. Erythropoietin, (EPO) the main cytokine of erythrocyte development binds to its receptor (EpoR) and leads to activation of transcription factor Stat5. This then triggers tyrosine phosphorylation signalling which induces immediate expression of the antiapoptotic gene *bcl-x.* Stat5 deficient mice are severely anaemic due to the decreased survival of foetal liver erythroid progenitors and a marked increase in apoptosis at E13.5 (Socolovsky et al., 1999).

### 1.3.3 Cytokines: Erythropoiesis

In definitive erythropoiesis, progenitor cells are dependent on EPO and EpoR for differentiation and maturation (Figure 1.5). The interaction between EPO and EpoR triggers internal cellular signalling which increases globin mRNA, transferrin receptor expression (CD235a/Glycophorin-a in humans and Ter119 in mice) and membrane structural proteins

characteristic to erythrocytes (Kendall, 2001). EPO plays a critical role in definitive erythropoiesis at the foetal liver stage and in bone marrow, evident by embryonic death at age E13.5 in EPO null mice due to severe anaemia. In primitive erythropoiesis (at the BFU-E), EPO deficiency did not seem to have detrimental effect on erythropoietic lineage commitment and only presented severe defects at the CFU-E stage (Wu et al., 1995). This suggests EPO and EpoR are major contributors in the survival of definitive erythroid progenitors beyond E12.5 *in utero* and postnatally in bone marrow haematopoiesis (Makita et al., 2001). *In utero*, EPO is manufactured in the foetal liver however into the latter stages of development and postnatally EPO is predominantly produced in the kidneys. Into adulthood, oxygen tension or hypoxic conditions tend to be the main driver for EPO production. This is regulated by Hypoxia inducible factor 1 (HIF1) whereby it binds to an enhancer region on the *Epo* gene, increasing expression and thus circulating levels of EPO to accelerate erythropoiesis (Bunn et al., 1998, Semenza et al., 1991).

### 1.3.4 Erythrocyte structure and function

Erythrocytes are the most abundant enucleate cell type in the circulation and their primary role is to transport oxygen around the body by haemoglobin. They have a characteristic biconcave disc shape to increase surface area and oxygen binding capacity as well as withstand blood flow shear stress. Haemoglobin is comprised of two subunits α-like globin and β-like globin peptide chains. *In utero*, embryonic-globin (ε-globin) is expressed in the yolk sac which then switches to foetal-globin (γ-globin) at the onset of primitive erythropoiesis in the foetal liver. γ- and α-globin chains make up total foetal haemoglobin (HbF) (Baron et al., 2013). The second switching event involving haemoglobin maturation occurs shortly after birth, γ-globin to β-globin occurs by a translational switch with erythroid progenitors in the bone marrow forming adult haemoglobin (HbA) (Sankaran and Orkin, 2013). Erythrocytes have also been suggested as critical players in platelet activation through phosphatidylserine (PS) exposure. PS exposure stimulates plasma thrombin generation and activates platelets

(Whelihan and Mann, 2013). Erythrocyte morphology has previously been explored with regard to thrombus stability. Their bioconcave shape not only allows cells to repond to shear stress but they are also able to change shape into ‘polyhedrocytes’ which allows tight formation of cells at the endothelium and the ability to alter their shape under different shear conditions (Ariens, 2015).

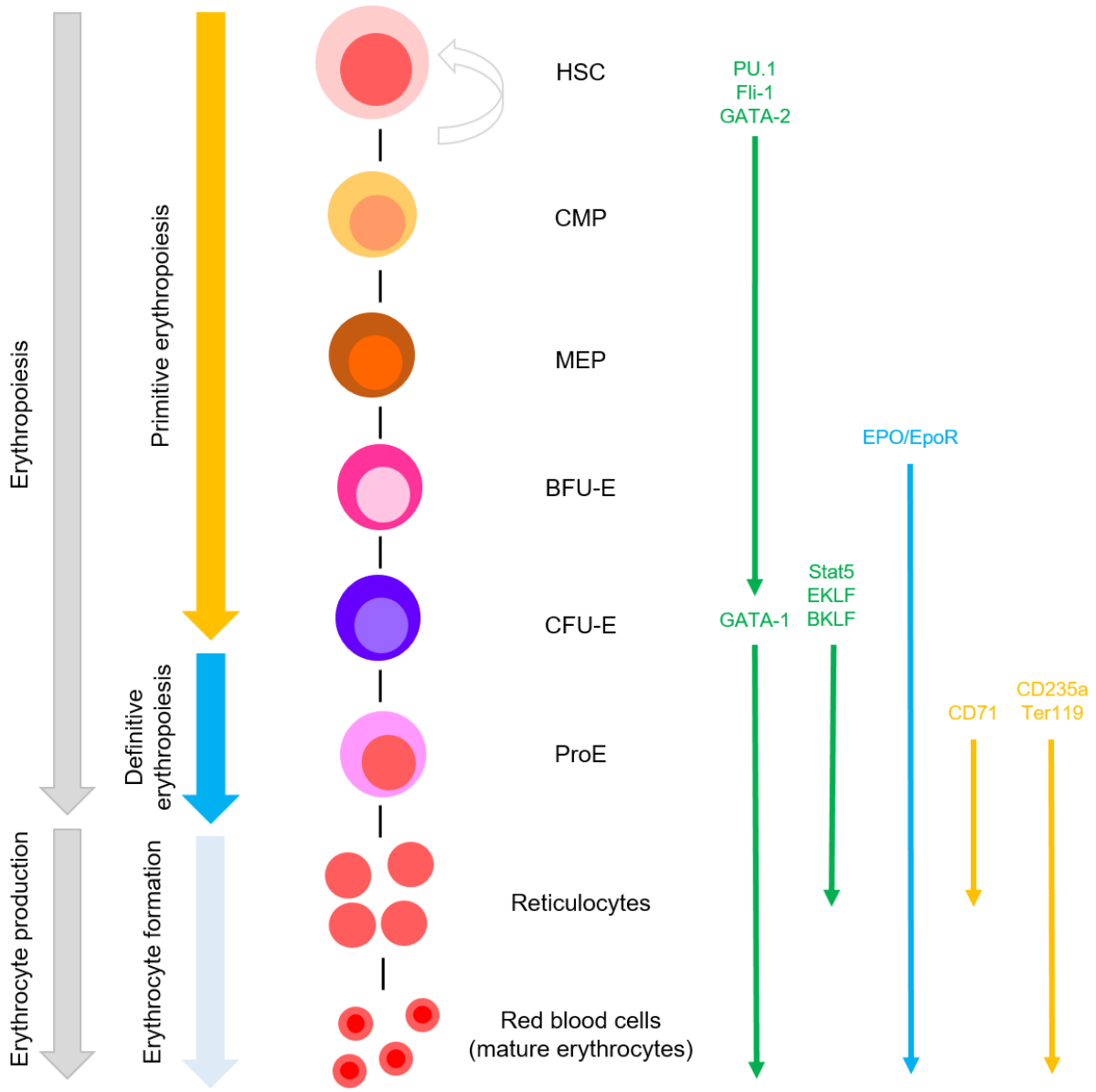


**Figure 1.5: Erythrocyte differentiation and red blood cell formation.** HSCs differentiate into myeloid committed CMPs with self-renewal capacity and further into MEPs. Here, the cytokine EPO and its respective receptor EpoR direct differentiation in the erythroid direction. BFU-E and CFU-E cells undergo further differentiation at the final stages of primitive erythropoiesis. The earliest identified cell of definitive erythropoiesis is the ProE. Here, the ProE undergoes several rounds of division producing cells which progressively decrease in size, losing CD71 expression and contain haemoglobin. The first stage of erythrocyte formation produces reticulocytes, which are enucleated immature red blood cells. They are larger than mature erythrocytes, containing residual ProE RNA and last approximately one day in the circulation before maturing into erythrocytes. Erythroid differentiation, maturation and erythrocyte formation is orchestrated by a series of transcription regulators (right hand side – green arrows) and cytokines (right hand side – blue arrows). Their involvement in this process varies and is highlighted by arrows of progression. Additionally, receptor expression can be used to highlight erythroid cells of varying age (right hand side – orange arrows).

## 1.4 Interactions: Platelets and Erythrocytes

### 1.4.1 Regulation of Megakaryopoiesis and Erythropoiesis

HSC differentiation appears to be regulated by two mechanisms. Firstly to maintain steady state haematopoiesis, based on the requirements of the body to produce sufficient blood cells for basal function. Secondly, to appropriately amplify haematopoiesis in response to haematopoietic stress, such as during infection, bleeding or hypoxia.

Platelets and erythrocytes are closely related, both originating from the same progenitor and sharing most transcription factors for development (Figure 1.1, Figure 1.2 and Figure 1.5). So the questions arises, where in lineage commitment do these differences occur and what controls whether their shared progenitor proliferates into a MK or erythroid progenitor? The distinct differences in cell types arise at the transcriptional and translational levels with lineage preferences altered in diseased states (Psaila et al., 2020). The genetic properties which determine a MK are different from that which determine erythroid committed cells and hence give rise to their different contents and functional differences. At the epigenetic level, it has been shown that long non-coding RNAs (lncRNAs) have been identified in erythroblasts, MKs and MEPs. While the specific functional capacity in these cell types remains unexplored, lncRNAs have been shown to regulate transcriptional control and mRNA stability – both factors which are also important to consider in endoribonucleolytic activity (Paralkar et al., 2014). If lncRNAs are regulated by TFs then this may function in the same capacity as the endoribonuclease SLFN14 altering haematopoietic cell lineage fate.

Some studies have suggested that expression of TFs holds two main roles in lineage direction. The first of which is to auto-upregulate and hold the lineage specified direction and the second is to actively down-regulate alternate pathways (Tsai et al., 1991). This has been shown with regard to GATA-1, whereby PU.1 inhibits transcriptional activity of GATA-1 in its target genes and vice versa (Zhu and Emerson, 2002).

### 1.4.2 GATA-1 and GATA-2

GATA-1 and GATA-2 are required for haematopoiesis and play particularly important roles in the differentiation of both MKs and erythroid cells. GATA binding proteins recognise a consensus target sequence 'T/A GATA A/G' found in promoters or enhancer regions of haematopoietic expressed genes (Tsai et al., 1991). There are 6 GATAs in total with GATA-1 and GATA-2 are expressed in MKs, erythroid cells, mast cells, eosinophils and other haematopoietic progenitors. GATA-3 is expressed at high levels in the lymphoid lineage (Merika and Orkin, 1993). GATA-4 to GATA-6 are not expressed in the haematopoietic lineage but rather involved in the development of cardiac cells and are termed 'non-haematopoietic' GATAs (Ikonomi et al., 2000, Pikkarainen et al., 2004).

Genetic manipulation of GATA-1 revealed *in vivo* the critical requirement for GATA-1 in the development of erythroid cells (Pevny et al., 1991). Erythroid differentiation did not proceed in response to GATA-1 null embryonic stem cells and similarly GATA-1 null mice are embryonic lethal at E10.5 (before foetal live haematopoiesis) (Tsai et al., 1991, Baron et al., 2013). GATA-2 null mice are also embryonic lethal due to failure of erythroid progenitor expansion (Baron et al., 2013). Although GATA-1, GATA-2 and GATA-3 recognise identical (or highly similar) promoter targets, the absence of either GATA-1, GATA-2 or both, means normal erythroid development does not occur (Fujiwara et al., 2004). The expression of GATA-1 and GATA-2 overlap in haematopoietic progenitors and the functional compensation in the erythroid lineage which occurs between GATA binding proteins is unknown (Fujiwara et al., 2004).

GATA-1 and GATA-2 present overlapping patterns of expression, with GATA-2 most highly expressed in early haematopoiesis and GATA-1 replacing it in terminally differentiating cells of both MK and erythroid origin (Weiss et al., 1994). It has been shown previously that GATA-2 may substitute in part for GATA-1 activity and the balance between GATAs in haematopoiesis is critical to normal cell development. GATA-1 is highly expressed in MKs

however GATA-1 deficient MKs exhibit reduced polyploidisation and form large colonies of immature MKs in the bone marrow. Platelets produced from these GATA-1 deficient MKs are low in number and have marked structural abnormalities (Vyas et al., 1999). One study suggested that the absolute level of GATA-2, as well as its amount compared to GATA-1 was critical in the regulation of erythroid differentiation (Ikonomi et al., 2000). Despite this, another study suggested that GATA-1 binds to genes common in both MK and erythroid lineages, however, this occurred at different binding sites, allowing for differential control between lineages (Doré et al., 2012).

Taken together, prior studies of GATA-1 and GATA-2 show they have significant involvement in the growth and survival of developing MK and erythroid precursors. However, it must be noted lineage fate is not solely controlled by GATAs and the involvement of co-factors or additional TFs remains unclear.

### 1.4.3 Extramedullary Haematopoiesis (EMH)

In healthy adults, the bone marrow is the primary site of haematopoiesis however in stress haematopoiesis, or in myeloproliferative neoplasms (MPN) other organs can take on this role (Tavassoli, 1991). Haematopoiesis is remarkably adaptable in its ability to shift in either myeloid or lymphoid directions in response to various diseases. Stresses such as haemorrhage or anaemia can shift haematopoiesis towards the myeloid direction and cause preferential priming of common progenitors in either MK or erythroid directions (Xavier-Ferrucio et al., 2019). EMH is typically identified as a secondary event to another disorder including haematological disorders or cancer (Yamamoto et al., 2016). In humans and mice this most commonly occurs in the liver and spleen but other sites such as lymph nodes have been identified (Wolf and Neiman, 1987, Schlitt et al., 1995, Sohawon et al., 2012). It is a compensatory mechanism which is closely related with bone marrow dysfunction with reduced capability to produce adequate progenitor and subsequent differentiated cells. In response to reduced erythrocyte numbers, erythropoietin production is upregulated which

initiates differentiation preference in the myeloid lineage or expansion of progenitors into the extramedullary space (Sohawon et al., 2012). In the spleen, EMH occurs in the red pulp. Despite the spleen's notoriously hypoxic, acidic conditions in the presence of digestive macrophages, HSCs appear to overcome this harsh microenvironment to compensate for particular stresses (Wolf and Neiman, 1987). Haematopoietic cells migrate to extramedullary organs and proliferate similarly to the bone marrow by production and cellular expression of endothelial expressed ligands such as CXCL12 and SCF (Miwa et al., 2013). Circulating haematopoietic progenitors may also be mobilised as a result of haematopoietic stress whereby cells 'seed' in non-medullary organs. Identifying multiple cells at different stages of differentiation supports that EMH can support maturation of cells from most immature HSC (CD34 negative) to most mature erythrocytes or platelets (Avecilla et al., 2004).

### 1.4.4 Platelets and Erythrocytes in Thrombosis and Haemostasis

Studies of thrombosis and haemostasis often focus on platelets as the primary cell of interest. However, emerging evidence suggests that red blood cells play a critical role in bleeding and thrombosis through blood rheology and viscosity, exposure of phosphatidylserine (PS), haemolysis as well as shear dependent morphological changes important in wound healing.

Patients with high haematocrits (high percentage of erythrocytes in the blood) such as in polycythaemia vera or supplementation of EPO are more susceptible to thrombotic disorders (Kroll et al., 2015). Erythrocytes contribute to blood viscosity by slowing down the flow of blood through vessels and increase platelet margination at the vessel wall (Barshtein et al., 2007). This initiates platelet hypercoagulability at the vessel wall and thus erythrocytes have an indirect effect on platelet activity based on haematocrit and flow conditions (Barshtein et al., 2007).

In normal cells at rest, PS is located on the inside of the plasma membrane, separating it from plasma coagulation factors (Kay and Grinstein, 2013). If cell damage occurs, caused by haemolysis, inflammation or shear stress, the erythrocyte membrane may be disrupted and PS exposed. Exposure of PS is a normal process of cell senescence (associated with programmed cell death pathways, apoptosis and eryptosis) but in cases of haemolysis where more cells are expressing PS it has been shown this can induce coagulability. PS is exposed on the membrane of activated platelets which functions to generate thrombin and further activate neighbouring platelets (Reddy and Rand, 2020). PS exposure on red blood cell membranes has been shown to function in the same way, stimulating plasma thrombin generation and activating platelets (Whelihan and Mann, 2013, Whelihan et al., 2012). This increases levels of circulating activated platelets despite no endothelial damage occurring and may induce spontaneous thrombosis and potential cardiovascular events (Whelihan and Mann, 2013, Whelihan et al., 2012).

RBCs interact with activated platelets through GPVI mediated adhesion under low shear rates (Goel and Diamond, 2002, Klatt et al., 2018). This ability of RBCs to interact with platelets is thought to be the reason for RBC presence in arterial thrombi which are known to be ‘platelet rich’, however any direct ligand between the two cell types is yet to be identified (Silvain et al., 2011). *In vivo* models of thrombosis in a mouse model of erythrocytosis and poikilocytosis showed reduced stability of thrombi at both arterial and venous shear rates despite normal platelet function (Stapley et al., 2021). This suggests thrombus formation at arterial shear rates is not solely dependent on platelets but the interaction of platelets and RBCs which mediate thrombus stability and platelet recruitment through secondary mediators such as platelet activation markers, PS exposure and plasma thrombin generation.

## 1.5 Studying genes and proteins in haemostasis and thrombosis

Platelets are small anucleate cells which play a critical role in primary haemostasis. In the bloodstream, platelets marginate against the endothelial wall for rapid detection of vessel

damage. Formation of a blood clot or thrombus at the site of injury is the best characterised function of platelets in order to stop bleeding and maintain vessel wall integrity (Machlus and Italiano, 2013). Exposure of sub-endothelial matrix proteins at the point of vessel injury, or generation of thrombin through the coagulation cascade cause platelet activation, adhesion and aggregation (Jackson, 2007). This response is augmented by release of feedback agonists from activated platelets such as thromboxane A2 and ADP. Platelets contain four types of secretory granules; dense (δ)-granules, alpha (α)-granules, multivesicular bodies and lysosomes, which contain small molecules, including platelet agonists and a range of cytokines, growth factors and coagulation proteins (Golebiewska and Poole, 2015, Heijnen et al., 1998). The platelet aggregate or thrombus is strengthened by fibrin crosslinking of activated platelets and is stabilised by 'clot retraction' subsequently securing the vascular plug to the damaged vessel wall (Undas and Ariëns, 2011). By these same mechanisms, unwarranted platelet activation can lead to the accumulation of thrombi and cause obstruction of blood flow or total occlusion of blood vessels. This can pose serious health risks in cardiovascular disease which as of 2020 accounted for approximately 27% of UK deaths (BHF, 2020). In comparison, defective platelets unable to aggregate at the site of injury can result in abnormal bleeding in some patients. As such, it is essential to understand the mechanisms for platelet activation, function and interactions with other blood cells which play a crucial part in preventing bleeding and/or thrombosis.

### 1.5.1 Inherited platelet disorders affecting haemostasis

Platelet function disorders comprise a wide variety of disorders typically characterised by defective production of platelets from megakaryocytes in the bone marrow or abnormal signalling pathways resulting in defective function. Inherited platelet disorders are a heterogeneous group of disorders making identifying a single attributable cause for such defects difficult. Thus far, platelet counting and light transmission aggregometry (LTA) remain two of the most useful techniques in identifying a single cause for platelet disorders. The

normal platelet count in humans is 150-400x$10^9$/L, maintained by equilibrium between platelet formation and consumption. A low platelet count, <150x$10^9$/L in humans is characterised as thrombocytopenia and may present platelet dysfunction or bleeding based on the reduced numbers of platelets in the circulation, unable to provide sufficient clot formation (Patel et al., 2005). In addition to this, while platelet number may be unaffected, platelet function disorders may arise due to defects in platelet activation or haemostatic signalling pathways. For example, Bernard-Soulier Syndrome (BSS) is a rare inherited platelet disorder that results from genetic defects in the genes *GPIBA*, *GPIBB* or *GP9*, where together these genes form the platelet membrane receptor GPIb/V/IX which plays a critical role in binding to von-willebrand factor (VWF) in thrombus formation. This can be assessed *in vitro* by aggregation in response to ristocetin. In addition to reduced platelet function, BSS patients have a macrothrombocytopenia, suggesting critical roles for *GPIBA*, *GPIBB* or *GP9* in platelet production. Grey Platelet Syndrome (GPS) is a bleeding disorder characterised by the complete absence of α-granules giving platelets their 'grey' appearance. Biallelic mutations in *NBEAL2* result in mild thrombocytopenia and bleeding tendencies (Raccuglia, 1971, Pluthero et al., 2018, Kahr et al., 2011).

There are many more inherited bleeding disorders linked to both defective platelet production and function (Table 1.1). Here, platelet defects are divided into three subgroups; megakaryopoiesis, platelet production and platelet clearance/other. Within each of these groups severity of the mutant platelet phenotype varies greatly with no one group presenting more severe defects than others. Heritable forms of thrombocytopenia are usually caused by mutations in genes involved in platelet production and megakaryocyte (MK) differentiation leading to defects in other platelet parameters as well as number including increased platelet size (MPV). Over 25 forms of IT have been described to date in OMIM (http://www.ncbi.nlm.nih.gov/omim), yet a causative gene remains to be identified in 50% of patients. Identification of such genes is fundamental in providing information on proteins

involved in normal platelet physiology. Furthermore, the functional investigation of platelet-related proteins is critical for developing our understanding of disease pathogenesis and for designing patient treatment regimens.

## 1.6 The Genotyping and Phenotyping of Platelets Study (GAPP Study)

The genotyping and phenotyping of platelets study (Watson et al., 2013, Maclachlan et al., 2017) recruited patients and their families with inherited bleeding disorders in order to identify genes and causative variants within these genes attributed to their bleeding. The study was launched in Birmingham with key collaborators from the universities of Bristol and Sheffield. To date, over 1000 patients have been recruited from over 25 collaborating haemophilia care centres across the UK and Ireland (Figure 1.6). The UK-GAPP workflow is standardised across all sites utilising techniques such as aggregometry and flow cytometry to characterise platelet function, as well as whole exome sequencing (WES) and Sanger sequencing of candidate genes to identify disease causing mutations involved in megakaryocyte development and platelet formation or platelet function (Watson et al., 2013). For newly recruited patients, whole blood samples are collected from referring centres for platelet phenotyping and sent to Birmingham for platelet protein and DNA extraction prior to sequencing. Several novel variants have been identified as a result of this study, such as those in *SLFN14, RUNX1* and *FLI1* providing patients with a definitive diagnosis of their disease (Table 1.1) (Fletcher et al., 2015) (Almazni et al., 2021, Almazni et al., 2019, Khan et al., 2020b). Three unrelated families with novel Schlafen 14 (*SLFN14)* variants were discovered in the UK-GAPP study (highlighted orange in Table 1.1).


**Figure 1.6: UK-GAPP patient recruitment sites shown by red point markers.** Collaborating hub laboratories were in Bristol and Sheffield with the main laboratory responsible for platelet functional testing at the University of Birmingham (blue star icon).

**Table 1.1: Genetic causes of inherited thrombocytopenia and associated syndromes. Taken from (Almazni et al., 2019).**

| Platelet Defect | Gene | Disorder | Syndrome or features | Reference |
|---|---|---|---|---|
| Megakaryopoiesis | *ANKRD26* | *ANKRD26*-related thrombocytopenia | Predisposition to leukaemia. Reduction of platelet α-granules. Normal in vitro platelet aggregation and mean platelet volume. Some patients have high level of haemoglobin and leukocyte. | (Bluteau et al., 2014, Pippucci et al., 2011) |
| | ETV6 | *ETV6*-related thrombocytopenia | Leukaemia predisposition. High erythrocyte mean corpuscular volume (MCV). Some patients have elevated red cell MCV. | (Noetzli et al., 2015) |
| | *FLI1* | Paris-Trousseau thrombocytopenia /Jacobsen syndrome | Abnormal development of heart and face. Intellectual disabilities. Large α-granules. Abnormal MKs morphology. Normal RBCs and WBCs counts. Moderate thrombocytopenia. | (Stevenson et al., 2015) |
| | *FYB* | *FYB*-related thrombocytopenia | Small platelets. Reduction of mature MKs in BM. Significant bleeding tendency. Normal WBCs count. Low mean platelet volume MPV. Mild iron deficiency anaemia. | (Koren et al., 2015) |
| | *GATA1* | GATA1-related disease: X-linked thrombocytopenia (XLT) and X-linked thrombocytopenia with thalassemia (XLTT) | Dyserythropoietic anaemia. Macrothrombocytopenia. Beta-thalassemia. Congenital erythropoietic porphyria. Erythrocyte abnormalities. Splenomegaly | (Freson et al., 2017) |
| | *GFI1B* | Macrothrombocytopenia and platelet function defects | Macrothrombocytopenia. Red cell anisopoikilocytosis. platelet dysfunction. Reduction of platelet α-granules. | (Stevenson et al., 2013b) |

| | | | | |
|---|---|---|---|---|
| | *HOXA11* | Amegakaryocytic thrombocytopenia with radio-ulnar synostosis | Bilateral radioulnar synostosis. Severe bone marrow failure. Cardiac and renal malformations. B-cell deficiency. Hearing loss. Clinodactyly. Some patients show skeletal anomalies. Some patients have developed pancytopenia. | (Horvat-Switzer and Thompson, 2006) |
| | *MECOM* | Congenital amegakaryocytic thrombocytopenia and radioulnar synostosis | | (Germeshausen et al., 2018) |
| | *MPL* | Congenital amegakaryocytic thrombocytopenia (CAMT) | Absence or reduced of MKs in BM. No physical anomalies. Development to BM aplasia in infancy. | (Ihara et al., 1999) |
| | *NBEAL2* | Grey Platelet Syndrome | Impaired platelet function. Severe reduction of platelet α-granules contents. Large platelets. Development of myelofibrosis and splenomegaly in some patients. Abnormalities in megakaryocyte development. | (Pluthero et al., 2018) |
| | *RBM8A* | Thrombocytopenia-absent radius syndrome | Bilateral radial aplasia. Elevated haemoglobin level in patients with 5'UTR SNP. Normal WBCs count and some patients have leucocytosis and eosinophilia. Anaemia. Skeletal, urogenital, kidney and heart defects. Reduced MKs in BM. | (Manukjan et al., 2017) |
| | *RUNX1* | Familial platelet disorder with propensity to acute myelogenous leukemia (FPD/AML) | Platelet defects. Variable platelet counts. Reduction in dense granule secretion observed in secondary qualitative abnormality. Myelodysplasia. Reduced response to several platelet agonists. | (Morgan and Daly, 2017) |
| | *SLFN14* | *SLFN14*-related thrombocytopenia | Giant platelets. Decreased ATP secretion. Reduced number of dense granules. | (Fletcher et al., 2015, Marconi et al., 2016, Saes et al., 2019) |
| | *SRC* | SRC-related thrombocytopenia | Myelofibrosis, bleeding, and bone pathologies. Hypercellular bone marrow with trilineage dysplasia. Platelets are dysmorphic and variable in size. Splenomegaly and congenital facial dysmorphism. | (Turro et al., 2016) |

| | | | | |
|---|---|---|---|---|
| | *THPO* | Inherited thrombocytopenia from monoallelic *THPO* mutation | Bone marrow aplasia. Normal or enlarged platelet morphology. | (Marconi et al., 2017) |
| | *PTPRJ* | Inherited thrombocytopenia | syndromic thrombocytopenia characterized by spontaneous bleeding, small-sized platelets. Impaired platelet function. | (Wen and Wang, 2019) |
| | *GALE* | Inherited thrombocytopenia | Dysplastic megakaryocytes. Some patients have mild anemia and febrile neutropenia. Big and pale platelets. Galactosemia, hypotonia, seizures, jaundice, galactosuria and hepatomegaly. | (Seo et al., 2019) |
| | *IKZF5* | Inherited thrombocytopenia | - | (Lentaigne et al., 2019) |
| | *NF-E2* | Inherited thrombocytopenia | - | (Luk et al., 2020) |
| Platelet production | *ACTIN1* | *ACTN1*-related thrombocytopenia | Congenital macrothrombocytopenia. Anisocytosis. Absent or mild bleeding diathesis. | (Kunishima et al., 2013) |
| | *CYCS* | CYCS-related thrombocytopenia | Normal platelet size and volume. | (Ong et al., 2017) |
| | *GNE* | *GNE* myopathy with congenital thrombocytopenia. | Rimmed vacuoles. Haematological complications are rare. Proteinuria and haematuria in some patients. Membranoproliferative glomerulonephritis. Platelets size are normal to large. | (Futterer et al., 2018, Revel-Vilk et al., 2018) |
| | *GP1BA*<br>*GPIBB*<br>*GP9* | Bernard-Soulier Syndrome (BSS)+ platelet type von-Willebrand disease (PTvWD) | Macrothrombocytopenia. Severe bleeding tendency with platelet function defect. Platelet anisocytosis. | (Othman and Emsley, 2017)<br>(Sivapalaratnam et al., 2017)<br>(Wright et al., 1993) |
| | *ITGA2B*<br>*ITGB3* | Glanzmann thrombasthenia | Impaired platelet function. | (Burk et al., 1991)<br>(Nurden et al., 2013) |

| | | | | |
|---|---|---|---|---|
| | | | | |
| | *MYH9* | *MYH9*-related disease (MYH9-RD) | Congenital macrothrombocytopaenia. Mild bleeding tendency. Development of kidney dysfunction, deafness, cataracts and Döhle-like bodies. Elevated liver enzymes. | (Balduini et al., 2011) |
| | *PRKACG* | *PRKACG*-related thrombocytopenia | Giant platelet. Impaired platelet function. | (Manchev et al., 2014) |
| | *TRPM7* | TRPM7-related thrombocytopenia | Macrothrombocytopenia. Atrial fibrillation. | (Stritt et al., 2016a) |
| | *TPM4* | Tropomyosin 4-related thrombocytopenia | Macrothrombocytopenia. All other blood cell counts are normal. Mild effect on platelet function. | (Pleines et al., 2017) |
| | *TUBB1* | *TUBB1*-related thrombocytopenia | Congenital macrothrombocytopenia. | (Kunishima et al., 2009) |
| | *WAS* | Wiskott-Aldrich syndrome, X-linked thrombocytopenia (XLT) | Mild or severe immunodeficiency, haematopoietic malignancies and eczema. Thrombocytopenia with small platelets. Autoimmune haemolytic anaemia. | (Massaad et al., 2013) |
| | *FLNA* | Filaminopathies A | X-linked dominant form of periventricular nodular heterotopia (FLNA-PVNH) and the otopalatodigital syndrome spectrum of disorders. Haemorrhage and coagulopathy. Abnormal platelet morphology. | (Nurden et al., 2011) |
| | *DIAPH1* | Macrothrombocytopenia (MTP) and hearing loss | _ | (Stritt et al., 2016b) |
| Platelet clearance/ other | *ABCG5 ABCG8* | Macrothrombocytopenia associated with Sitosterolemia. | Xanthomas and premature coronary atherosclerosis due to hypercholesterolemia. Haematologic abnormality. | (Bastida et al., 2017) (Bardawil et al., 2017) |
| | *STIM1* | Stormorken Syndrome and York platelet syndrome | Tubular myopathy and congenital miosis. Severe immune dysfunction. | (Shahrizaila et al., 2014, Markello et al., 2015) |

| | | | | |
|---|---|---|---|---|
| | *ORAI1* | Stormorken syndrome | CRAC channelopathy. Severe combined immunodeficiency, autoimmunity, muscular hypotonia, and ectodermal dysplasia. | (Lacruz and Feske) |
| | *vWF* | Von Willebrand disease type IIB | _ | (Cooney et al., 1991) |
| | *MASTL* | Autosomal dominant thrombocytopenia | _ | (Hurtado et al., 2018) |
| | *ADAMTS13* | Thrombotic thrombocytopenia purpura | Upshaw-Schulman syndrome. Anaemia. | (Levy et al., 2001) |

### 1.6.1 *SLFN14* mutations in unrelated families with a dominant form of thrombocytopenia

A novel thrombocytopenia causing gene was identified in three unrelated families, namely *SLFN14*, through the British Heart Foundation (BHF) funded UK-GAPP study (Fletcher et al., 2015). Patients harbouring *SLFN14* mutations displayed an analogous phenotype that consisted of moderate thrombocytopenia, enlarged platelets, decreased ATP secretion and a dominant inheritance pattern (Figure 1.7). Three heterozygous missense mutations were identified in affected family members and predicted to encode amino acid substitutions (K218E, K219N, V220D). Since the discovery of *SLFN14* related thrombocytopenia (SLFN14-RT), an additional mutation (p.R223W) was identified in 3 family members with an inherited thrombocytopenia (IT) (Family D, Figure 1.7) (Marconi et al., 2016) and most recently, (Saes et al., 2019) a further patient with an alternative base change at nucleotide c.657 resulting in the same K219N mutation (Family E, Figure 1.7). The R223W mutation led to reduced megakaryocyte maturation and decreased proplatelet formation in cultured megakaryocytes derived from patient peripheral blood and the proband identified by Saes et al. presented with bleeding, macrothrombocytopenia and an unspecified secretion defect, consistent with preliminary data from the GAPP study (Saes et al., 2019). All these variants apart from R223W (Variant ID: 17-33884415-G-A) were not reported in the gnomAD (genome aggregation database) highlighting their rarity amongst different populations and confinement to the published four families. All patients were recruited based on a bleeding phenotype but it is unclear at this stage if any of the mutations within *SLFN14* present a more severe platelet phenotype than others. Endogenous SLFN14 expression was reduced in platelets from all patients from the UK-GAPP cohort and mutant SLFN14 expression was decreased by approximately 65-80% compared to wild-type SLFN14 when overexpressed in transfected cells (Fletcher et al., 2018). Whole mount electron microscopy revealed a reduced number of dense granules in affected patient platelets, correlating with a decreased

ATP secretion observed in lumiaggregometry studies (Fletcher et al., 2015). These results identified *SLFN14* mutations as cause for an IT with excessive bleeding, outlining a fundamental role for *SLFN14* in platelet formation and function. Interestingly, thrombocytopenia was moderate in the patients studied, suggesting that the increased bleeding was also due to impaired platelet function thus *SLFN14* appears to regulate platelet function as well as number (Fletcher et al., 2015). All of the *SLFN14* mutations identified to date are within an ATPase-AAA-4, GTP/ATP binding region of *SLFN14* conserved between species with the exception of V220D which is semi-conserved (Figure 1.8).

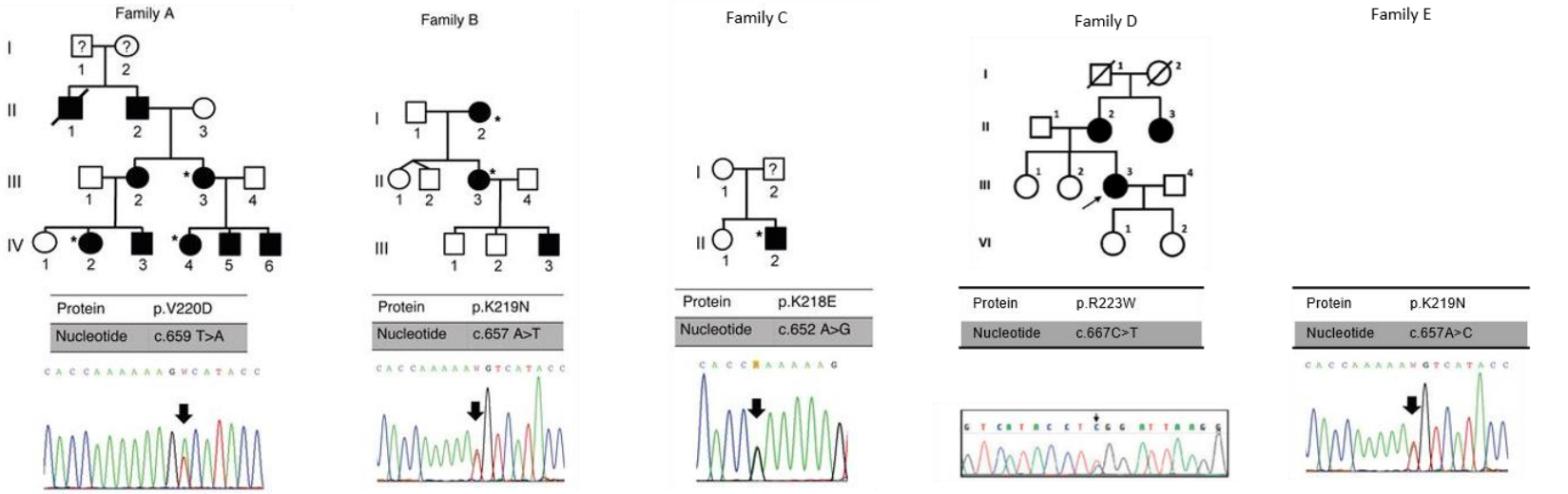


| Patient | Platelet Count ($x10^3/\mu l$) |
|---|---|
| III 2 | 140 |
| III 3 | 74 |
| IV 2 | 110 |
| IV 4 | 100 |
| IV 5 | 116 |

| Patient | Platelet Count ($x10^3/\mu l$) |
|---|---|
| I 2 | 83 |
| II 3 | 68 |

| Patient | Platelet Count ($x10^3/\mu l$) |
|---|---|
| II 2 | 89 |

| Patient | Platelet Count ($x10^3/\mu l$) |
|---|---|
| II 1 | 87 |
| II 2 | 91 |
| III 3 | 79 |

| Patient | Platelet Count ($x10^3/\mu l$) |
|---|---|
| I 1 | Not reported |

**Figure 1.7: SLFN14 mutations identified in 5 unrelated families with inherited thrombocytopenia and bleeding.** Figure adapted using pedigree and Sanger sequencing traces. (Fletcher et al., 2015, Marconi et al., 2016, Saes et al., 2019). Affected family members are shown by shaded symbols, * in families A, B and C used in GAPP phenotyping assays and arrow in family D by Marconi et al. No familial information for family E was available by Saes et al.

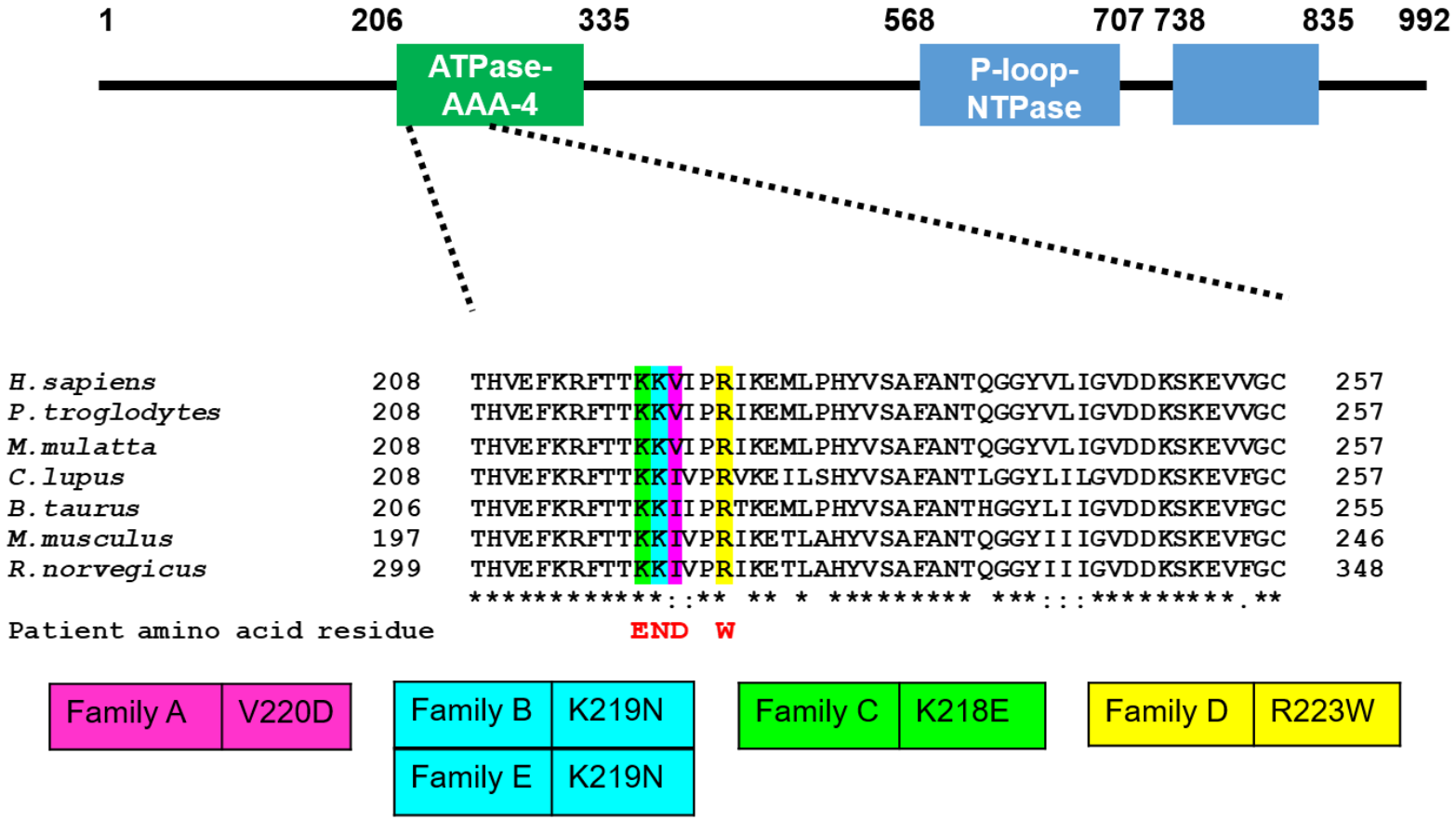


**Figure 1.8: *SLFN14* mutations are conserved between species with the exception of V220D.** Figure adapted from Fletcher et al to show all 5 unrelated familial mutations in *SLFN14* conserved between species (Fletcher et al., 2015, Marconi et al., 2016, Saes et al., 2019)

## 1.7 The *SLFN* family of genes and proteins

After the identification of *SLFN14*, its structure and cellular function was studied in more detail. The *SLFN* family of genes were initially discovered in mice by Schwarz et al., involved early in the T cell lineage, regulating differentiation, maturation and in some instances ablating growth (Schwarz et al., 1998). Overexpression of *SLFN1* resulted in cell cycle arrest at the G0/G1 phase and as such was named “Schlafen” translated from German as “to sleep” (Schwarz et al., 1998). Subsequent studies classified the *SLFNs* into three distinct subgroups based on size and domain homology (Kaiser et al., 2004, Neumann et al., 2008). 10 mouse and 6 human *SLFN* genes have been identified to date involved in viral replication and translational control (Seong et al., 2017, Yang et al., 2018, Liu et al., 2018, Mavrommatis et al., 2013). All 10 mouse *SLFN* genes possess a core region containing a unique “slfn box” with an unknown function. Subgroups II and III contain an extra domain conserved by a region flanked by the five amino acid signature (Ser-Trp-Ala-Asp-Leu) ‘SWADL’ appearing to be *SLFN* specific. This was discovered in early characterisation of the *SLFN* family whereby *SLFNs* 3 and 4 possessed an additional 200 amino acid sequence not found in subgroup I (Schwarz et al., 1998). Adjacent to this is the C-terminal ‘ATPases associated with diverse cellular activities’ (AAA) domain. Based on protein homology, the AAA motif is thought to function similarly to classical AAA domains in ATP/GTP binding in DNA and RNA metabolism (Hanson and Whiteheart, 2005, Lupas and Martin, 2002). Another protein was discovered with significant similarity to those in subgroup II, extending C-terminal a further 400 amino acids. When aligned, the first 570 amino acids were homologous to *SLFNs* 3 and 4 while the remainder was unique to *SLFN8* leading to the classification of the final *SLFN* subgroup, III (Kaiser et al., 2004). Additional homologous genes to *SLFN8* were identified as *SLFN5, SLFN9, SLFN10* and *SLFN14*, whereby the last two coding exons are confined to this final subgroup. NCBI conserved domain database (CDD) searches revealed significant homology to motifs typical of superfamily I of RNA/DNA helicases which are known to mediate DNA and RNA metabolism (Kaiser et al., 2004). Based on length and homology, *SLFN14* belongs to subgroup III (Figure 1.9) (Stapley et al.,

2020). It is currently unclear the exact roles these SLFNs play in health and disease and more specifically the physiological roles of the members in each subgroup. Subgroup structure is consistent between humans and mice as identified in early studies by Kaiser et al. however it is unclear at this stage if SLFNs between species have the same endoribunucleolytic active site. SLFN5 and SLFN14 are the only two subgroup III SLFNs shared between humans and mice (Puck et al., 2015). In both species, subgroup III SLFNs localise within the nucleus whereas subgroups I and II reside in the cytoplasm (Neumann et al., 2008). This reveals potential reasons for subgroup III SLFNs to have a direct impact on protein translation in cell differentiation and proliferation. Additionally, multiple SLFNs with the same structure and function may act in a compensatory fashion whereby some SLFNs may be functionally redundant or in the case of mutant forms, one or more other SLFNs may be able to take over its role in transcriptional control.

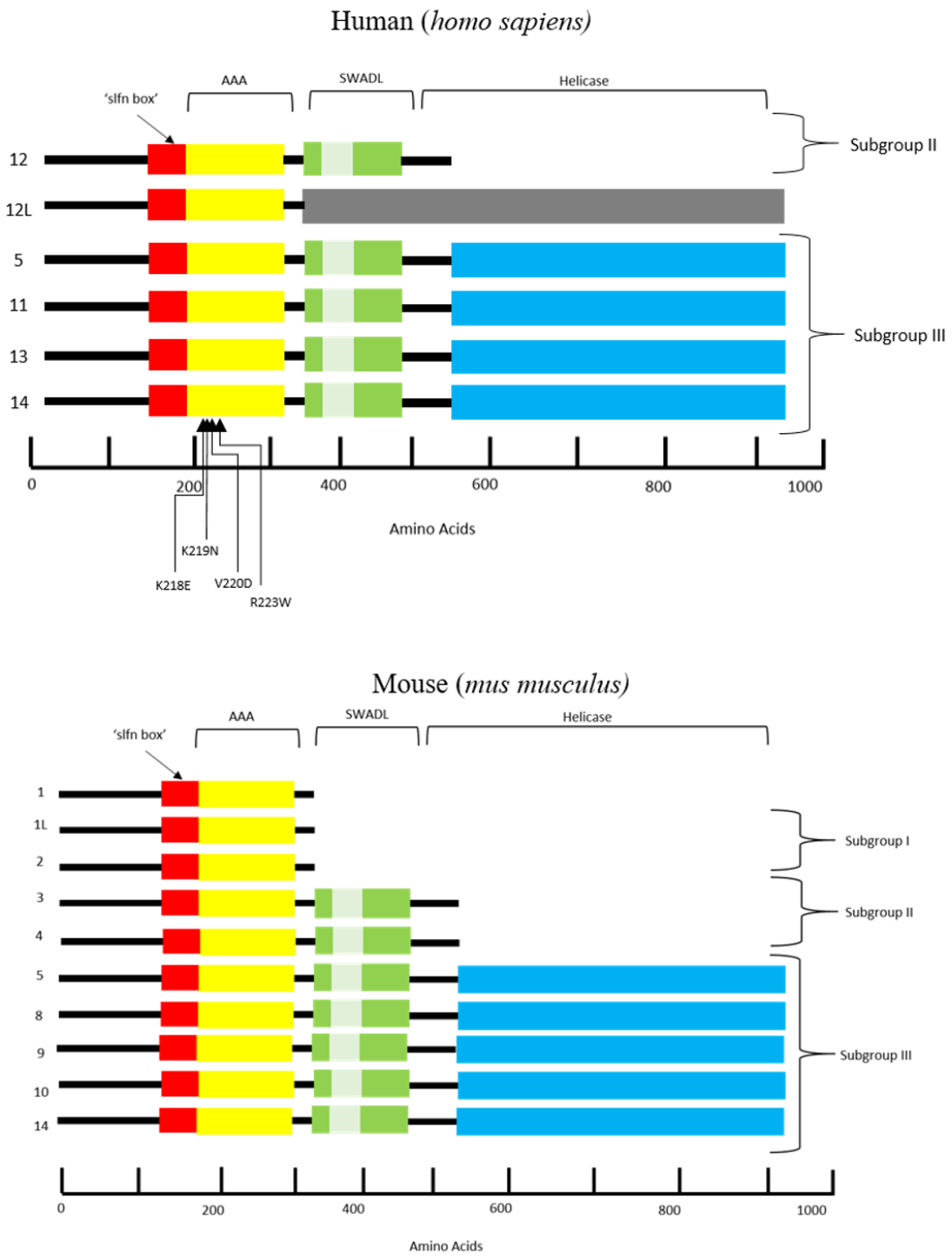


**Figure 1.9: SLFN family of genes highlighting domains and regions in both *Homo sapiens* and *Mus musculus*.** 'slfn' box is unique to *SLFN* proteins and function remains unknown. The AAA domain is responsible for DNA and RNA metabolism and in humans is the region of mutations associated with thrombocytopenia and bleeding. SWADL region, believed to be *SLFN* specific, is a sequence flanked by SWA and DL amino acids. Helicase regions at the C-terminal end of the protein are known to mediate DNA and RNA metabolism. (Stapley et al., 2020).

### 1.7.1 *SLFN14* is a ribosome-associated endoribonuclease

Very little is known about the SLFN protein family, especially SLFN14, and the mechanism through which *SLFN14* mutations might cause thrombocytopenia and bleeding. The single nucleotide variants in *SLFN14* identified within the patients are predicted to result in substitutions within the highly conserved ATPase-AAA-4 domain of SLFN14 species (Figure 1.8). SLFN14 also contains a C-terminus with homology to superfamily I of DNA/RNA helicases (Schwarz et al., 1998, Geserick et al., 2004). Recent evidence suggests shorter SLFN14 isoforms are bound to ribosomes and function as an endoribonuclease, regulating rRNA and ribosome-associated mRNA cleavage and translational control (Pisareva et al., 2015). While the longer SLFN14 isoform is found to localise to the nucleus and lack endoribonuclease activity, yet its function is still unknown (Pisareva et al., 2015). SLFN14 has a direct orthologue in mice with approximately 70% shared protein sequence homology. Studies by Rowley et al. show high levels of *SLFN14* mRNA in murine platelets suggesting that SLFN14 may play a role in murine MK and platelet development or function and platelets may indeed translate their own SLFN14 protein maintaining overall function (Rowley et al., 2012). In patients where platelet SLFN14 expression is reduced, this may contribute to their reduced platelet count and function although the mechanism for this remains to be explored.

In reticulocytes, SLFN14 is strongly overexpressed tethered to ribosomes, and appears to be one of the major ribosome-associated proteins (Pisareva et al., 2015). SLFN14 binds to ribosomes and ribosomal subunits in the low part of the body and cleaves RNA but preferentially rRNA and ribosome-associated mRNA (Fletcher et al., 2018). Importantly, only a few endoribonucleases participating in ribosome-mediated processes are characterised to date, and none of them are shown to be directly associated with the ribosome. Consistently, in megakaryocyte-like cell lines (Dami cells), SLFN14 wild-type and thrombocytopenia-related mutants co-localise with ribosomes and reveal endoribonucleolytic activity resulting in reduced rRNA staining (Fletcher et al., 2018). In addition, SLFN14 is shown to cleave

RNA at the ribosomal unit and in HEK293T cells, each SLFN14 mutant displayed rRNA/tRNA/mRNA degradation by the presence of rRNA fragments. Notably, the mechanisms of mRNA and ribosomal decay in platelets are not known nor is it clear if SLFN14 cleaves any RNA it encounters during translation or more specific RNAs involved in haematopoiesis. It is well-known that the turnover of rRNA/tRNA/mRNA plays an important role in translation control and regulating gene expression (Tomecki and Dziembowski, 2010). As such compared to SLFN14 wild-types, expression of K218E mutants is dramatically reduced as a result of post-translational degradation due to partial misfolding of the protein (Fletcher et al., 2018).

### 1.7.2 The physiological role of endoribonucleases

mRNA turnover is a means of controlling cellular transcription by degrading RNA which occurs by two main processes in most, if not all eukaryotic mRNAs. The first is termed mRNA surveillance, which involves shortening of the mRNA to an oligo which is no longer capable of binding to Pab1p, the major binding protein for transcription in eukaryotes (Dunckley and Parker, 2001). The second process involves direct cleavage within the body of the mRNA catalysed by sequence-specific endoribonucleases (Dunckley and Parker, 2001). This sequence specificity means endoribonucleases can target RNAs which are involved in cell differentiation processes and lead to the development of disease. This has previouslty been explored by Mattijssen et al, 2010 in the context of autoimmune disorders (Mattijssen et al., 2010).

Endoribonucleases mediate ribosomal clearance and ribosomal, messenger and mitochondrial RNA turnover however, mutant variants of ribosome-related proteins, such as SLFN14, may cause errors in both ribosome homeostasis and subsequent haematopoietic lineage dysfunction (Ricciardi et al., 2015, Narla and Ebert, 2010, Seong et al., 2017). Given the structural similarity of *SLFN13* to other subgroup III genes (such as *SLFN14*) and the recent report on SLFN13's role as an endoribonuclease it seems plausible to hypothesise

that *SLFN14* may be impacting haematopoietic differentiation and more specifically platelet synthesis in humans by acting as an endoribonuclease, inhibiting translation and preventing complete protein synthesis within the haematopoietic lineage (Yang et al., 2018). Taking into account ribosomal association and RNA degradation activities of SLFN14, it may contribute to the expression of genes or transcription factors directly involved in haematopoietic programming.

## 1.8 Research hypothesis and aims

Based on previous findings, it was hypothesised that SLFN14 is a key regulator in haematopoiesis and platelet function and as such, mutations within *SLFN14* may impact differentiation and function of platelets.

This hypothesis lead to the development of the following research aims:

1. To develop a viable mouse model with homologous *SLFN14* mutation to patients (K219N in patients and K208N in mice). (Chapter 3)

2. To investigate the role of *SLFN14*-K208N in platelet function using *in vitro* and *in vivo* platelet function assays. (Chapter 4)

3. To investigate the role of *SLFN14*-K208N and in haematopoiesis with particular focus on the myeloid lineage of platelet and erythrocyte differentiation. (Chapter 5)

4. To develop a viable *SLFN14* platelet specific knockout mouse using the PF4Cre loxP system (*SLFN14 PF4Cre*) to investigate the involvement of *SLFN14* specifically in megakaryopoiesis and platelet function. (Chapter 6)

# Chapter 2

## Materials and Methods

# Chapter 2 – Materials and Methods

## 2.1 Materials

All antibodies and platelet agonists are listed in Table 2.1 and Table 2.2.

### 2.1.1 Mice

Targeting strategies for the generation of all genetically modified mice is detailed in the corresponding results chapters. In short, a *SLFN14*-K208N point mutation mouse was generated using in house CRISPR-Cas9 gene editing to induce the G>T mutation observed in K219N patients. MK and platelet specific *SLFN14* knockout mice (*SLFN14-PF4Cre*) were generated using the Cre-LoxP system published by Tiedt et al. whereby a floxed *SLFN14* allele was generated and bred with PF4Cre mice leading to MK/platelet specific deletion of exons 2 and 3 in *SLFN14*. All mice were generated on a C57BL/6J background. Animal care and welfare was controlled in accordance with Home Office regulations and the use of Animals in Scientific Procedures Act 1986 (ASPA 1986) under PPLs P53D52513 and Pp3749922. Animals were housed at the Biomedical Services Unit at the University of Birmingham.

**Table 2.1: Table of antibodies**

| Antibody | Host species, conjugate, catalogue number | Manufacturer | Dilution |
|---|---|---|---|
| CD41 (αIIb) – mouse | Rat, APC, 133913 | Biolegend | FCC 1:200<br>FC 1:100 |
| Ter119 – mouse | Rat IgG2b, FITC, 116205 | Biolegend | FCC & FC 1:100 |
| Ter119 - mouse | Rat IgG2b, APC e-780, 15371660 | eBioscience | FC 1:100 |
| CLEC2 - mouse | Rat, FITC, 17D9MCA5700F | Bio-Rad Laboratories | FC 1:100 |
| CD42a (GpIb) – mouse | Rat, FITC, M040-1 | Emfret Analytics | FC 1:100 |
| CD49b (α2) – mouse | Rat, FITC, M071-1 | Emfret Analytics | FC 1:100 |
| CD41/CD61 (integrin αIIbβ3) – mouse | Rat, FITC, M025-1 | Emfret Analytics | FC 1:100 |
| GPVI – mouse | Rat, FITC, M011-1 | Emfret Analytics | FC 1:100 |
| CD62P (P-selectin) – mouse | Rat, FITC, M130-1 | Emfret Analytics | FC 1:100 |
| CD41/CD61 activated (JON/A) – mouse | Rat, PE, M023-2 | Emfret Analytics | FC 1:100 |
| CD42c (GPIbβ) – mouse | Rat, DyLight488, X488 | Emfret Analytics | IV 0.1µg/g |
| CD71 (transferrin receptor) – mouse | Rat, PE, 553267 | BD Biosciences | FC 1:100 |
| CD41 (αIIb) – mouse | Rat, AlexaFluor®488, 133907 | Biolegend | CM 1:100 |
| CD71 (transferrin receptor) – mouse | Rat, AlexaFluor®647, 563504 | BD Biosciences | CM 1:100 |
| Ter119 – mouse | Rat, , AlexaFluor®488, 116215 | Biolegend | CM 1:100 |
| CD45 – mouse | Rat, APC e-780, 47-0451-82 | ThermoFisher | FC 1:100 |
| CD45 – mouse | Rat, APC, 17-0451-82 | ThermoFisher | FC 1:100 |
| CD45 – mouse | Rat, FITC, 11-0451-85 | ThermoFisher | FC 1:100 |
| CD45 – mouse | Rat, PE, 12-0451-82 | ThermoFisher | FC 1:100 |
| **Isotype controls** | | | |
| IgG | Rat, FITC, P190-1 | Emfret Analytics | FC 1:100 |
| IgG2a | Rat, PE, 400507 | Biolegend | FC 1:100 |
| IgG1 | Rat, APC, 400411 | Biolegend | FC 1:100 |
| IgG2b | Rat, FITC, MCA6006F | Bio-Rad Laboratories | FC 1:100 |
| IgG2b | Rat, APC e-780, 15321650 | eBioscience | FC 1:100 |

FCC, flow cytometry counting; FC, flow cytometry; IV, *In vivo* labelling; CM, confocal microscopy; b/w, body weight

**Table 2.2: Table of platelet agonists**

| Agonist | Receptor interaction | Manufacturer, catalogue number |
|---|---|---|
| ADP | P2Y1, P2Y12 | Sigma, A2754 |
| Collagen | GPVI, αIIbβ3 | Takeda, 1130630 |
| CRP (collagen related peptide) | GPVI | Provided by Prof. Farndale; cross-linked in-house |
| Fibrinogen | αIIbβ3 | Enzyme research, FIB3 |
| PAR4-peptide | PAR4 | Alta biosciences |
| Thrombin | PAR1, PAR4 (PAR3 and PAR4 in mice) | Sigma, T4648 |
| U46619 | TP (thromboxane $A_2$) | Sigma, D8174 |
| Rhodocytin | CLEC-2 | Isolated as previously described. (Shin and Morita, 1998). |

## 2.2 Molecular Biology

Genotyping of *SLFN14-PF4Cre* mice was determined by polymerase chain reaction (PCR) and *SLFN14*-K208N mice by PCR and subsequent Sanger sequencing. All primers are shown in Table 2.3. Due to the COVID-19 pandemic, from March 2020, ear clips from *SLFN14*-K208N mice were sent to Transnetyx®, TN US for automated genotyping.

### 2.2.1 DNA Extraction

Ear clips from 3 week old mice prior to weaning were provided by the Biomedical Services Unit (BMSU) and DNA was extracted as per the Qiagen DNeasy Blood and Tissue extraction kit (Qiagen, UK, #69504). DNA was subsequently stored at -20°C for short term and then moved to -80°C for long term storage.

### 2.2.2 PCR: genotyping *SLFN14-PF4Cre* knock-out mouse

PCR was performed for detection of the floxed (fl) and wildtype (WT) allele. A separate PCR reaction was used to detect Cre deleter expression. Primers were purchased from Sigma-Aldrich® and run on Bio-Rad DNA Engine Tetrad® Peltier Thermal Cycler (Table 2.4).

### 2.2.3 PCR: genotyping *SLFN14*-K208N knock-in mouse

PCR was performed with primers purchased from Sigma-Aldrich® using same equipment as and protocol in Table 2.5.

**Table 2.3: PCR and Sanger sequencing primers**

| Gene Target | Forward primer | Reverse primer |
|---|---|---|
| *SLFN14*$^{fl}$ | GGCTCAGTTGGTAGCTAGAG | CAGACATGACCTCATGGAAC |
| PF4Cre | CCCATACAGCACACCTTTTG | TGCACAGTCAGCAGGTT |
| *SLFN14*-K208N | GATATTAAGATGTGTGCCTTGG | GTTTTTAGTGAGTCGGGGTTCAC |

**Table 2.4: PCR protocols for SLFN14$^{fl}$ and *PF4Cre*; mixtures and cycling conditions**

| ***SLFN14*$^{fl}$ PCR: Per reaction (11µl)** | ***PF4Cre* PCR: Per reaction (11µl)** |
|---|---|
| 5µl NEB LongAmp® *Taq* 2X Mater Mix | 5µl Sigma-Aldrich® REDTaq® Ready Mix$^{TM}$ |
| 0.5µl (10µM) forward primer | 0.5µl (10µM) forward primer |
| 0.5µl (10µM) reverse primer | 0.5µl (10µM) reverse primer |
| 3µl dd$H_20$ | 3µl dd$H_20$ |
| 2µl DNA (neat) | 2µl DNA (neat) |
| (+2µl 6X Loading dye post PCR #N0550S) | |
| 95°C for 2 minutes | |
| 95°C for 30 seconds | |
| 56°C for 1 minute x34 cycles | |
| 68°C for 4 minutes | |
| 72°C for 3 minutes | |
| Incubate at 4°C | |
| Product sizes – flox 2120bp WT 2086bp | Product sizes - + 200bp; - no band |

**Table 2.5: PCR protocols for *SLFN14*-K208N*;* mixtures and cycling conditions**

| ***SLFN1*-K208N PCR: Per reaction (25µl)** | |
|---|---|
| 12.5µl Sigma-Aldrich® REDTaq® Ready Mix™ | |
| 0.5µl (10µM) forward primer | |
| 0.5µl (10µM) reverse primer | |
| 9.5µl $ddH_20$ | |
| 2µl DNA (neat) | |
| 94°C for 3 minutes | |
| 94° for 1 minute | x30 cycles |
| 60°C for 1 minute | |
| 72°C for 1 minute | |
| 72°C for 5 minutes | |
| Incubate at 4°C | |
| Fragment size: 263bp for Sanger sequencing | |

### 2.2.4 Agarose gel electrophoresis

*SLFN14*-K208N PCR products were visualised using gel electrophoresis. A 1% agarose gel made with TAE buffer was stained with Safe View dye (1µl per 15ml gel) and PCR products were run at 100V for 25 minutes. *SLFN14-PF4Cre* PCR products were loaded on a 1.5% gel with 2µl 6X loading dye and run at 60V for 1 hour to ensure clear separation of similar sized bands. All gels were loaded with 5µl NEB Quick-Load® purple 1Kb plus DNA ladder. Gels were imaged using ultraviolet trans-illuminator (Syngene, Gene Genius Bio Imaging System) and Genesnap software (version 6.03.00) for visualisation of PCR bands.

## 2.3 Sanger Sequencing of PCR products

### 2.3.1 Post PCR purification

2.4µl of PCR product was added to a 96 well plate and an equal volume of microCLEAN (Microzone Ltd) solution added to each well using the Eppendorf Multipette Stream®. The plate was spun at 1900 G for 40 minutes using the Hettich® Universal 320R plate centrifuge to pellet the PCR product and then upside down onto tissue at 30 G for 30 seconds to remove supernatant. Purified PCR pellets were then ready for Sanger sequencing PCR.

### 2.3.2 Sequencing PCR

After purification, concentrated PCR pellets were amplified for Sanger sequencing using a final concentration of 4pmol of the original primers in combination with the BigDye® Terminator v3.1 cycle sequencing kit from ThermoFisher UK. After a brief vortex and pulse centrifuge, the PCR mix below was run as per conditions in Table 2.6.

**Table 2.6: PCR protocols for *SLFN14*-K208N Sanger sequencing; mixture and cycling conditions**

| ***SLFN14*-K208N Sanger sequencing PCR: Per reaction (10µl)** | |
|---|---|
| 0.5µl BigDye® Ready Reaction Mix | |
| 2µl BigDye® Terminator 5x Sequencing Buffer | |
| 0.4µl (10µM) forward or reverse primer | |
| 7.1µl $dH_20$ | |
| 96°C for 30 seconds | |
| 50°C for 15 seconds | x30 cycles |
| 60°C for 4 minutes | |
| Incubate at 4°C | |

### 2.3.3 Post-Sequencing PCR purification

Sequencing reactions were purified by adding 2µl 0.125M EDTA to each well with 30µl 100% ethanol. The plate was centrifuged for 20 minutes at 500 G and then upside down for 30 seconds at 30 G to remove supernatant. 90µl of freshly prepared 70% ethanol was added to each well, spun for 10 minutes at 500 G, upside down for 30 seconds at 30 G and then repeated for a second time. After this, pellets were left to air dry for 5 minutes before preparing samples for the sequencer.

### 2.3.4 Preparation of samples for ABI 3730XL Sequencer

10µl Hi-Di™ Formamide from Applied Biosystems™ was added to each well and mixed to resuspend pellet. DNA was denatured for 2 minutes at 94°C on the Tetrad® and immediately snap-chilled on ice to prevent re-annealing of single stranded DNA.

### 2.3.5 Sequencing Analysis

The plate was sequenced using Applied Biosystems™ 3730XL Automated Sequencer which uses capillary electrophoresis for separation of DNA fragments. Data was uploaded to the University of Birmingham sequencing directory and sequences were analysed with Chromas Version 2.4 software against reference *SLFN14* sequences downloaded from ensembl cDNA sequence database (Ensembl, 2018). Any samples with high background or suspected contamination were repeated using the same protocol.

## 2.4 Haematological analysis

### 2.4.1 Blood collection by exsanguination

Mice were selected based on genotype and age; all mice used were aged 8-16 weeks (adult) and sex matched. Litter matched controls were used for comparison in all experiments and genotype abbreviations are given in each relevant chapter. Exsanguination took place in the BMSU under terminal anaesthesia by inhalation of isoflurane/$O_2$ (5%) gas. Blood was drawn from the inferior vena cava (IVC) using a 25 gauge needle into 10% acid citrate dextrose

(ACD). Following collection, blood was inverted in an Eppendorf gently to mix and prevent coagulation.

### 2.4.2 Automated blood counting

An automated HORIBA Medical Pentra ES 60 blood counter was used to count whole blood in *SLFN14* indel and *SLFN14-PF4Cre* colonies. 65µl of whole blood mixed with ACD anticoagulant was used. Data was adjusted to correct for anticoagulant dilution.

### 2.4.3 Histological analysis

Whole blood was taken from exsanguinated mice into EDTA anticoagulant and peripheral whole blood smears were prepared using a laboratory standardised protocol and stained with ThermoFisher Shandon™ Kwick Diff™ stain kit (ThermoFisher, UK, #9990700).

Spleens and femurs were collected from sex and age matched mice exsanguinated schedule 1 culled. Spleen length and weight were measured. Spleens were stored in formalin solution 10% neutral buffered with 4% paraformaldehyde (PFA) for histological sectioning. Spleens and decalcified bones were embedded in paraffin wax, sectioned at 5µm, mounted onto microscope slides and stained with Haematoxylin and Eosin (H&E). After staining, slides were scanned using light microscopy on the Zeiss Axio ScanZ1 slide scanner (Carl Zeiss Ltd, Cambridge, UK).

## 2.5 Flow Cytometry

### 2.5.1 *SLFN14-* K208N mouse platelet and erythrocyte counts

For each mouse 5µl of well mixed whole blood was taken into a 5ml FACS tube. 45µl of antibody mix composed of PBS, CD41 APC and Ter119 FITC was added (Table 2.1). The staining solution was left to incubate in the dark for 15 minutes (1:10 dilution) followed by the addition of 2950µl of PBS pipette mixed 6 times (1:60 dilution). 50µl of this was transferred into a new 5ml FACS tube and made up to 1000µl (1:20 dilution). Overall this resulted in a dilution factor of 12,000 which was identified as the optimum dilution eliminating coincidence

events with red blood cells and platelets in the flow cytometer. All samples were individually gently pipette mixed 6 times prior to measurement ensuring sample homogeneity. The Accuri™ C6 flow cytometer (BD, UK) measured 30µl of sample at slow flow rate and threshold set to 35,000 to exclude debris. Gates were set for platelet and red blood cell populations indicated by a positive staining shift from an unstained control. The number of cells were calculated using the value of events in 30µl and correcting by the overall dilution factor. Size was quantified by forward scatter area histograms (Mean-FSC-A) (Masters and Harrison, 2014).

### 2.5.2 Platelet glycoprotein surface expression

For each mouse 25µl of well mixed whole blood was added to 225ul PBS (1:10 dilution) and stained with CD41 by adding 1µl into an Eppendorf. 25µl of stained blood for each mouse was then aliquoted across 7 wells in a 96 well flat bottom plate. Major platelet glycoprotein antibodies (Isotype control CLEC-2, CLEC-2, GP1Bα, α2, αIIbβ3, GPVI and FITC control) were diluted as per Table 2.1 and 25µl of this mix was added to one well for each sample. The plate was left to incubate in the dark for 15 minutes then 100µl PBS was added to each well, mixing with a pipette to end the reaction. 5000 events in the CD41 positive channel were measured and sample mean fluorescence intensity (MFI) was calculated.

### 2.5.3 Immature platelet fraction (IPF) in whole blood using SYTO13 nucleic acid dye

Mice were anaesthetised and terminally bled from the IVC into 100µl ACD anticoagulant as before. 3µl SYTO13 dye, 5µl whole blood, CD41 (αIIbβ3) antibody at a final concentration of 1:400 and PBS were left to incubate at room temperature for 20 minutes in the dark. 200µl 1% PFA was added and samplers run on an Accuri™ C6 flow cytometer (BD.UK). CD41 positive cells were selected and the percentage of this population also positive for SYTO13 in the FL1 channel was recorded as the immature platelet fraction. Gates were set based on a SYTO13 negative control.

### 2.5.4 Integrin activation and platelet degranulation by flow cytometry

Whole blood was collected as in 2.4.1 and labelled with APC conjugated CD41. CD41 stained platelets were activated using agonists from Table 2.2 diluted in PBS. FITC conjugated P-selectin and PE conjugated JON/A (directly binding to only the activated from of integrin αIIbβ3) were used to measure degranulated and activated platelets by flow cytometry. 10,000 platelet events (CD41 single positive) were collected and percentage of double positive JON/A and P-Selectin events analysed.

## 2.6 Platelet preparation

### 2.6.1 Preparation of washed mouse platelets

Mice were bled under terminal anaesthesia from the IVC by isoflurane/$O_2$ (5%) and collected into a 1ml syringe containing 100µl ACD. Following collection, Tyrode's-HEPES buffer was warmed in 37°C and 200µl of this was added to each Eppendorf containing the blood and ACD mixture before spinning in a MicroCentaur for 5 minutes at 45 G. The supernatant containing plasma and around one third of the red blood cells (~700µl) was pipetted into a new labelled Eppendorf using cut tips (to avoid shear stress and unintended platelet activation). These were centrifuged using the Thermo-Scientific™ Heraeus™ swinging bucket Megafuge™ 16R (Loughborough UK) for 6 minutes at 200 G. Platelet rich plasma (PRP) and buffy coat were then placed into another new labelled Eppendorf and 200µl of Tyrode's-HEPES buffer was added to the original tube containing red blood cells. This was spun for a second time to maximise number of platelets from whole blood and pooled with the original plasma. Tyrode's-HEPES buffer was added to achieve total volume of 1ml PRP and 1µl $PGI_2$ (prostacyclin) at 10µg/ml (to prevent platelet activation) was added and gently inverted to mix. Eppendorfs were centrifuged at high speed for 6 minutes at 1000 G to form a platelet pellet. Supernatant was aspirated and the platelet resuspended in Tyrode's-HEPES buffer before diluting to the desired concentration.

### 2.6.2 Counting mouse washed platelets

5µl of washed platelet pellet suspension was added to 10ml COULTER®ISOTON®II diluent and gently mixed. Platelets were counted three times using the Z$^{TM}$2 Series COULTER COUNTER® (Beckman Coulter®) and an average calculated. Platelets were diluted to 2x10$^{8}$/ml for light transmission aggregometry (LTA), 2x10$^{7}$/ml for platelet spreading and 4x10$^{8}$/ml for biochemical assays with Tyrodes-HEPES buffer. All suspensions were left to rest for 30 minutes prior to further experimentation.

## 2.7 Platelet Functional Assays

### 2.7.1 Platelet Aggregation Assay

LTA was performed using the Chrono-Log Lumi-Dual aggregometer and measured against a control sample of Tyrodes-HEPES solution containing no platelets. Aggregations were performed on the same day as exsanguination using 300µl washed platelets per test at a concentration of 2x10$^{8}$/ml. Samples were pre-warmed to 37°C for 60 seconds in glass cuvettes and then under stirring conditions (1200 rotations per minute) for a further 60 seconds before addition of an agonist. Aggregation was monitored for a further 6 minutes after agonist addition. Agonists and their concentrations are highlighted in Table 2.2. Aggregation curves were scanned and control traces overlaid with test samples. Percentage aggregation was also quantified. In *SLFN14-PF4Cre* mice, area under the curve (AUC) was calculated using the AGGROLINK8 software. Representative traces were generated from individual data points collated into an Ascii file using Microsoft Excel and exporting these into GraphPad Prism.

### 2.7.2 Platelet Secretion Assay

Dense granule release was measured by detecting ATP at the same time as aggregation. Chrono-lume (diluted 1:300) was used to measure platelet ATP release in each channel in

response to platelet agonist addition. AUC was calculated using the AGGROLINK8 software. 2 nmol ATP standard was used to calibrate Chrono-lume at the start of each experiment.

### 2.7.3 Platelet Spreading

13mm round glass coverslips were washed with 100% ethanol, rinsed with PBS and placed in a 24 well cell culture plate. 300µl of 100µg/ml fibrinogen in PBS and 10µg/ml collagen in collagen diluent was added to the top of the coverslip and left to incubate overnight at 4°C. Coverslips were then blocked with 300µl 5mg/ml denatured fatty acid free BSA in PBS for 1 hour at room temperature. $2x10^7$/ml resting washed platelets were allowed to spread on coated coverslips for 45 minutes at 37°C. Some washed platelets were pre-activated with an addition of final concentration 0.1U/ml thrombin and allowed to spread on fibrinogen under the same incubation conditions. Platelets were aspirated and coverslips washed once with PBS to remove non-adhered cells. 10% formalin was added to each well to fix cells for 10 minutes and then washed 3 times with PBS. Platelets on the coverslips were incubated with 50mM $NH_4Cl$ for 10 minutes to quench residual formalin and washed 3 times with PBS. Cells were permeabilised with 0.1% TritonX-100 in PBS for 5 minutes, washed with PBS and incubated in immunofluorescence blocking buffer (1% BSA and 2% goat serum in PBS). Filamentous actin (F-actin) was stained with Alexa488-conjugated phalloidin diluted in blocking buffer for 1 hour at room temperature in the dark. All coverslips were mounted onto microscope slides using Hydromount, covered and stored at 4°C. Images were captured on a Zeiss Epifluorescence microscope with 63X objective and blinded for analysis of the following parameters: adhered platelets, platelet surface area and platelet perimeter using KNIME high-throughput platelet spreading analysis software (Khan et al., 2020).

### 2.7.4 *Ex vivo* flow adhesion assay

Coverslips were coated with micro spots of Horm collagen, human collagen type III and fibrinogen. Blood was collected as above into 5U/ml heparin (diluted in saline) in the presence of 40µM PPACK to inhibit thrombin generation. Whole blood was flowed over the

micro spots for 3.5 minutes at either 1700/s or 1000/s. Brightfield images were captured and immediately after perfusion, thrombi were stained with FITC conjugated P-selectin, PE conjugated JON/A and Aexa-647 conjugated annexin V for PS exposure. Images were blinded and analysed for differences in thrombi surface area coverage, P-selectin expression, JON/A activation, PS exposure and thrombus morphological scoring in FIJI. These experiments were conducted by Natalie Jooss in collaboration with Johan Heemskerk of Maastricht University, Netherlands.

### 2.7.5 Clot retraction

Blood was collected from wild type and heterozygous mice as previously described. Whole blood was spun at 200g for 8 minutes in the presence of 10µg/ml $PGI_2$ (final concentration). The PRP layer was removed into a new Eppendorf and adjusted to a final concentration of $2x10^8$/ml with PPP obtained from the same whole blood (spun at 1000g for 10 minutes). It is often necessary to sacrifice extra wild type mice for PPP to dilute platelets. Tyrodes-HEPES buffer was supplemented with 2mM $CaCl_2$ and 175µl added to a cuvette along with 50µl PRP at $2x10^8$/ml, 5µl erythrocytes for colour (obtained from high speed PPP isolation step) and 20µl thrombin at a final concentration of 1U/ml to stimulate clot formation. An unbent paperclip was added to each cuvette with the loop at the base of the cuvette for the clot to adhere. Clots were allowed to form over the course of 2 hours, visual observations were recorded and a photo taken every 30 minutes. At the end of the time course the clot and paperclip were weighed and solution volume remaining in the cuvette was measured to calculate clot volume as a percentage of the original starting volume.

## 2.8 *In vivo* Platelet Function Assays

### 2.8.1 Tail bleeding Haemostasis Assay

Mice were weighed to ensure they were within the correct weight boundary (20-29g) then anaesthetised under isofluorane/$O_2$ (5%) on a 37°C heat mat to maintain consistent body

temperature. Isoflurane/$O_2$ was reduced to approximately 3% after transferring the mouse to the heat mat to avoid gasping and regulate breathing rate (this was assessed on an individual basis). 2-3mm of tail tip (to ensure cut was made through both lateral tail veins and accounting for tail thickness differences between mice) was excised using a sterilised razor blade and submerged into 50ml 37°C prewarmed saline. Time until first cessation of bleeding or up to 20 minutes was recorded in seconds. Erythrocytes were lysed in 1ml $dH_20$ and stored at -20°C for haemoglobin absorbance assay.

### 2.8.2 Haemoglobin Assay

Two mice of each genotype were bled and known volumes of red blood cells were lysed to generate standard curves for absorbance. Absorbance from 50µl lysed erythrocytes per test sample was measured at wavelengths 550nm and 575nm in a flat bottom 96 well plate in a microplate reader. Samples were assessed in duplicate.

### 2.8.3 *In vivo* Thrombosis – Laser Injury

Mice were anaesthetised and cremaster muscle arterioles were exposed. Mice were injected with Dylight488-conjugated anti-GPIbβ antibody (0.1µg/g body weight x488). Thrombus formation in the arterioles was induced by laser injury and accumulation of platelets (green) at the site was observed. Brightfield and fluorescence images were acquired to show thrombus size and platelet contribution.

### 2.8.4 *In vivo* Thrombosis – Ferric Chloride ($FeCl_3$)

Mice were anaesthetised and injected with the same antibody as above. The carotid artery of each mouse was exposed and subjected to 10% ferric chloride for 3 minutes to induce thrombus formation. $FeCl_3$ acts by damaging the vascular wall and subsequently endothelium which in turn generates reactive oxygen species, activating platelets and erythrocytes to accumulate at the site of injury. Time to vessel occlusion was assessed through fluorescence and brightfield imaging.

## 2.9 *Ex vivo* bone marrow and organ analysis

### 2.9.1 Immunohistochemistry

Femurs, tibias and spleens were collected from terminally anaesthetised mice as described in 2.3.1. Spleen connective tissue removed and length and weight was measured. All flesh was removed from femurs and tibias and ends cut to expose bone marrow. All tissues were fixed in 3.7% paraformaldehyde. Following decalcification of the bones, tissues were embedded in paraffin and sectioned at 5µm thickness. Samples were mounted on glass microscope slides and subsequently stained with haematoxylin and eosin and reticulin stain Spleen sections were additionally stained with Perl's Prussian blue stain for free iron content (Advanced Histopathology Laboratory, London, UK). All slides were imaged using a Zeiss Axio ScanZ1 light microscope.

### 2.9.2 Haematopoietic stem cell progenitor detection by flow cytometry – Bone Marrow

Mouse femurs and tibias were cleaned of flesh and bone marrow drawn out by centrifugation for 10 seconds at high speed into FACS buffer (1% FBS and 2mM EDTA in PBS). Cell suspensions were gently pipette mixed and spun at 500 G for 4 minutes. Supernatant was removed, pellet suspended in fresh ice cold FACS buffer and filtered through a 70µm cell strainer to remove cell debris. The cell suspension was then divided into separate Eppendorf's for each test (200µl per test) and antibodies added at their respective concentrations (Table 2.1). Cells were left to incubate at 4°C in the dark for 20 minutes. 100µl 1% PFA was added, incubated for 10 minutes and spun 3 times at 200 G removing supernatant and resuspending in ice cold FACS buffer between each centrifugation step. After this wash step, 200µl of the cell suspension was added to a 96 well flat bottom plate and 50,000 events were collected at a fast aperture rate. Live, single cells were gated and progenitor levels detected by relevant staining patterns.

### 2.9.3 Haematopoietic stem cell progenitor detection by flow cytometry - Spleens

Mouse spleens were cleaned of connective tissue and homogenised using the end of a 5ml syringe in FACS buffer (1% FBS and 2mM EDTA in PBS). Cell suspensions were gently pipette mixed and spun at 500 G for 4 minutes. Supernatant was removed, pellet suspended in fresh ice cold FACS buffer and filtered through a 70µm cell strainer to remove cell debris. The cell suspension was then divided into separate Eppendorf's for each test (200µl per test) and antibodies added at their respective concentrations (Table 2.1). Cells were left to incubate at 4°C in the dark for 20 minutes. 100µl 1% PFA was added, incubated for 10 minutes and spun 3 times at 200 G removing supernatant and suspending in ice cold FACS buffer between each centrifugation step. After this wash step, 200µl of the cell suspension was added to a 96 well flat bottom plate and 50,000 events were collected at a fast aperture rate determined by the BD Accuri system. Live, single cells were gated and progenitor levels detected by relevant staining patterns.

### 2.9.4 Fluorescent Activated Cell Sorting (FACS) of Haematopoietic Progenitor Cells

Bone marrow was prepared as in section 2.9.2. 500µl of bone marrow suspension was stained with FITC conjugated CD42b, PE conjugated CD71, APC conjugated CD41, APC-Cy7 conjugated Ter119 and incubated for 20 minutes at 4°C in the dark. 200µl of bone marrow was used for single stained and unstained controls and in addition, a PE fluorescence minus one (FMO) sample was prepared using the CD45 antibodies in Table 2.1 for colour compensation. After incubation, 100µl 1% PFA was added, incubated for 10 minutes and spun once at 1000 G for 5 minutes. The stained bone marrow pellet was then resuspended in 1.5ml FACS buffer without EDTA along with 5µl 7-AAD cell viability stain 10 minutes prior to sorting. Cells were sorted using BD-FACS Aria cell sorter by the flow cytometry facility at the University of Birmingham.

## 2.10 Quantitative Real Time PCR (qRT-PCR)

### 2.10.1 RNA extraction of Haematopoietic Progenitor Cells

RNA was extracted from sorted MK, ProE and MEP cells using the Qiagen RNeasy micro kit as per manufacturer instructions. RNA was stored at -20°C until required.

### 2.10.2 qRT-PCR of bone marrow RNA

*SLFN14* and *GATA1* expression were assessed in whole bone marrow RNA from *SLFN14*-K208N mice. This was to briefly investigate the effect of *SLFN14*-K208N mutation on haematopoiesis with particular interest in *GATA1* which plays an important role in proliferation and differentiation of cells in both megakaryocyte and erythroid lineages. Isolated bone marrow RNA was reverse transcribed for cDNA using the High-Capacity cDNA Reverse Transcription Kit (Life Technologies) and amplified with respective primers (Table 2.7) using SYBR-green based technology (Power SYBR-green Master Mix, Life Technologies). Quantification of gene expression was performed using the ABI Prism 7500HT sequence detection system (Applied Biosciences, Foster City, CA, USA). Relative gene expression was calculated according to the comparative GAPDH endogenous control and data presented as a percentage of wild-type gene expression.

**Table 2.7: qRT-PCR primer sequences**

| Target | Forward | Reverse |
|---|---|---|
| SLFN14 | 5’-CCTGATGACACCAGCTTTGTC-3’ | 5’-CCCTTGTTCTCACGGCATTG-3’ |
| GATA1 | 5'-CCGCAAGGCATCTGGCAAA-3' | 5'- CGGGAGGTAGAGGCAGGA-3' |
| GAPDH | 5’−GAAGGTGAAGGTCGGAGT−3’ | 5’GAAGATGGTGATGGGATTTC−3’ |

## 2.11 Statistical analysis

All statistical analyses were conducted using GraphPad Prism software v8.4 and presented as mean ± standard error of the mean (SEM) unless otherwise stated. Student t-tests and one-way ANOVA were used to determine differences between means with correction for unequal sample sizes where applicable. All significance values are reported as * $p<0.05$, ** $p< 0.01$, *** $p<0.001$, **** $p<0.0001$.

# Chapter 3

Generation of CRISPR mouse models

# Chapter 3 – Generation of CRISPR mouse models

## 3.1 Aim

The aims of this chapter were to successfully develop viable mouse models to investigate the involvement of *SLFN14* in platelets and megakaryopoiesis, and more specifically how this causes abnormal bleeding in patients. In order to address the overall research question CRISPR-Cas9 genome editing was performed, generating mouse models with homologous mutations in S*LFN14* which have been found in human patients. It was hypothesised that the K219N missense mutation, homologous to a K208N mutation in mice would phenocopy the platelet defects observed in patients.

## 3.2 Introduction

Laboratory rats have been used to study physiology, toxicology, nutrition, behaviour and immunology for over 150 years (Kawamata and Ochiya, 2010). Over 95% of animal models used are mice due to their protein homology and gross cellular similarity to humans (Vandamme, 2014).

Genetically modified animals are organisms where specific genes have been altered, added or knocked out, whereas transgenic animals are those who carry one or more foreign genes specifically introduced into the genome. These manipulations allow scientists to mimic human disease and study the mechanism for its development in further detail. Traditional gene targeting methods used isolated embryonic stem cells (ESCs) from mouse blastocysts which were re-injected into pseudo-pregnant females generating chimeric mice. When the ESCs are reintroduced into a blastocyst they contribute to the formation of all tissues creating a global chimeric mouse (Capecchi, 1989). These methods yield high success rates however are typically very time consuming to generate an established model (Gupta and Musunuru, 2014).

Expanding knowledge of the bacterial adaptive immune system has resulted in generation of gene targeting technology to interrogate mammalian gene function. The most rapidly

developing is RNA-guided endonucleases known as Cas9 from the bacterial immune system and termed ‘clustered regularly interspaced short palindromic repeats’ (CRISPR). The CRISPR array is targeted by Cas9 after it identifies a sequence denoted by the protospacer-adjacent motif (PAM). The PAM sequence highlights the desired region for Cas9 mediated double strand breaks (DSBs) (Gupta and Musunuru, 2014) (Figure 3.1). CRISPR derived RNA (crRNA) guides the Cas9 complex to the guide RNA which is formed of an 18-25 base pair sequence of interest. Cas9 cleaves chromosomal DNA upstream from the -NGG PAM sequence producing site specific DSBs. These breaks are then repaired by non-homologous end joining (NHEJ) leading to ‘indel’ mutations or homologous recombination (HR) using specific donor oligonucleotides for precise gene editing (Jin and Li, 2016, Technologies, 2012) (Figure 3.1).

Unlike other methods of genome editing (zinc finger nucleases (ZFNs) and transcription activator-like effector nucleases (TALENs)), CRISPR-Cas9 can edit small fragments of DNA and donor oligonucleotides can be used to initiate single nucleotide changes. Multiple guide RNAs can be used simultaneously in CRISPR, targeting multiple genes at once in large scale applications and due to the frequently repeating PAM sequence, the guide RNA can be re-targeted to cleave another sequence at a different site. In other instances the PAM sequence can be mutated in the donor oligonucleotide to avoid Cas9 re-cutting the DNA resulting in unwanted additional mutations. Despite the pioneering discoveries of these gene editing techniques, CRISPR-Cas9 efficiency needs to be assessed for potential off target effects. In mouse genetics, breeding strategies need to be developed in order to minimise the generational effect of this and breed out any off target mutations which are not of particular interest (Gaj et al., 2013).

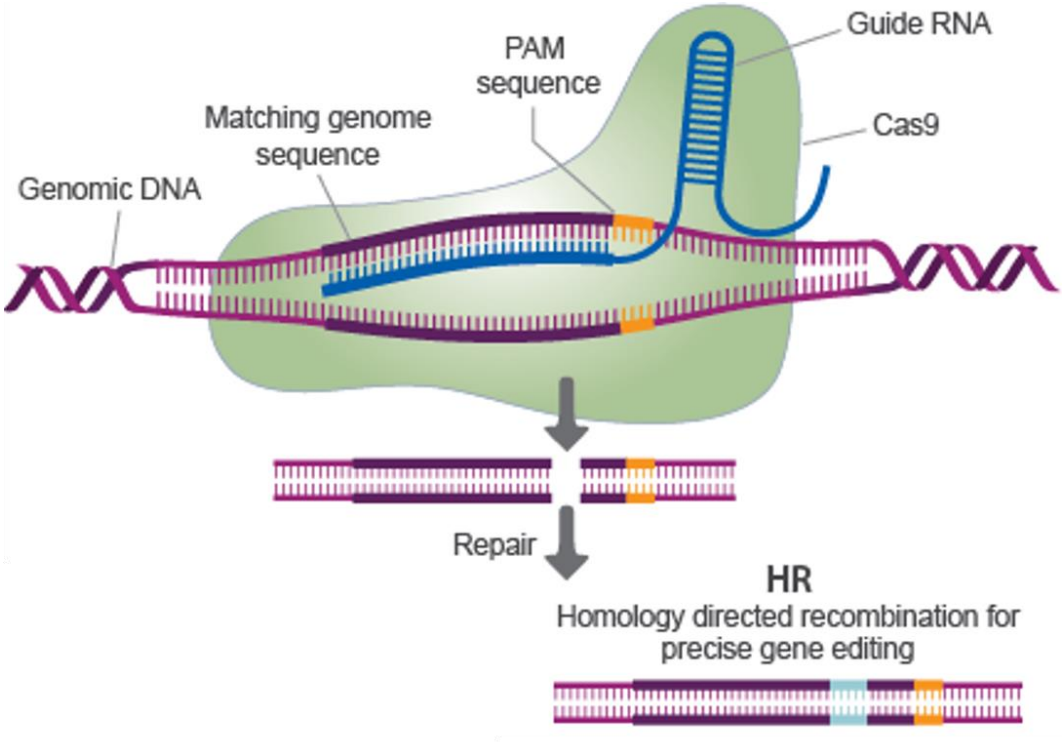


**Figure 3.1: Clustered Regulatory Interspaced Short Palindromic Repeats (CRISPR) mechanism.** Exploitation of bacterial immune system's ability to cut and insert genes to induce single nucleotide changes in the target genome. Protospacer adjacent motif (PAM) sequence highlights the desired region for Cas9 enzyme mediated double stranded breaks of genomic DNA. Guide RNA contains template sequence for homologous repair (HR) and gene editing mediated by oligonucleotide sequence. Figure adapted from Technologies, 2012.

To study megakaryopoiesis and thrombopoiesis in humans, bone marrow biopsies are required which involves a painful, invasive procedure, posing additional risks to those with bleeding tendencies. Manipulation of mouse models and *in vivo* investigation is the only viable option to uncover such critical mechanisms in platelet production. Currently, no *in vitro* methods exist to model platelets and while primary megakaryocyte cell cultures can produce platelets for small scale studies, they do not produce platelets in the same quantity or with the level of reactivity of those *in vivo* (Thon and Italiano, 2010, Strassel et al., 2018). The absence of nuclei in platelets means they cannot be cultured or genetically altered to recapitulate such mutations in *SLFN14*.

This chapter highlights the process used in order to induce the *SLFN14*-K208N mutation using CRISPR-Cas9 genome editing with donor K208N oligonucleotides. In addition to this, there were several off-target mutations generated from the CRISPR repair, producing different insertion/deletion (indel) mutations. These indel mutations are not present in *SLFN14* patients but through initial platelet phenotyping assays such as whole blood counting and aggregation, it will allow investigation into the role of SLFN14 in platelet production and function. Different length truncations of SLFN14 protein may give insight into potential functional redundancy in the AAA domain of *SLFN14* with particular emphasis on platelet function.

## 3.3 Results

### 3.3.1 Generation of a CRISPR *SLFN14*-K208N mouse model

Thus far, five families worldwide have been reported with mutations within the AAA domain of *SLFN14*. In order to investigate these specific mutations and how they are causative of thrombocytopenia and bleeding, the K208N mouse model was generated using CRISPR. CRISPR is a method used to exploit the bacterial immune system's ability to delete and insert short fragments of foreign DNA. This was discovered by Hovarth and colleagues in 2007 who described after viral challenges, bacteria can insert new 'spacers' in their genome derived from phage genomic DNA. This subsequently provides memory and future resistance against phages which aim to destroy the bacteria (Barrangou et al., 2007). Using donor oligonucleotides homologous to the patient K219N mutation previously reported (Fletcher et al., 2015) the CRISPR mechanism was used to constitutively induce the homologous single amino acid change, generating the K208N mutation in mice. Donor sequences containing the K208N mutation (c.624 G>T base change) were co-injected with a single guide RNA (sgRNA). Genomic DNA was cut by the Cas9 enzyme (often described as molecular scissors) at a specific –NGG site denoted by the sgRNA and protospacer adjacent motif (PAM) site, 3 nucleotides downstream from the 5' end of the donor sequence (Figure 3.2A). Here, the donor strand is inserted into the genome and is used as a complementary strand for homology directed repair (HDR). Free nucleotides form bonds with their complementary base on the partner strand to form repaired, double stranded DNA containing the mutation. ES cells containing the mutations were inserted into pseudo-pregnant female mice and subsequently bred with wild-type mice to produce heterozygote K208N offspring (Figure 3.2B). To ensure optimum targeting specificity, the sgRNA sequence was manufactured at optimum length and the PAM site was mutated to prevent the Cas9 enzyme re-cutting at non-specific sites minimising off-target annealing (Figure 3.2A).

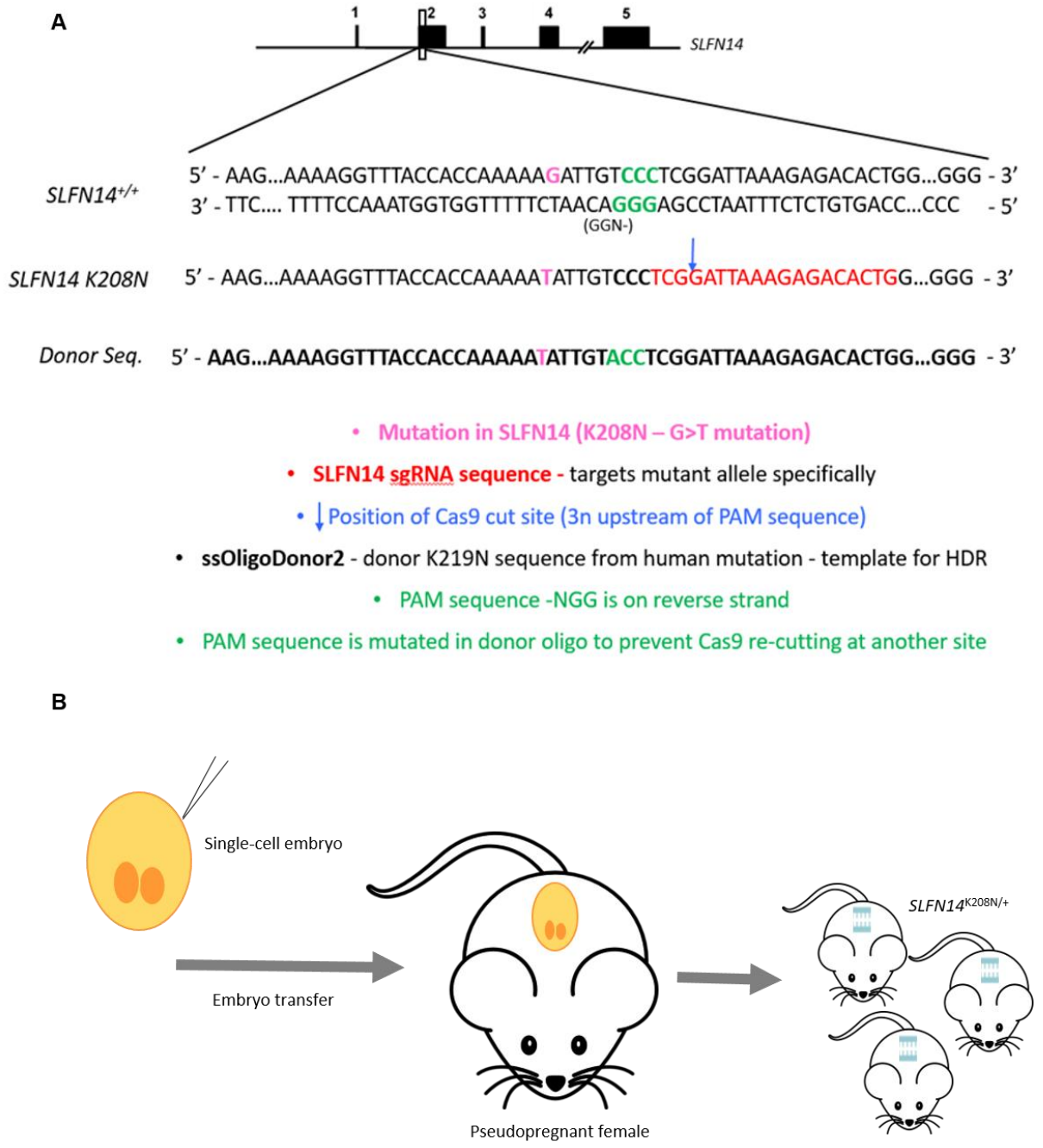


**Figure 3.2: Generation of a SLFN14-K208N mouse model using CRISPR and HDR gene editing.** (A) Oligonucleotide donor templates of K208N mutation were co-injected with single guide RNA (sgRNA) as per the CRISPR-Cas9 mechanism. Homologous repair resulted in the G>T single base change and subsequent K208N mutation. (B) ES cells which contained the mutation were inserted into pseudo pregnant female mice to produce *SLFN14*$^{K208N/+}$ offspring.

### 3.3.2 Separation of 'indel' mutations from CRISPR knock-in mechanism

The first generation of CRISPR offspring often contains indel mutations where the HR is not completely specific. This is a common problem faced by many in the field as a consequence of the CRISPR repair mechanism (Adli, 2018). As observed in the Sanger Sequencing trace, male 1 (L36 M1) possessed the successful CRISPR mutation of G>T, along with the -ACC mutated PAM site, shown by the orange and blue arrows respectively (Figure 3.3A and B). PAMs are mutated in this instance to avoid Cas9 re-cutting and inserting at additional locations. Beyond this point in the sequence, there are a series of frameshift mutations as observed by the 'messy' appearance of the Sanger sequence trace if the region of view is expanded (Figure 3.3Ci). Clonal sequencing of the single PCR product (exon 1 of SLFN14) from this individual mouse showed the various mutations which arose as a result of the HR CRISPR repair strategy (Figure 3.3Cii, iii and iv). All mutations shown are homozygous since they are clones. This mouse was used in breeding with wild-type mice generating viable offspring which were heterozygous for the K208N and 'other' mutations. As the indel mutations occurred in the same region as the desired K208N mutation (AAA domain) it was hypothesised they may reveal significant information with regards to *SLFN14* in platelet production and function.

The final three separate indel colonies generated were *SLFN14:* c.634_642del CGGATTAAA, p.Arg212Lys214del (9bpdel); *SLFN14:* c.624_625delGA, p.Lys208Asnfs*6 (delGA); *SLFN14:* c.624_627delGATT, p.Lys209Lysfs*23 (4bpdel). The predicted effect of all the CRISPR generated indel mutations on the SLFN14 protein are given in Figure 3.4. The 9bpdel was in-frame and therefore predicted to only delete three amino acids from the total protein length but in the critical AAA domain of the SLFN14 protein. Frameshift mutations delGA and 4bpdel resulted in truncation of 687 and 669 amino acids respectively with potentially most harmful effects on overall protein function. The K208N mutation did not

affect total protein length but as has been shown previously is thought to affect protein folding and overall structure (Fletcher et al., 2018) (Figure 3.4).

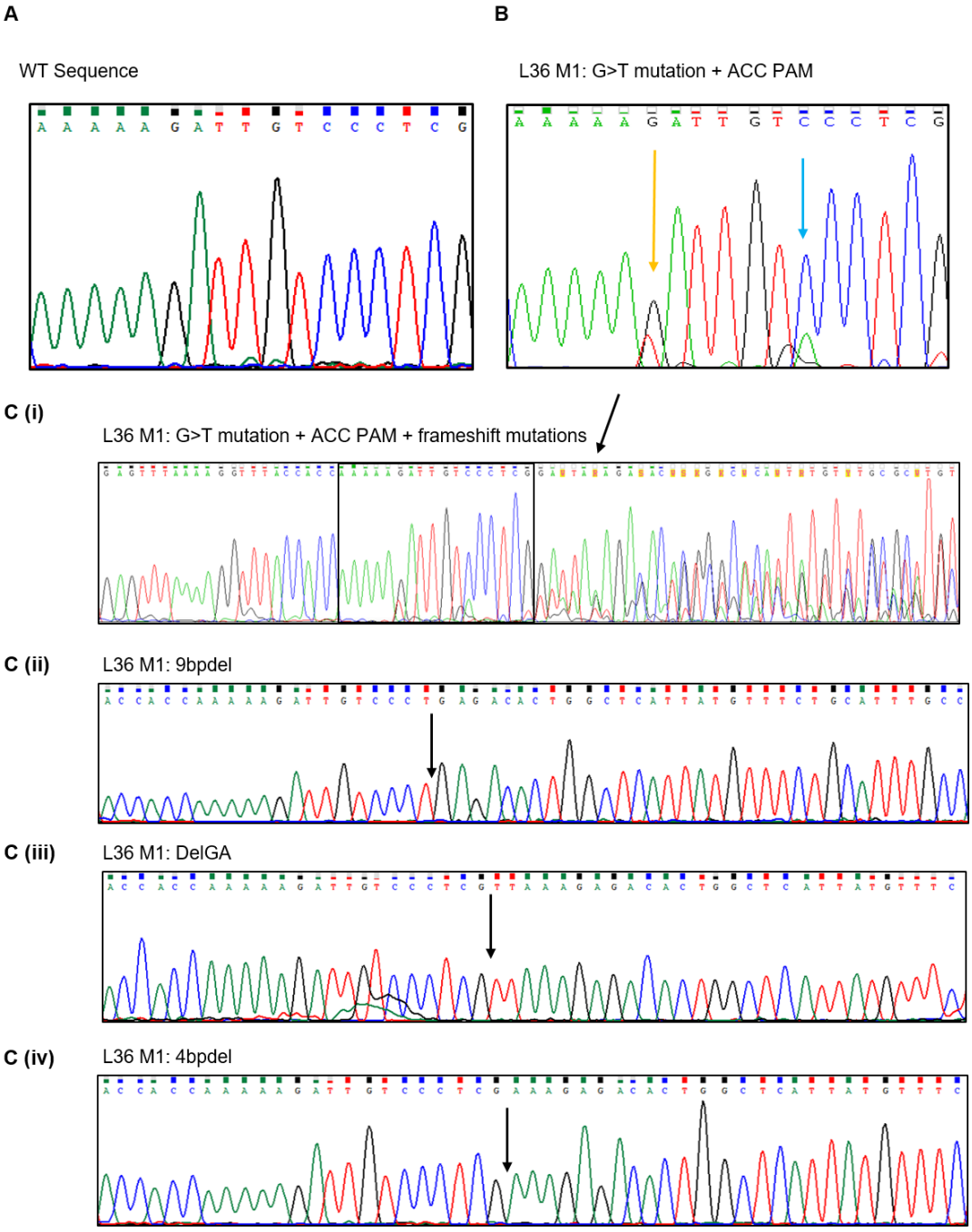


**Figure 3.3: Verification of *SLFN14-K208N* mutation by Sanger sequencing and clonal sequencing of indel colonies from CRISPR homology directed repair.** (A) SLFN14 wild-type sequence. (B) SLFN14$^{K208N/+}$ Sanger sequencing trace containing G>T substitution (orange arrow) and mutated PAM sequence (blue arrow). (C) Expanded view of Sanger sequencing trace from mouse L36 M1 containing G>T substitution, -ACC PAM sequence and frameshift mutations. (ii) Arrow denotes position of 9bp deletion. (iii) Arrow denotes position of deletion of bases GA. (iv) Arrow denotes position of 4bp deletion. All traces in (C) are representative homozygous traces arising from clonal expansion of L36 M1 PCR products and subsequent colony breeding.

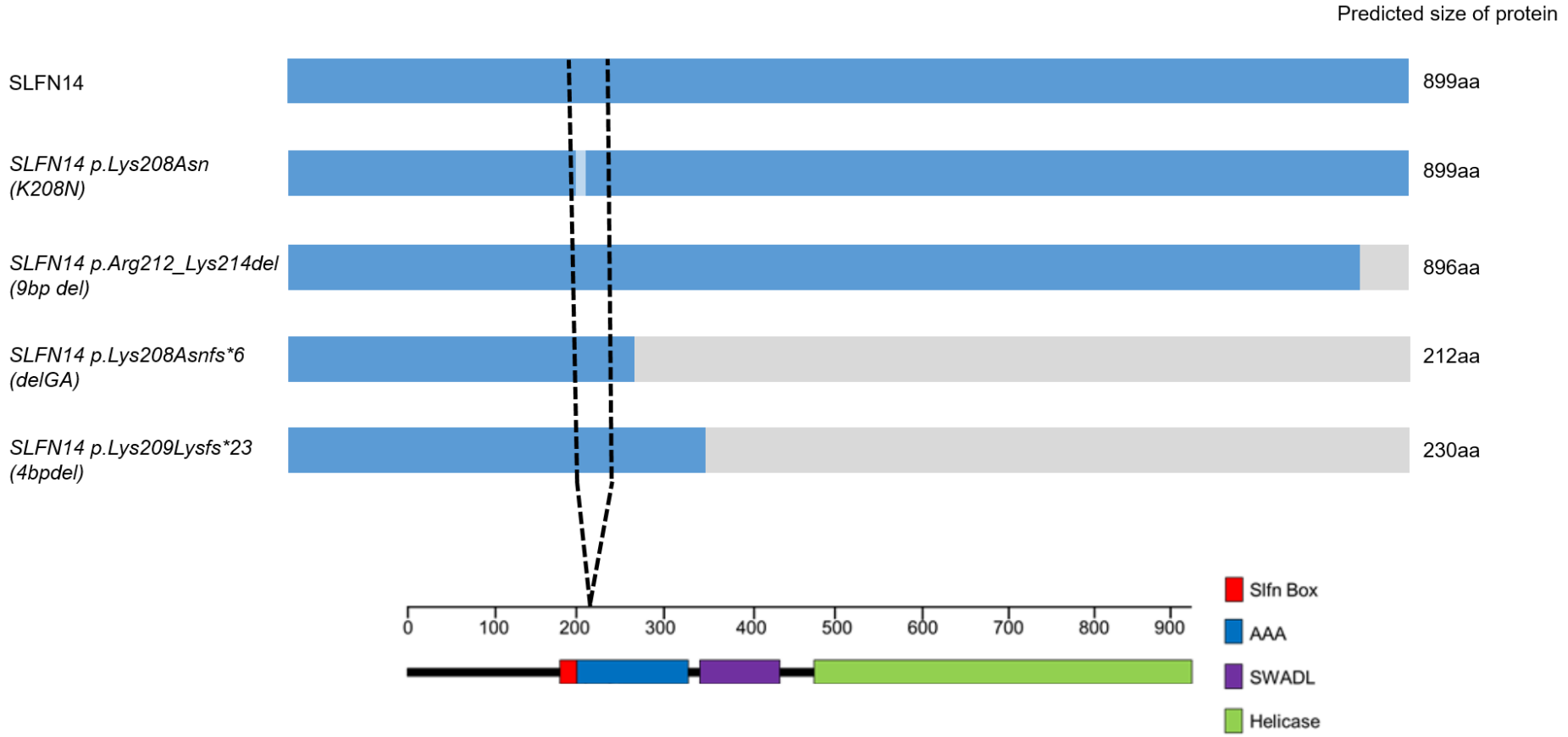


**Figure 3.4: Predicted protein effect of *SLFN14* indel mutations on SLFN14 protein transcription. ‘**slfn’ box - unique to SLFN proteins and function remains unknown. AAA domain - responsible for DNA and RNA metabolism. SWADL region - believed to be SLFN specific, region flanked by SWA and DL amino acids only present in subgroups II and III of the SLFN gene/protein family. Helicase region - C-terminal end of the protein are known to mediate DNA and RNA metabolism.

### 3.3.3 *SLFN14 9bpdel* mice displayed normal platelet counts and morphology

Automated whole blood counting was used to assess gross haematological parameters in *SLFN14 9bpdel* mice compared to littermate wild-type controls. Platelet count and size was consistent across all groups. As discrepancies in red blood cell parameters were observed in the *SLFN14*-K208N model (Chapter 4), particular attention was paid to erythrocyte count and size however, no significant differences were observed (Table 3.1).

### 3.3.4 *SLFN14 9bdel* mice display normal platelet function

To investigate platelet function in greater detail, resting glycoprotein expression was assessed in whole blood by flow cytometry. Samples were stained with CD41 APC antibody and co-stained with relevant FITC conjugated platelet antibodies. Heterozygous and homozygous *SLFN14 9bpdel* mice displayed similar levels of major platelet glycoprotein expression (Figure 3.5).

Although platelet glycoprotein receptors under resting conditions were normal, to assess overall platelet function, light transmission aggregometry (LTA) was used in washed platelets. Samples at $2x10^8$ platelets/ml were subjected to platelet agonists at different doses and aggregation was observed for a total of 6 minutes. Thrombin (acting on receptors PAR3 and PAR4 in mice), collagen (for receptors GPVI and integrin αIIbβ3) and CRP (specifically for GPVI) were used to initiate platelet aggregation. End point percentage aggregation was measured (Figure 3.6D). No differences were observed in the platelet function profiles in response to any agonists at any dose. Greater variation to thrombin at the intermediate dose (0.03U/ml) was observed although this did not affect significance (Figure 3.6Aii).

Despite the predicted removal of three amino acids from the total length of the SLFN14 protein, *SLFN14 9bpdel* did not appear to affect platelet count, size or function in these mice and therefore were not studied further.

**Table 3.1: Gross haematological analysis of *SLFN14 9bpdel* mice.** Significance measured by two-way ANOVA with Tukey's correction for multiple comparisons. Data presented is from n=6-30 mice per genotype, mean ± SD. ns, not significant.

| Blood Parameter | *SLFN14*$^{+/+}$ | *SLFN14*$^{9bpdel/+}$ | *SLFN14*$^{9bpdel/9bpdel}$ | Significance |
|---|---|---|---|---|
| Platelet count ($10^3$/µl) | 766.52 ± 87.78 | 788.08 ± 84.06 | 783.55 ± 92.63 | ns |
| Mean platelet volume (µm$^3$) | 5.01 ± 0.12 | 4.94 ± 0.10 | 5.14 ± 0.21 | ns |
| Plateletcrit (%) | 0.33 ± 0.05 | 0.34 ± 0.05 | 0.36 ± 0.04 | ns |
| Red blood cell count ($10^6$/µl) | 8.64 ± 0.38 | 9.22 ± 0.80 | 8.35 ± 0.44 | ns |
| Haemoglobin concentration (g/dl) | 13.03 ± 1.01 | 13.32 ± 1.03 | 12.50 ± 1.12 | ns |
| Haematocrit (%) | 38.07 ± 1.38 | 39.01 ± 3.09 | 36.03 ± 3.03 | ns |
| Red blood cell distribution width (%) | 13.33 ± 0.98 | 12.83 ± 0.71 | 13.40 ± 0.76 | ns |
| Mean corpuscular volume (µm$^3$) | 51.00 ± 1.63 | 50.37 ± 1.59 | 49.50 ± 1.38 | ns |
| Mean corpuscular haemoglobin (pg) | 17.46 ± 2.03 | 14.48 ± 2.18 | 14.97 ± 1.31 | ns |
| White blood cell count ($10^3$/µl) | 5.46 ± 1.86 | 8.25 ± 2.88 | 7.18 ± 3.96 | ns |
| - Lymphocyte (%) | 72.20 ± 5.17 | 74.83 ± 11.00 | 77.08 ± 11.52 | ns |
| - Monocyte (%) | 9.46 ± 2.33 | 7.87 ± 3.14 | 7.28 ± 2.92 | ns |
| - Neutrophil (%) | 17.05 ± 4.00 | 14.86 ± 5.81 | 15.15 ± 9.76 | ns |
| - Eosinophil (%) | 0.24 ± 0.36 | 0.44 ± 1.15 | 0.25 ± 0.52 | ns |
| - Basophil (%) | 0.26 ± 0.13 | 0.24 ± 0.09 | 0.23 ± 0.10 | ns |

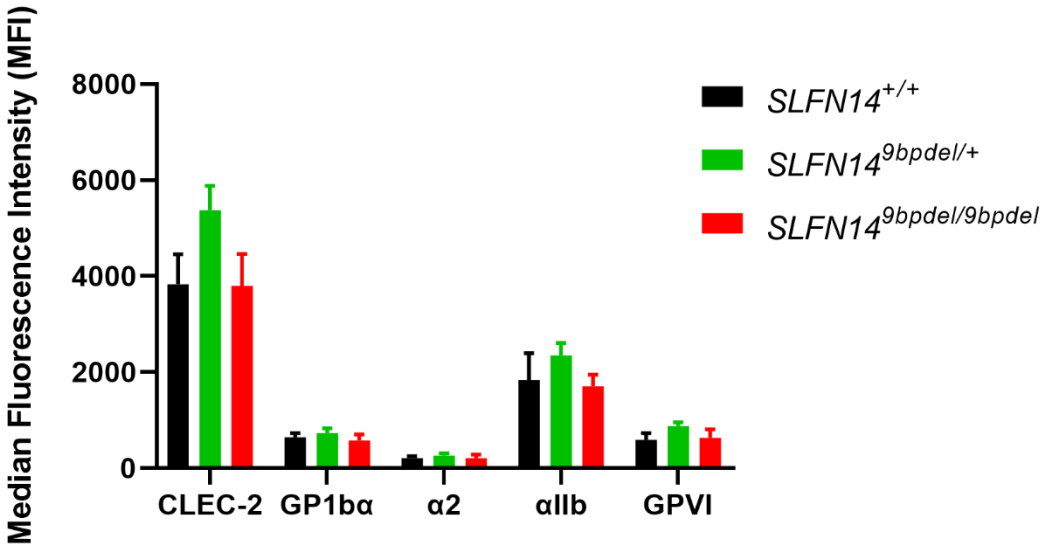


**Figure 3.5: Platelet glycoprotein expression in whole blood under resting conditions is normal.** Major platelet glycoproteins are expressed at normal levels in *SLFN14 9bpdel* mice compared to littermate controls. Data is from n=4-13 mice per genotype, mean ± SEM, two-way ANOVA with Tukey's correction for multiple comparisons.

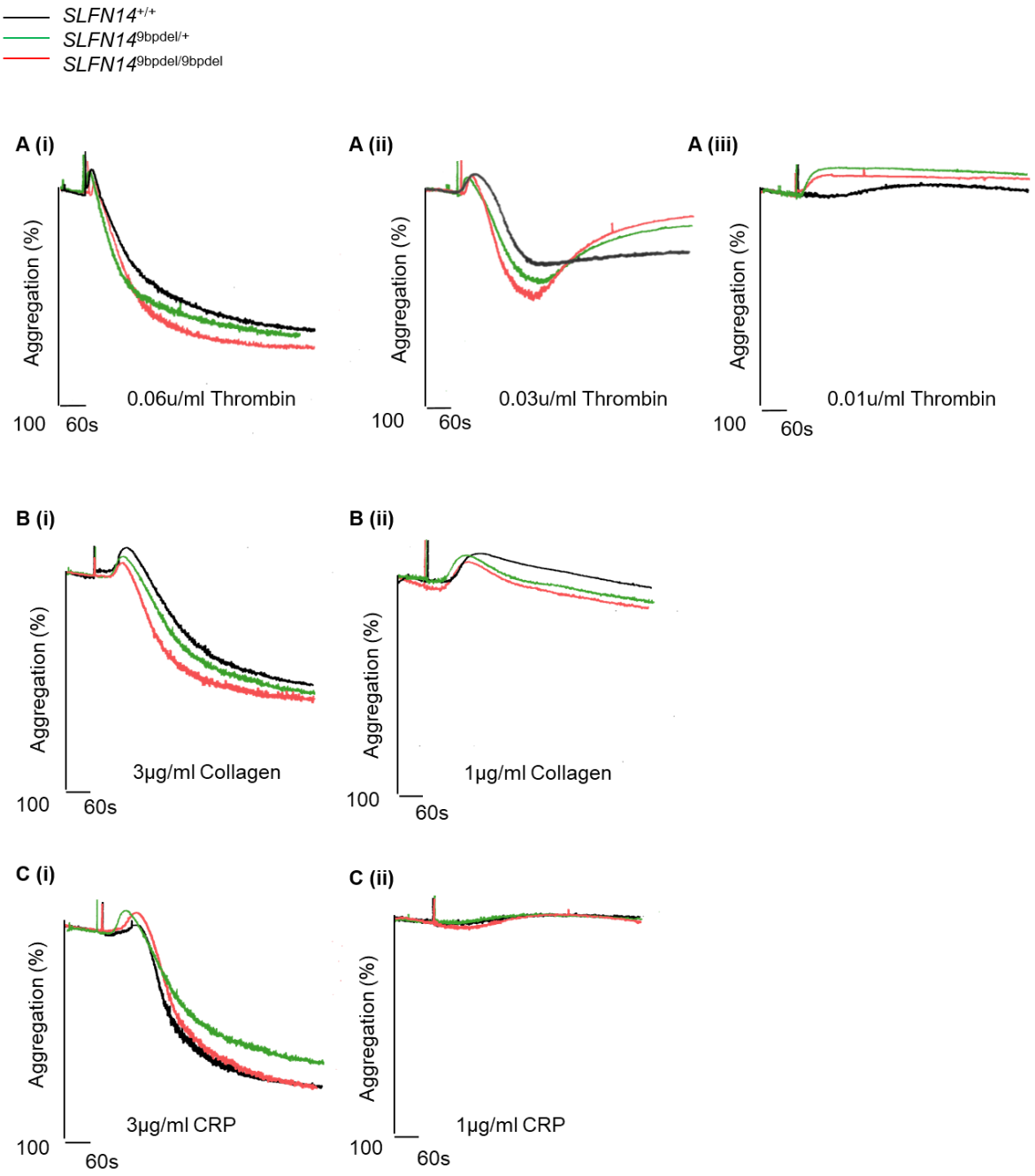
SLFN14+/+
SLFN149bpdel/+
SLFN149bpdel/9bpdel
A (i)
Aggregation (%)
0.06u/ml Thrombin
100
60s
A (ii)
Aggregation (%)
0.03u/ml Thrombin
100
60s
A (iii)
Aggregation (%)
0.01u/ml Thrombin
100
60s
B (i)
Aggregation (%)
3µg/ml Collagen
100
60s
B (ii)
Aggregation (%)
1µg/ml Collagen
100
60s
C (i)
Aggregation (%)
3µg/ml CRP
100
60s
C (ii)
Aggregation (%)
1µg/ml CRP
100
60s

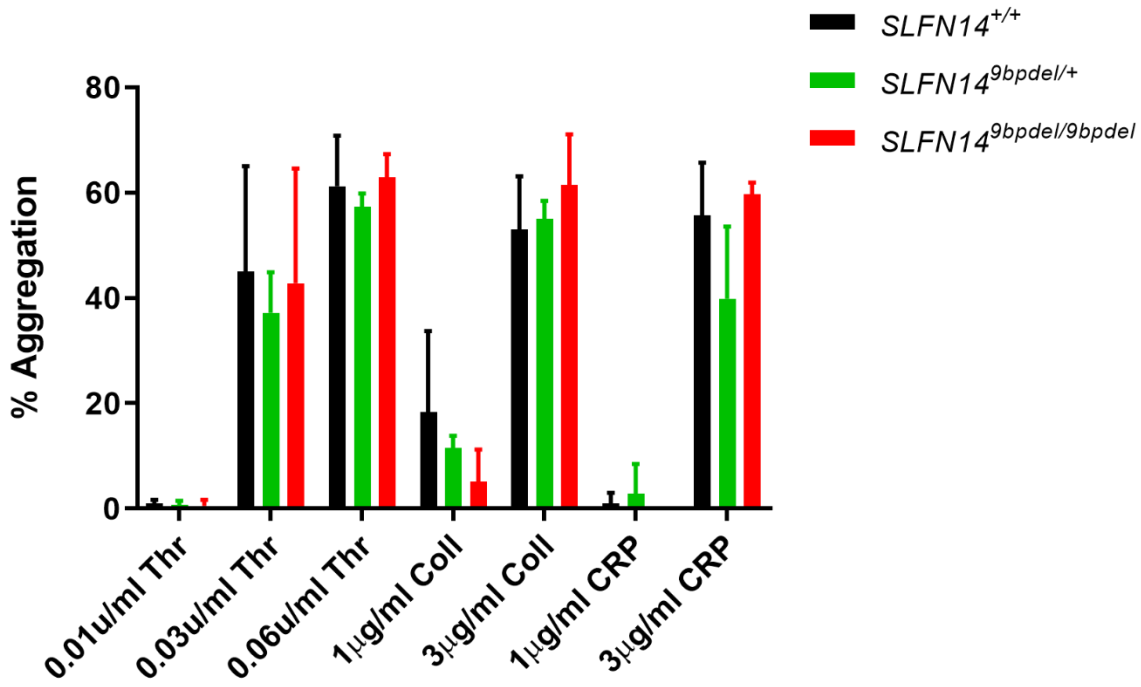


**Figure 3.6: Platelet function in SLFN14 9bpdel mice is normal.** (A, B and C) Platelet function assessed by LTA in washed platelets under stirring conditions showed normal responses to agonists thrombin, collagen and CRP at varying doses. (D) Summary of final percentage aggregation. Data is from n=3-5 mice per genotype mean ± SEM two-way ANOVA with correction for multiple comparisons.

### 3.3.5 *SLFN14 delGA* mice displayed slight increased platelet count

Deletion of 'GA' of the *SLFN14* sequence resulted in a frameshift mutation as shown by Sanger sequencing traces in Figure 3.3. Whole blood counting in homozygous and heterozygous *SLFN14 delGA* mice was used to assess differences in blood cell parameters with particular focus on platelet count and size. *SLFN14*$^{delGA/+}$ and *SLFN14*$^{delGA/delGA}$ mice displayed a mild thrombocythaemia compared to littermate controls ($p<0.0001$) while MPV remained consistent between all groups (Table 3.2). All other blood cell parameters remained unchanged. Reasons behind this increase in platelet count at this stage were unclear.

### 3.3.6 *SLFN14 delGA* mice display normal platelet function

Platelet glycoprotein markers were measured in whole blood (stained with CD41 APC to identify platelet population) and in both genotypes no differences in the expression level was observed. In heterozygotes there was a slightly increased MFI of CLEC-2 and αIIb however this did not reach significance (Figure 3.7).

To investigate platelet function LTA was used. Thrombin, collagen and CRP were used at various doses each to measure platelet function *in vitro.* Over the 6 minute time course, at high doses of all agonists (0.06U/ml thrombin, 3µg/ml collagen and 3µg/ml CRP) both *SLFN14*$^{delGA/+}$ and *SLFN14*$^{delGA/delGA}$ platelets reached maximum aggregation alongside *SLFN14*$^{+/+}$ controls (Figure 3.8Ai, Bi and Ci). Following this, a reduced dose (0.03U/ml thrombin, 1µg/ml collagen and 1µg/ml CRP) showed platelets did not aggregate (Figure 3.8Aii, Bii and Cii). *SLFN14 delGA* platelets mirrored controls in terms of platelet function and no defect, to any agonist or dose tested was observed (Figure 3.8D).

The increase in platelet count did not appear to affect overall platelet function and it remains unclear why this increase in homozygotes was observed. The range between genotypes was consistent across the three groups so this deviation was concluded to be sample variation and although statistically significant, this was not physiologically relevant in the

assays tested. Under all conditions both heterozygote and homozygote platelets mirrored their controls and the delGA mutation did not appear to play a role in thrombocytopenia or defective platelet function.

**Table 3.2: Gross haematological analysis of *SLFN14 delGA* mice.** Significance measured by two-way ANOVA with Tukey's correction for multiple comparisons. Data presented is from n=9-13 mice per genotype, mean ± SD. ns, not significant, **** p<0.0001.

| Blood Parameter | *SLFN14*$^{+/+}$ | *SLFN14*$^{delGA/+}$ | *SLFN14*$^{delGA/delGA}$ | Significance |
|---|---|---|---|---|
| Platelet count ($10^3$/µl) | 723.17 ± 116.00 | 787.16 ± 92.13 | 867.28 ± 87.98 | **** |
| Mean platelet volume (µm$^3$) | 5.00 ± 0.14 | 5.12 ± 0.18 | 5.15 ± 0.16 | ns |
| Plateletcrit (%) | 0.35 ± 0.11 | 0.34 ± 0.04 | 0.38 ± 0.07 | ns |
| Red blood cell count ($10^6$/µl) | 9.08 ± 0.37 | 9.37 ± 0.34 | 8.96 ± 0.40 | ns |
| Haemoglobin concentration (g/dl) | 12.72 ± 0.39 | 13.00 ± 0.66 | 12.54 ± 0.66 | ns |
| Haematocrit (%) | 40.29 ± 2.02 | 39.74 ± 2.41 | 37.35 ± 5.79 | ns |
| Red blood cell distribution width (%) | 12.81 ± 0.60 | 12.84 ± 0.84 | 13.89 ± 0.89 | ns |
| Mean corpuscular volume (µm$^3$) | 50.50 ± 2.17 | 49.78 ± 1.72 | 49.46 ± 1.81 | ns |
| Mean corpuscular haemoglobin (pg) | 16.01 ± 0.72 | 16.24 ± 1.09 | 17.08 ± 3.56 | ns |
| White blood cell count ($10^3$/µl) | 11.24 ± 7.72 | 8.98 ± 4.03 | 8.40 ± 4.21 | ns |
| - Lymphocyte (%) | 77.07 ± 4.66 | 77.91 ± 3.18 | 79.28 ± 4.09 | ns |
| - Monocyte (%) | 9.18 ± 3.12 | 8.30 ± 1.89 | 7.49 ± 2.81 | ns |
| - Neutrophil (%) | 13.46 ± 2.69 | 13.36 ± 1.80 | 12.9 ± 3.40 | ns |
| - Eosinophil (%) | 0.12 ± 0.19 | 0.23 ± 0.24 | 0.56 ± 1.55 | ns |
| - Basophil (%) | 0.17 ± 0.16 | 0.21 ± 0.15 | 0.16 ± 0.11 | ns |

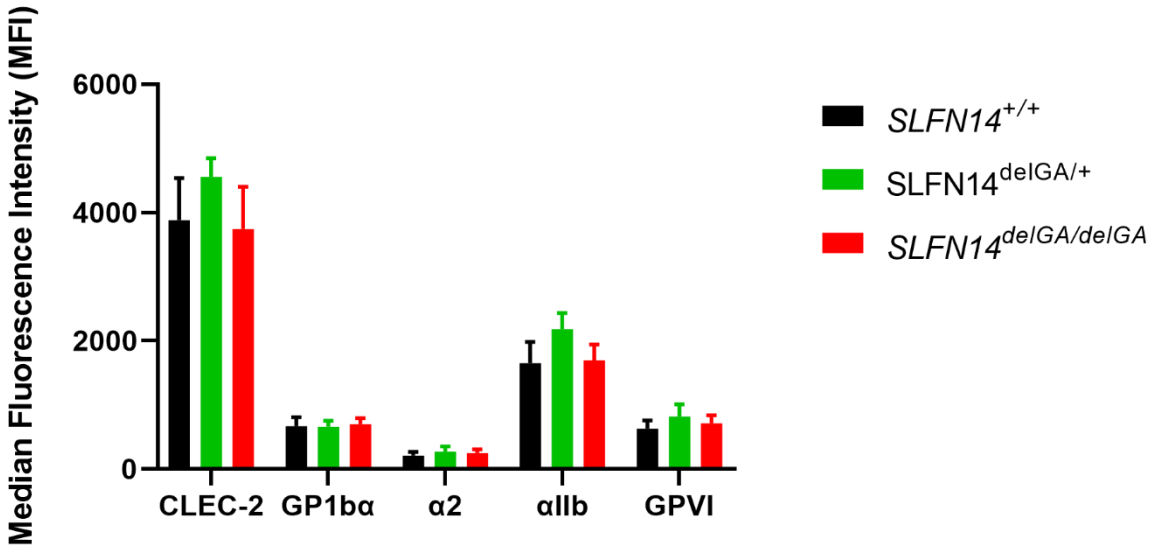


**Figure 3.7: Platelet glycoprotein expression in whole blood under resting conditions is normal.** Major platelet glycoproteins are expressed at normal levels in *SLFN14 delGA* mice compared to littermate controls. Data is from n=6-8 mice per genotype, mean ± SEM, two-way ANOVA with Tukey's correction for multiple comparisons.

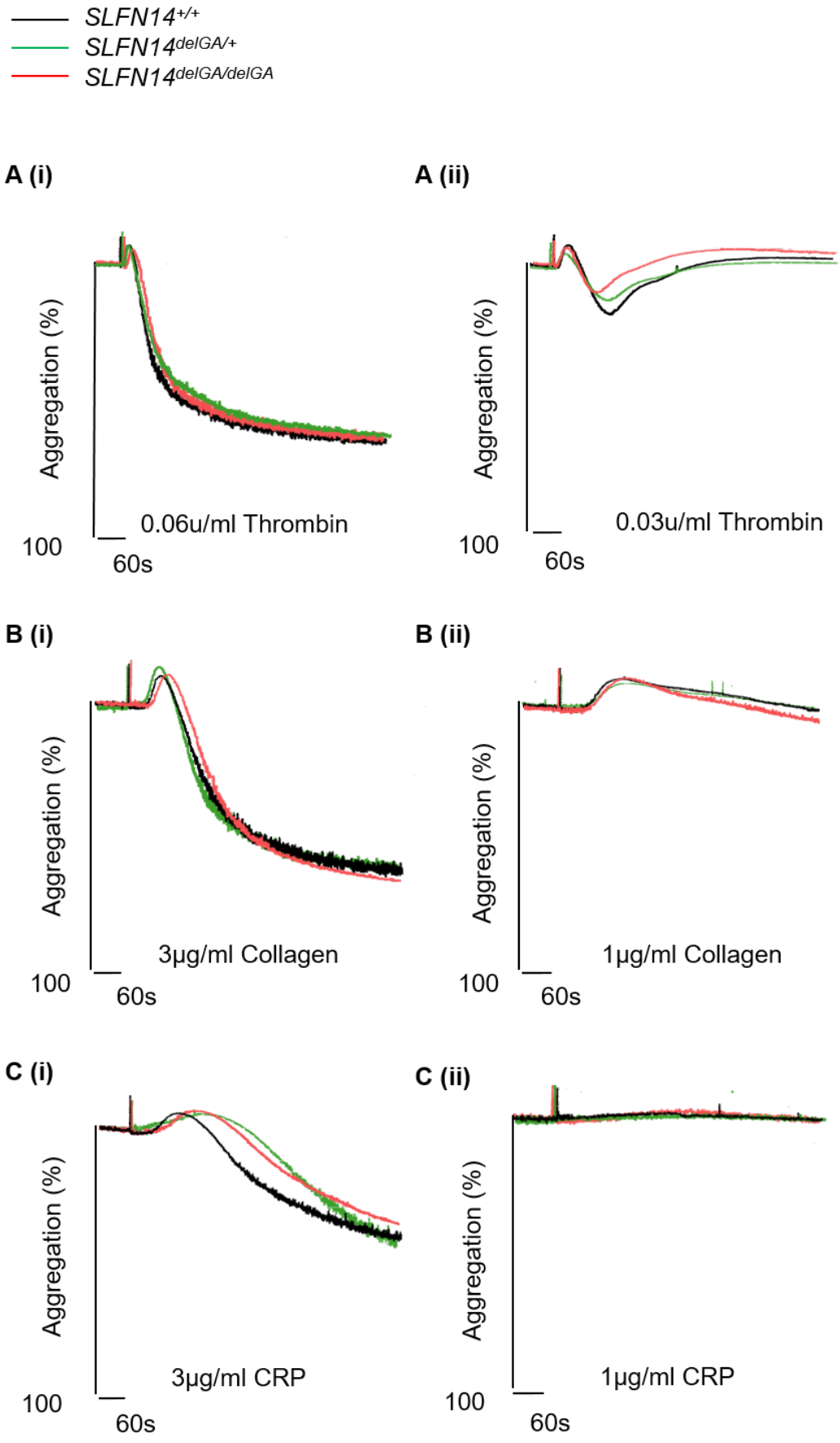
SLFN14+/+
SLFN14delGA/+
SLFN14delGA/delGA
A (i)
A (ii)
Aggregation (%)
100
0.06u/ml Thrombin
60s
0.03u/ml Thrombin
B (i)
B (ii)
3µg/ml Collagen
1µg/ml Collagen
C (i)
C (ii)
3µg/ml CRP
1µg/ml CRP

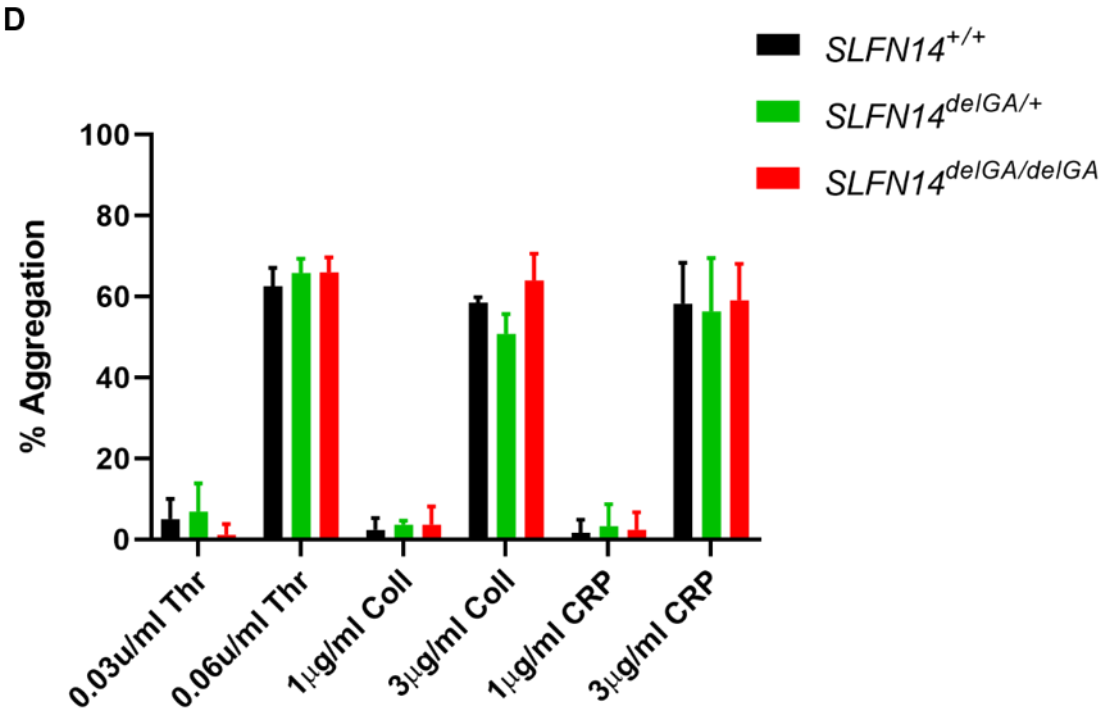


**Figure 3.8: Platelet function in SLFN14 delGA mice is normal.** (A, B and C) Platelet function assessed by LTA in washed platelets under stirring conditions showed normal responses to agonists thrombin, collagen and CRP at varying doses. (D) Summary of final percentage aggregation. Data is from n=3-6 mice per genotype mean ± SEM two-way ANOVA with correction for multiple comparisons.

### 3.3.7 *SLFN14 4bpdel* mice displayed no platelet morphological or functional abnormalities

Deletion of 4 base pairs in the SLFN14 mice in this colony resulted in a frameshift mutation, shown in Figure 3.3Civ. Whole blood counting was used in *SLFN14 4bpdel* mice to assess differences in platelet count and morphology. Platelet count and MPV was consistent across all genotypes as well as all other blood cell parameters measured (Table 3.3).

Platelet glycoprotein markers were measured in whole blood and in both genotypes no differences in the expression level was observed, indicating the 4 base pair deletion did not affect platelet production or morphology at their resting state (Figure 3.9).

Similarly to the other indel colonies, platelet function was assessed by LTA in washed platelets. Thrombin, collagen and CRP were used as agonists under different concentrations to initiate platelet aggregation. All genotypes were assessed using thrombin at high, intermediate and low doses and did not present any functional defect (Figure 3.10A). At a high dose of collagen no defect was observed between controls and heterozygous or homozygous mice (Figure 3.10Bi). Due to the COVID-19 pandemic and reduced capacity of animal housing facilities, breeding in this colony was terminated before homozygote platelet function could be fully assessed in response to collagen and CRP at intermediate and low doses. This unfortunately resulted in the loss of all mice for future experiments. Before breeding ceased, heterozygous platelets showed no difference in response to collagen at 1µg/ml or CRP at 3µg/ml and 1µg/ml (Figure 3.10Bii and Ci and ii).

Initial phenotyping showed that the 4bpdel mice did not cause any platelet defect in these mice. However, the inability to confirm platelet function in homozygotes leaves this question unanswered.

**Table 3.3: Gross haematological analysis of *SLFN14 4bpdel* mice.** Significance measured by two-way ANOVA with Tukey's correction for multiple comparisons. Data presented is from n=4-13 mice per genotype, mean ± SD. ns, not significant.

| Blood Parameter | *SLFN14*$^{+/+}$ | *SLFN14*$^{4bpdel/+}$ | *SLFN14*$^{4bpdel/4bpdel}$ | Significance |
|---|---|---|---|---|
| Platelet count ($10^3$/µl) | 812.24 ± 69.57 | 813.71 ± 96.27 | 838.46 ± 115.61 | ns |
| Mean platelet volume (µm$^3$) | 5.05 ± 0.08 | 5.07 ± 0.12 | 5.05 ± 0.06 | ns |
| Plateletcrit (%) | 0.36 ± 0.04 | 0.36 ± 0.05 | 0.36 ± 0.05 | ns |
| Red blood cell count ($10^6$/µl) | 9.00 ± 0.38 | 9.03 ± 0.42 | 9.25 ± 0.30 | ns |
| Haemoglobin concentration (g/dl) | 12.55 ± 0.48 | 12.65 ± 0.49 | 12.68 ± 0.29 | ns |
| Haematocrit (%) | 38.59 ± 0.95 | 39.31 ± 1.71 | 38.33 ± 3.09 | ns |
| Red blood cell distribution width (%) | 12.98 ± 1.02 | 12.92 ± 0.69 | 13.60 ± 0.45 | ns |
| Mean corpuscular volume (µm$^3$) | 49.64 ± 0.92 | 50.54 ± 0.97 | 49.50 ± 0.58 | ns |
| Mean corpuscular haemoglobin (pg) | 16.12 ± 0.59 | 16.23 ± 0.54 | 16.51 ± 1.19 | ns |
| White blood cell count ($10^3$/µl) | 5.36 ± 2.71 | 5.77 ± 4.91 | 3.30 ± 2.52 | ns |
| - Lymphocyte (%) | 76.57 ± 2.98 | 69.23 ± 14.02 | 63.43 ± 29.39 | ns |
| - Monocyte (%) | 7.86 ± 1.96 | 9.05 ± 2.31 | 8.33 ± 4.02 | ns |
| - Neutrophil (%) | 15.32 ± 1.77 | 17.22 ± 9.34 | 18.80 ± 9.23 | ns |
| - Eosinophil (%) | 0.06 ± 0.08 | 0.28 ± 0.48 | 0.23 ± 0.17 | ns |
| - Basophil (%) | 0.17 ± 0.13 | 0.14 ± 0.14 | 0.17 ± 0.15 | ns |

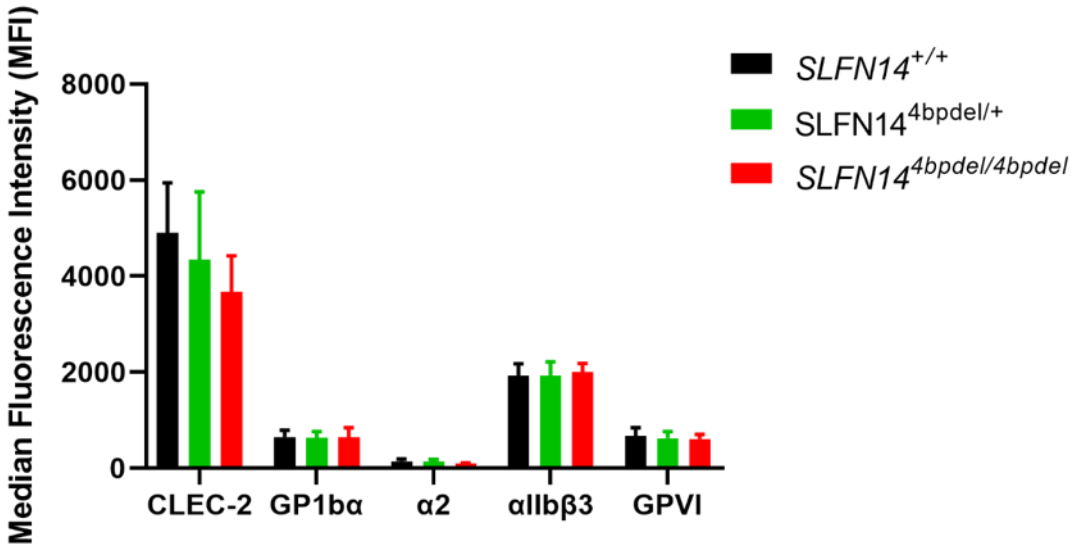


**Figure 3.9: Platelet glycoprotein expression in whole blood under resting conditions is normal.** Major platelet glycoproteins are expressed at normal levels in *SLFN14 4bpdel* mice compared to littermate controls. Data is from n=3-8 mice per genotype, mean ± SEM, two-way ANOVA with Tukey's correction for multiple comparisons.

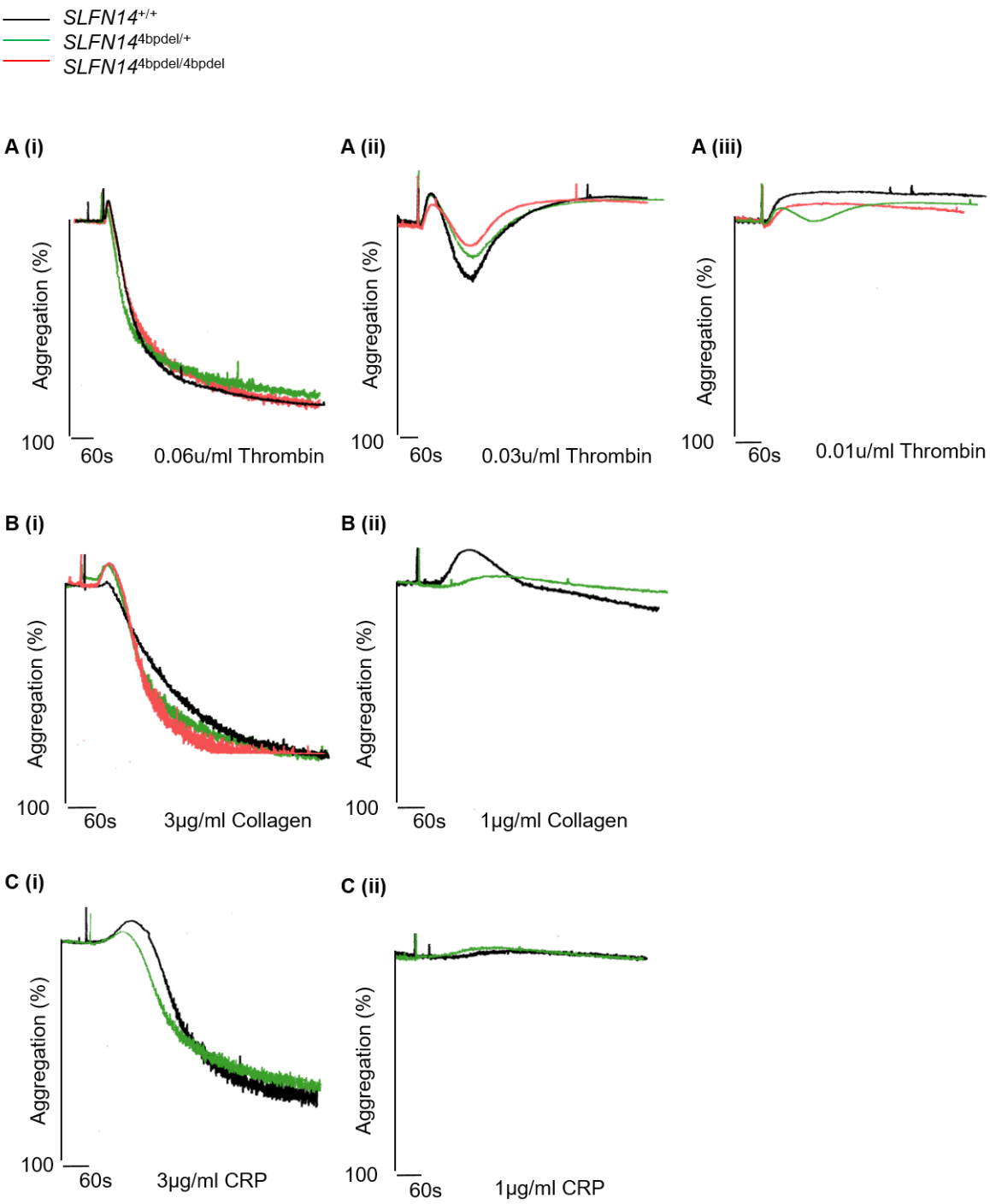
SLFN14+/+
SLFN14 4bpdel/+
SLFN14 4bpdel/4bpdel
A (i)
A (ii)
A (iii)
Aggregation (%)
100
60s
0.06u/ml Thrombin
0.03u/ml Thrombin
0.01u/ml Thrombin
B (i)
B (ii)
3µg/ml Collagen
1µg/ml Collagen
C (i)
C (ii)
3µg/ml CRP
1µg/ml CRP

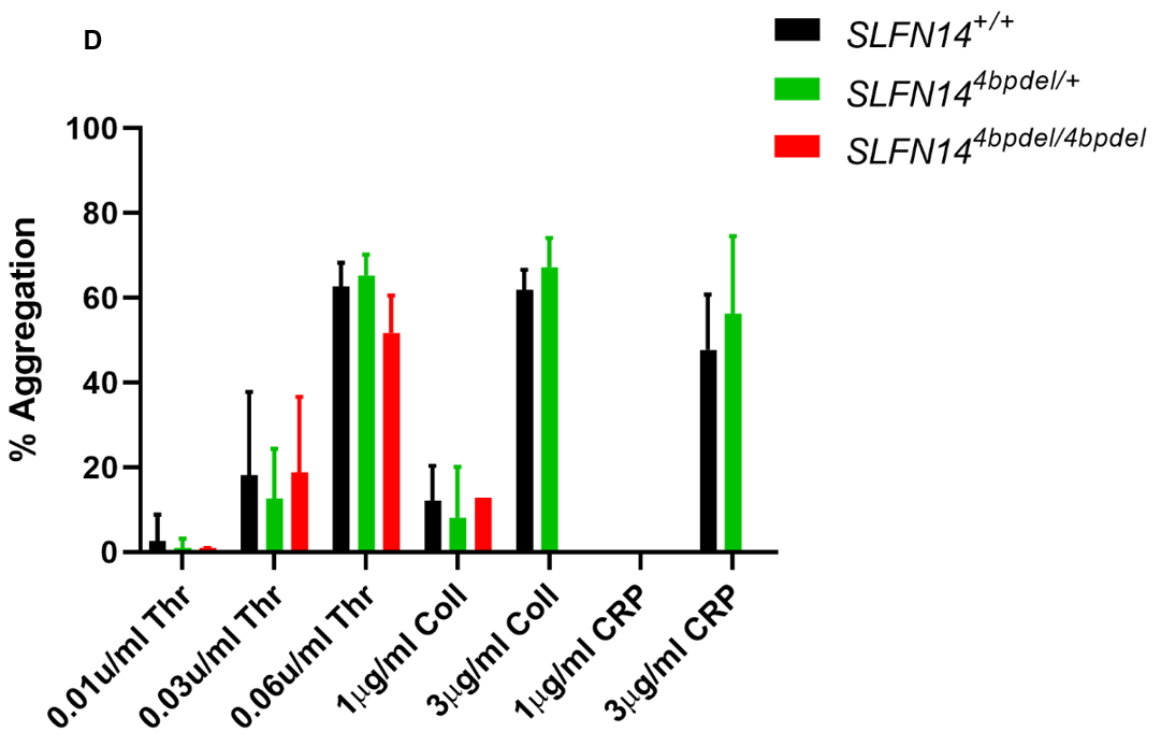


**Figure 3.10: Platelet function in SLFN14 4bpdel mice is normal.** (A, B, C) Platelet function assessed by LTA in washed platelets under stirring conditions showed normal responses to agonists thrombin, collagen and CRP at various doses. (D) Individual traces were used to calculate percentage final aggregation as shown in quantification graph, mean percentage aggregation ± SEM, n=1-9 mice per genotype, (homozygotes were unavailable in some cases due to animal housing restrictions during the COVID-19 pandemic). Significance assessed by two-way ANOVA with correction for multiple comparisons and students t-test for conditions with only two genotypes.

## 3.4 Discussion

Within this chapter, the *SLFN14*-K208N mouse model was developed using CRISPR mediated genome editing to initiate a single nucleotide substitution mutation which has previously been identified in a series of patients with inherited bleeding. As a consequence of the HR in the CRISPR repair mechanism, several indel mutations were obtained effectively as a by-product and deemed worthy of investigating further. These 4 separate colonies were used in order to help uncover the reasons behind abnormal platelet production and function observed in patients. 9bpdel, delGA and 4bpdel colonies all produced viable homozygote offspring whereas *SLFN14*-K208N mice only produced heterozygotes (explored further in Chapter 4). This led reason to believe that the platelet phenotype of homozygotes may be more severe and applicable to the mechanism of K219N patients and potential role in haemostasis.

In the indel colonies, basic phenotyping involving whole blood counting, assessment of glycoprotein receptors on resting platelets and platelet aggregation in response to thrombin, collagen and CRP did not reveal abnormal platelet phenotypes. In all models, platelet count, size and function was consistent between all genotypes. This was surprising given the K219N mutation in humans, in the same region, produces a severe macrothrombocytopenia and bleeding.

All these mutations occur in exon 2 which is the first coding exon in the *SLFN14* gene, also within the AAA domain. Indel mutations resulted in predicted truncations of the SLFN14 protein whereas the K208N mutation meant protein length was retained at 899 amino acids. Unfortunately, SLFN14 protein size was not investigated in these indel models. Priority was given to LTA experiments to decipher any platelet function defect and due to the COVID-19 pandemic further samples for proteomic studies could not be obtained. In this model with no differences to platelet production or function it may be suggested that these truncations had little to no effect on either sufficient transcription of SLFN14 or its role in platelet biology. At

this stage it was important to continue investigating the K208N mutation as it is homologous to the patient K219N mutation. As will be explored in further detail in Chapter 5, the K208N mutation did have a significant effect in haematopoiesis, suggesting it is not the length or truncation of sections of the protein but rather the folding and overall structure which ultimately affect platelet production and function in humans. It may also be plausible that the truncated section of the SLFN14 protein is functionally redundant or another subgroup III protein may take over its role in this scenario.

In 2018 Yang et al. revealed the crystal structure of SLFN13 in rats (Yang et al., 2018). *SLFN13* is also a member of SLFN subgroup III. They revealed that it is the substitution of conserved charged residues which impact protein folding and nucleolytic activity of SLFN13 (Yang et al., 2018). This may also be applicable in mouse *SLFN14* whereby it is the substitution of residues in the AAA domain which results in protein misfolding and haematopoietic defects in mice rather than truncation or minor alterations to protein length. This has previously been explored by Fletcher at al. with regards to the K218E mutation whereby the change of a lysine to glutamine reside at position p.218 resulted in changes in tertiary protein structure and post translational degradation (Fletcher et al., 2018). The exact mechanism for potential protein misfolding in the mouse K208N model remains to be explored.

# Chapter 4

## Initial phenotypical characterisation of the *SLFN14*-K208N mouse model

# Chapter 4 – Initial phenotypical characterisation of the *SLFN14*-K208N mouse model

## 4.1 Aim

The aim of this chapter was to investigate the effect of the *SLFN14*-K208N mutation in mice with particular focus on platelet production and function. Here, the K208N CRISPR model was characterised, a mutation which is homologous to the *K219N* observed in *SLFN14* patients. The overall aim of this chapter was to interrogate the platelet phenotype in mice compared to that of the *K219N* mutation in humans. In mice, it was hypothesised that K208N would produce the same if not very similar effects on platelet production and function to *SLFN14* patients.

## 4.2 Introduction

In the GAPP study, initially three extended families were identified with heterozygous mutations in *SLFN14.* Since this, two additional families have been discovered with similar mutations also presenting with a bleeding phenotype. In mice, *SLFN14* is located on chromosome 11 and in humans, chromosome 17. *SLFN* genes are highly conserved through all mammalian species and located in close proximity to other genes involved in T-cell differentiation and development (Stapley et al., 2020, Bustos et al., 2009, Schwarz et al., 1998). This provides further evidence that mutations within *SLFN14* may specifically affect haematopoiesis and the overall function of haematopoietic derived cells. Currently there are no mouse models with these missense mutations accompanied by a macrothrombocytopenia or bleeding phenotype similar to that in *SLFN14* patients. Here, the generation of a CRISPR knock-in mouse will allow investigation of the phenotypical characterisation of *SLFN14* and more specifically, how the K208N mutation within the AAA domain contributes to thrombocytopenia and platelet function defects. The generation of this mouse model was detailed more in the previous chapter but briefly, donor oligonucleotides from the *K219N* mutation observed in patients (Family B in Fletcher et al., 2015) were used to initiate a single

nucleotide change within *SLFN14* in mice on a C57/BL6J background. DNA was repaired using homology directed repair and resulted in a single amino acid change from Lysine to Asparagine at position 208 with. In humans, the *K219N* variant is shown to colocalise with ribosomes and mediate rRNA endonucleolytic degradation. Compared to SLFN14 wild-types, mutant protein is significantly reduced as a result of post translational degradation from partial misfolding of the protein (Fletcher et al., 2018).

This chapter demonstrates that the platelet phenotype in *SLFN14*-K208N transgenic mice is largely indifferent from wild-type controls with the only difference being slightly enlarged platelets. This did not seem to affect platelet reactivity to agonists under static or aggregating conditions. Erythrocyte count was elevated by approximately 30%. Erythrocytes were smaller, in some instances half the size of wild-types, irregularly shaped and had lower haemoglobin content giving rise to severe anaemia and most likely the cause of death in homozygote offspring prior to weaning. This red blood cell phenotype contributes to thrombus instability in laser and ferric chloride induced injury models. The phenotype of this mouse is unique and not only highlights the importance of investigating cell-cell interactions in *in vivo* physiological studies and assays in whole blood but also the species-specific differences which can arise when studying homologous mutations in transgenic models.

## 4.3 Results

### 4.3.1 *SLFN14*$^{K208N/K208N}$ mice do not survive to weaning due to severe anaemia

Initial breeding strategies revealed heterozygote/heterozygote pairs did not produce live homozygote offspring. The average litter size for heterozygote breeding pairs was 6, with an average 3 heterozygote mice and 3 wild-types. The average pre-wean loss across 15 litters was 1.5 mice. According to Mendelian inheritance, 25% offspring should be homozygotes however this was not observed. Expected and observed values are significantly different by Chi square analysis (Figure 4.1Ai and ii). These values, accompanied by the lack of live homozygote mice suggests that all pre wean losses are homozygotes and thus do not survive to weaning age. Timed mating experiments were used to investigate the stages of embryo development in *SLFN14* mutants. *In utero,* at embryonic day 12.5 (E12.5), both heterozygotes and homozygotes appeared paler than wild-type controls. At E14.5, a similar phenotype was observed with vasculature appearing less defined, most likely due to severely low haemoglobin content and inability to clearly distinguish blood vessels (Figure 4.2). These two time points are critical in embryonic development with particular impact on platelet and erythroid lineages. No embryo resorption sites were seen at either time point suggesting homozygotes do survive to full term but die shortly after birth due to severe anaemia before weaning and before genotyping samples could be obtained. No size or developmental differences were observed between the genotypes at either stage. Subsequent breeding to avoid homozygous loss involved wild-type/heterozygote pairs which produced mice at normal Mendelian ratios by Chi square analysis (Figure 4.1Aiii). Heterozygote mice produced from these were indistinguishable from wild-type littermates and used in further analysis of the *SLFN14* phenotype. Therefore, all comparisons made in this chapter are between heterozygotes (*SLFN14*$^{K208N/+}$) and litter matched wild-type controls (*SLFN14*$^{+/+}$).

**A (i)**

| $SLFN14^{K208N/+}$ X $SLFN14^{K208N/+}$ | Expected Ratio |
|---|---|
| $SLFN14^{+/+}$ | 0.25 |
| $SLFN14^{K208N/+}$ | 0.50 |
| $SLFN14^{K208N/K208N}$ | 0.25 |

**(ii)**

| $SLFN14^{K208N/+}$ X $SLFN14^{K208N/+}$ | Expected | Observed |
|---|---|---|
| $SLFN14^{+/+}$ | 22 | 36 |
| $SLFN14^{K208N/+}$ | 44 | 47 |
| $SLFN14^{K208N/K208N}$ | 22 | 0 |
| CHITEST P value | | >0.0001 |
| Cross 2 average litter size | 6 | |

**(iii)**

| $SLFN14^{K208N/+}$ X $SLFN14^{+/+}$ | Expected | Observed |
|---|---|---|
| $SLFN14^{+/+}$ | 96 | 87 |
| $SLFN14^{K208N/+}$ | 96 | 97 |
| CHITEST P value | | 0.552 |
| Cross 1 average litter size | 8 | |

**Figure 4.1: *SLFN14*-K208N homozygote mice do not survive to weaning and inheritance differs from Mendelian patterns.** (A) Mendelian inheritance of *SLFN14* heterozygote/heterozygote breeding pairs. (i) Predicted ratios of genotypes based on Mendel's law of inheritance. (ii) No *SLFN14*-K208N homozygotes were observed from heterozygote/heterozygote breeding pairs. Data from 13 litters. (iii) Heterozygote/wild-type breeding pairs produced live offspring at expected Mendelian inheritance ratios and Chi square test of deviation was not significant. Data from 24 litters.

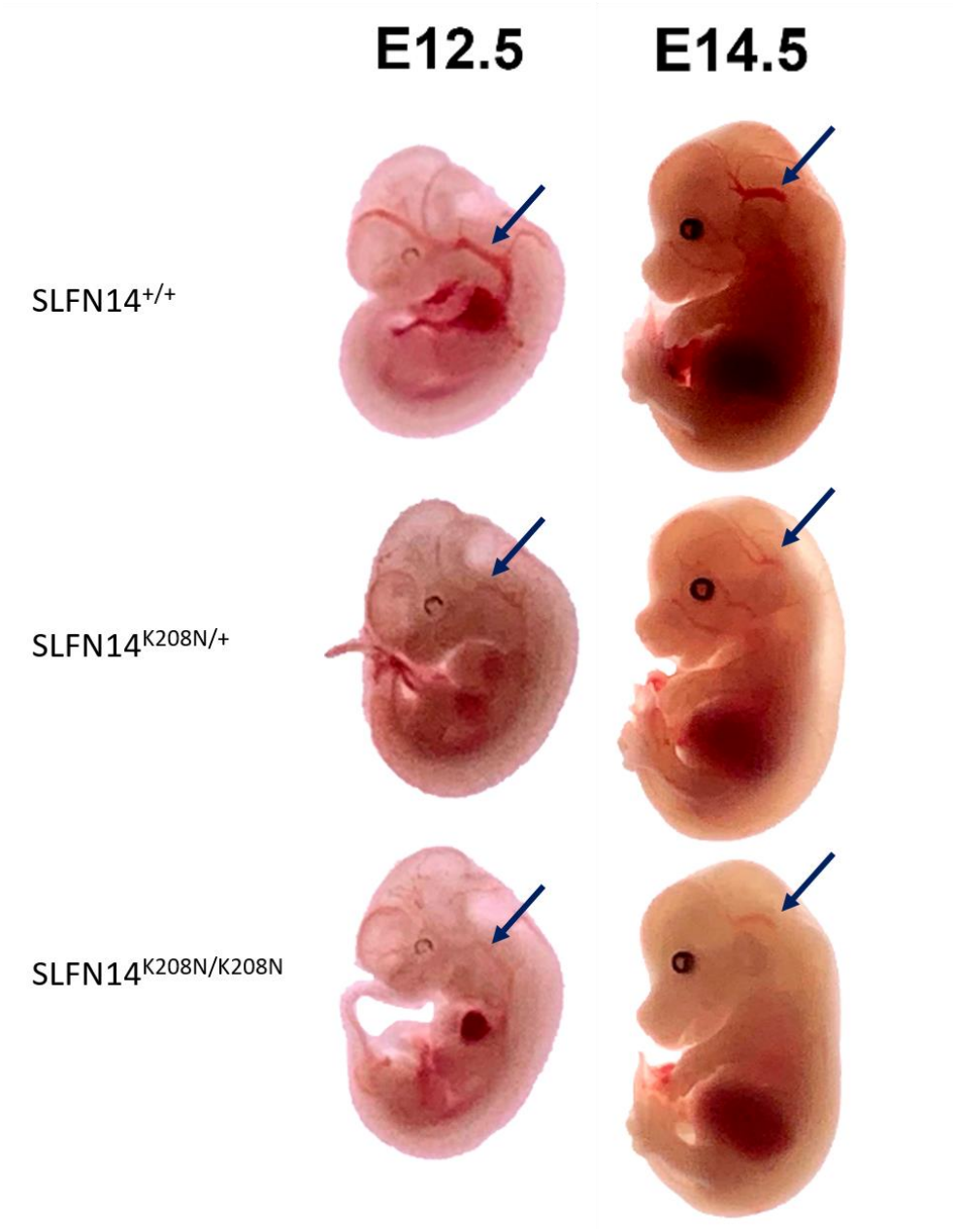


**Figure 4.2: *SLFN14*-K208N homozygote mice do not survive to weaning and appear much paler than wild-types.** Embryos obtained from timed mating experiments at E12.5 and E14.5. Arrows indicate aortic arch at both time points which is progressively less visible with homozygosity.

### 4.3.2 Haematological analysis of SLFN14-K208N whole blood using automated impedance based haematology analyser

In humans, the *SLFN14*$^{K219N/+}$ mutation causes thrombocytopenia. Therefore, before investigating platelet function, whole blood counts were used to assess the circulating levels of platelets and other major blood cell components. Blood was collected from mice under terminal anaesthesia and analysed using an ABX Pentra ES60 automated blood counter. After an anticoagulant dilution correction was applied, whole blood counts were analysed. Initially, a significant increase in platelet count and size was observed (Figure 4.3Ai and ii). However, upon studying other blood parameters in further detail it appeared this was inaccurate. This counter is based on an impedance mechanism whereby cells are classified by size. Each cell within pre-set size boundaries is classified to a category of either platelets or erythrocytes and the number of cells passing through each chamber is calculated to give cell count. While erythrocyte count remained unchanged, size was significantly reduced (Figure 4.3Bi and ii). Histograms present the cell size of each category and upon observation erythrocytes were outside the counter's predetermined normal range leading to the conclusion that a proportion of these small erythrocytes were of similar size to platelets (Figure 4.3C). These microcytes were determined by the analyser as platelets and incorrectly included in the platelet parameters thus increasing the overall platelet count. Therefore, this platelet count was in fact a combination of platelets and micro-erythrocytes and could not be considered an accurate representation of the initial phenotyping process.

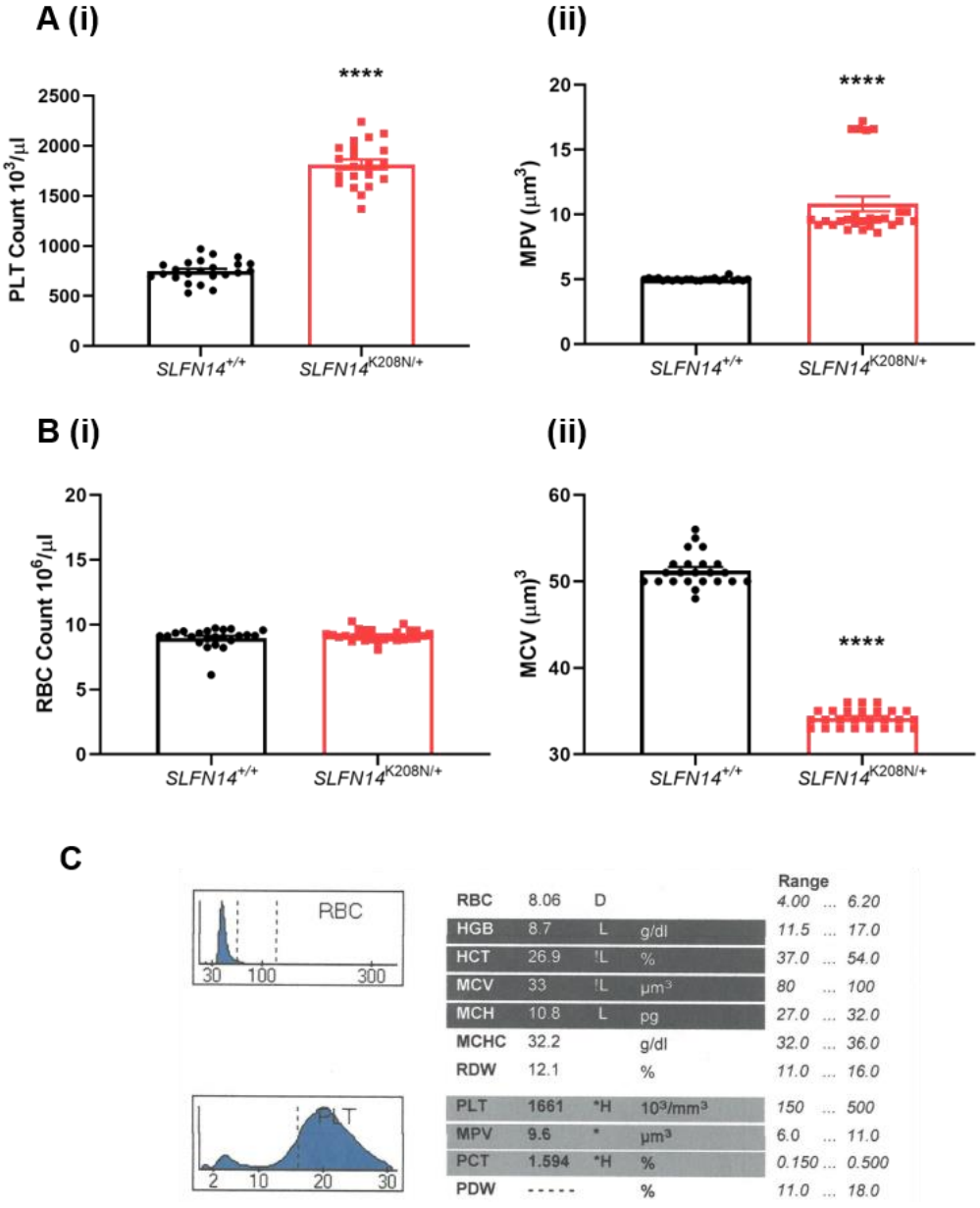


**Figure 4.3: Automated haematology analyser results from *SLFN14*-K208N mice showed first evidence of erythrocytosis.** (A) Anticoagulated whole blood was collected from *SLFN14*$^{+/+}$ (n=23) and *SLFN14*$^{K208N/+}$ (n=26) mice and platelet parameters analysed on ABX Pentra ES60 blood counter. (i) Significantly increased platelet count and (ii) significant increase in platelet size was observed in heterozygotes compared to wild-type controls. (B) Erythrocyte parameters. (i) No difference in red blood cell count was observed between genotypes. (ii) Significantly reduced red blood cell size. (C) Representative histogram from SLFN14$^{K208N/+}$ mouse shows significant reduction in red blood cell size (below normal range shown by dotted boundaries). All data presented as mean ± SEM; unpaired t-test with Welch's correction **** *P*<0.0001.

### 4.3.3 Flow cytometry cell counting assay for platelets and erythrocytes

In order to accurately count platelets and red blood cells, a flow cytometry based counting assay was developed using specific cell markers. Whole blood was stained with CD41 (αIIb) conjugated to APC and Ter119 (also known as glycophorin A or GPA) conjugated to FITC. Ungated plots (Figure 4.4Ai) showed a slight overlap in the platelets (green) and red blood cells (red) in the *SLFN14*$^{K208N/+}$ panel which confirms similarities in size between some cells identified by the automated analyser. 30µl of stained blood was used and single positive gates were applied to calculate the number of stained cells per microliter (Figure 4.4Aii). Forward scatter information was used as an indication of cell size (Figure 4.4Aiii). By this specific labelling method, platelet count was unchanged between genotypes, but in similarity to the automated analyser, platelet size was significantly increased (Figure 4.4Bi and ii). Red blood cell count was significantly increased by approximately 30% (Figure 4.4Ci) accompanied by a stark reduction in red blood cell size (Figure 4.4Cii). This provides further evidence that the automated analyser was counting a population of red blood cells as platelets and thus appearing to increase the overall count.

Increased platelet size is often associated with immature platelets. Young platelets released into the circulation by pro-platelet extensions (pre-platelets) often contain high yields of residual megakaryocyte RNA. This RNA degrades as platelets age thus suggesting a high RNA content is indicative of young platelets in the circulation. *SLFN14*$^{K219N}$ patients have a high immature platelet fraction (IPF) which is notably related to their macrothrombocytopenia. To investigate this in mice, SYTO13 was used in a flow cytometry assay to bind RNA. SYTO13 has recently been identified as a more specific and more stable marker of RNA content than the previously used Thiazole orange (Hille et al., 2019). CD41 was used to identify the platelet population and CD41$^{+}$/SYTO13$^{+}$ cells were used in analysis. The IPF in *SLFN14*$^{K208N/+}$ mice was 15% higher than wild-type controls which provides a suitable explanation for increased platelet size in Figure 4.4D.

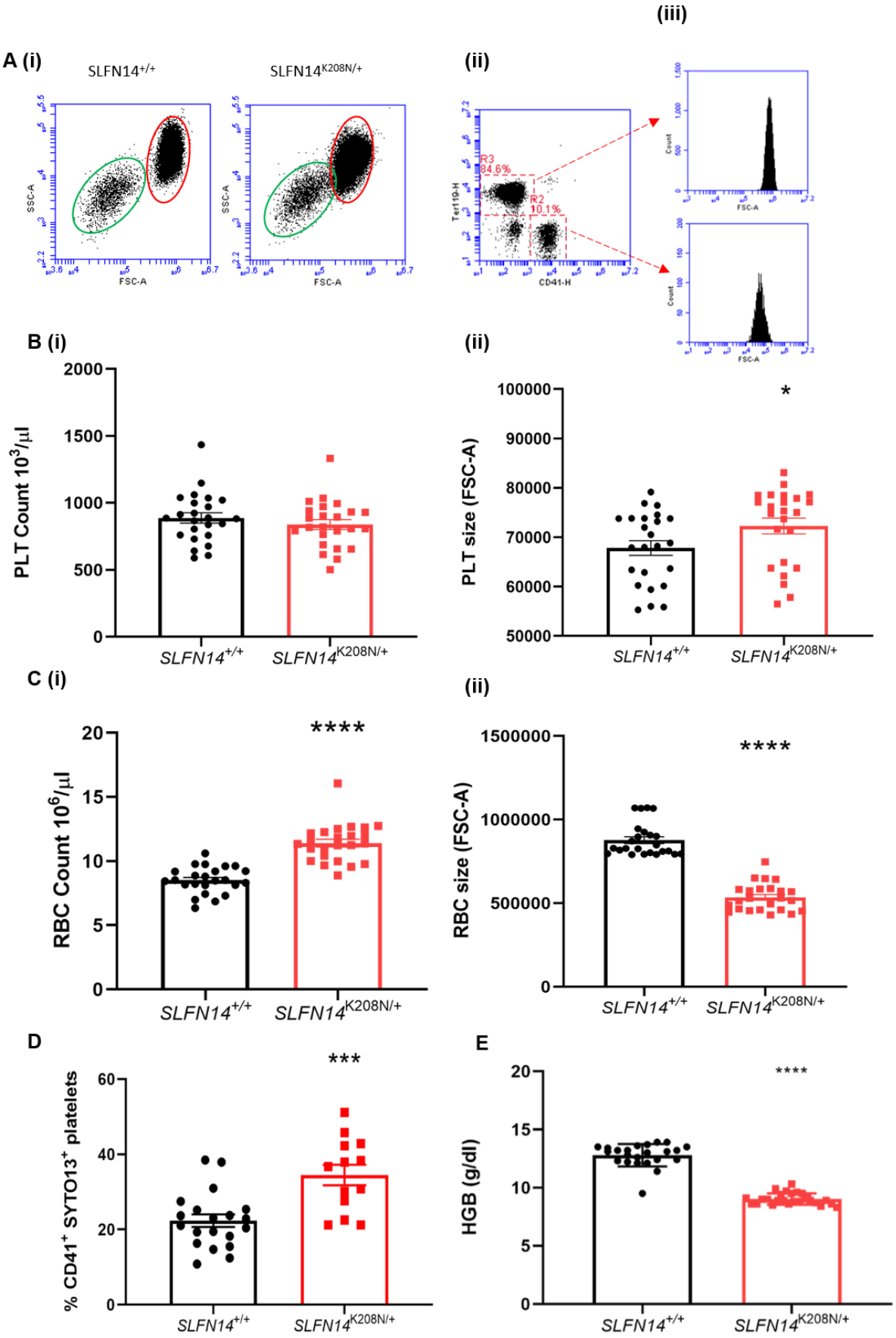
A (i)
SLFN14+/+
SLFN14K208N/+
SSC-A
FSC-A
(ii)
(iii)
R3
84.6%
R2
10.1%
Ter119-H
CD41-H
Count
B (i)
PLT Count 10³/µl
(ii)
PLT size (FSC-A)
*
C (i)
RBC Count 10⁶/µl
****
(ii)
RBC size (FSC-A)
****
D
% CD41⁺ SYTO13⁺ platelets
***
E
HGB (g/dl)
****

**Figure 4.4: Flow cytometry based haematological cell counting analysis of *SLFN14*$^{K208N/+}$ mice** (A) Flow cytometry based counting of platelets and erythrocytes. (i) Flow cytometry forward and side scatter plots showing size overlap of erythrocyte and platelet populations. Platelets (green) and erythrocytes (red). (ii) Gating method shown for double stain using CD41 (R2) and Ter119 (R3). Representative plots of n=18 mice per genotype. (iii) Forward scatter histograms used for cell size quantification. (Bi and ii) Platelet counts and size from flow cytometry based counting. Mean ± SEM, n=18 mice per genotype. (C) Erythrocyte counts and size from flow cytometry based counting. Mean ± SEM, n=18 mice per genotype. (D) Immature platelet fraction in *SLFN14*$^{K208N/+}$ mice. CD41 positive platelets were gated and immature platelet population assessed by SYTO13 staining. Mean ± SEM, n=13-20 mice per genotype. (E) *SLFN14*$^{K208N/+}$ mice are anaemic. Haemoglobin levels were measured by an automated haematology analyser in *SLFN14*$^{K208N/+}$ mice compared to wild-type controls. Mean ± SEM, n=23-26 mice per genotype. *p<0.05, ***p<0.001, ****p<0.0001

### 4.3.4 *SLFN14*-K208N mice exhibit poikilocytosis and severe anaemia

Given the discrepancies in erythrocyte counts and size, erythrocyte morphology was assessed in further detail using whole blood smears stained with haematoxylin and eosin (H&E). Microcytes identified in both automated and flow cytometry based counting assays were substantially smaller, in some cases approximately half the size of wild-type controls. Wild-type erythrocytes displayed characteristic 'plump' and rounded shapes while *SLFN14*$^{K208N/+}$ cells were irregularly shaped, with some membrane indentations (poikilocytosis) as shown in Figure 4.5. In addition to light microscopy, scanning electron microscopy was used, which is a more advanced technique used in cell morphological studies. Here, red blood cells were isolated from whole blood using a series of centrifugation steps and leukocyte depletion filters. Erythrocytes were fixed using 2.5% glutaraldehyde fixation solution. Cells were air dried and imaged at a 1500X magnification. Aside from some 'star shaped' cells which appear in both genotypes, *SLFN14*$^{K208N/+}$ erythrocytes are irregularly shaped and appear smaller than neighbouring wild-type cells highlighted in Figure 4.6A and B (green and red circled cells). Star shaped cells are a common feature in SEM and often arise due to the osmotic differences between cells and the fixation solution. Osmolality matching is notoriously difficult in the field of SEM and occurs at low levels in all samples but progressively increases with time the cells are in fixation solution (Mustafa et al., 2016). In the wild-type samples there is some level of spiking but in *SLFN14*$^{K208N/+}$ mice this appears increased (Figure 4.6). All samples were prepared and imaged at the same time using identical solutions, negating the possibility these differences were due to sample preparation or the length of time cells were in fixation solution. As will be explored later in the subsequent chapter, *SLFN14* mutant cells may be more sensitive to haemolysis. As observed in wild-types, haemolysis does occur but perhaps mutant erythrocytes, with their membrane irregularity, renders them more susceptible to these osmolality changes, resulting in the appearance of a greater quantity of 'spiked' erythrocytes under resting conditions (Figure 4.6B). In addition, *SLFN14*$^{K208N/+}$ erythrocytes appeared paler than controls in whole blood

smear images in panel A, supporting a 35% reduction in haemoglobin content and severe anaemia (Figure 4.4E). The lower haemoglobin content is likely due to the reduced size and lower carrying capacity. Additionally, haemoglobin synthesis may be impacted by the endoribonucleolytic activity of *SLFN14* which mediates translation at ribosomes. This hypothesis will be addressed in the next chapter.

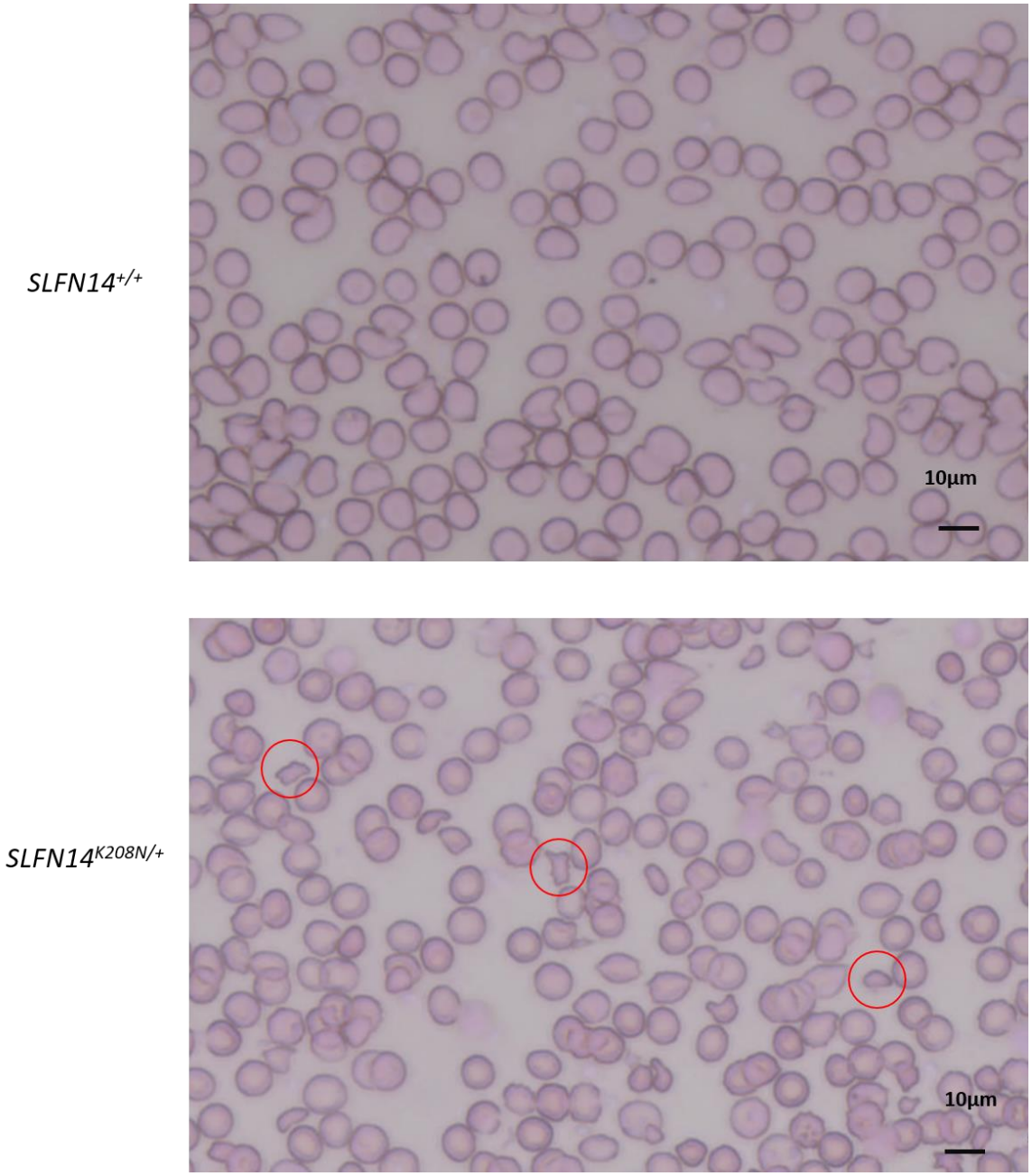


**Figure 4.5: Poikilocytosis in *SLFN14*$^{K208N/+}$ erythrocytes.** (A) Whole blood smears from wild-type and *SLFN14*$^{K208N/+}$ mice. Blood smears were stained with H&E histological stain to view blood cell size and morphology. Poikilocytes (irregular shaped cells) are circled in red. Representative images of n=6-7 mice per genotype.

*SLFN14*$^{+/+}$

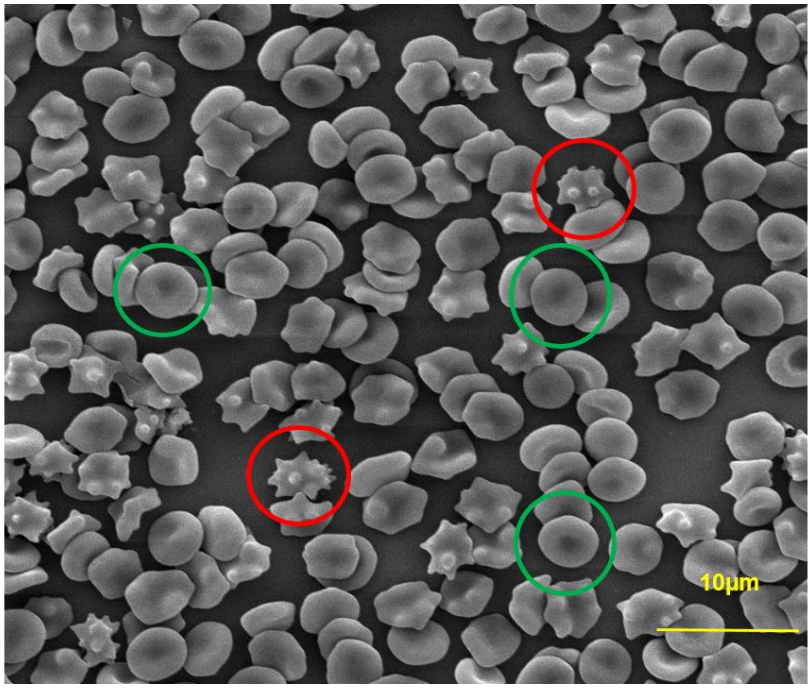


*SLFN14*$^{K208N/+}$

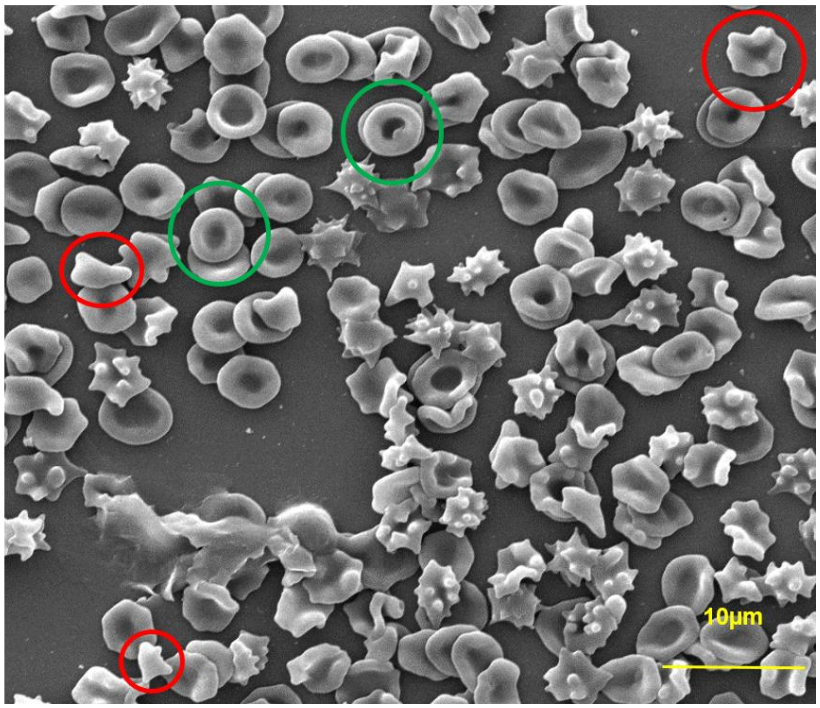


**Figure 4.6: Scanning electron microscopy images of isolated erythrocytes.** Normal round and plump erythrocytes are shown in wild-types and *SLFN14*$^{K208N/+}$ mice (green circles) and irregularity in shape and size of erythrocytes more susceptible to haemolysis in *SLFN14*$^{K208N/+}$ mice (red circles). Representative images of n=3 mice per genotype.

### 4.3.5 *SLFN14*-K208N platelets show normal distribution of granules by transmission electron microscopy

Upon activation, platelets experience a series of activation and degranulation steps in to change conformation leading to platelet activation, adhesion and ultimately thrombus formation. Transmission electron microscopy (TEM) can identify ultrastructural abnormalities in platelet granule content and give indication of potential functional defects such as that observed in gray platelet syndrome, whereby alpha granules are completely absent. Resting washed platelet suspensions were fixed in 2.5% glutaraldehyde solution. The fixed cells were embedded with 100% resin and sectioned at 0.8µm with an ultra-microtome. Sections were viewed under a transmission electron microscope. Alpha and dense granules were identified in platelet sections (Figure 4.7Ai). The number and size of alpha and dense granules was consistent between genotypes (Figure 4.7Aii). In addition, a number of other platelet structures were visible and highlighted in Figure 4.7Ai. This work was conducted in collaboration with the School of Metallurgy and Materials, University of Birmingham.

### 4.3.6 *SLFN14*-K208N mice have normal platelet glycoprotein levels

Following verification of normal levels of platelets in the circulation, platelet function was investigated in further detail. Although platelet count was retained, it was unclear at this stage if platelet function may be defective as seen in *SLFN14* patients. Some mutations in platelet specific genes have been found to affect the levels of glycoproteins on the platelet surface which subsequently affect downstream platelet signalling and function (Alan and Paquita, 2020, Almazni et al., 2020). Given the platelet defects observed in patients it was important to check these levels as a first indication of a potential platelet function defect. Whole blood was stained with CD41 (conjugated to APC) and a series of FITC conjugated antibodies for major glycoprotein receptors on platelets (CLEC-2, GP1Bα, α2, αIIbβ3 and GPVI). CD41 staining ensured only the platelet population was selected and no contamination occurred from micro-erythrocytes. Median fluorescence intensity (MFI) was

used to measure glycoprotein expression levels on the platelet surface. All receptors were present at normal levels between genotypes (Figure 4.8A). Therefore, *SLFN14*$^{-}$K208N does not affect expression of glycoproteins at the platelet surface under resting conditions.

### 4.3.7 *In vitro* platelet activation in whole blood by flow cytometry showed normal alpha granule secretion and activated integrin exposure

Normal levels of platelet glycoproteins and granule contents were observed under resting conditions, however in some cases, glycoprotein exposure and degranulation may be impaired depending on agonist stimulation. Upon agonist detection, alpha granules within platelets release their contents. One of these substances is platelet activation marker P-selectin which is exposed on the cell surface. In addition, one of the major platelet glycoproteins, αIIbβ3, undergoes conformational changes upon detection of agonists. This is then present in an 'active form' which in mice, is detected by the antibody JON/A. Whole blood was stained with FITC conjugated P-Selectin and PE conjugated JON/A and activated by the addition of platelet agonists at various doses. Activation marker expression was measured in whole blood by flow cytometry and the percentage of double positive platelets for both P-selectin and JON/A was calculated. Overall, a dose response effect was present but no differences were observed between genotypes for either P-selectin expression or JON/A detection after platelet activation using any of the agonists (Figure 4.8B).

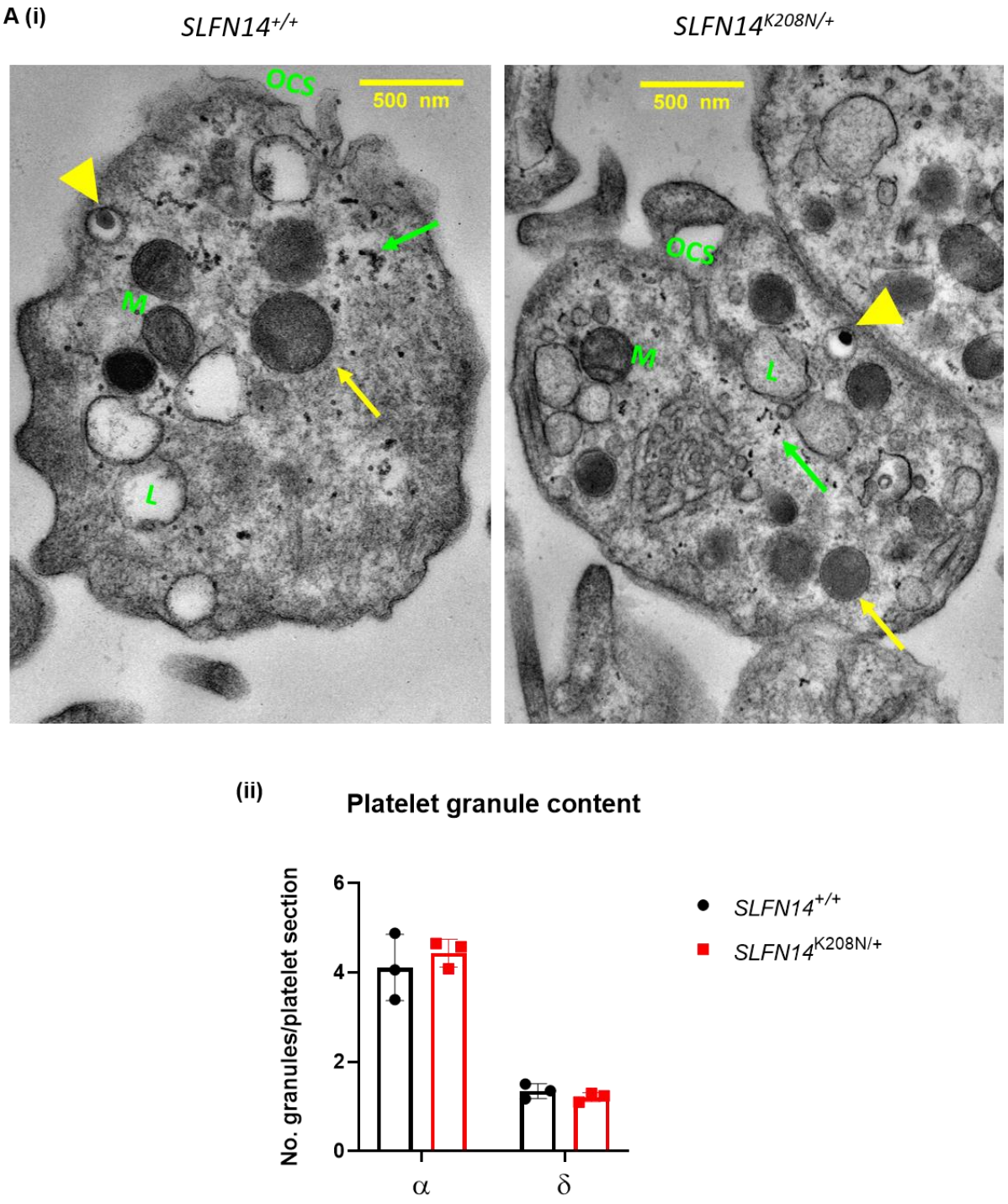


**Figure 4.7: Platelet transmission electron microscopy (TEM) in *SLFN14*-K208N mice.** (A) Representative images of TEM sections of wild-type and *SLFN14*$^{K208N/+}$ mice respectively. (i) Alpha (α) granules (yellow arrow), dense (δ) granules (yellow arrowhead). Other platelet ultrastructure features include: Mitochondria (M), Lysosomes (L), Open canalicular system (OCS) glycogen (green arrow). (ii) Quantification of platelet granules from TEM images. Data presented is mean ± SEM from 60 and 66 platelets from wild-types and *SLFN14*$^{K208N/+}$ mice respectively. All images were analysed blind and unblinded after quantification was complete. Unpaired t-test with Welch's correction. N=3 mice per genotype.

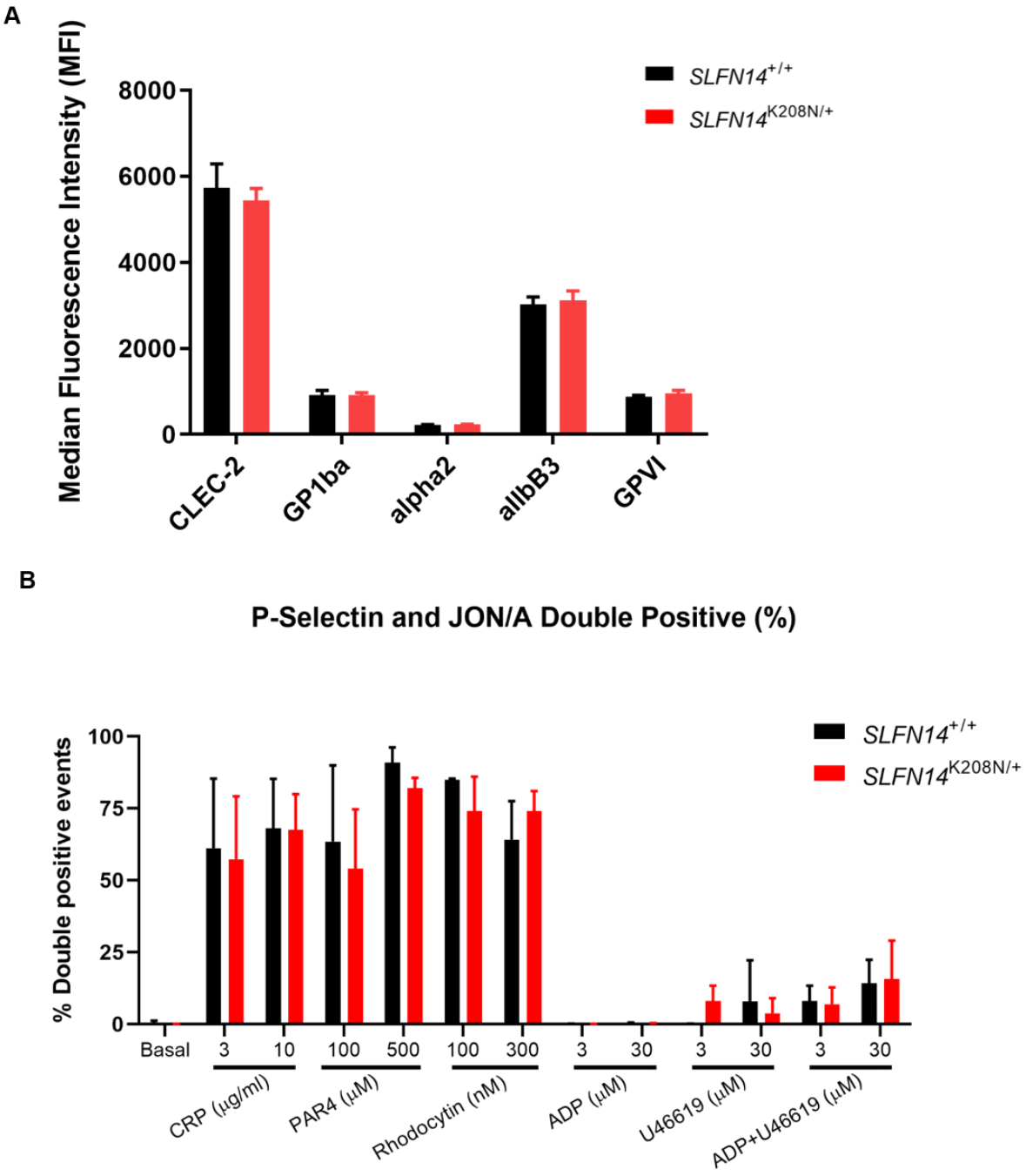


**Figure 4.8: *In vitro* assessment of platelet glycoprotein receptors and activation in *SLFN14*$^{K208N/+}$ mice** (A) Resting platelet surface glycoprotein expression levels. GP1ba$^{+}$ platelets were co-stained for indicated surface receptors in whole blood. Median fluorescence intensity (MFI) from n=4-6 mice per genotype. Mean±SEM; significance assessed by Welch's t-test for multiple comparisons. (B) P-selectin and activated αIIbβ3 (JON/A) expression on *SLFN14*$^{K208N/+}$ mouse platelets in response to indicated agonist stimulation. Data presented is the percentage of platelet double positive (P-Selectin and JON/A) events (mean±SEM) of n=3-6 mice per genotype per condition. Significance assessed by two-way ANOVA with Bonferroni correction for multiple comparisons.

### 4.3.8 *SLFN14*-K208N platelets display normal aggregation and secretion in response to collagen, collagen-related peptide and thrombin in light transmission aggregometry

As mentioned previously, *SLFN14* patients show defective platelet aggregation in response to protease activated-1 (PAR-1), ADP and collagen. To investigate platelet function in the K208N mouse model, light transmission aggregometry (LTA) was used. LTA is considered the gold standard for investigating platelet function, particularly in isolated platelets whereas whole blood aggregation assays may often involve interactions between different blood cells. LTA captures platelet responses from initial activation mediated shape change, followed by sustained granule release. The two main activation pathways of platelet aggregation are through G protein-coupled receptors (G-PCR) and ITAM/receptor tyrosine kinases, stimulated in this model by thrombin, collagen and collagen-related peptide (CRP) respectively. A clear dose response was observed in response to thrombin (Figure 4.9Ai, ii and iii). The PAR-1 defect seen in patients (which signals using the G-PCR pathway) is not mirrored in these mice using thrombin. Collagen and CRP both signal using the ITAM/receptor tyrosine kinase pathway and although dose response reactions were observed, these were not different between genotypes (Figure 4.9B and C). Final platelet aggregation was measured 6 minutes after agonist addition and no statistical differences were observed in response to these three agonists between genotypes (Figure 4.9D). Therefore, SLFN14-K208N mice do not show the same platelet aggregation defects experienced by SLFN14 patients with the same mutation. Dense granule release was indirectly measured by luminescence produced by activated luciferase in the presence of ATP. No differences in ATP release were identified between genotypes in response to any of the agonists tested (Figure 4.9E).

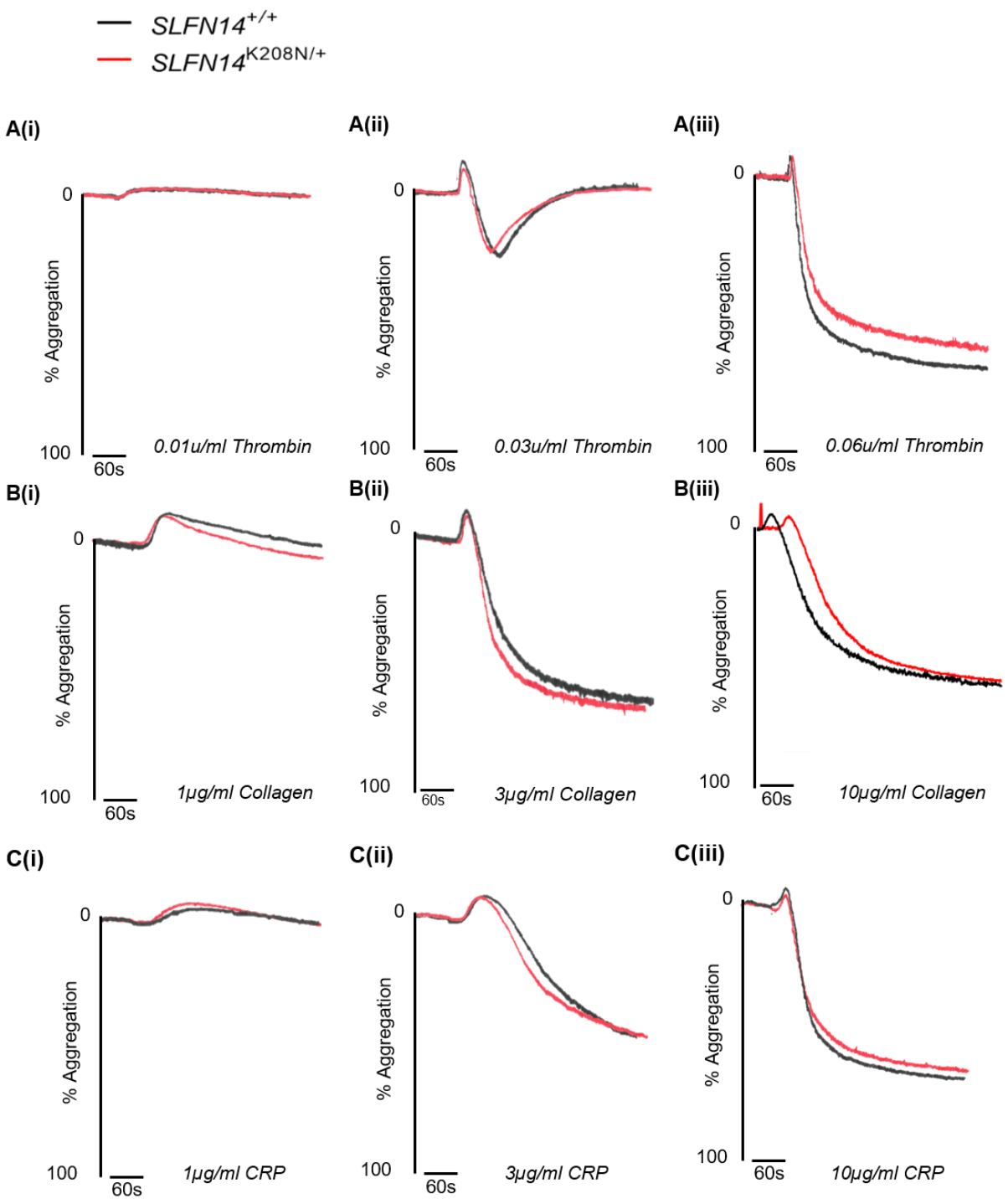
SLFN14+/+
SLFN14K208N/+
A(i)
A(ii)
A(iii)
0
100
% Aggregation
60s
0.01u/ml Thrombin
0.03u/ml Thrombin
0.06u/ml Thrombin
B(i)
B(ii)
B(iii)
1µg/ml Collagen
3µg/ml Collagen
10µg/ml Collagen
C(i)
C(ii)
C(iii)
1µg/ml CRP
3µg/ml CRP
10µg/ml CRP

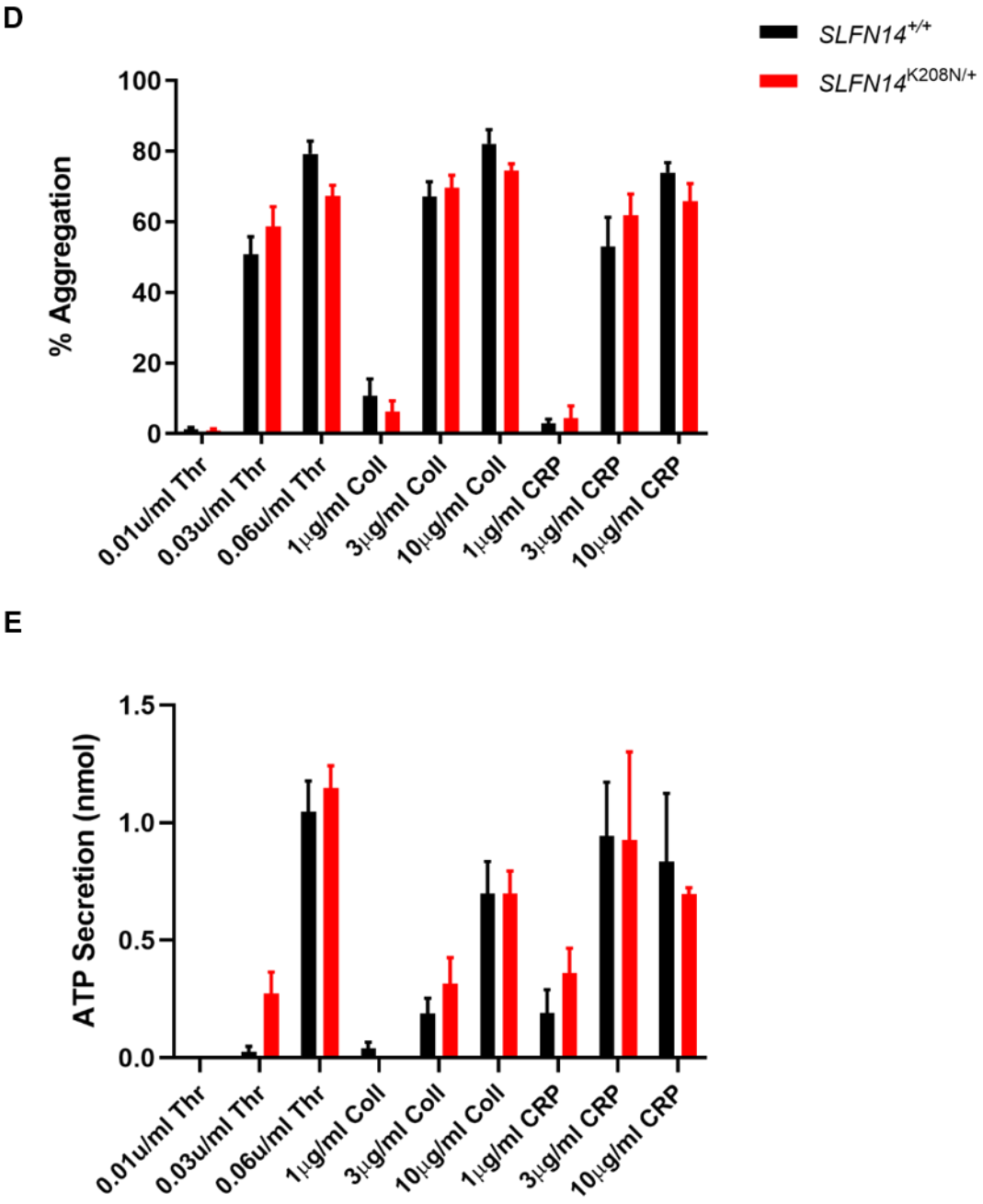


**Figure 4.9: *SLFN14*-K208N mice show normal aggregation responses to major platelet agonists**. (A) Platelet responses to thrombin at doses (i) 0.01U/ml (ii) 0.03U/ml and (iii) 0.06U/ml. (B) Platelet responses to collagen at doses (i) 1µg/ml, (ii) 3µg/ml and (iii) 10µg/ml. (C) Platelet responses to CRP at doses (i) 1µg/ml, (ii) 3µg/ml and (iii) 10µg/ml. Representative traces from n=4-14 mice per genotype per condition. (D) Percentage total aggregation was calculated for each condition. No differences were observed between genotypes. (E) ATP secretion was measured in nmol in response to each platelet agonist. No differences in secretion was observed. Data presented is mean ± SEM, n=4-14 mice per genotype per condition. Significance was measured by student's t-test with correction for multiple comparisons

### 4.3.9 *SLFN14*-K208N platelets show normal spreading on collagen and fibrinogen under resting and thrombin stimulated conditions

In addition to platelet's ability to activate and adhere to one another, haemostasis also involves adhesion to vessel walls. Upon injury, the vessel wall integrity is compromised, sub endothelial cell damage occurs and collagen and fibrinogen are exposed on the extracellular matrix (ECM). Here, it is the role of platelets to adhere to the vessel surface through GPVI, αIIbβ3 and the GP-V-IX complex, triggering platelet spreading and plug formation. Wild-type and *SLFN14*$^{K208N/+}$ washed platelets were allowed to spread on collagen and fibrinogen coated surfaces for 45 minutes. Platelets were labelled with Alexa-flour 488 conjugated phalloidin stain to visualise cytoskeleton dynamics under these different conditions (Figure 4.10A). Blinded images were used to train a machine learning assisted automated cell segmentation programme which was used to detect spread and unspread platelets. This was used to calculate area and perimeter of each platelet in each image (Figure 4.10B and C). No significant differences in mean platelet area or perimeter were identified on collagen spread platelets (Figure 4.10Bi and ii). Similarly, under basal and pre-activated conditions (presence of 0.1U/ml thrombin) area and perimeter of platelets spread on fibrinogen coverslips was not significantly different (Figure 4.10Ci and ii). Mouse platelets do not fully spread on fibrinogen unless pre-activated. As such, across both genotypes, platelet area increased, whereas perimeter reduced during spreading due to the absence of platelet membrane indentations caused by cytoskeletal rearrangement, filopodia and lamellipodia formation which form before fully spreading. In all conditions, *SLFN14*$^{K208N/+}$ platelet's area was greater than wild-types. Although this was not significantly different under spreading conditions, this increase is likely attributable to the significant difference in platelet size at resting state (from blood counting data) due to the higher immature platelet fraction observed previously using SYTO13 staining (Figure 4.4D).

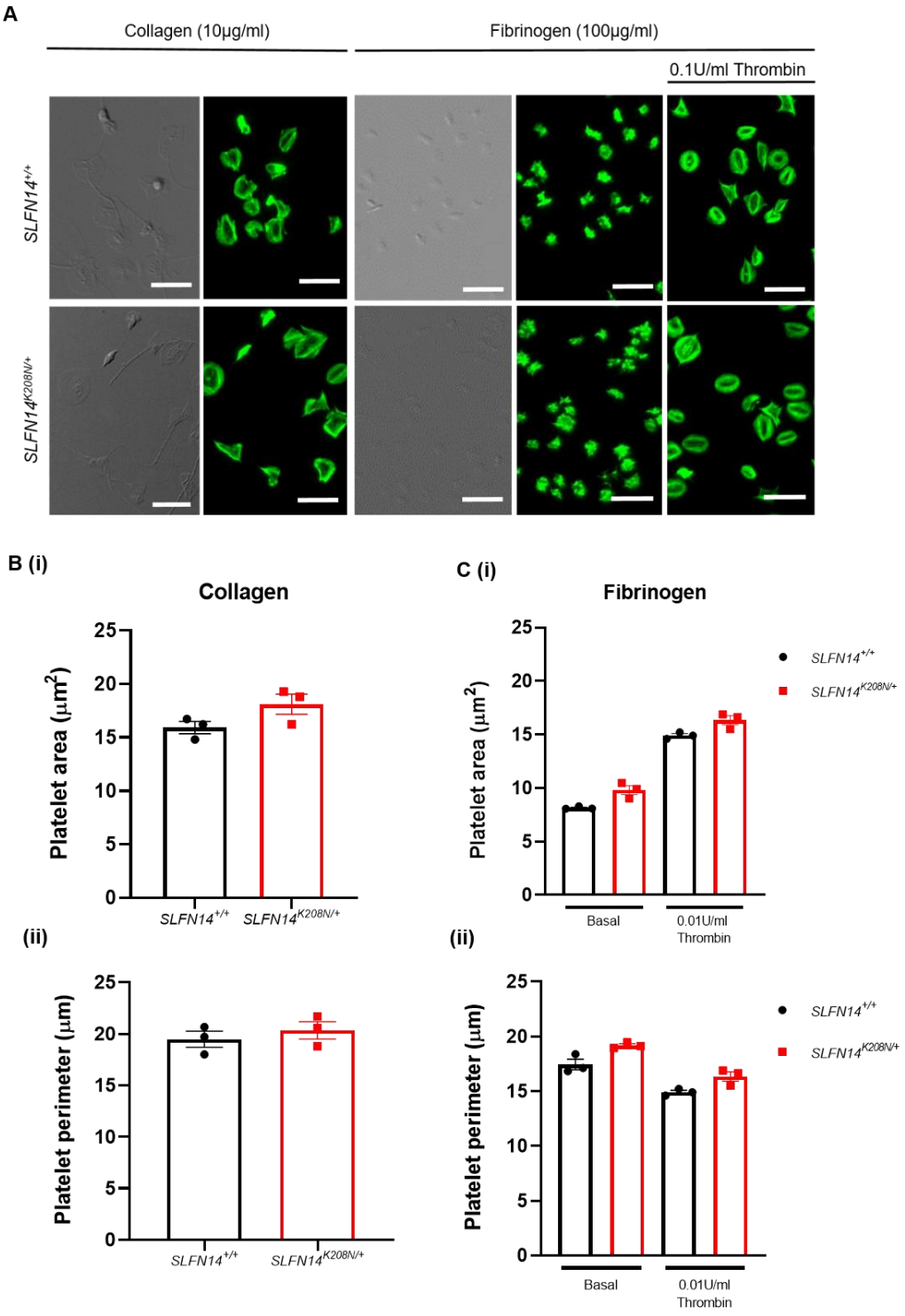


**Figure 4.10: Platelet spreading and adhesion in *SLFN14*$^{K208N/+}$ mice.** (A) Representative differential interference contrast (DIC) and fluorescent phalloidin stained *SLFN14*$^{K208N/+}$ platelets spread on collagen and fibrinogen under resting and thrombin pre-activated conditions (0.1U/ml thrombin). (B and C) Quantification of platelet spreading using a semi automated machine learning based anlaysis tool. (i) Platelet area, µm$^2$. (ii) Platelet perimeter, µm. Data presented is mean ± SEM, unpaired student's t test with Welch's correction, n=3 mice per genotype/condition.

### 4.3.10 *SLFN14*-K208N mice do not present with a bleeding phenotype

Platelet adhesion to the ECM and spreading are the first stages in maintaining haemostasis. In some cases of impaired platelet function, as observed in *SLFN14* patients, platelets are unable to adhere to the ECM, aggregate and form a clot thus presenting a bleeding phenotype. To investigate if this same bleeding phenotype was present in *SLFN14* mice, bleeding time was assessed by removing 2-3mm of tail tip and immersed in saline. The time taken for bleeding to cease was recorded. All mice bled for below 2 minutes and 30 seconds and times were not significantly different between *SLFN14*$^{K208N/+}$ and wild-types (Figure 4.11Ai). This, accompanied by aggregation and spreading data shows *SLFN14*-K208N does not affect *in vitro* platelet function in mice and does not show the same platelet defect as observed in *SLFN14* patients.

While the time for bleeding to cease was indifferent between the genotypes, the haemoglobin absorbance assay was used to measure blood loss. Using a microplate reader, a standard curve for each genotype was generated using known volumes of erythrocytes to measure haemoglobin absorbance at 575 and 550nm. This haemoglobin absorbance at both wavelengths was indifferent between genotypes indicating *SLFN14*$^{K208N/+}$ mice did not lose more blood than controls during the assay (Figure 4.11Aii).

### 4.3.11 *SLFN14*-K208N platelets show normal clot retraction

An important factor in platelet plug formation and maintenance of vessel wall integrity is the ability of platelets to trigger conversion of fibrinogen to fibrin. This process involves outside-in signalling by the platelet integrin αIIbβ3 which ultimately results in clot contraction, drawing edges of the clot together to become mechanically stable. This process is driven by a secondary wave of platelet activation and subsequent processing of prothrombin to thrombin leading to conversion of plasma fibrinogen to fibrin which forms a dense network of fibres for thrombus stabilisation (Tucker et al., 2012). Here in *SLFN14*$^{K208N/+}$ mice platelets were stimulated by a high dose of thrombin to trigger retraction. There was no visual difference

observed over the time course nor in clot weight heterozygote mice and controls suggestive that platelet outside-in signalling is functional and fibrin formation mediated by thrombin activity is not hindered by this mutation model (Figure 4.11Bi and ii).

A (i)

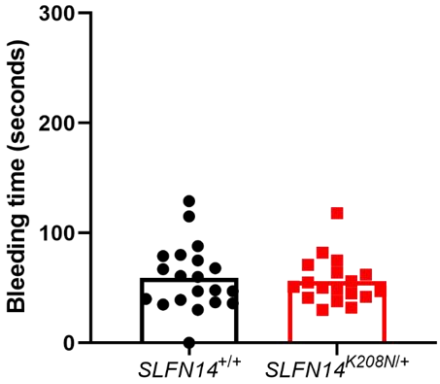


(ii)

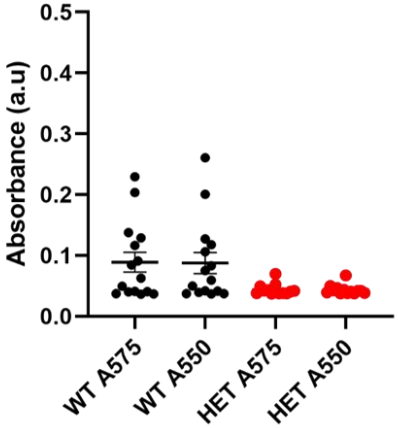


B (i)

Time (min)

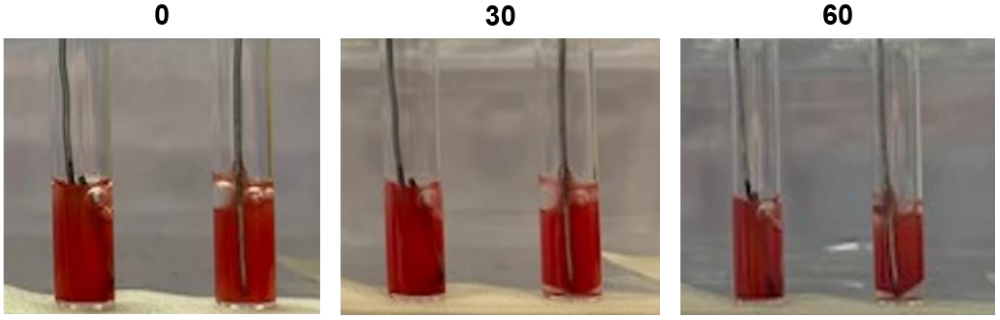


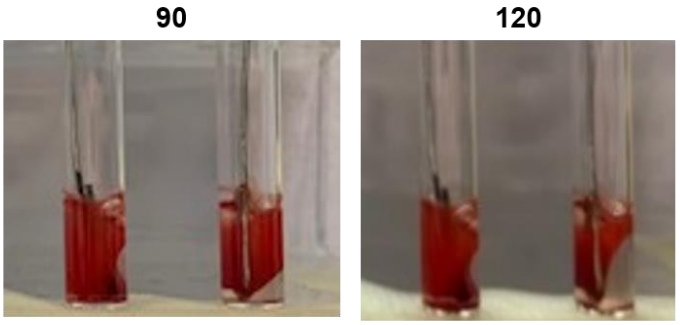


(ii)

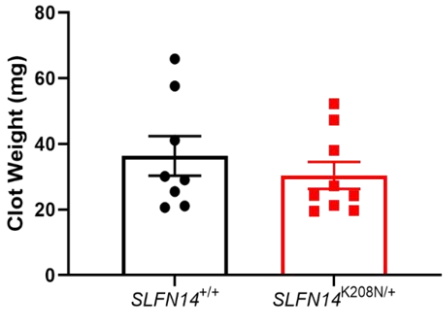

**Figure 4.11: Haemostasis and clot retraction assay in *SLFN14*$^{K208N/+}$ mice.** (A) Tail bleeding time assay. (i) 2-3mm tail was removed and mice bleeding time until first stop was measured. Data presented is mean time in seconds. (ii) Haemoglobin absorbance assay as an indication of blood volume lost during haemostsis assay. Each data point represents one animal. N=18-20 mice per genotype. (B) Clot retraction of *SLFN14*$^{K208N/+}$ mouse platelets in PRP. Clots were formed by stimulating $2x10^8$/ml platelets with 0.1U/ml thrombin and monitored over a 2 hour timecourse. (i) Representative images and (ii) final clot weight in mg. Data presented is mean±SEM, n=8-9 mice per genotype.

### 4.3.12 *SLFN14*-K208N mice have tendency to from smaller, more unstable thrombi in *in vivo* laser and ferric chloride induced injury models

The primary role of platelets is to protect and maintain vessel wall integrity and to prevent blood loss. However, heightened platelet reactivity can also be detrimental in and thrombus formation which occludes vessels can be life threatening in some conditions. Thrombus formation was assessed by laser injury of the cremaster arterioles (Figure 4.12 Ai and ii). In wild-type mice, thrombi formed within the first 15 seconds of injury with many platelets recruited to the site. Here, embolism of the thrombus occurred at a steady rate over the remaining three minutes. In contrast, in *SLFN14*$^{K208N/+}$ mice fewer platelets were recruited to the site of injury as measured by thrombus area in pixels (Figure 4.12Aiii) and were embolised substantially quicker, although the thrombus did form at a similar rate to controls, (Figure 4.12Ai and ii). Given the normal *in vitro* platelet function and *in vivo* haemostatic response, this reduced thrombus formation is likely due to the contributions of abnormal erythrocytes which are known to promote thrombus stability at venous shear rates.

At arterial shear in the carotid artery, the $FeCl_3$ model of thrombus formation did not show such significance. In both mice occlusive thrombi did form although in *SLFN14*$^{K208N/+}$ mice this took progressively longer with some embolization occurring between 10 and 12 minutes (Figure 4.12 Bi, ii and iii). Arterial thrombi are known to be platelet rich and erythrocytes do not form an integral part to their formation. This suggests, thrombus formation in the arteries is not significantly impaired in this model but all K208N thrombi do have a tendency to embolise and generally fewer platelets are recruited to the site of injury.

### 4.3.13 *SLFN14*-K208N platelets display minor functional differences under *ex vivo* flow conditions

*In vitro* platelet aggregation and spreading assays allow detailed analysis of individual platelet signalling pathways. However, their physiological relevance in terms of platelet behaviour with other blood cells may be questioned. As shown previously by *in vivo*

thrombosis data, shear rates can form an integral part of platelet behaviour and response to various activation stimuli. *Ex vivo* analysis by whole blood flow adhesion can capture the interactions of platelets with other blood cells under flow conditions similar to that in the vascular system. Glass coverslips were coated with Horm collagen, human collagen type III and fibrinogen to assess GPVI, α2β1 and αIIbβ3 function. Here, whole blood (thrombin inhibited by the addition of PPACK) was flowed over each surface for 3.5 minutes at either 1000/s or 1700/s (Figure 4.13, Figure 4.14, Figure 4.15). These shear rates correspond to venous and arterial pressures in mice respectively (Panteleev et al., 2021). Brightfield images were obtained in addition to fluorescent images where platelets were stained for P-selectin, JON/A and phosphatidylserine (PS) (Figure 4.13A, Figure 4.14A, Figure 4.15A). These experiments and analysis was performed by Natalie Jooss and in collaboration with Johan Heemskerk of Maastricht University, Netherlands.

Under both shear rates and all surfaces, no significant differences were observed between the mean surface area coverage of platelets between genotypes (Figure 4.13Bi, Figure 4.14Bi and Figure 4.15Bi). However, as determined by the multi-layered score, *SLFN14*$^{K208N/+}$ aggregates were significantly larger than wild-types on human collagen type III however the explanation for this remains unclear (Figure 4.14Bv). Activation markers P-selectin and JON/A were expressed at normal levels under all conditions however platelet PS exposure was slightly increased in *SLFN14*$^{K208N/+}$ mice across all surfaces. This difference may be attributed slight pre-activation caused by experimental delay before sampling or differences between experiment days. Mean platelet coverage on the fibrinogen surface was largely variable (Figure 4.15Bi). In addition to this, although fairly consistent between genotypes, P-selectin, JON/A and PS exposure were very low. Fibrinogen is a substantially weaker activation surface than horm and human collagen thus meaning aggregates differ in size and the strength of expression markers is much reduced in comparison (Figure 4.15B ii and iii).

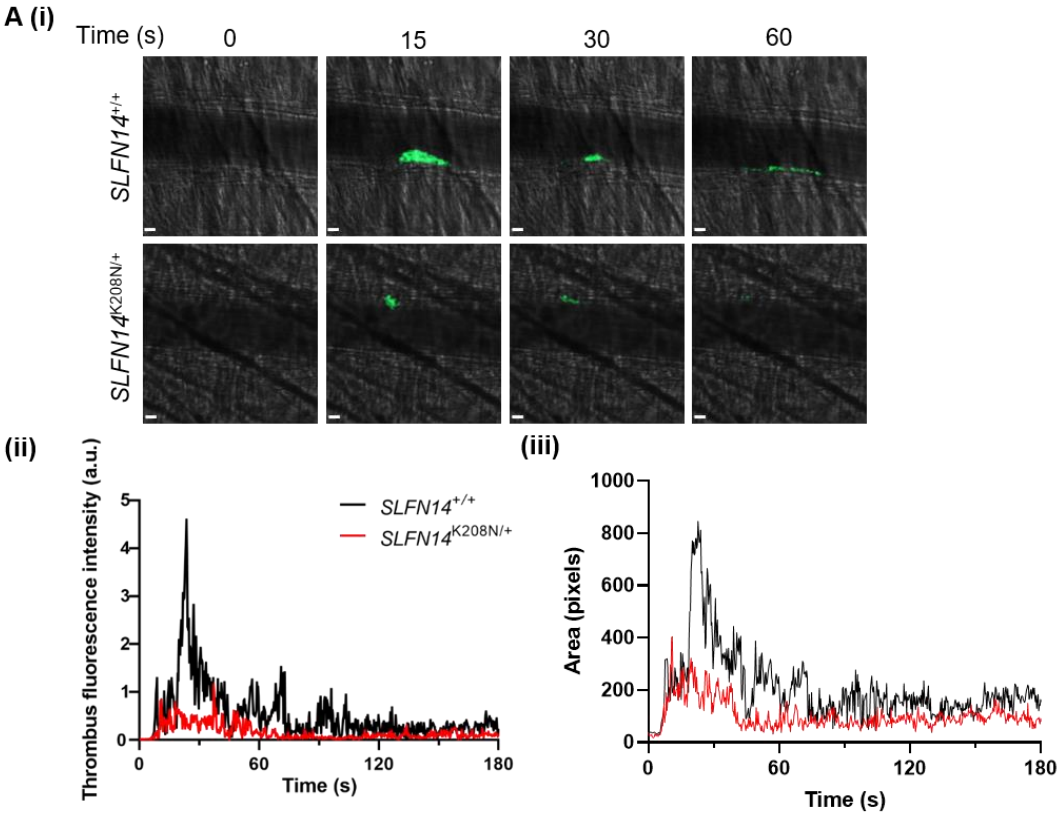
A (i)
Time (s)
0
15
30
60
SLFN14+/+
SLFN14K208N/+
(ii)
Thrombus fluorescence intensity (a.u.)
SLFN14+/+
SLFN14K208N/+
Time (s)
(iii)
Area (pixels)
Time (s)

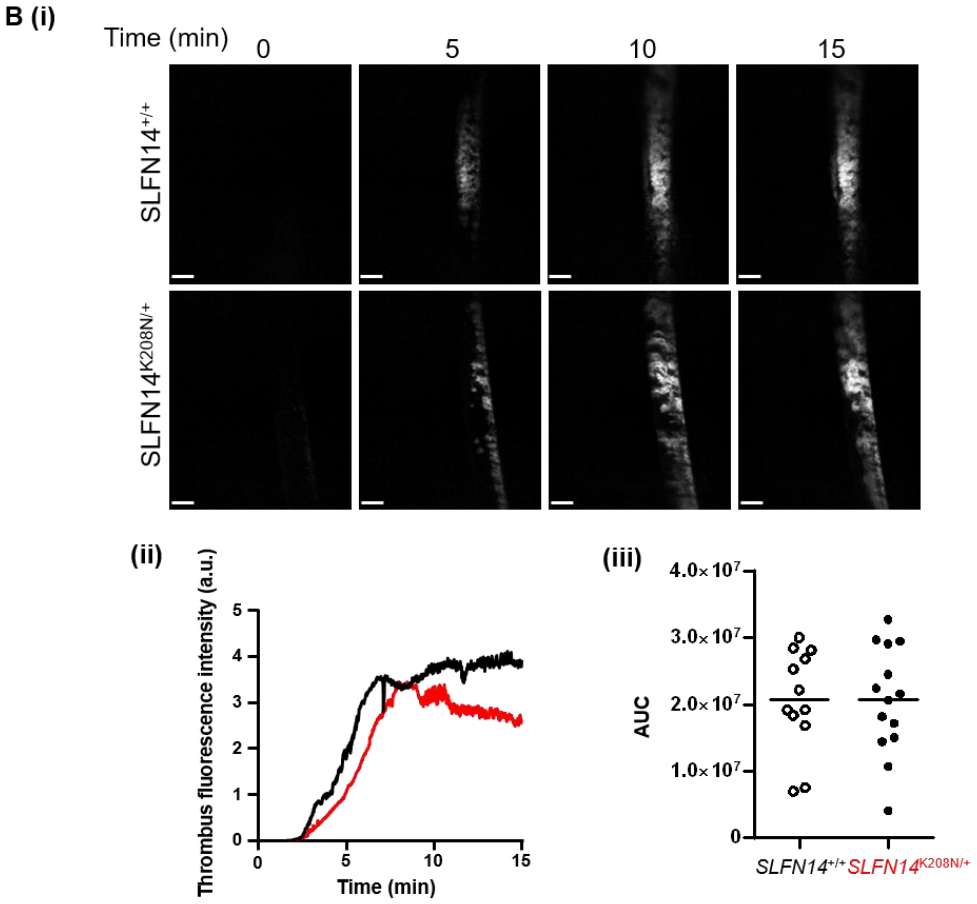
B (i)
Time (min)
0
5
10
15
SLFN14+/+
SLFN14K208N/+
(ii)
Thrombus fluorescence intensity (a.u.)
Time (min)
(iii)
AUC
4.0×10^7
3.0×10^7
2.0×10^7
1.0×10^7
0
SLFN14+/+
SLFN14K208N/+

**Figure 4.12: Functional role of SLFN14$^{K208N/+}$ in *in vivo* thrombosis.** (A) Laser induced thrombus formation in vivo. (i) Representative composite brightfield and fluorescence images of thrombus formation. Mice were injected with anti-GPIbβ DyLight488 (0.1µg/g body weight). Arterioles of the cremaster muscle were subsequently injured by laser and thrombi fluorescence measured, scale bar 10µm. (ii) Curves represent median integrated thrombus formation fluorescence intensity in arbitrary units (a.u.) for 31-32 injuries in 4 mice per genotype. (iii) Curves represent median integrated thrombus formation and area in pixels of the thrombus. This was not statistically significant. (B) Ferric chloride-induced thrombus formation. Mice were injected with DyLight488-conjugated anti-GPIbβ antibody (0.1 µg/g body weight) and carotid artery subsequently injured with 10% ferric chloride solution for 3 minutes. (i) Representative fluorescence images of platelets (GPIbβ). Scale bar 200 µm. (ii) Curves represent median integrated thrombus fluorescence in arbitrary units (a.u.), and (iii) area under the curve of the integrated fluorescence density in aribitrary units (a.u). Data is mean, n=11-12 mice per genotype.

Horm

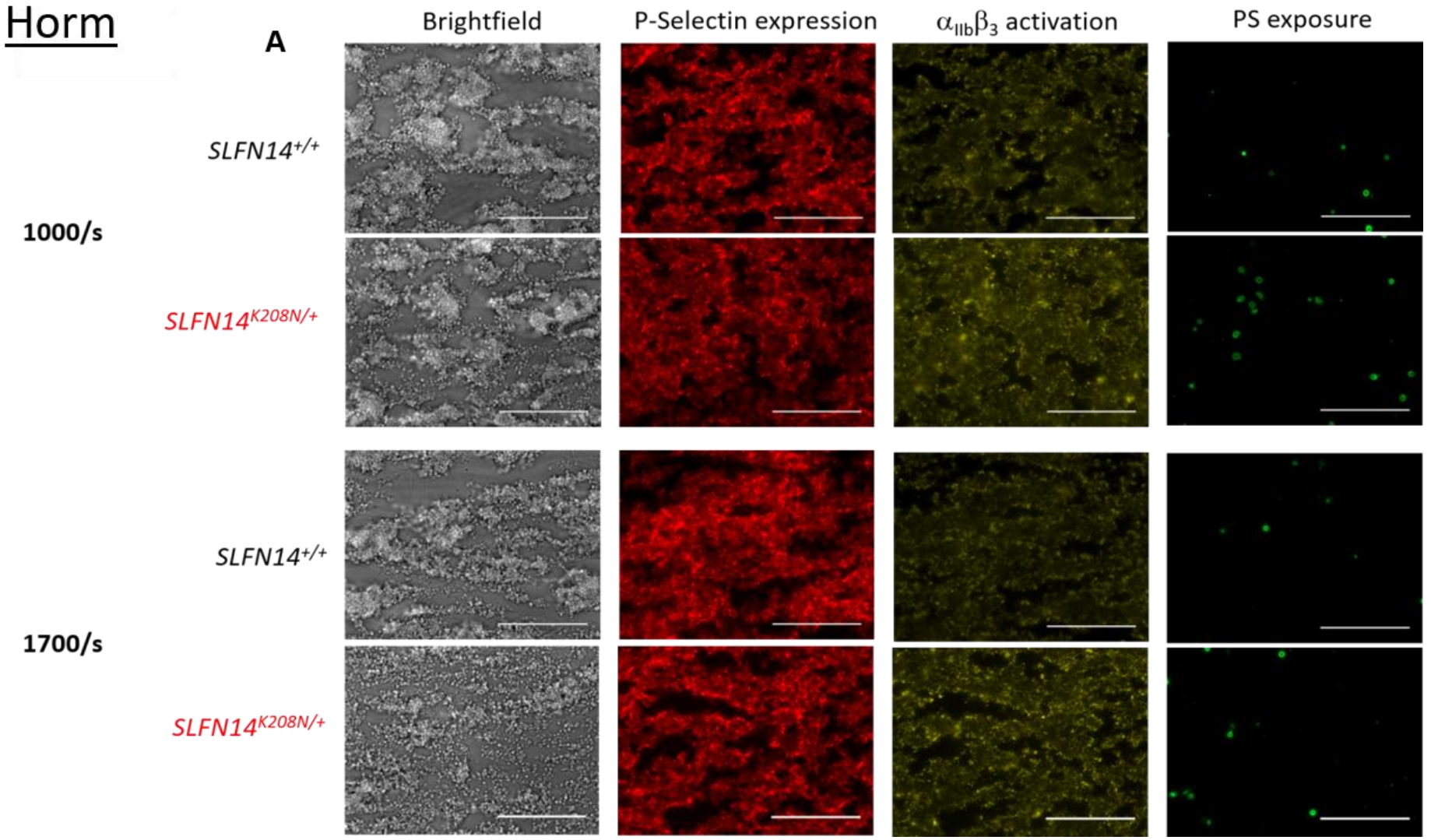
A
Brightfield
P-Selectin expression
$\alpha_{IIb}\beta_3$ activation
PS exposure
SLFN14+/+
1000/s
SLFN14K208N/+
SLFN14+/+
1700/s
SLFN14K208N/+

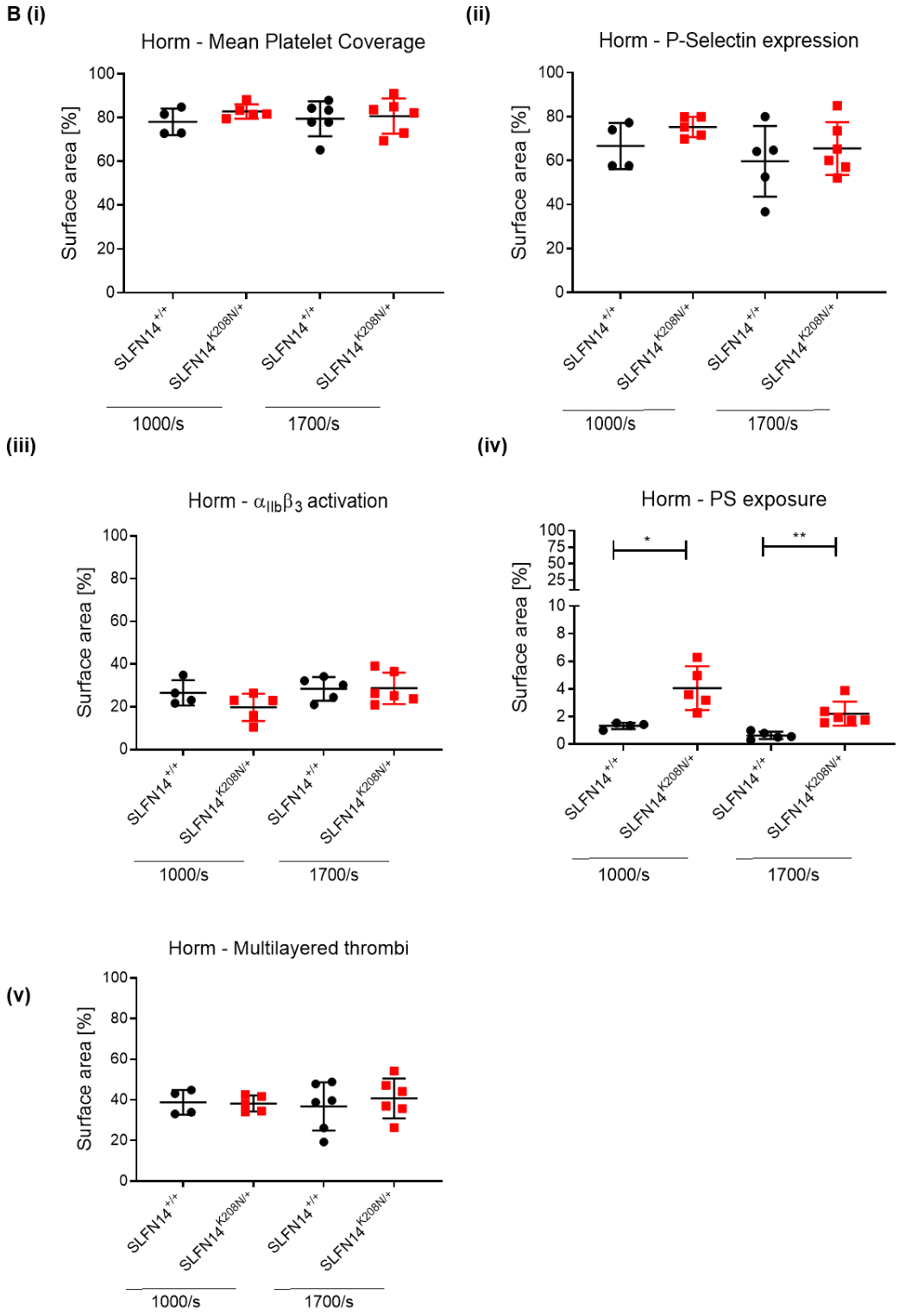


**Figure 4.13: Adhesion and activation of platelets under flow conditions on Horm collagen.** Heparin-PPACK anticoagulated blood was flown over Horm collagen coated surfaces for 3.5 minutes at 100/s and 1700/s shear rates. (A) Representative brightfield and fluorescent images. (B) Mean platelet area coverage of adhered platelets was quantified from brightfield images. Surface area coverage of P-Selectin, JON/A and PS exposure were quantified from fluorescence images (JON/A – PE, P-Selectin – FITC, Annexin V – alexa fluor 647). N= 4-6 mice per genotype per condition, unpaired t-test with Mann Whitney correction. * $p<0.05$, ** $p<0.005$. Experiments and analysis performed by Natalie Jooss.

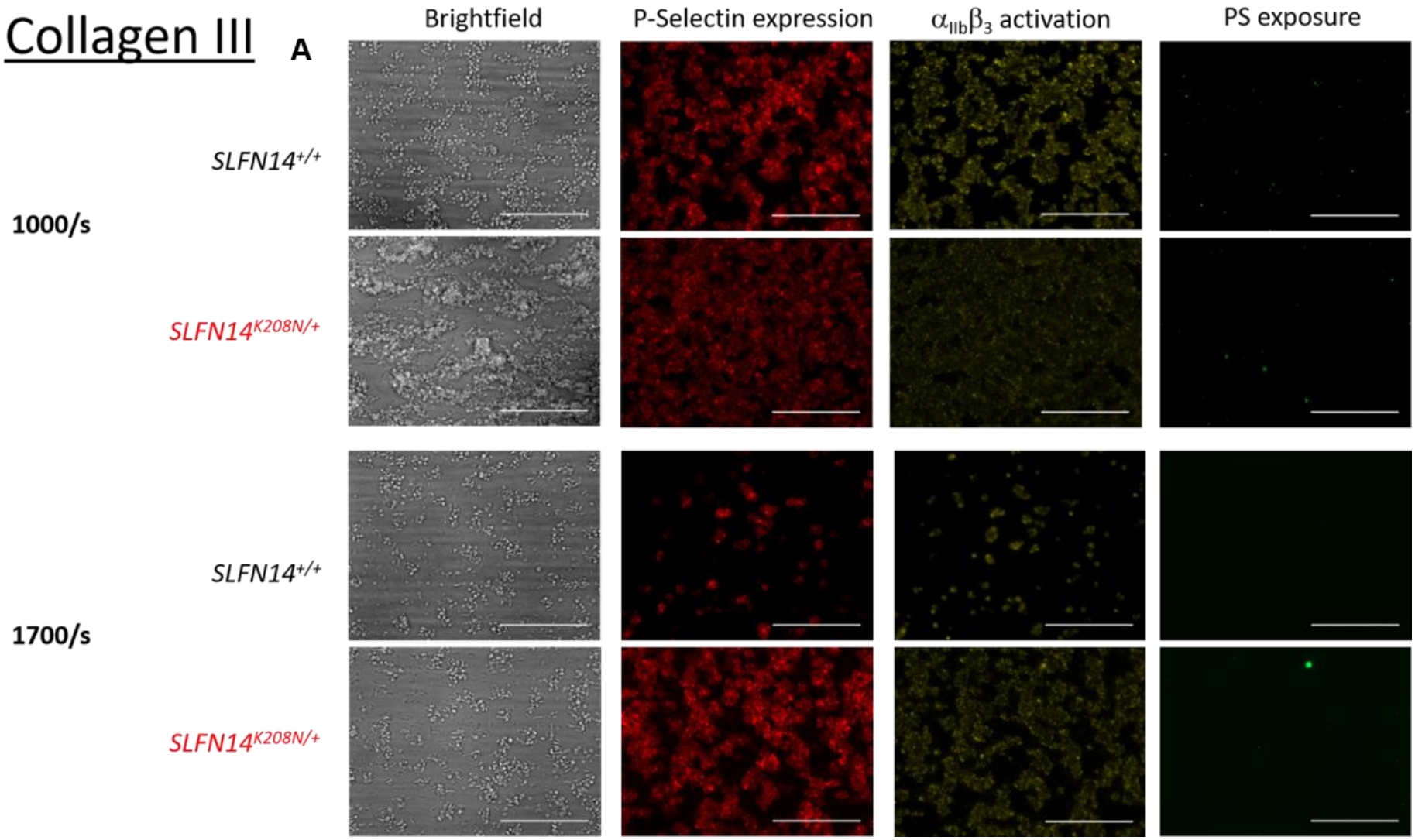
Collagen III
A
Brightfield
P-Selectin expression
αIIbβ3 activation
PS exposure
SLFN14+/+
1000/s
SLFN14K208N/+
SLFN14+/+
1700/s
SLFN14K208N/+

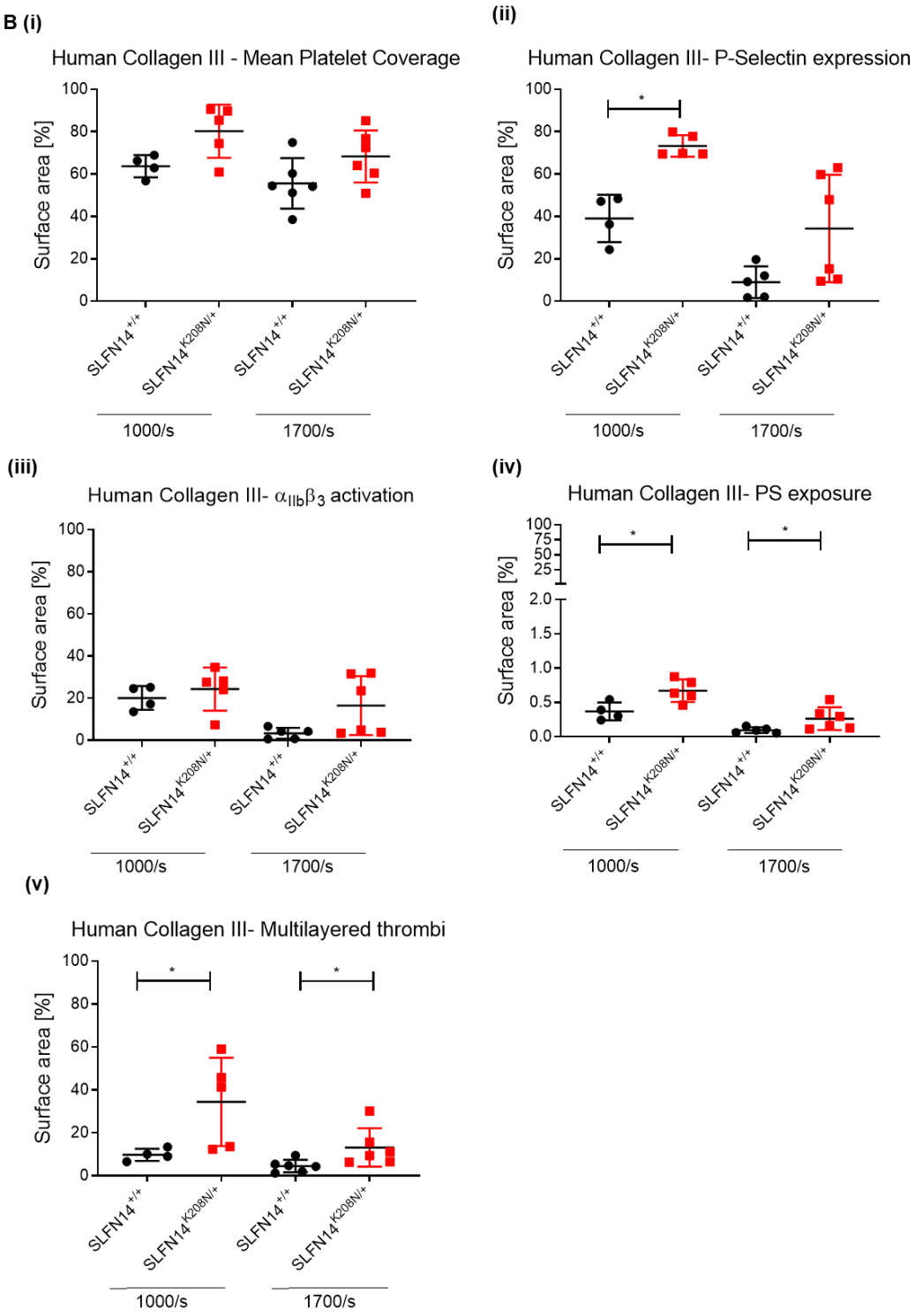


**Figure 4.14: Adhesion and activation of platelets under flow conditions on Human collagen type III.** Heparin-PPACK anticoagulated blood was flown over human collagen type III coated surfaces for 3.5 minutes at 100/s and 1700/s shear rates. (A) Representative brightfield and fluorescent images. (B) Mean platelet area coverage of adhered platelets was quantified from brightfield images. Surface area coverage of P-Selectin, JON/A and PS exposure were quantified from fluorescence images (JON/A – PE, P-Selectin – FITC, Annexin V – alexa fluor 647). N= 4-6 mice per genotype per condition, unpaired t-test with Mann Whitney correction. * $p<0.05$. Experiments and analysis performed by Natalie Jooss.

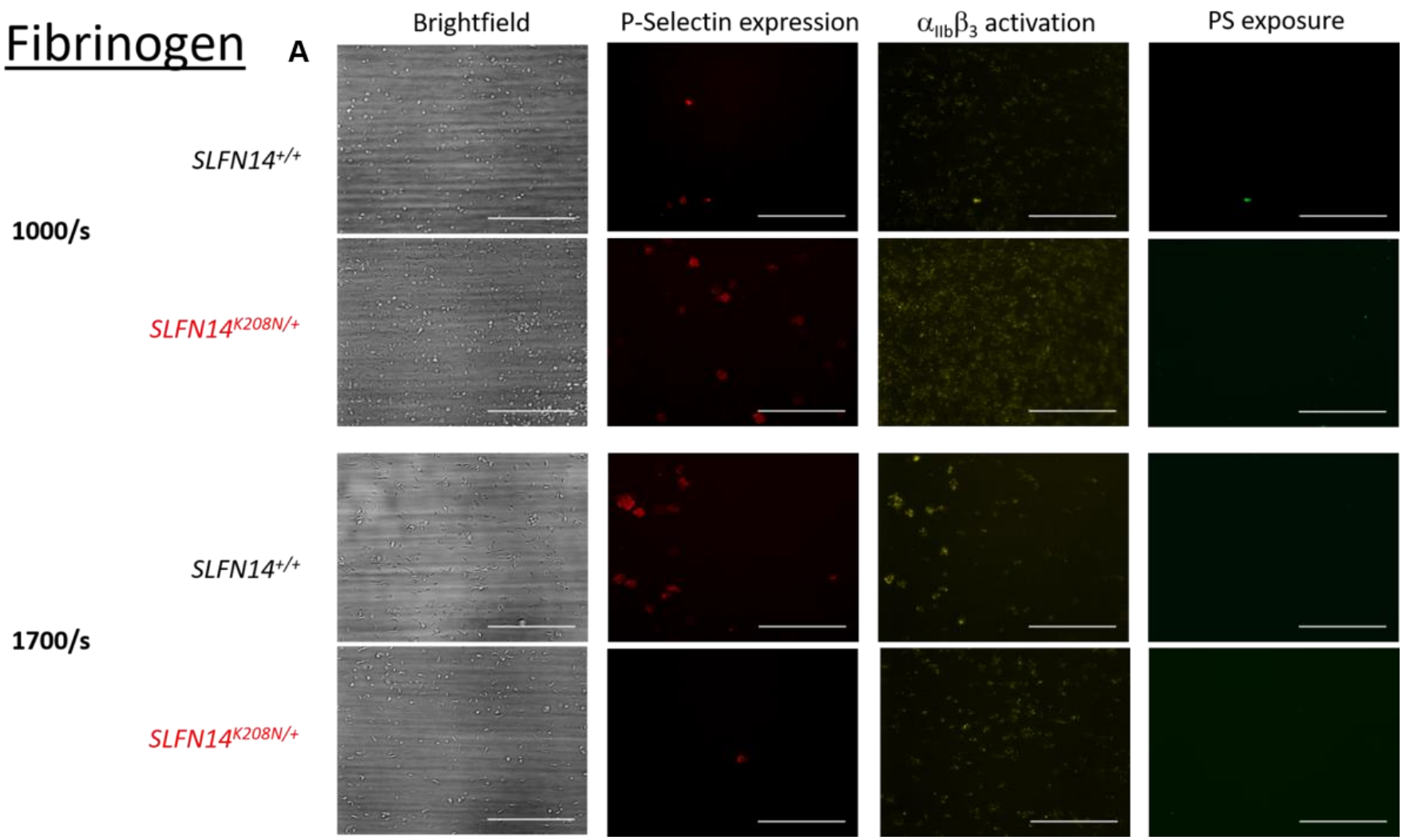
Fibrinogen
A
Brightfield
P-Selectin expression
αIIbβ3 activation
PS exposure
SLFN14+/+
1000/s
SLFN14K208N/+
SLFN14+/+
1700/s
SLFN14K208N/+

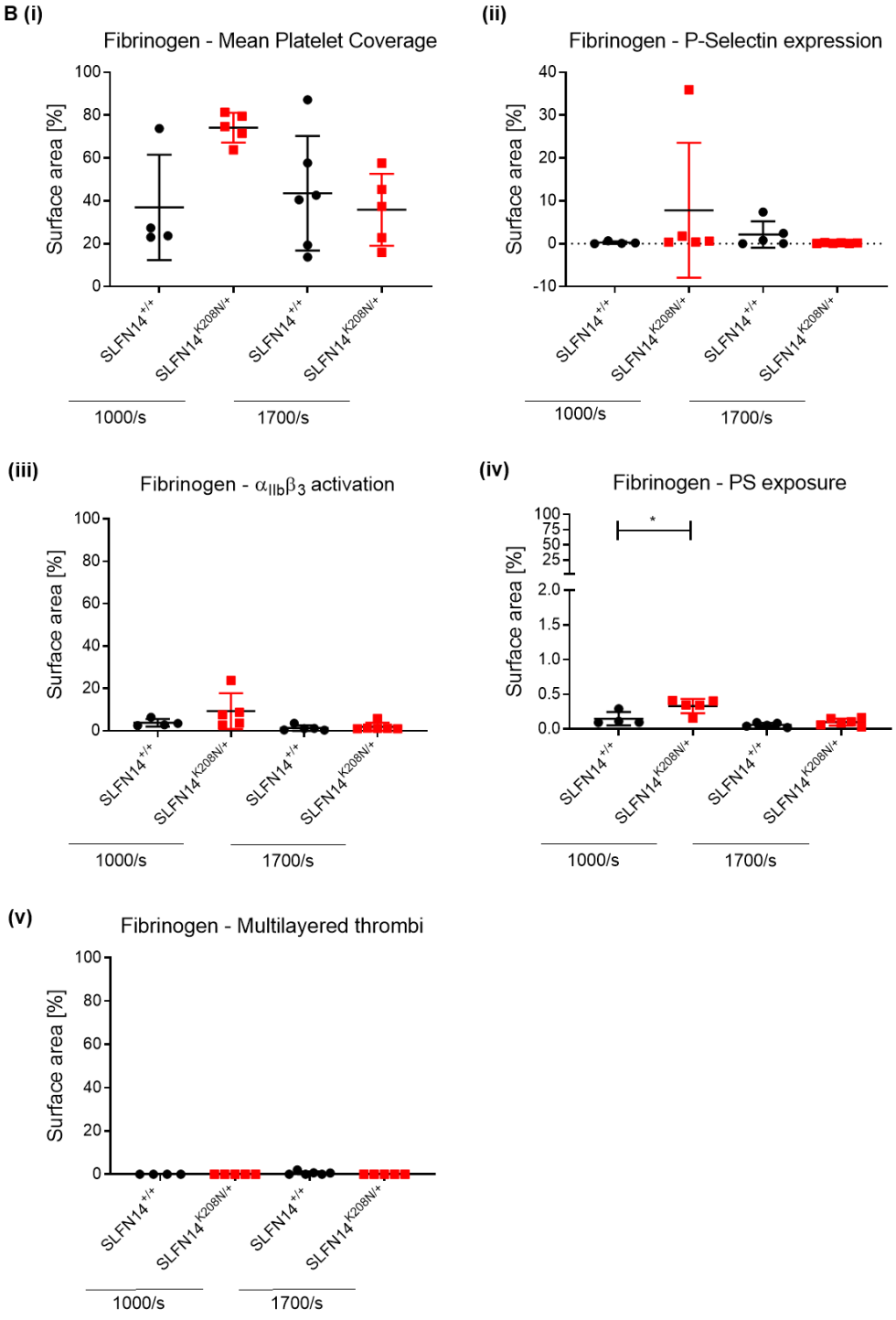


**Figure 4.15: Adhesion and activation of platelets under flow conditions on fibrinogen.** Heparin-PPACK anticoagulated blood was flown over fibrinogen coated surfaces for 3.5 minutes at 100/s and 1700/s shear rates. (A) Representative brightfield and fluorescent images. (B) Mean platelet area coverage of adhered platelets was quantified from brightfield images. Surface area coverage of P-Selectin, JON/A and PS exposure were quantified from fluorescence images (JON/A – PE, P-Selectin – FITC, Annexin V – alexa fluor 647). N= 4-6 mice per genotype per condition, unpaired t-test with Mann Whitney correction. * $p<0.05$. Experiments and analysis performed by Natalie Jooss.

## 4.4 Discussion

Within this chapter, in depth phenotyping assays reveal that platelet function is largely retained in these mice. The K208N mutation is inherited in a heterozygote manner, the same as in the *SLFN14* patients suggesting homozygote *SLFN14* mutations are lethal in both mouse and humans with the primary explanation for this in mice being a severe anaemia. The exact cause for the lack of homozygous *SLFN14* patients is not yet known, however it may be plausible to speculate the platelet defect or bleeding tendency is so severe in these patients, miscarriage may occur in a similar way to that observed in patients with inherited platelet disorders and menorrhagia (Lowe et al., 2019, Bick, 2000). In mice, the cause for this anaemia is not currently clear, although blood cell formation and haematopoiesis analysis in the following chapter may provide some evidence for this. At embryonic days 12.5 and 14.5, K208N mouse embryos were paler than wild-type controls, likely due to the severe anaemia making blood vessels much less clear. Investigating embryos at earlier time points or using *in vitro* expansion of foetal liver derived HSCs, may give insight into the emergence of red blood cell defects earlier in development and potential interactions between SLFN14 and other regulatory proteins in erythropoiesis (Baron et al., 2013).The extent of this anaemic phenotype has not yet been explored but using blood gas analysis would help to explore the reduction in oxygen carrying capacity of deformed erythrocytes. Measuring plasma EPO levels, particularly in the kidneys where EPO is generated, may reveal differences in EPO production between K208N mice and wild-types or highlight a disrupted EPO feedback loop in erythropoiesis.

The platelet phenotype in these mice is largely retained and does not present similar defects as observed in patient studies. I*n vitro* assays involving isolated platelets and *in vivo* haemostasis and thrombosis assays in whole blood do not show either impaired or amplified platelet function in response to various stimuli. The mechanism for significant increase in IPF is unclear given normal megakaryocyte production in the bone marrow although the

extramedullary haematopoiesis in the spleen may provide some explanation for this (detailed further in chapter 5). A higher IPF is often associated with hypersensitivity in platelets, presenting a higher risk of spontaneous thrombosis and cardiovascular events in patients (Grove et al., 2009). In this model, platelets were not more responsive or procoagulant suggesting overall function is not altered by circulating immature platelets. In contrast to *SLFN14* patients, *SLFN14*$^{K208N/+}$ mice did not display a bleeding phenotype by the bleeding time assay. Deviation in *in vivo* thrombosis was observed in the ferric chloride model whereby stable thrombus formation is dependent on interactions between platelets, erythrocytes and the endothelium. Erythrocytes are the primary determinant of blood rheology and promote platelet margination, increasing their concentration near the endothelium to enable rapid formation of thrombi in response to vessel damage (Byrnes and Wolberg, 2017, Turitto and Baumgartner, 1975, Turitto and Weiss, 1980). Erythrocytes are known to have significant contribution to thrombus stability at venous shear rates and indeed reduced thrombus formation has been shown previously in models of anaemia suggesting it is in fact the abnormal erythrocytes in this instance which cause the thrombosis defect (Klatt et al., 2018). In addition, it may also present the hypothesis that the role of platelets is to hold erythrocytes at the site of injury, but anaemia and poikilocytosis in this model, means platelets are not secure at the endothelium and results in embolization. The same theory applies at arterial shear rates, with fewer platelets recruited and held at the site of injury as shown by faster embolization than wild-type controls.

The flow adhesion model was used to uncover mechanisms for these differences in platelet function between *in vitro* and *in vivo* models. Horm collagen (equine tendon collagen), human collagen type III and fibrinogen were all used in flow adhesion assays to trigger the GPVI, α2β1 and αIIbβ3 receptors and signalling pathways. These are the most common substances exposed on the endothelial matrix upon vessel injury. There was slight increase in the PS exposure on platelets in response to all surfaces at both shear rates but this may

have arisen from slight pre-activation due to delays in experimentation and variation across the two experiment days. This slight pre-activation was not enough to trigger enhanced granule release (P-selectin) or significantly raise activated integrin αIIbβ3 on the platelet surface. Comparing the results of flow assays with *in vivo* thrombosis assays highlights that platelet function is retained. Platelets remain fully functional in their ability to adhere to and spread on endothelial surfaces but it is the embolization process, potentially mediated by erythrocytes which is key in this model.

Given the significant differences in platelet and erythrocyte characteristics of *SLFN14* mice compared to patients, it is clear the same mutation acts in a species dependent manner affecting megakaryocytes and platelets in humans but erythrocytes in mice. The question then arises as to how *SLFN14,* as an endoribonuclease, mediates these changes depending on species and where within haematopoiesis do these changes manifest which ultimately affect the production and function of terminally differentiated blood cells.

# Chapter 5

*SLFN14*-K208N as an endoribonuclease in haematopoiesis, platelet and erythroid lineage commitment

# Chapter 5 – *SLFN14-K208N* as an endoribonuclease in haematopoiesis, platelet and erythroid lineage commitment

## 5.1 Aim

The aim of this chapter was to investigate the effect of the *SLFN14*-K208N mutation with particular interest in haematopoiesis and blood cell differentiation. As detailed in the previous chapter, *SLFN14*$^{K208N/+}$ mice present with significant differences in erythrocyte and platelet populations within the circulation, leading to altered platelet and red blood cell function. In this chapter bone marrow progenitors specific to MK and erythroid lineages were studied to distinguish how the K208N mutation can cause these differences in cell number and function. The primary site of blood cell production and maturation is the bone marrow, hence this was the primary location for studying haematopoietic progenitors but additionally, due to splenomegaly in these mice, it was anticipated this may also be contributing to haematopoiesis. In parallel to this, it has previously been reported by Fletcher et al that *SLFN14* is an endoribonuclease. Here, *SLFN14's* endoribonucleolytic properties were explored with regards to haematopoiesis and stem cell differentiation.

The main hypothesis for this chapter was that *SLFN14* mediates haematopoiesis, particularly in MK and erythroid lineages. It was anticipated that *SLFN14* may regulate critical coding RNAs or TFs involved in haematopoiesis and as such mutations within *SLFN14* can cause defective cell production and function directly involved in thrombosis and haemostasis.

## 5.2 Introduction

Haematopoiesis is the process of blood cell production from progenitor cells in the bone marrow. All blood cells are produced from HSCs which are pluripotent stem cells, capable of differentiation into any cell lineage, but predominantly determined by a series of cytokines and TFs specific to the desired lineage. The precise progression of differentiation in recent years is very much a topic of discussion in the field. The classical hierarchal structure of haematopoiesis clearly illustrated identified stages whereby cells differentiate in a stepwise

fashion. Now, with advances in technologies especially single cell sequencing, and the identification of numerous cell signatures, haematopoiesis is seen to be much more of a continuous differentiation process, whereby cells can bypass intermediate steps (Zhang et al., 2018). Haematopoietic diseases such as inherited thrombocytopenia and anaemia are often caused by defects in TFs early in haematopoiesis (Lu et al., 2018). In some cases, these underlying defects can cause differentiation bias toward certain lineages (Xavier-Ferrucio et al., 2019). In addition, errors arising in haematopoiesis may impair the function of terminally differentiated cells, such as that in *GFI1B* mutations and associated Grey Platelet Syndrome. Genetic variations in *GFI1B* results in complete absence of platelet α-granules and subsequently platelet dysfunction and severe bleeding (Stevenson et al., 2013a). GFI1B, like many TFs, is expressed early in haematopoiesis meaning such variants and platelet dysfunction is determined at the early stages of megakaryopoiesis (Möröy et al., 2015). Similarly in the erythroid lineage, severe anaemia can arise due to mutations in the EPOr rendering cells hyposensitive to EPO stimulated proliferation in erythropoiesis (Watowich et al., 1999). MKs and erythroid cells are closely related, sharing most TFs in lineage development (Zhu and Emerson, 2002). Therefore, highlighting where in haematopoiesis *SLFN14* can affect lineage commitment is critical.

SLFN14 acts as an endoribonuclease, although there is very minimal literature about the function of endoribonucleases. Generally, *SLFNs* are reported in relation to mediating cellular development, replication and degradation processes (Schwarz et al., 1998, Song et al., 2018, Puck et al., 2015, Okamoto et al., 2021). This suggests, *SLFN14* plays a pivotal role in haematopoiesis and may be responsible for mediating lineage bias with regard to MK and erythroid lineages.

## 5.3 Results

### 5.3.1 *SLFN14*-K208N mice display normal megakaryocytes in the bone marrow

Although platelet counts in *SLFN14*$^{K208N/+}$ mice were unchanged, there was a slight increase in platelet size which was due to slightly increased IPF. This often arises due to improper platelet formation or premature proplatelet release into the circulation and in some instances 'young' platelets are hyper-reactive in the circulation which leads to spontaneous thrombosis. To assess thrombopoiesis, bone marrow sections were stained with H&E histology stain and MKs were counted. *SLFN14*$^{K208N/+}$ MKs were comparable in appearance from wild-types showing characteristic polyploid nucleus and large cytoplasmic region (Figure 5.1A). This was further quantified by flow cytometry and no differences were observed in MK number in the bone marrow suggesting platelet production and thrombopoiesis is normal in this model (Figure 5.1Bi and ii). As seen from *in vitro* platelet function assays, K208N platelets did not appear to be more reactive than controls and mice were healthy with no evidence of increased thrombosis as a result of increased IPF *SLFN14*-K208N erythroid progenitors, which are largely indifferent from controls.

### 5.3.2 *SLFN14*-K208N mice display normal proportions of erythroid progenitors in the bone marrow

To identify erythroid progenitors in the bone marrow, CD71 and Ter119 markers were used (Figure 5.2A). ProEs are the largest erythroid progenitors in the bone marrow, and here detected by CD71 and Ter119 double stained events. There was no difference in the number of ProEs in the bone marrow of *SLFN14*$^{K208N/+}$ mice (Figure 5.2Bi). Erythroid maturation can be measured by progressive loss of CD71 expression. Ter119$^{hi}$ gated cells are erythroid progenitors committed to the erythroid lineage which are further segregated by size using forward scatter. As observed in Figure 5.2Bii there is a tendency for more Ter119$^{hi}$ cells in the bone marrow. When Ter119hi cells are segregated by size, three erythrocyte populations are observed: EryA are the largest of these erythroid committed progenitor cells most

prevalent in the bone marrow, EryB are of intermediate size, smaller than their EryA progenitors and maturing towards fully differentiated EryC cells (Figure 5.2Biii). EryC cells are the most mature erythrocytes, hence very few are detected in the bone marrow itself (Figure 5.2Biii). A slight increase in the proportion of EryB cells was observed although this did not reach significance (Figure 5.2Biii). Perhaps most interesting is the distribution of EryB cells within *SLFN14*$^{K208N/+}$ bone marrow. Cells within this gate show a 'spread' distribution towards the EryC boundary (Figure 5.2A).

### 5.3.3 *SLFN14*-K208N bone marrow contains higher proportions of MEPs

MKs and erythroid progenitors arise from a common progenitor, the Megakaryocyte Erythroid Progenitor (MEP) (Figure 5.3A). A very small population of MEPs were detected in the bone marrow using CD71 and CD41, markers common to both subsequent lineages as shown previously by Psaila et al 2016 (Figure 5.3Bi) (Psaila et al., 2016). MEPS are difficult to detect *in situ* but here there was a slight increase in the proportion of MEPs in *SLFN14*$^{K208N/+}$ bone marrow, however this did not reach significance (Figure 5.3Bii). In addition, there was approximately 50% increase in single CD71 positive cells in this panel, suggestive that *SLFN14*$^{K208N/+}$ MEPs have a more prevalent erythroid signature and potential preference to erythroid differentiation (Figure 5.3Bi).

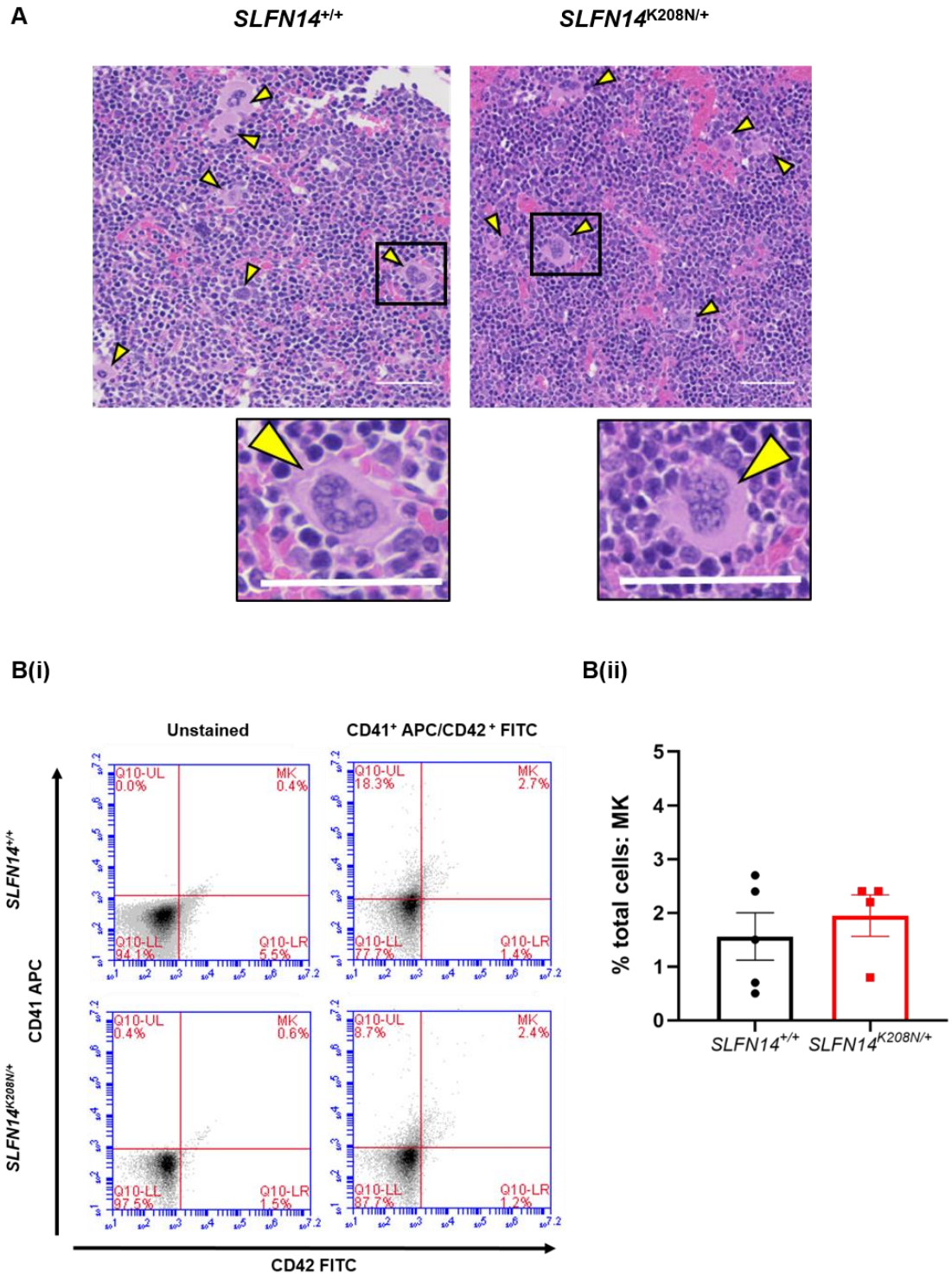


**Figure 5.1: Proportion of megakaryocytes in the bone marrow of *SLFN14*-K208N mice was consistent with wild-types.** (A) Representative images of H&E stained femur sections from SLFN14$^{+/+}$ and SLFN14$^{K208N/+}$ mice. Scale bar 50µm. (B) Flow cytometry quantification of MKs in bone marrow. (i) Whole bone marrow was stained with CD41 and CD42 antibodies. MKs were double positive events. (ii) Quantification of MKs in whole bone marrow. Figures shown as percentage of total cells CD41/CD42 double positive. No difference was observed in proportion of MKs in the bone marrow. Data presented is mean ± SEM, student's t-test with correction for unequal sample sizes. N=4-5 mice per genotype.

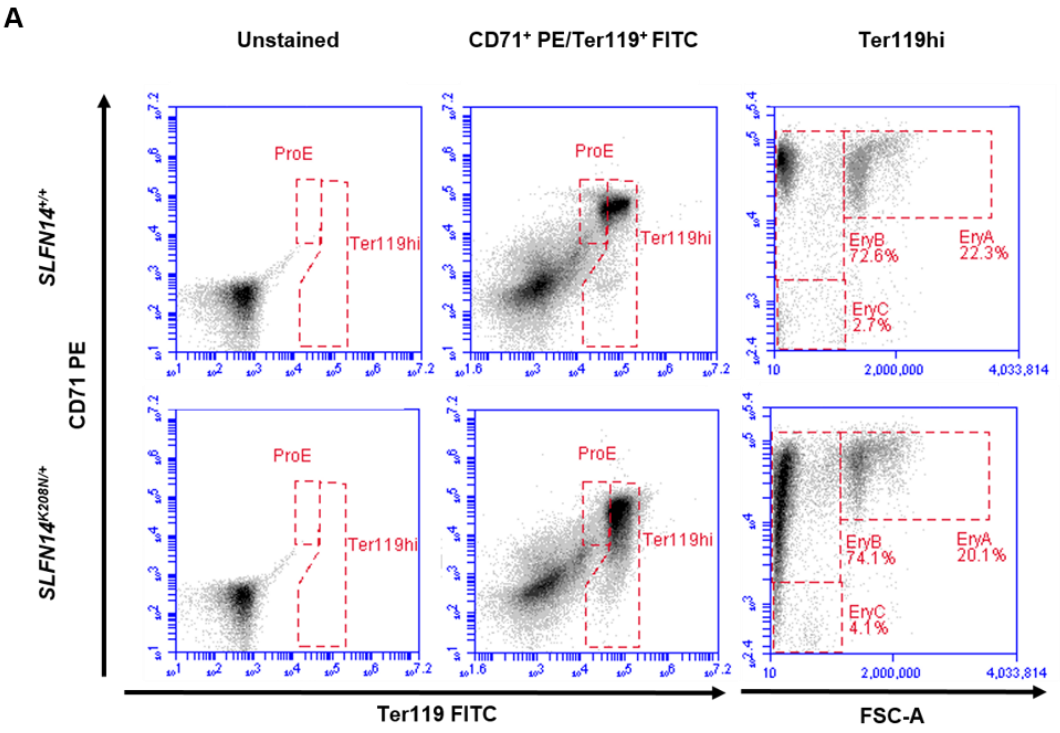
A
Unstained
CD71+ PE/Ter119+ FITC
Ter119hi
SLFN14+/+
SLFN14K208N/+
CD71 PE
ProE
Ter119hi
EryB
72.6%
EryA
22.3%
EryC
2.7%
EryB
74.1%
EryA
20.1%
EryC
4.1%
10
2,000,000
4,033,814
Ter119 FITC
FSC-A

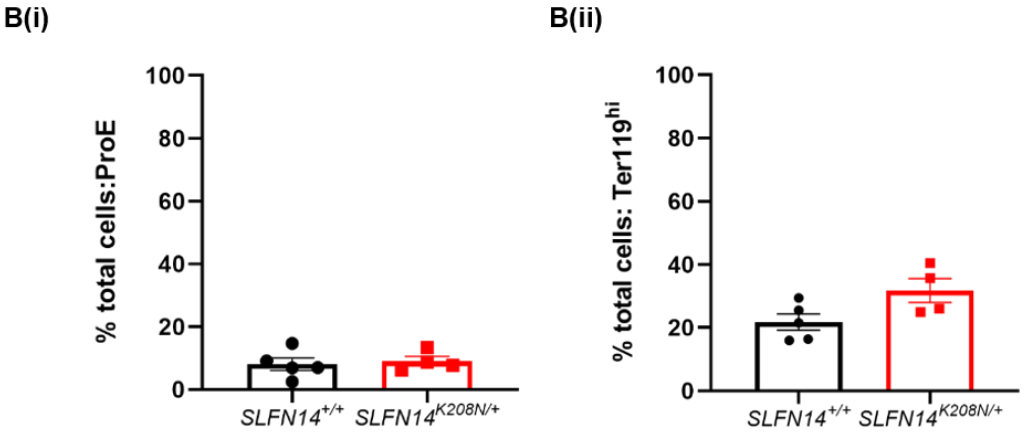
B(i)
% total cells:ProE
100
80
60
40
20
0
SLFN14+/+
SLFN14K208N/+
B(ii)
% total cells: Ter119hi
100
80
60
40
20
0
SLFN14+/+
SLFN14K208N/+

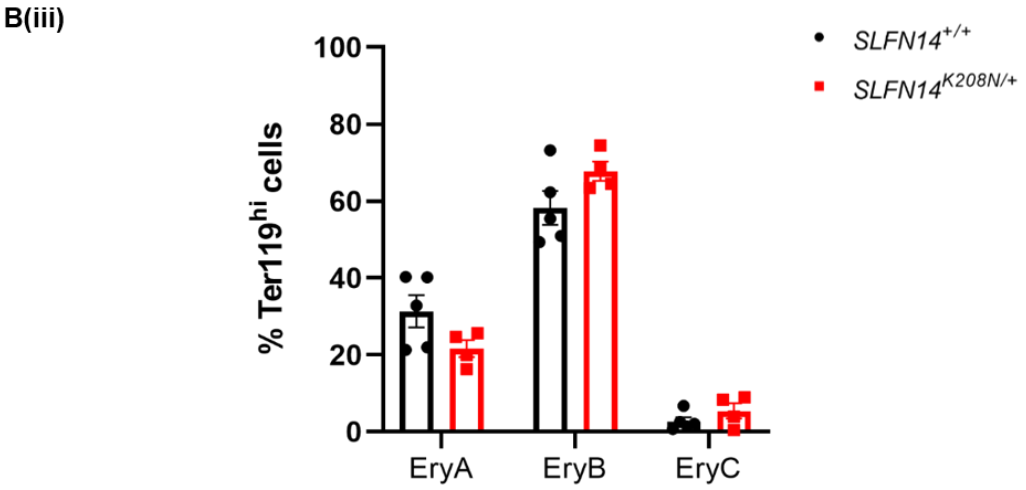
B(iii)
% Ter119hi cells
100
80
60
40
20
0
EryA
EryB
EryC
SLFN14+/+
SLFN14K208N/+

**Figure 5.2: Proportion of erythroid committed progenitors in the bone marrow of *SLFN14*-K208N mice was consistent with wild-types.** (A) Whole bone marrow flow cytometry to quantify proportion of Proerythroblasts (ProE) and erythroid committed cells (Ter119hi). ProE, CD71/Ter119 double positive events; Ter119hi, Ter119 bright events. (B) Flow cytometry quantification of erythroid cells. (i) Proportion of ProEs was consistent between genotypes. (ii) Ter119hi cells were consistent across both genotypes. (iii) Ter119hi cells segregated based on size to further separate populations. All cells were in consistent proportions between genotypes with few EryC (most mature erythrocytes) detected. Figures shown as percentage of total cells with specified staining pattern. Data presented is mean ± SEM, student's t-test with correction for unequal sample sizes. N=4-5 mice per genotype.

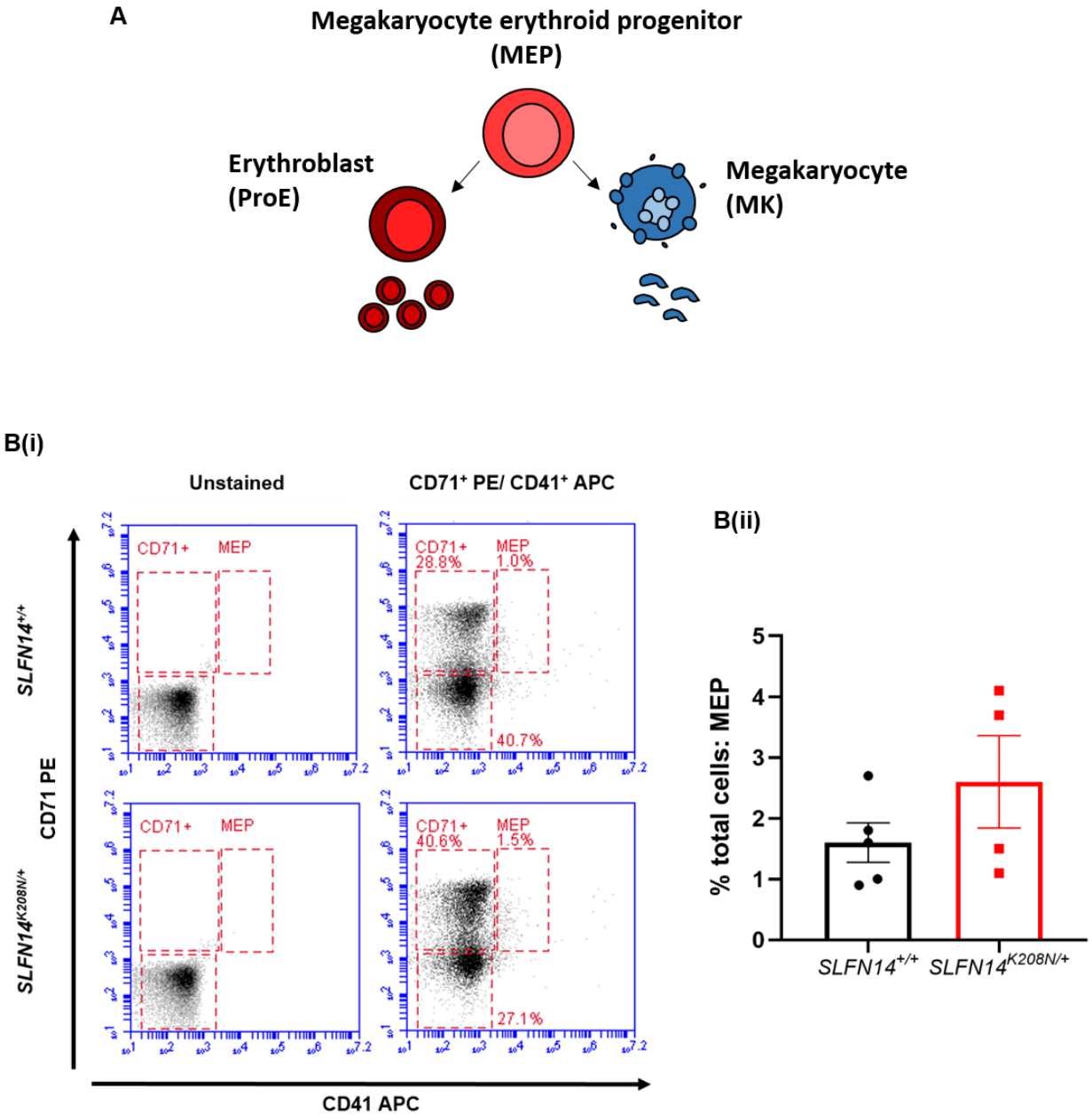


**Figure 5.3: *SLFN14*-K208N bone marrow contains higher proportions of MEPs.** (A) MKs and erythroid progenitors originate from the same progenitor (MEP). (B) Quantification of MEPs in the bone marrow. (i) Whole bone marrow was stained with CD41 and CD71 to identify MEPs. *SLFN14*$^{K208N/+}$ mice showed higher CD71 single positive events. (ii) *SLFN14*$^{K208N/+}$ mice has slightly increased proportion of MEPs than wild-type controls in the bone marrow but this was not significant. Data presented is mean ± SEM with correction applied for unequal sample sizes. N=4-5 mice per genotype.

### 5.3.4 *SLFN14*$^{K208N/+}$ mice exhibit splenomegaly and haemolysis

The spleen is a major organ involved in filtering and clearing blood cells from the circulation. Spleen morphology is an important consideration when assessing blood cell production and clearance. Spleens from *SLFN14*$^{K208N/+}$ mice were found to be significantly larger than wild-type controls (Figure 5.4Ai and ii). In addition, *SLFN14*$^{K208N/+}$ spleens appeared darker than wild-types which only had slight pigmentation due to macrophage mediated haemolysis (Figure 5.4Ai and B). Perl's Prussian blue staining was used and identified a significant increase in the sites of free iron staining within the spleen (Figure 5.4B). Free iron was present in both red and white pulp of the spleen indicative of upregulated haemolysis. The exact mechanism for this haemolysis is unclear at this stage.

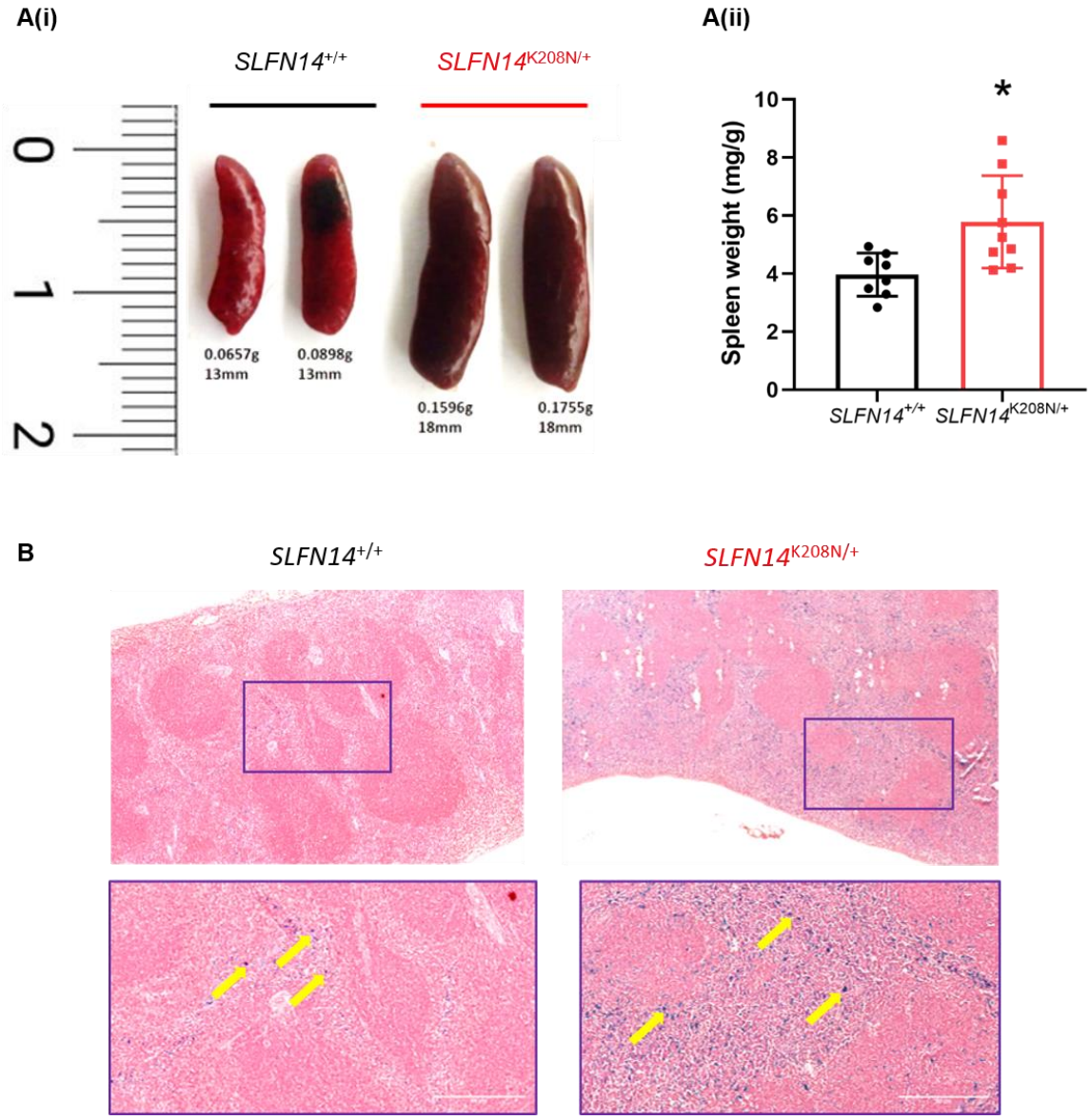


**Figure 5.4: *SLFN14*-K208N mice exhibit splenomegaly and increased heamolysis.** (A) *SLFN14*$^{K208N/+}$ spleens. (i) *SLFN14*$^{K208N/+}$ spleens were significantly larger thank wild-type controls. (ii) Spleen size was increased by approximately 50%. (B) Spleen sectioning and staining using Perl's Prussian blue showed more sites of free iron, indicative of increased heamolysis (free iron is stained in blue and highlighted by yellow arrows). Scale bar is 50µm. Data presented is mean ± SEM, student's t-test for significance with correction for unequal sample size. N=8-9 mice per genotype. * $p<0.05$.

### 5.3.5 *SLFN14*-K208N show splenic extramedullary haematopoiesis (EMH)

The spleen morphology was particularly striking and although differences in pigmentation could be addressed by upregulated haemolysis, it was unclear at this stage what was contributing to the significant increase in size. Homogenised spleen samples were stained with the same progenitor panel antibodies as in the bone marrow. As above, MKs were identified by histology sectioning and staining, showing characteristic large nuclei and cytoplasmic regions (Figure 5.5A). No differences in size or number were observed when quantified by flow cytometry (Figure 5.5Bi and ii).

The erythroid progenitor panel was applied to homogenised spleen samples (Figure 5.6A) and although ProEs were present in the spleen, proportions where significantly lower than that observed in the bone marrow. SLFN14$^{K208N/+}$ spleens contained higher proportions of ProEs and it was evident at this stage the spleen was a site of extramedullary erythropoiesis in SLFN14$^{K208N/+}$ mice (Figure 5.6Bi). There was also approximately 20% increase in Ter119$^{hi}$ cells which constituted both intermediate progenitors (EryB) and a significantly higher proportion of mature erythrocytes (EyrC) (Figure 5.6Bii and iii). Similar to the bone marrow, the ‘spread’ distribution in EryB cells was also observed in spleen samples consistent with progressive loss of CD71 expression, indicative of erythrocyte maturation and extramedullary erythropoiesis from intermediate progenitors in the spleen (Figure 5.6A).

In similarity to the bone marrow, there was a tendency for an increased proportion of MEPs within the spleen but this did not reach significance (Figure 5.7Ai and ii).

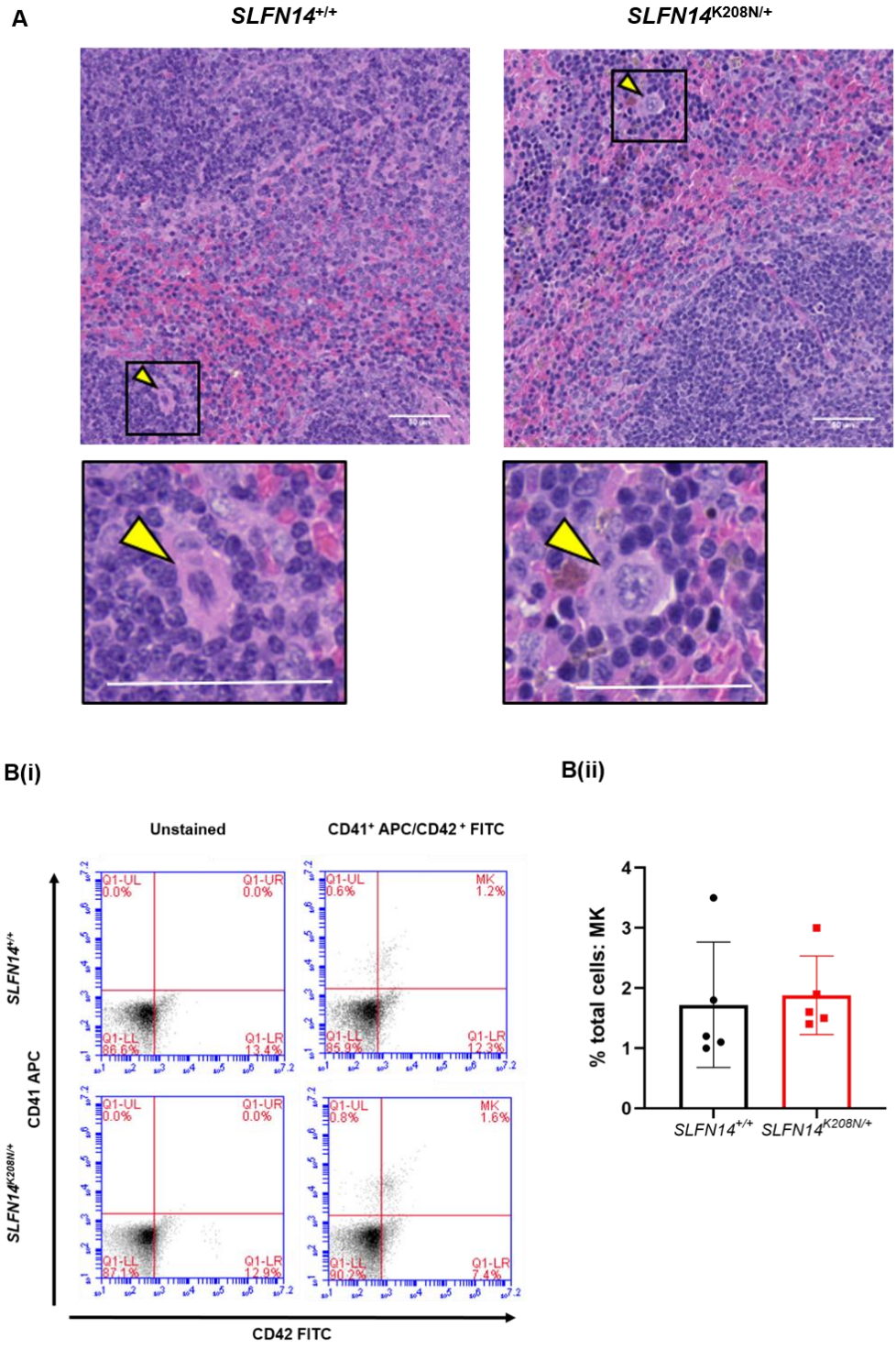


**Figure 5.5: Proportion of megakaryocytes in the spleen of *SLFN14*-K208N mice was consistent with wild-types.** (A) Representative images of H&E stained femur sections from SLFN14$^{+/+}$ and SLFN14$^{K208N/+}$ mice. Scale bar 50µm. (B) Flow cytometry quantification of MKs in homogenised spleen. (i) Spleen homogenate was stained with CD41 and CD42 antibodies. MKs were double positive events. (ii) Quantification of MKs. Figures shown as percentage of total cells CD41/CD42 double positive. No difference was observed in proportion of MKs in the spleen. Data presented is mean ± SEM, student's t-test. N=5 mice per genotype.

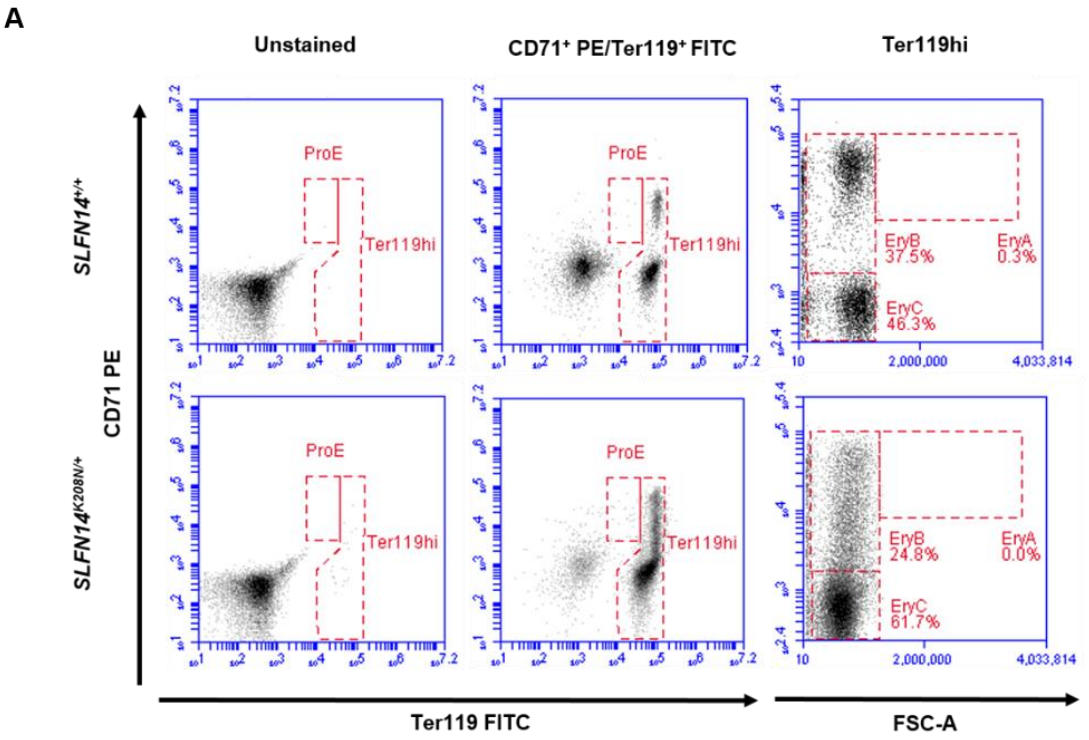
A
Unstained
CD71+ PE/Ter119+ FITC
Ter119hi
SLFN14+/+
SLFN14K208N/+
CD71 PE
ProE
Ter119hi
EryB
37.5%
EryA
0.3%
EryC
46.3%
EryB
24.8%
EryA
0.0%
EryC
61.7%
10
2,000,000
4,033,814
Ter119 FITC
FSC-A

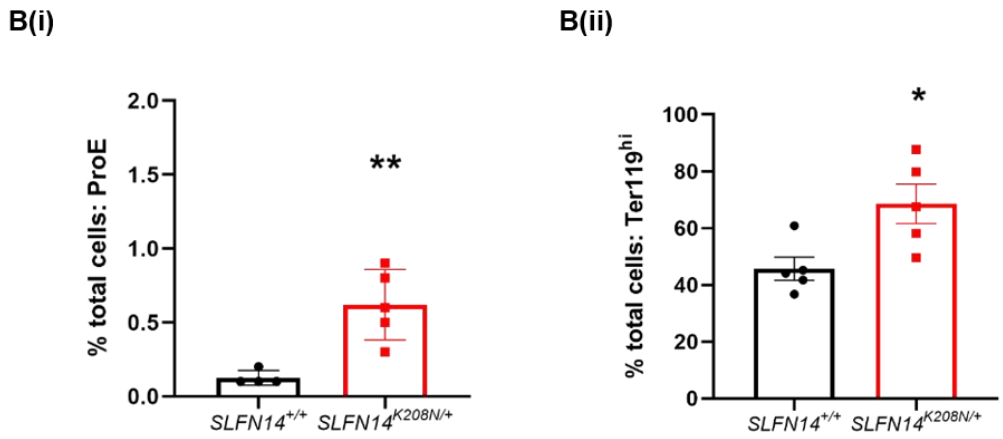
B(i)
% total cells: ProE
2.0
1.5
1.0
0.5
0.0
**
SLFN14+/+
SLFN14K208N/+
B(ii)
% total cells: Ter119hi
100
80
60
40
20
0
*
SLFN14+/+
SLFN14K208N/+

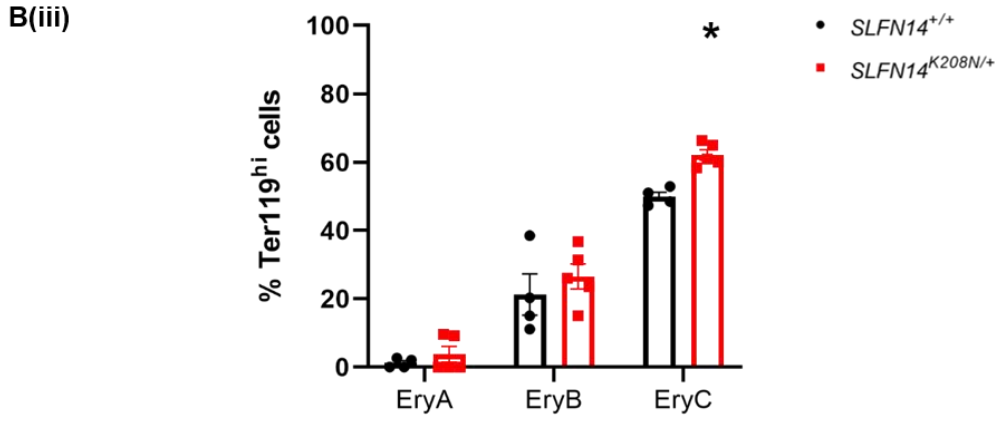
B(iii)
% Ter119hi cells
100
80
60
40
20
0
*
SLFN14+/+
SLFN14K208N/+
EryA
EryB
EryC

**Figure 5.6: *SLFN14*-K208N mice show extramedullary erythropoiesis in the spleen.** (A) Flow cytometry on homogenised spleens to quantify proportion of ProE and erythroid committed cells (Ter119hi). ProE, CD71/Ter119 double positive events; Ter119hi, Ter119 bright events. (B) Flow cytometry quantification of erythroid cells. (i) Proportion of ProEs was significantly increased in *SLFN14*$^{K208N/+}$ mice. (ii) Significantly greater proportion of Ter119hi cells in the spleen of *SLFN14*$^{K208N/+}$ mice than wild-type controls. (iii) Ter119hi cells segregated based on size to further separate populations. EryA and EryB cells were in consistent proportions between genotypes. Increased proportion of EryC cells detected consistent with haemolysis and clearance. Figures shown as percentage of total cells with specified staining pattern. Data presented is mean ± SEM, student's t-test. N=5 mice per genotype. *p<0.05, ** p<0.01.

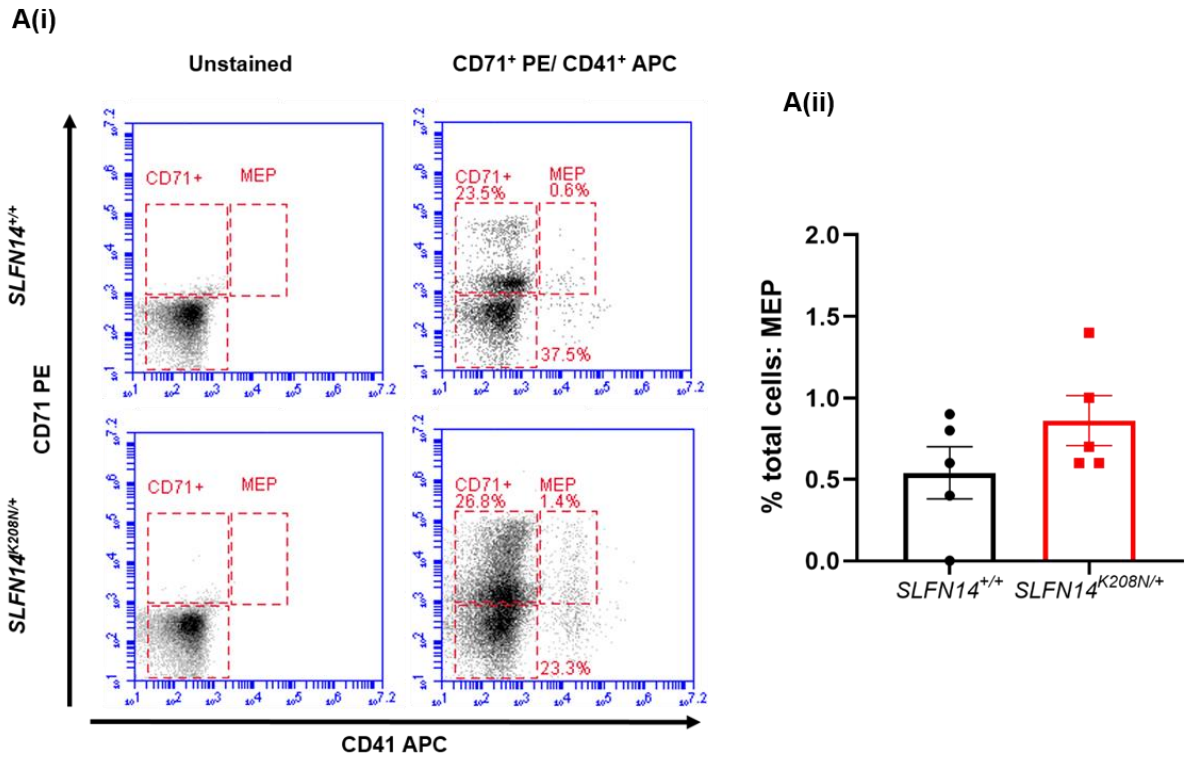


**Figure 5.7: *SLFN14*-K208N spleens contains higher proportions of MEPs.** (A) Quantification of MEPs in the homogenised spleen samples. (i) Spleens were stained with CD41 and CD71 to identify MEPs. (ii) *SLFN14*$^{K208N/+}$ mice has slightly increased proportion of MEPs than wild-type controls in the spleen but this was not significant. Data presented is mean ± SEM, student's t-test. N=5 mice per genotype.

### 5.3.6 EMH in *SLFN14*$^{K208N/+}$ mice is non-neoplastic and not due to bone marrow fibrosis

The presence of haematopoietic progenitors and differentiating erythrocytes in the spleen is evidence of EMH. Usually EMH occurs in cases of myelofibrosis or bone marrow dysfunction, however, given the normal appearance and proportions of these progenitors in the bone marrow this was not the case. EMH, in either the spleen or liver occurs in two instances, neoplastic or non-neoplastic EMH. Reticulin staining was used as previously described by Geer et al. G6b-B knock-in mouse model (Geer et al., 2018). These images were used as positive controls for myelofibrosis showing clear bone marrow dysfunction and fibrosis similar to that observed in G6b deficient mice and patients (Figure 5.8). Reticulin staining of the bone marrow did not reveal fibrosis and it was concluded the EMH in *SLFN14*$^{K208N/+}$ mice was indeed non-neoplastic (Figure 5.8).

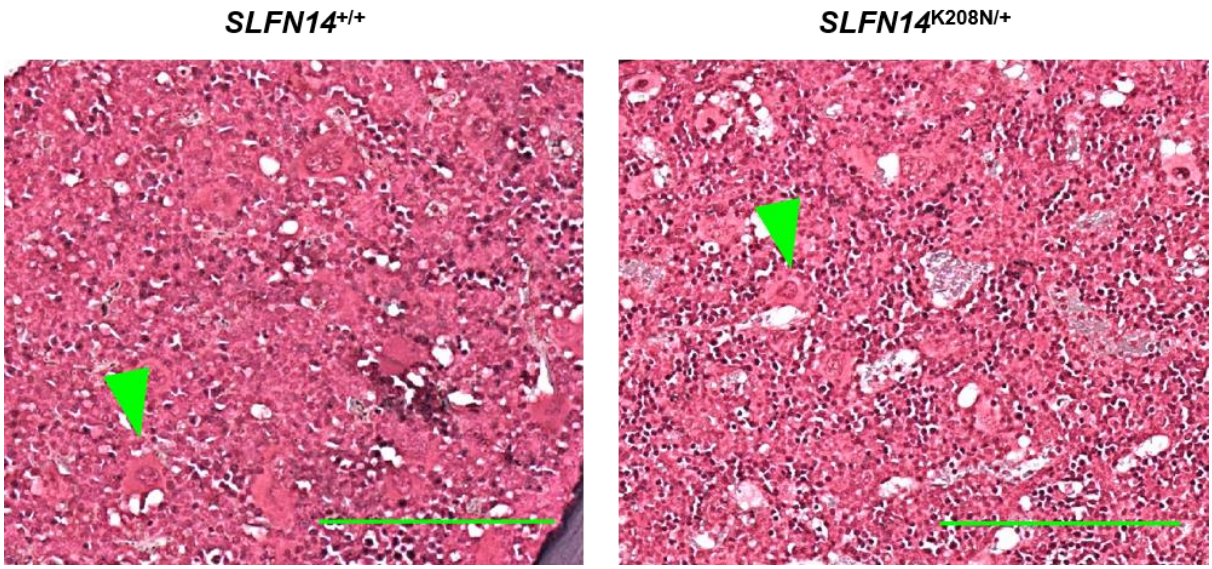


**Figure 5.8: Reticulin staining in *SLFN14*-K208N mice.** Reticulin staining of the bone marrow did not show evidence of myelofibrosis. Green arrowheads denote bone marrow megakaryocytes, scale bar 100µm. N=3 mice per genotype.

### 5.3.7 qRT PCR shows reduced *SLFN14* and *GATA1* expression in whole bone marrow mRNA

At this stage, it was clear the *SLFN14*-K208N mutation played an important role in haematopoiesis, with particular emphasis on the erythroid lineage. SLFN14 as an endoribonuclease functioning by cleaving and degrading RNA, which then results in a reduction in quantity or viability of intact RNA. This can be observed from Figure 5.9A whereby Fletcher et al. explored the activity of SLFN14 endoribonuclease in rRNA cleavage. With this in mind, it was hypothesised there may be differential expression of haematopoietic RNAs as a result of the *SLFN14*-K208N mutation. This may then ultimately affect the differentiation process of MKs and erythroid cells, subsequently altering platelet and mature erythrocyte function.

qRT-PCR of whole bone marrow RNA revealed *SLFN14* mRNA itself was approximately 50% of the level seen in wild-types (Figure 5.9Bi). *GATA1*, is involved in haematopoiesis with particular impact in myeloid cell differentiation. *GATA1* mRNA was reduced by approximately 60% in *SLFN14*$^{K208N/+}$ mice compared to wild-type controls (Figure 5.9Bii). It was hypothesised that the presence of mutant *SLFN14* (or more specifically the *SLFN14*$^{K208N/+}$ mutation) was significantly altering the quantity and perhaps quality of TF mRNA in the bone marrow, subsequently disrupting haematopoiesis with particular impact on the erythroid lineage.

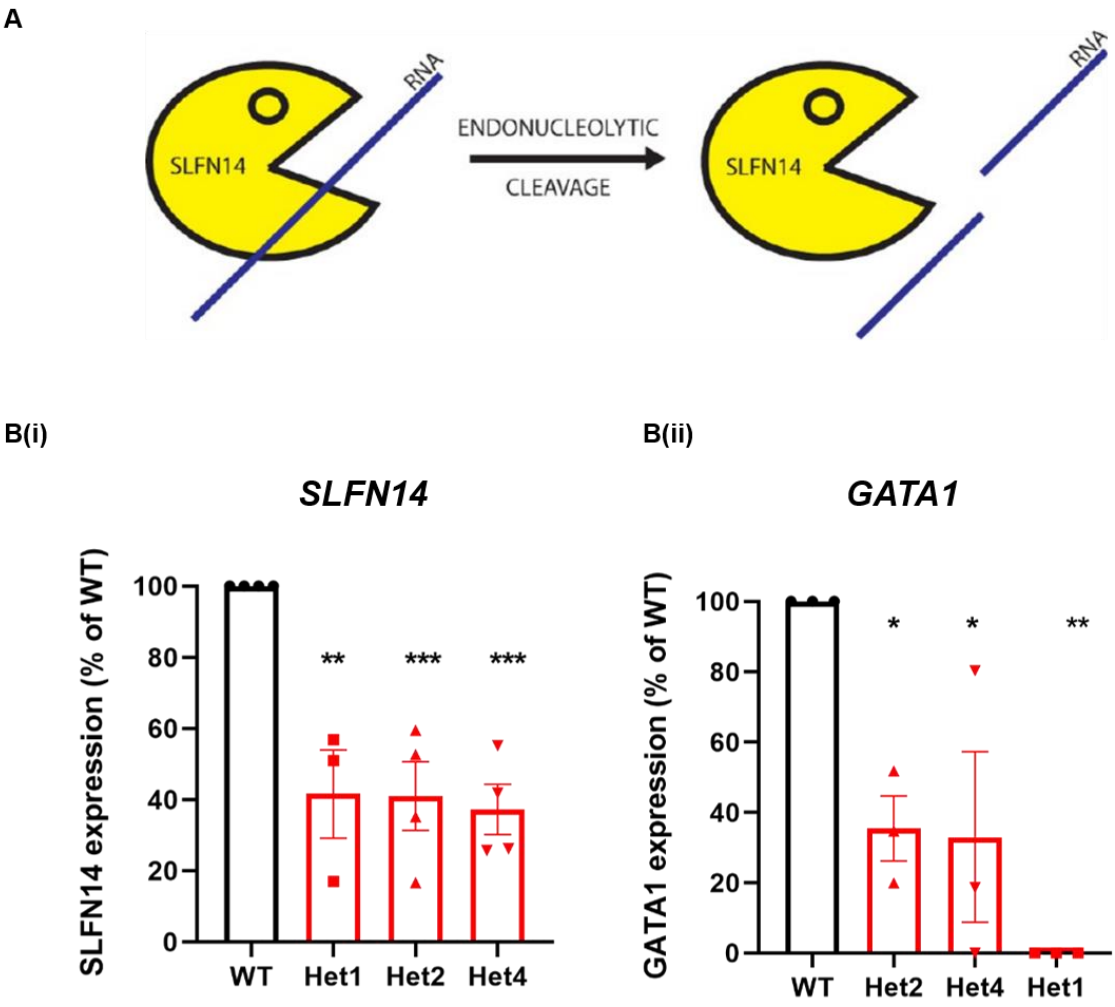


**Figure 5.9: SLFN14 endoribonucleolytic activity in haematopoiesis.** (A) Schematic taken from Pisareva et al. whereby SLFN14 can cleave and degrade ribosomal RNA causing RNA degradation (Pisareva et al., 2015). (B) Quantification of (i) SLFN14 and (ii) GATA1 mRNA in whole bone marrow as measured by qRT-PCR. *SLFN14*$^{K208N/+}$ mRNA presented as a percentage of wild-type controls. N=1-3 mice per genotype with each mouse measured in triplicate. Mean ± SEM, assessed by one-way ANOVA. *p<0.05, **p<0.01, ***p<0.001.

## 5.4 Discussion

This chapter has addressed the involvement of *SLFN14* in haematopoiesis with particular focus on MK and erythroid lineages given the differences in platelet and erythrocyte function observed in Chapter 4. Here, histology staining supported flow cytometry data showing consistent proportions of MKs in the bone marrow. In addition to this, erythroid progenitors and MEPs were also consistent, suggesting medullary haematopoiesis in *SLFN14*$^{K208N/+}$ mice was normal. However, this appeared to differ in the spleen. Severe splenomegaly was observed whereby mutant mouse spleens were approximately twice as large as wild-type controls. Their darker appearance was due to increased haemolysis mediated by macrophage clearance of erythrocytes in the circulation. At this stage, it is unclear whether this is due to accelerated erythrocyte clearance however, cell lifespan assays in the future aim to address this (Hoffmann-Fezer et al., 1991).

The most interesting factors with regards to progenitor populations were those identified in the spleen. In some instances, the spleen and liver act as secondary sites for haematopoiesis in a compensatory fashion to maintain adequate numbers of blood cells in the circulation. This has been shown to be true in both mouse and human cases of myeloproliferative disorders (Imai et al., 2017, Shide et al., 2008). This is termed extramedullary haematopoiesis (EMH) which can be divided into two categories: non-neoplastic; the accumulation of haematopoietic precursor cells in the splenic red pulp; and neoplastic; whereby the spleen acts as the primary site of haematopoiesis due to haematologic malignancy which renders the bone marrow dysfunctional. Often in the most severe cases, neoplastic EMH can be an indication of disease transformation (Orazi and Czader, 2010). In this chapter, *SLFN14*$^{K208N/+}$ spleens contained higher proportions of ProEs, erythroid committed cells (Ter119hi) and EryC cells. However, the distribution of EryB cells within the gate showed progressive loss of CD71 expression and subsequent maturation. This showed EMH in the context of erythropoiesis. Currently the working hypothesis is that

erythrocytes are produced in the spleen, in addition to the bone marrow in order to compensate for their smaller size and lower oxygen carrying capacity. Greater numbers of circulating erythrocytes suggests that the anaemia in these mice is somewhat controlled, which is not the case *in utero* of homozygotes rendering them lethal beyond E16.5. Repeating these experiments in both bone marrow and spleens will allow full interrogation of this haematopoietic phenotype which may currently be somewhat limited by small samples of mice used.

SLFN14 has previously been identified as an endoribonuclease. Studies by Fletcher et al explored this in rabbit reticulocytes and identified that SLFN14 had the ability to cleave RNA and cause RNA degradation. With respect to haematopoiesis, qRT-PCR was used to assess mRNA levels of GATA1 expression – a TF known to play important roles in both MK and erythroid lineage differentiation. The presence of the K208N mutation resulted in approximately 60% reduction in GATA1 mRNA expression. Although there was a reduction in TF mRNA, progenitor cell proportions were consistent in the bone marrow suggesting this reduction did not affect overall cell proliferation, but their propensity or lineage bias toward MK or erythroid directions is unclear at this stage. This theory has previously been explored by Xavier-Ferrucio et al. where in cases of iron deficiency anaemia, MEPs show a greater lineage bias toward MKs (Xavier-Ferrucio et al., 2019). This is worth exploring in the future given the observed anaemia but retained platelet function. RNA sequencing of individual progenitor populations will reveal how reduced TF mRNA and the K208N mutation affects platelet and erythrocyte cell development and function and in addition, if other TF RNAs are affected during haematopoiesis giving rise to an erythrocyte defect in *SLFN14*-K208N mice and platelet defect in *SLFN14* patients.

# Chapter 6

## Generation and platelet phenotyping of *SLFN14 PF4Cre* mouse

# Chapter 6 – Generation and platelet phenotyping of *SLFN14 PF4Cre* mouse

## 6.1 Aim

The aim of this chapter was to successfully develop a viable conditional knockout of *SLFN14* to investigate its specific role in platelets and megakaryopoiesis. In addition to the global K208N mouse model, the conditional knockout was generated to address this research question with particular focus on platelets and megakaryocytes. It was hypothesised that this *SLFN14-PF4Cre* mouse would result in thrombocytopenia and a platelet defect similar to that observed in human patients.

## 6.2 Introduction

Conditional knockout mouse models have long been a viable option used to study pathologies with particular interest in single genes or signalling pathways. Deletion of genes ubiquitously expressed may result in harmful phenotypes and off target effects which may hinder discovery of mechanisms specific to the cell type of interest. To overcome this, conditional gene inactivation is a viable option whereby the whole or specific regions of genes can be deleted in a tissue specific manner. The global functional properties of SLFN14 remain to be explored and so here, it was important to consider the wider effects of constitutive deletion. The loxP-Cre system has been widely used in several genes implicated in the platelet and megakaryocyte lineage including Gp1ba and PF4 (Nagy et al., 2019, Tiedt et al., 2007).

Platelet factor 4 (PF4) is a marker specific to the platelet/megakaryocyte lineage where the PF4Cre recombinase transgene was initially constructed by Tiedt et al. using homologous recombination in bacteria. This was the first generation of a conditional knockout mouse used to induce selective deletion of genes in the megakaryocyte lineage (Tiedt et al., 2007). The Gp1ba-Cre model was developed by Nagy et al. whereby they explored its highly specific deletion of floxed genes only in the megakaryocyte lineage. Platelets are becoming increasingly associated in immune related pathologies and many have found that the PF4Cre

transgene is also expressed in a variety of leukocyte populations. Subsequently, in some instances this presented difficulties in attributing deletion of floxed genes to either megakaryocyte or leukocyte lineages (Shi et al., 2014, Abram et al., 2014, Calaminus et al., 2012, Pertuy et al., 2015).

Selecting the most appropriate Cre deleter strain is important for interpreting accurate tissue specific results and generating animal colonies which are viable with limited off target effects. In this chapter, the *SLFN14-PF4Cre* strain is explored with regards to platelet function. Within the haematopoietic lineage *SLFN14* mRNA is expressed in myeloid cells (namely megakaryocyte and erythrocyte lines) however SLFN14 expression was detected at very low levels in T-cells and undetectable in monocytes and monocyte-derived dendritic cells (Puck et al., 2015). This suggests that the *SLFN14-PF4Cre* model should have very little to no impact on functionality of leukocytes. In addition, *SLFN14* in mice is located on chromosome 11 (location 11, 50.30cM) in very close proximity to the locus of mouse Gp1ba (location 11, 3.20cM) whereas PF4 is on mouse chromosome 5 (Bult et al., 2019). With SLFN14 and PF4 loci well separated, this makes the PF4Cre targeting strategy more appropriate than GP1ba.

In this chapter *SLFN14* homozygous floxed mice in the presence of PF4Cre recombinase present with a moderate macrothrombocytopenia. While heterozygous mice follow the same trend, this did not reach significance. Further investigation of haemostatic function in these mice is required but from initial phenotyping, the reduction in circulating platelet number appears to arise from a reduced proportion of megakaryocytes in the bone marrow. At this stage it is unclear how this may impact platelet function *in vivo*.

Due to mouse breeding constraints during the COVID-19 pandemic and the lack of homozygote flox mice suitable for breeding, *SLFN14*$^{fl/fl}$ *PF4Cre* mice could not be generated in time for further functional work within this chapter. Therefore, *SLFN14*$^{fl/+}$ *PF4Cre* mice are used in most experiments as the sample group with work to be completed on *SLFN14*$^{fl/fl}$ *PF4Cre* mice once breeding increases and access to the animal facility allows.

## 6.3 Results

### 6.3.1 Generation of *SLFN14-PF4Cre* colony

In order to broadly investigate the physiological function of *SLFN14* in platelets and megakaryocytes, a conditional knockout mouse was generated. A mutant form of the *SLFN14* allele (SLFN14$^{fl}$) was engineered whereby exons 2 and 3 were selectively removed upon expression of the PF4Cre recombinase. The previously reported K219N and K208N mutations respectively, are located in exon 2, hence removal of this exon may give insights into the functional capacity of this region in megakaryopoiesis and platelet function.

First, a targeting vector was constructed for generation of the modified or transformed *SLFN14* allele (*SLFN14$^{T}$*). Homologous recombination occurred in embryonic stem (ES) cells in which an internal ribosome entry site (IRES) FRT-neo-FRT-LoxP cassette was inserted after exon 3 and a LoxP site inserted before exon 2. These sites are as shown in Figure 6.1. Chimeric mice were generated from the ES cell clone containing the targeted locus with heterozygous offspring from wild-type C57BL/6J mice. The –neo- sequence was removed by intercrossing transgenic Flp recombinase positive mice resulting in *SLFN14*$^{fl}$ whereby 'fl' denotes '**f**ixed **L**oxP' sites. These sites highlight the region which is to be targeted in conditional deletion (Figure 6.1). Texas A&M Institute for Genomic Medicine produced the embryonic stem cell (ESC) lines. Following insertion and validation of the floxed sites, clones were inserted into mouse blastocysts and transferred into psuedopregnant female mice. Specific inactivation in the megakaryocyte lineage was achieved by breeding these *SLFN14* floxed mice with externally sourced platelet factor 4 Cre recombinase expressing (PF4Cre) animals, to produce *SLFN14$^{fl}$ PF4Cre* offspring (Tiedt et al., 2007). Subsequent breeding steps using positive PF4Cre expressing mice resulted in the germline deletion of exons 2 and 3 in a conditional manner. Mice were bred in either heterozygous flox/heterozygous flox or heterozygous flox/wild-type breeding pairs (*SLFN14$^{fl/+}$* X *SLFN14$^{fl/+}$* or *SLFN14$^{fl/+}$* X *SLFN14$^{+/+}$* respectively). In general the PF4Cre positive mouse was the male breeder, to

control for any potential postpartum haemorrhage due to the presence of floxed allele in female mice. In experiments, mice negative for PF4Cre were grouped and used as controls against those positive for PF4Cre which were assessed in separate sample groups. This ensured any effect of the PF4Cre recombinase on the wild-type allele was controlled for.

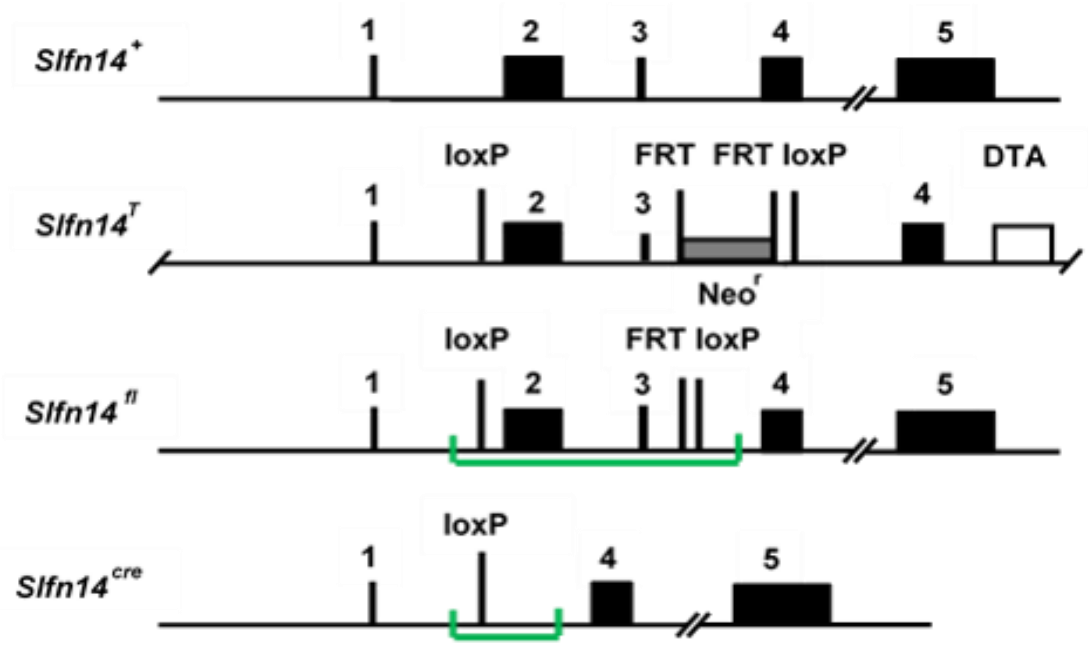


**Figure 6.1: Generation of a SLFN14 conditional knock-out mouse model.** Targeting strategy used to generate the *SLFN14* flox mouse model. Green banded regions highlight regions susceptible to deletion upon Cre expression by loxP sites. Slfn14$^{cre}$ shows conditional knockout of exons 2 and 3 after PF4Cre recombinase activity.

### 6.3.2 PF4Cre mediated deletion of exons 2 and 3 in *SLFN14*

PCR genotyping was used to identify the presence of flox alleles. Primers were designed to include the loxP site before exon 2 to distinguish between floxed and wild-type alleles. The presence of a larger band identified the floxed allele (presence of loxP) and wild-type allele 34 base pairs shorter (Figure 6.2A). In order to resolve bands 34 base pairs apart, a 1.5% agarose gel was run at 60V for an hour to ensure slow separation of fragments. Expression of the PF4Cre recombinase was determined in a separate PCR reaction (Figure 6.2B). Mendelian inheritance was assessed by a Chi-Square goodness of fit test (Figure 6.2C). Observed numbers of mice with each genotype were compared to those expected based on ratios as stated by Mendel's law. Cross types 4 and 5 (with Cre positive on floxed mice and wild-type mice respectively) did not show significant deviation from Mendelian inheritance (Figure 6.2Ci and ii). Cre expression in flox or wild-type breeders (cross 4 versus cross 5 respectively) was not favourable to a particular genotype. Assessment is ongoing for assessing inheritance of homozygous floxed mice.

### 6.3.3 *SLFN14 PF4Cre* mice present with mild macrothrombocytopenia

Having observed macrothrombocytopenia in *SLFN14* patients, whole blood counting was used to establish if this conditional knock-out mouse phenocopies human patients. Blood samples were collected from terminally anaesthetised mice as described in 'Methods and Materials' and 65µl was run on an automated haematology analyser (HORIBA Pentra ES 60). Platelet counts in *SLFN14*$^{fl/fl}$ *PF4Cre* mice were significantly reduced (p=0.001) and *SLFN14*$^{fl/+}$ *PF4Cre* mice also appeared to have reduced platelet count compared to controls, however this did not reach significance (Figure 6.3Ai). In addition to this, mean platelet volume was significantly increased in *SLFN14*$^{fl/fl}$ *PF4Cre* mice (p=0.006) but not heterozygotes (Figure 6.3Aii). Erythrocyte count and size was consistent across all genotypes Figure 6.3Bi and ii) and leukocyte counts were consistent across all genotypes

indicating PF4Cre alone and in the presence of *SLFN14* flox, did not affect overall leukocyte count in these animals (Figure 6.4).

A

SLFN14

1. SLFN14$^{fl/fl}$
2. SLFN14$^{fl/+}$
3. SLFN14$^{+/+}$

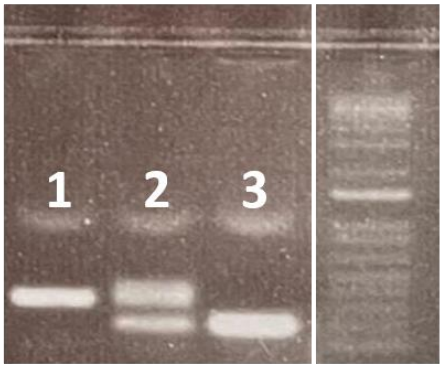


B

PF4Cre

1. PF4Cre –ve
2. PF4Cre +ve

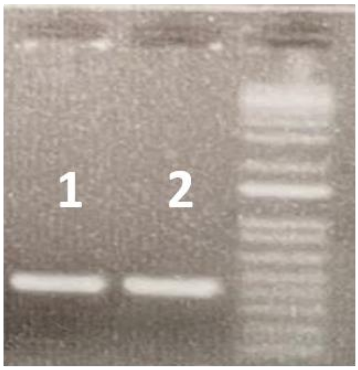


C(i)

**fl wt +** X **wt wt -**

| Outcome | Expected | Observed |
|---|---|---|
| fl wt PF4Cre - | 7 | 3 |
| fl wt PF4Cre + | 7 | 8 |
| wt wt PF4Cre - | 7 | 2 |
| wt wt PF4Cre + | 7 | 10 |
| TOTAL | 26 | 23 |
| Chi-square | | 7.500 |
| P value (two-tailed) | | 0.057 |
| P value summary | | ns |

C(i)

**fl wt -** X **wt wt +**

| Outcome | Expected | Observed |
|---|---|---|
| fl wt PF4Cre - | 8 | 7 |
| fl wt PF4Cre + | 8 | 12 |
| wt wt PF4Cre - | 8 | 6 |
| wt wt PF4Cre + | 8 | 8 |
| TOTAL | 32 | 33 |
| Chi-square | | 2.625 |
| P value (two-tailed) | | 0.453 |
| P value summary | | ns |

**Figure 6.2: *SLFN14-PF4Cre* genotyping and inheritance.** (A) Detection of *SLFN14$^{fl}$* alleles by PCR and agarose gel electrophoresis. Genotypes 1, 2 and 3 are *SLFN14$^{fl/fl}$*, *SLFN14$^{fl/+}$* and *SLFN14$^{+/+}$* respectively. DNA ladder is from same gel but additional wells removed. (B) Detection of PF4Cre expression by PCR and agarose gel electrophoresis. Genotypes 1 and 2 are negative and positive for PF4Cre respectively. These two fragments were amplified separately but together, form the full mouse genotype. (C) Chi square analyses to assess for Mendelian inheritance patterns. (i) Cross type 4: fl wt Cre + X wt wt Cre - crosses resulted in offspring following Mendelian inheritance ratios (p=0.057). (ii) Cross type 5: fl wt - X wt wt + crosses resulted in offspring following Mendelian inheritance ratios (p=0.453). Data is from 4 and 5 litters of each cross respectively. Chi-square goodness of fit test in GraphPad prism software.

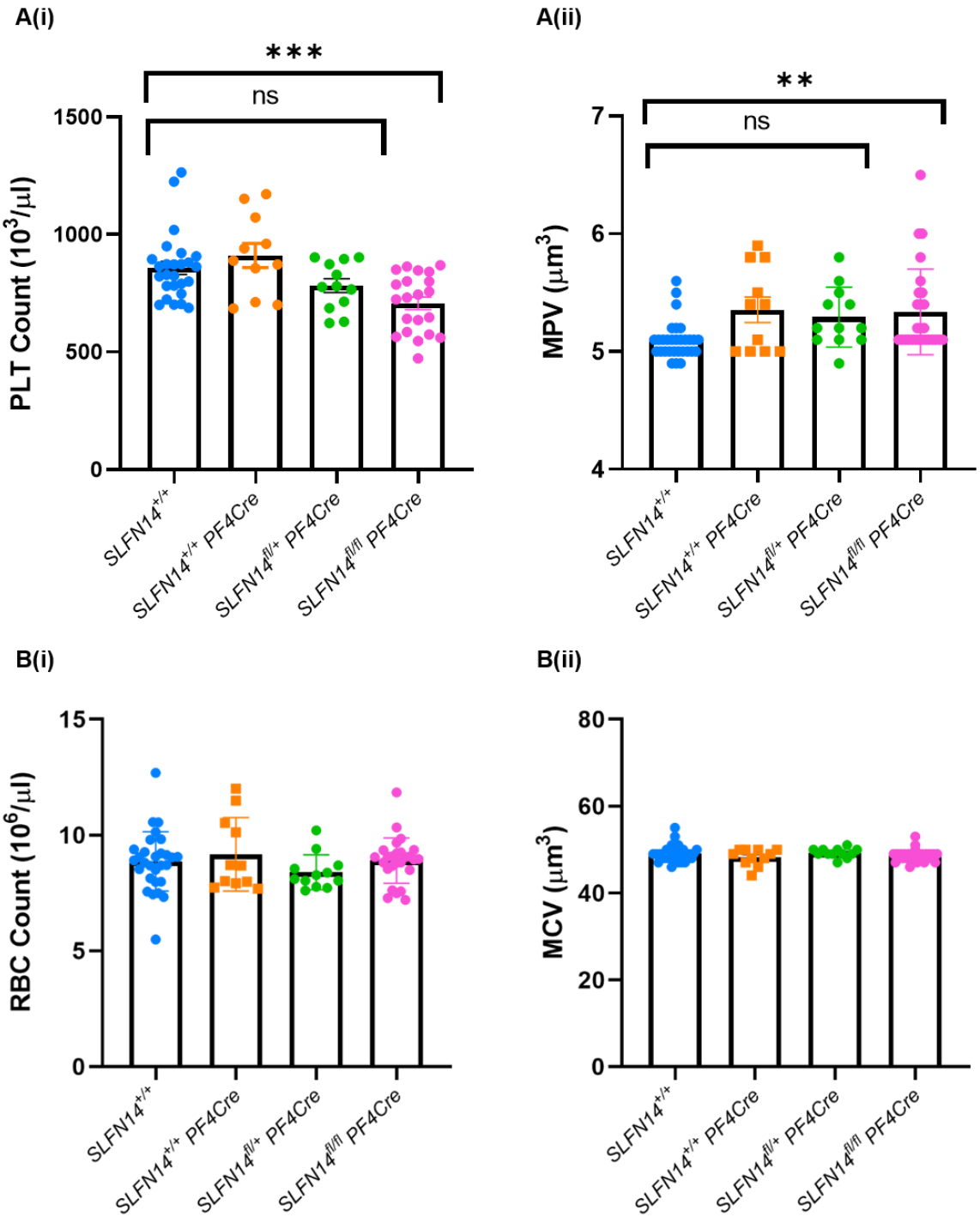


**Figure 6.3: *SLFN14-PF4Cre* platelet and erythrocyte counts.** (A) Platelet counts and MPV in *SLFN14-PF4Cre* mice. (i) *SLFN14*$^{fl/fl}$ *PF4Cre* mice present a mild thrombocytopenia (p=0.001) compared to controls (*SLFN14*$^{+/+}$). (ii) *SLFN14*$^{fl/fl}$ *PF4Cre* platelets are significantly enlarged compared to controls (p=0.006). *SLFN14*$^{fl/+}$ *PF4Cre* mice followed similar trend but this did not reach significance. (B) Red blood cell counts and MCV in *SLFN14-PF4Cre* mice. (i) Erythrocyte count and (ii) size were consistent across all genotypes. Data presented is mean ± SEM, one way ANOVA with correction for multiple comparisons. N=11-30 mice per genotype. ***p<0.001, **p<0.01, ns; not significant.

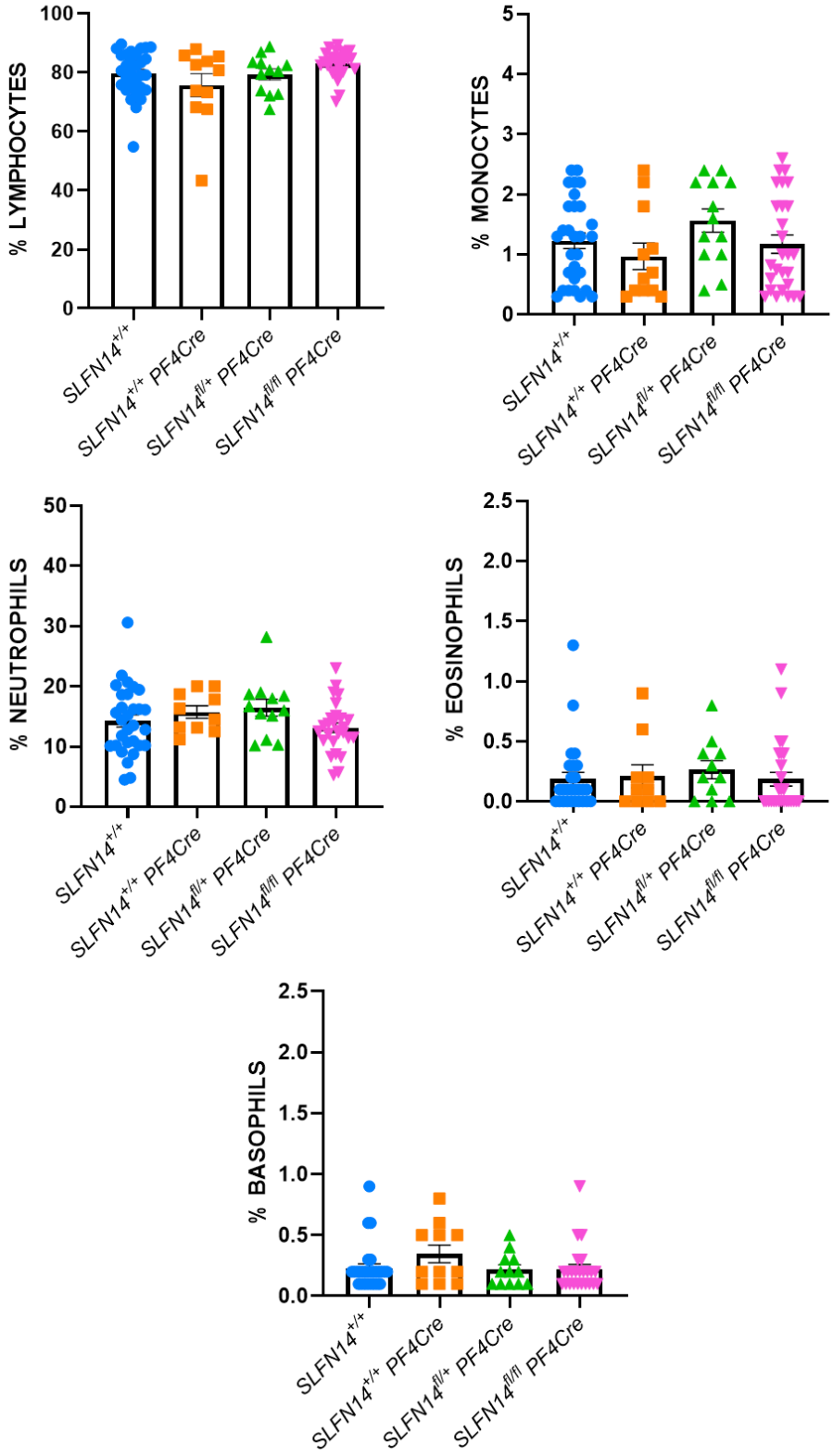


**Figure 6.4: Leukocyte counts in *SLFN14-PF4Cre* mice were consistent across all genotypes.** Data presented is mean ± SEM, one way ANOVA with correction for multiple comparisons. N=11-30 mice per genotype.

### 6.3.4 *SLFN14-PF4Cre* mice present with normal levels of major glycoprotein receptors and activation markers

Surface expression of major platelet glycoprotein receptors was quantified by flow cytometry in whole blood. Despite reduced circulating platelet count, *SLFN14*$^{fl/+}$ *PF4Cre* and *SLFN14*$^{fl/fl}$ *PF4Cre* displayed normal levels of major glycoprotein receptors under resting conditions (Figure 6.5A). Upon stimulation with major platelet agonists, alpha-granules release their contents and P-selectin is exposed on the platelet surface. In addition, upon agonist stimulation, the αIIbβ3 integrin undergoes a conformational change and can be detected by the JON/A antibody. From all platelet events, the percentage of double positive P-selectin and JON/A platelets were measured. Across all genotypes this was consistent, with some reduced activity in response to weaker agonists ADP and U46619 (Figure 6.5B). Unfortunately, at the time of experiment, *SLFN14*$^{fl/fl}$ *PF4Cre* mice were unavailable for activation studies due to reduced breeding over the COVID-19 pandemic.

### 6.3.5 *SLFN14-PF4Cre* mice show normal platelet granule content by transmission electron microscopy

Washed platelet pellets were suspended in 2.5% glutaraldehyde fixation solution in phosphate buffer, embedded in 100% resin and sectioned at 0.8µm. Sections were viewed using a transmission electron microscope and images taken for quantification (Figure 6.6Ai). All images were analysed blind. *SLFN14*$^{fl/+}$ *PF4Cre* mice were compared to *SLFN14*$^{+/+}$ and no differences were observed between the number of alpha or dense granules per platelet (Figure 6.6Aii). In addition to granule content, other features in platelets such as lysosomes, mitochondria and glycogen deposits did not appear different between genotypes (Figure 6.6Aii). 35 platelets per mouse were assessed across 3 different mice per genotype. Unfortunately, at the time of experiment, *SLFN14*$^{fl/fl}$ *PF4Cre* mice were unavailable due to reduced breeding over the COVID-19 pandemic.

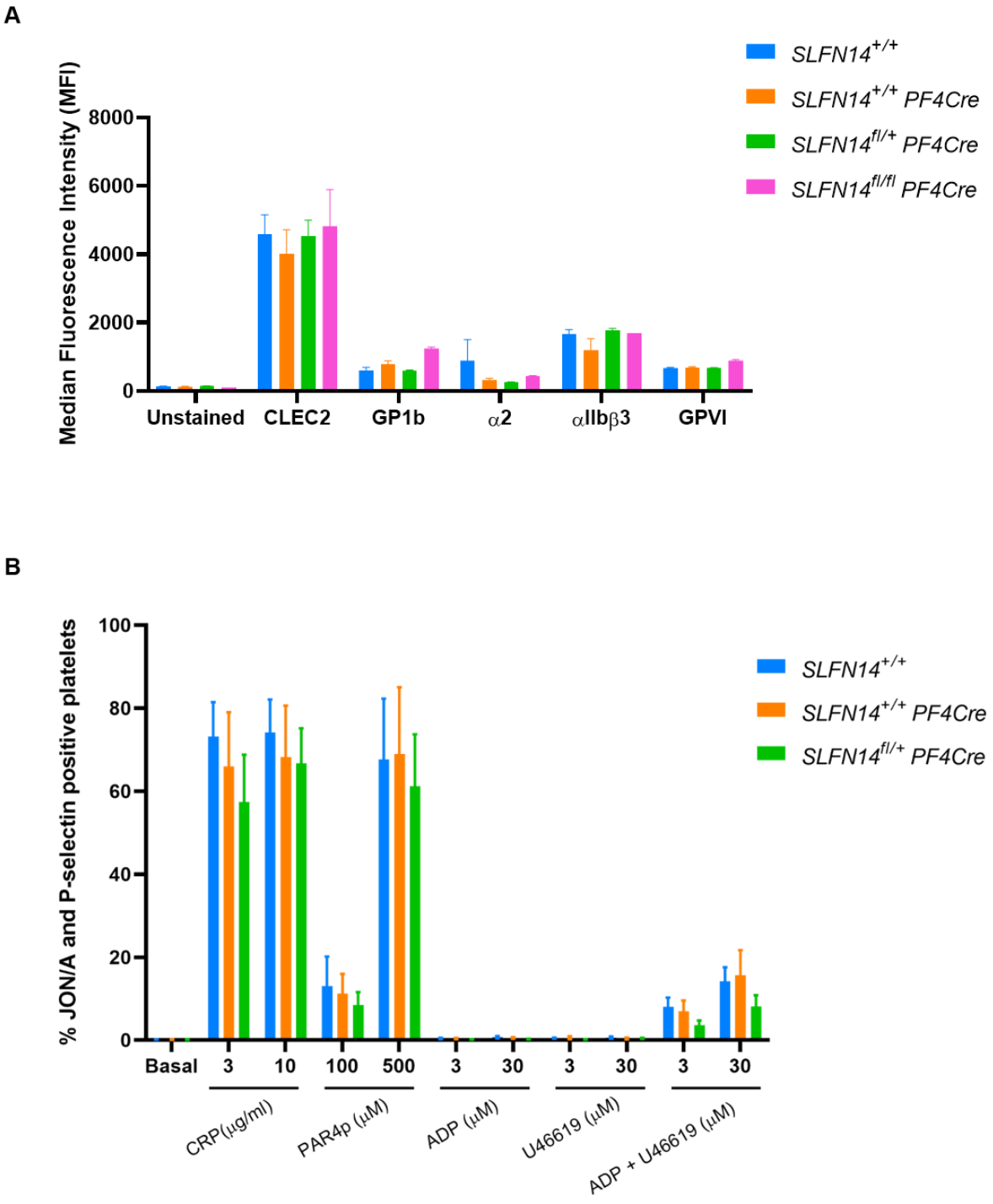


**Figure 6.5: *In vitro* assessment of platelet glycoprotein receptors and activation in *SLFN14-PF4Cre* mice** (A) Resting platelet surface glycoprotein expression levels. GP1ba$^{+}$ platelets were co-stained for indicated surface receptors in whole blood. Median fluorescence intensity (MFI) from n=3-6 mice per genotype. Mean ± SEM; significance assessed by one way ANOVA with correction for multiple comparisons. (B) P-selectin and activated αIIbβ3 (JON/A) expression on *SLFN14-PF4Cre* mouse platelets in response to agonist stimulation. Data presented is the percentage of double positive (P-Selectin and JON/A) platelet events. Mean ± SEM of n=5-7 mice per genotype per condition. Significance assessed by two-way ANOVA with correction for multiple comparisons.

**A(i)**

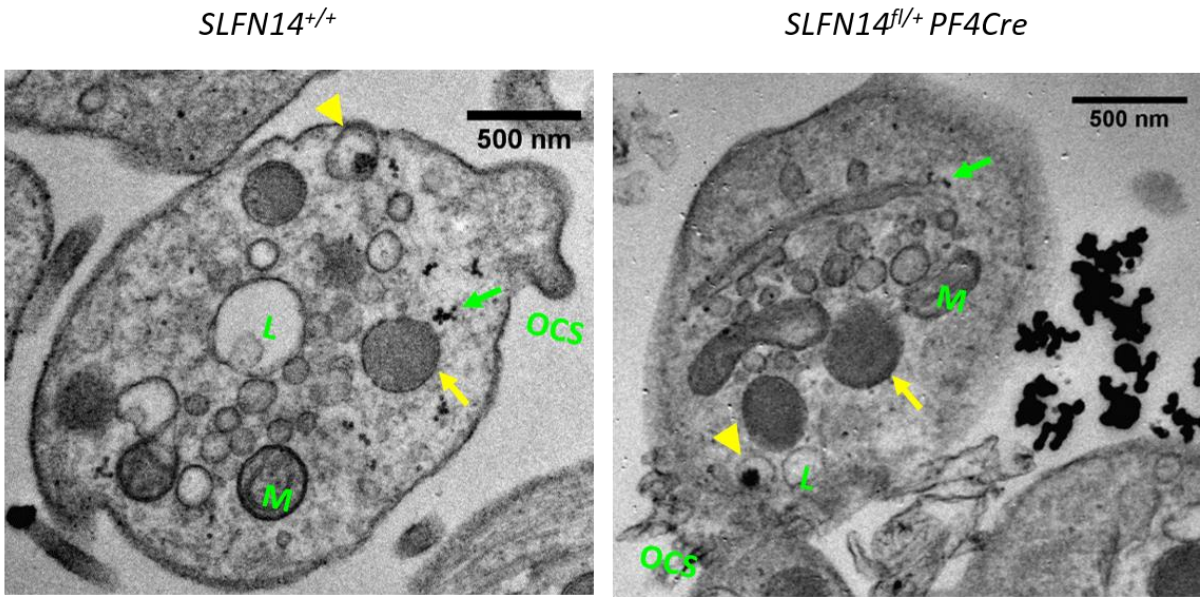


**A(ii)**

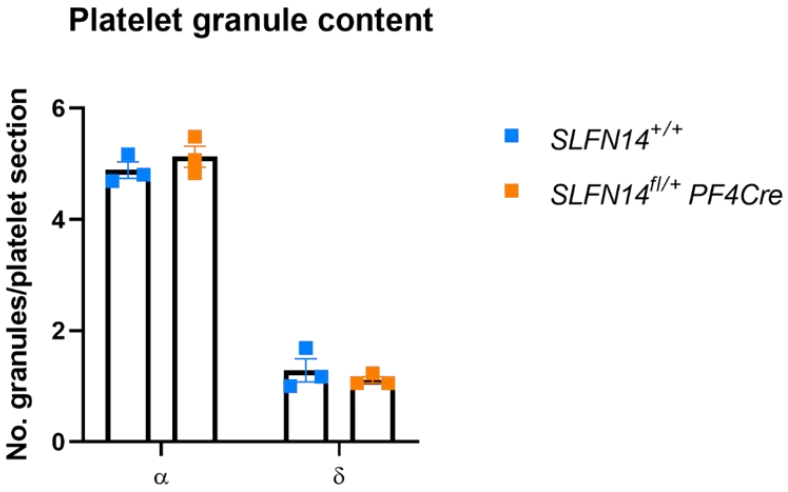


**Figure 6.6: Platelet transmission electron microscopy (TEM) in *SLFN14-PF4Cre* mice.** (Ai) Representative images of TEM sections in *SLFN14*$^{+/+}$ and *SLFN14*$^{fl/+}$ *PF4Cre* mice respectively. Alpha (α) granules (yellow arrow), dense (δ) granules (yellow arrowhead). Other platelet ultrastructure features include: Mitochondria (M), Lysosomes (L), Open canalicular system (OCS) glycogen (green arrow). (ii) Quantification of platelet granules from TEM images. Data presented is mean ± SEM from 35 platelets per mouse, n=3 mice per genotype. Significance assessed by unpaired t-test with Welch's correction.

### 6.3.6 *SLFN14-PF4Cre* mice show normal aggregation in response to major agonists

LTA was used to assess *in vitro* platelet function. Agonists collagen, CRP and thrombin were used at various doses to investigate platelet response via the two main activation pathways (G-PCR and ITAM/receptor tyrosine kinases) (Figure 6.7). Platelets of all genotypes showed clear dose responses to all agonists with increasing concentration as shown in representative traces in Figure 6.7A, B and C and summary in Figure 6.7D. Total ATP secretion was measured alongside the aggregation and similarly, all platelets showed ATP secretion indifferent from controls. There was some variation in the total secretion at 10µg/ml CRP and 0.06U/ml thrombin in *SLFN14*$^{fl/+}$ *PF4Cre* mice however this did not reach significance (Figure 6.7E).

### 6.3.7 *SLFN14*$^{fl/+}$ *PF4Cre* mice have fewer megakaryocytes in the bone marrow

*SLFN14*$^{fl/fl}$*PF4Cre* mice showed a reduced platelet count and *SLFN14*$^{fl/+}$ *Pf4Cre,* although not significant, also showed a similar trend. To investigate the cause of this reduced platelet count, adult mouse bone marrow was assessed by flow cytometry, staining specifically for progenitor populations. In Chapter 5 it was shown that *SLFN14* mutations can affect normal haematopoiesis and it was suggested *SLFN14,* with its endoribonucleolytic properties, may be acting as to cleave RNAs critical in haematopoiesis. This will subsequently affect the differentiation and maturation of progenitor cells which controls the levels of circulating mature blood cells. In this chapter, *SLFN14*$^{fl/+}$ *Pf4Cre* mice showed significantly reduced proportions of MKs in the bone marrow (Figure 6.8A, p=0.033). Unfortunately homozygote mice were not available at the time of these experiments but this reduction in MK population may be further reduced in *SLFN14*$^{fl/fl}$*PF4Cre* mice contributing to the further reduced platelet count observed (Figure 6.3Ai). Erythroid committed cells and MEP populations remained consistent in PF4Cre mice (Figure 6.8B and C). This exact mechanism for this reduction in proportion of MKs in the bone marrow remains to be explored.

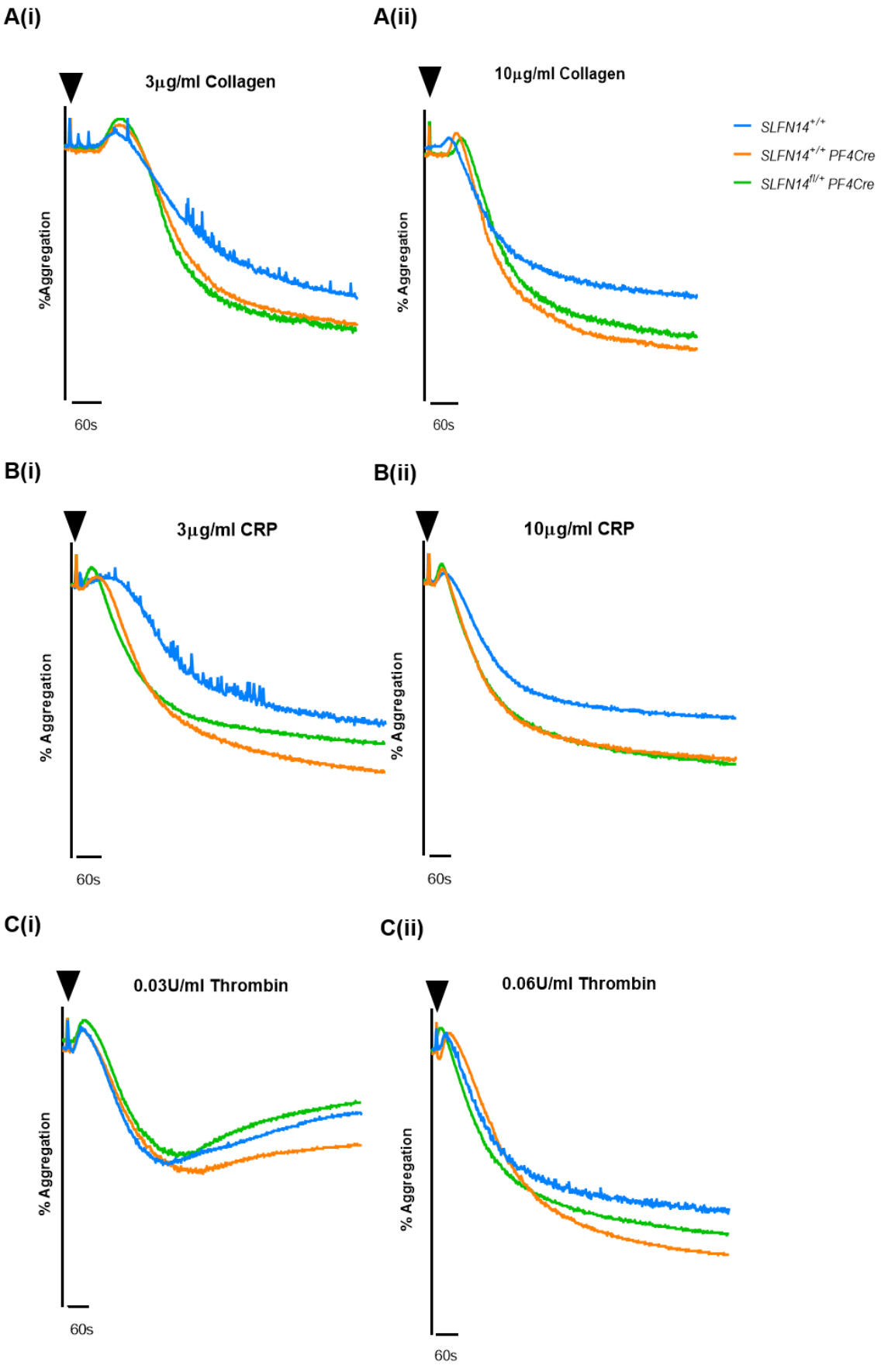
A(i)
3µg/ml Collagen
%Aggregation
60s
A(ii)
10µg/ml Collagen
% Aggregation
60s
SLFN14+/+
SLFN14+/+ PF4Cre
SLFN14fl/+ PF4Cre
B(i)
3µg/ml CRP
% Aggregation
60s
B(ii)
10µg/ml CRP
% Aggregation
60s
C(i)
0.03U/ml Thrombin
% Aggregation
60s
C(ii)
0.06U/ml Thrombin
% Aggregation
60s

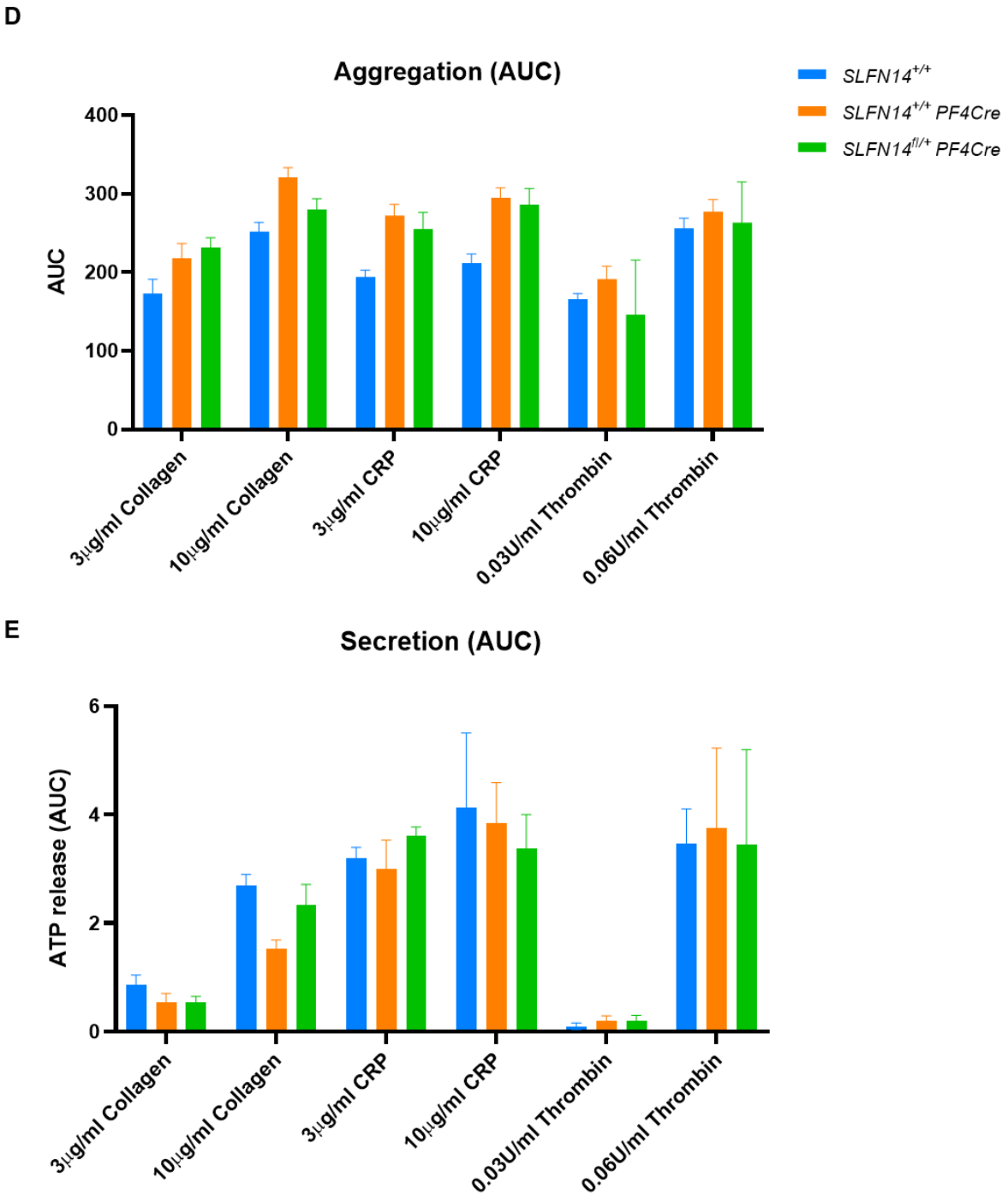


**Figure 6.7: *In vitro* assessment of platelet function in *SLFN14-PF4Cre* mice.** (A, B and C) Platelet function assessed by LTA in washed platelets under stirring conditions showed normal responses to collagen, CRP and thrombin at varying doses. (D) Summary of area under the curve (AUC) for aggregation and (E) summary of AUC for ATP release measured by Chrono-lume. Data is mean ± SEM, n=3-5 mice per genotype. Two-way ANOVA with correction for multiple comparisons.

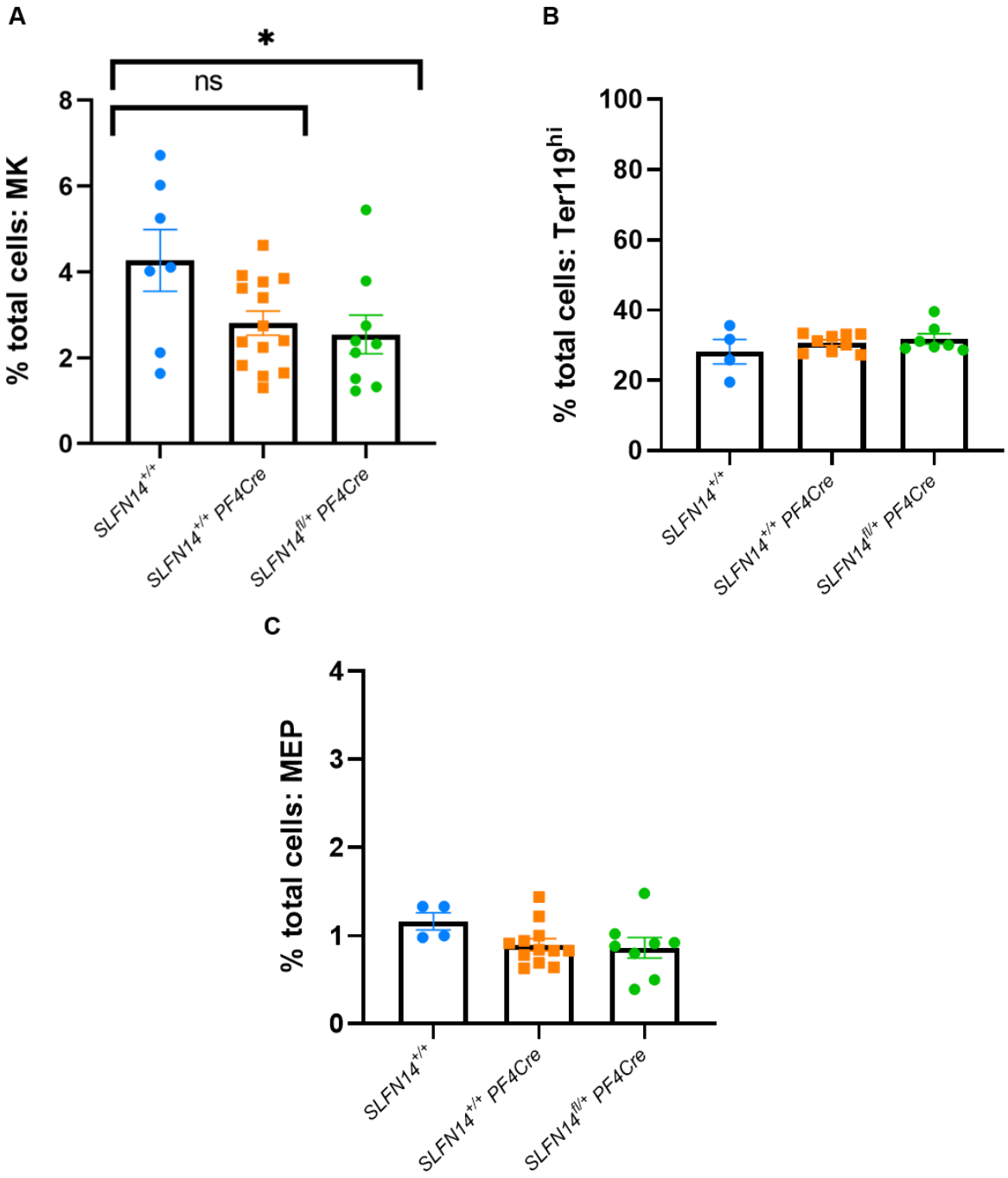


**Figure 6.8: Quantification of bone marrow progenitors in *SLFN14-PF4Cre* mice by flow cytometry.** (A) *SLFN14$^{fl/+}$PF4Cre* mice showed reduced proportion of MKs in whole bone marrow (p=0.033) *SLFN14$^{+/+}$PF4Cre* (p=0.0510). (B) Ter119hi or erythroid committed progenitors and (C) megakaryocyte-erythroid progenitors (MEPs) were unchanged. Data presented is mean ± SEM, n=4-12 mice per genotype analysed blind. Significance was assessed by one-way ANOVA with correction for multiple comparisons.

## 6.4 Discussion

This chapter has explored the generation of the conditional knockout mouse model of *SLFN14* in MKs and platelets using the PF4Cre loxP system. The PF4Cre system has been a longstanding gold standard for MK and platelet conditional mouse models since its discovery in 2007 (Tiedt et al., 2007). Here, exons 2 and 3 were selectively removed when flox mice were also positive for the PF4Cre recombinase. Exon 1 is a non-coding region, with exons 2, 3, 4 and 5 all coding exons. All previously identified mutations in *SLFN14* known to cause thrombocytopenia and bleeding were located in exon 2, therefore it was important to delete this region while exons 4 and 5 remain intact. With exon 2 (and the start codon removed) it is unlikely that exons 4 and 5 result in translated protein unless 'ATG' or an alternative methionine start codon is present within exon 4. Therefore any differences in platelet function could be attributed to the selective deletion of exons 2 and 3 in MKs and platelets. The PF4Cre conditional model has recently been described as being 'leaky' and in some instances such as those described by Nagy et al, having off target effects in leukocyte populations (Nagy et al., 2019). To ensure the PF4Cre model was suitable, *SLFN14* expression was investigated using expression atlas software and previously published data. It was clear that *SLFN14* is not expressed or at undetectable levels in leukocyte populations and in haematopoiesis, is confined to MK and erythroid lineages (Madeira et al., 2019) (Figure 6.9). In addition, *SLFN14* in mice is located on chromosome 11 in very close proximity to the locus of mouse *Gp1ba* whereas *PF4* is on mouse chromosome 5 (Bult et al., 2019). This would make targeting specific regions of *SLFN14* with loxP sites and not to affect *GP1ba* transcription very difficult. Together, this ensured the PF4Cre recombinase model was most suitable to investigate *SLFN14* function in MKs and platelets.

Platelet counts in *SLFN14*$^{fl/fl}$*PF4Cre* mice were significantly reduced, accompanied by an increased MPV. In *SLFN14*$^{fl/+}$*PF4Cre* mice, platelet count and size was reduced and increased respectively, although this did not reach significance. All other blood cell counts

were consistent between genotypes, providing assurance that floxed *SLFN14* (without expression of PF4Cre) did not impact blood cell production in other lineages. Platelet function measured by activation, degranulation and aggregation was retained in both heterozygous and homozygous floxed mice. This is dissimilar to the *in vitro* platelet function defect observed in patients (Fletcher et al., 2015). Despite this, at this stage it is unclear if these mice replicate the bleeding phenotype observed in *SLFN14* patients. This will be investigated in future experiments with *in vivo* haemostasis and thrombosis assays.

The reduced circulating platelet count most likely arises from the reduced proportion of MKs in the bone marrow. Naturally, fewer MKs in the bone marrow will give rise to fewer pro-platelets released and subsequently mature platelets but this should be explored further using more mice to assess any differences in MK proportion are significant. In addition, platelets were enlarged and as previously reported, enlarged platelets are associated with increased reactivity. This did not appear to be the case in *SLFN14*$^{fl/fl}$ *PF4Cre* mice *in vitro* (Loo and Martin, 1999). Enlarged *SLFN14*$^{fl/fl}$ *PF4Cre* platelets presented with similar numbers of major glycoprotein receptors and granule content compared to controls, suggesting the packaging and processing of platelets in megakaryopoiesis is indifferent from controls which ultimately does not affect their function.

However, it remains to be explored how this reduction in MKs may contribute to reduced circulating platelets. Histology staining will reveal potential differences in MK structure, nuclear ploidy and distribution within the bone marrow. *SLFN14* is an endoribonuclease, where it may be plausible that conditional knockout of exons 2 and 3 results in cleavage of RNAs or transcription factors critical in megakaryopoiesis. As such, conditional removal of these may affect thrombopoietin (TPO) binding to c-Mpl receptors, one of the primary mechanisms critical in stimulating expansion and differentiation of MKs (Xu et al., 2018). Disruption to the c-Mpl/TPO signalling pathway is just one potential hypothesis for the reduced levels of enlarged circulating platelets which at present is unclear. The *SLFN14*-

*PF4Cre* conditional mouse model will be invaluable to study *SLFN14* in megakaryopoiesis. While the *SLFN14*-K208N model will reveal endoribonucleolytic function at the global level which has been shown to affect MK and erythroid lineages, this PF4Cre mouse will specifically target the MK lineage and be more applicable to platelet defects in *SLFN14* patients (Stapley et al., 2021).

**Mus musculus**

**Figure 6.9: *SLFN14* expression in various tissues from Mus musculus.** *SLFN14* expression is confined to MK and erythroid haematopoietic lineages. Expression was below cut-off range for detection in leukocyte and lymphoid tissues. Screenshot taken from ebi.ac.uk Expression Atlas (accessed 06/05/2021).

# Chapter 7

General Discussion

# Chapter 7 – General Discussion

## 7.1 *SLFN14* mutant mouse models and phenotype summary

The first aim of this thesis was to develop a genetically modified mouse model with the K208N mutation using CRISPR Cas-9 genome editing. This was used to further investigate the effect of the patient K219N mutation with particular focus on platelet development and function. The work presented in Chapter 3 shows that this CRISPR mouse model was viable in heterozygotes and as a result of the CRISPR HDR repair mechanism, generated several other mutations within the same region of *SLFN14*. This is a common problem in the field and although CRISPR engineering is highly specific, some errors still occur which should be appreciated when assessing its success. Sanger sequencing was used to validate the K208N substitution and subsequently these extra *SLFN14* mutations were separated, bred out and retained for further study, ensuring any differences were only attributable to one mutation. These 'indel' mutations did not present differences in platelet count, morphology or *in vitro* function compared to wild-types, suggesting it is the specific amino acid change K208N, rather than truncation of SLFN14 protein, which causes altered platelet and erythrocyte function in *SLFN14* mice.

*SLFN14*-K208N was a global genetically modified model and from initial blood counting it was clear erythrocytes were also affected. At this point it was important to consider not only platelet function but the involvement of abnormal erythrocytes particularly in *in vivo* assays. As set out in aim 2 the plan of this thesis was to investigate *SLFN14*-K208N with respect to platelet function only. However, given the observations described in Chapter 4 it became clear this presented significant species-specific differences between cell types. Thus, to understand *SLFN14* with respect to platelet function and reveal potential mechanisms for the platelet defect in humans, the *SLFN14 PF4Cre* mouse model was used in preference. Selective deletion of exons 2 and 3 was obtained using the Cre loxP system on a PF4 background. *SLFN14* is expressed at very minimal levels in leukocytes and its proximity to

the GP1b locus (an alternative platelet and MK Cre specific strain) meant PF4 was a more suitable selective marker. Here, flox mice (both heterozygous and homozygous) expressing PF4Cre presented with a mild macrothrombocytopenia but retained platelet function. This reduced circulating platelet count is similar to *SLFN14* patients, potentially highlighting a mechanism for *SLFN14* involved in megakaryopoiesis regardless of species. However, the reason for the difference in reduced platelet function in patients remains unclear.

In summary of this thesis, novel genetically modified mouse models of *SLFN14* have been developed and present significantly different phenotypes. In a global *SLFN14*-K208N mouse model, erythrocytes are of abnormal quantity, shape and appear to impair thrombus stability *in vivo* at lower shear rates, while platelet count, morphology and function is retained. However, in *SLFN14 PF4Cre* mice, preliminary studies show platelet count is reduced due to reduced proportions of CD41/CD42 stained MKs in the bone marrow potentially affecting MK maturation and subsequent proplatelet release. However, at this stage this does not appear to affect *in vitro* platelet function. *In vivo* assays with particular focus on tail bleeding haemostasis assay will be required to fully define the effect of *SLFN14 PF4Cre* in bleeding. To date, this is the first investigation of SLFN14 involvement in platelet and erythrocyte function. The summary of these phenotypes, in comparison to that observed in *SLFN14* patients is summarised in Figure 7.1.

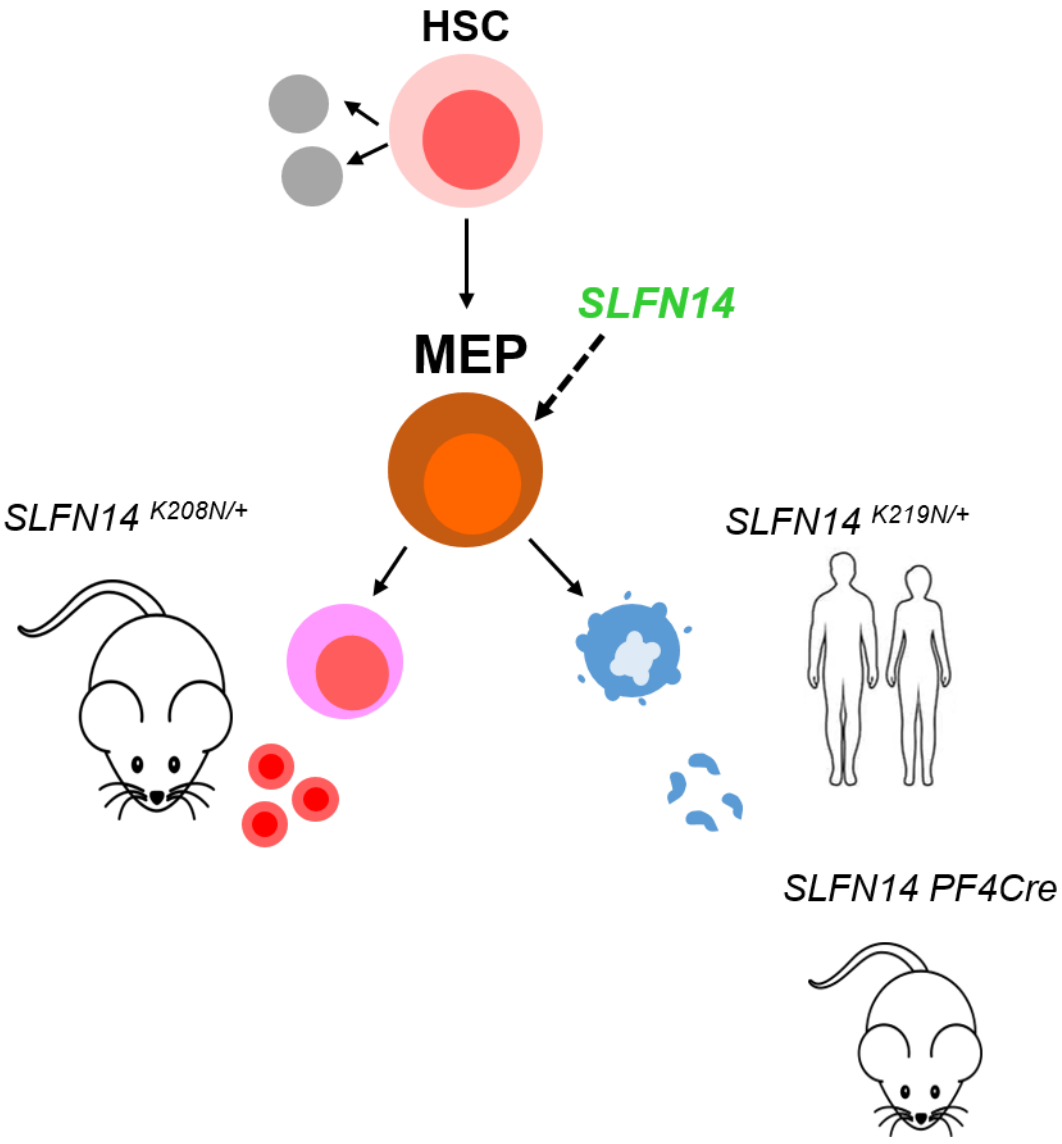


**Figure 7.1: Schematic adapted from Stapley et al. showing species-specific phenotype differences of mutations in SLFN14.** Human K219N patients present with macrothrombocytopenia and bleeding and SLFN14 PF4Cre mice also have macrothrombocytopenia. However, mice with the homologous mutation (*SLFN14*-K208N) do not have a platelet defect but show microcytosis and anaemia. SLFN14 is predicted to function at the MEP cleaving RNAs critical to lineage commitment giving rise to species and lineage dependent phenotypes. (Stapley et al., 2021)

## 7.2 *SLFN14* in platelet function

*SLFN14 in vitro* platelet function is retained in K208N mice but appears to contribute to reduced thrombus stability in *in vivo* models. It has been shown that increased erythrocyte count and subsequently haematocrit can affect blood rheology and increase platelet margination at the vessel wall rendering platelets hyper-reactive (Barshtein et al., 2007). However, upon vessel injury thrombus formation occurred at a similar rate to controls and platelets were not more reactive. In contrast, thrombi embolised quicker than controls, particularly under lower shear rates in the cremaster arterioles suggestive that the abnormal erythrocytes play a major factor in thrombus stability. It has been shown that erythrocytes form polyhedrocytes to seal clots, while platelets mainly provide the fibrin meshwork needed for clot elasticity (Ariens, 2015). Interestingly, the same research group have shown that erythrocytes and platelets can interact directly with fibrinogen in comparable affinity in a β3 integrin dependent manner (Ariens, 2015). In the case of *SLFN14*-K208N it may be proposed that abnormal erythrocyte membrane dynamics may in fact disrupt this interaction. Clot stabilisation in wild-type mice is dependent on the contribution of both fully functional fibrinogen interactions of platelets and erythrocytes, but with only functional platelet binding, this may not be achieved in K208N mice. However, it is unclear if this mechanism still applies in haemostasis. Further exploration of this mechanism is needed through clot composition with labelling fibrin, erythrocytes and platelets.

Clot instability of the IVC has been explored previously whereby CLEC-2 knockout mice (global inducible deletion or platelet specific deficient) are protected from deep vein thrombosis (DVT) based on their inability to interact with podoplanin at the vessel wall (Payne et al., 2017). This is based on a thrombo-inflammatory mechanism where CLEC-2 is a major receptor contributing to platelet-leukocyte interactions. CLEC-2 knockout mice in similarity to *SLFN14*-K208N have normal *in vitro* aggregation responses to collagen, CRP and thrombin (Haining et al., 2017, May et al., 2009) Contrastingly, β-thalassemia patients

are known to have an increased risk of thrombosis based on their chronic platelet activation and microcytic anaemia (Succar et al., 2011). It will be interesting to investigate DVT in these mice and assess the extent of platelet-erythrocyte interactions at the vessel wall, as well as whether their haemolytic anaemia is a major contributor of thrombosis, in a similar way to thalassemia patients.

Other than contributing to reduced thrombus stability, it appears the erythrocyte defect did not play any part in increasing thrombosis risk through thrombin generation or spontaneous activation of platelets.

### 7.3 SLFN14 is a key regulator in haematopoiesis

Transcription factors involved in megakaryopoiesis and erythropoiesis have very similar expression patterns, occurring at early stages in haematopoiesis and as suggested previously, there is significant overlap of GATA-1 and GATA-2 factors contributing to differentiation in both lineages. It was proposed that the binding sites of transcription regulators are different depending on the lineage but this is currently unclear and as such cytokines remain the major contributor to deciding lineage fate (Doré et al., 2012). In order to investigate this further RNA sequencing of different progenitors (MEP, ProE and MK) will highlight transcriptional differences throughout different lineages and highlight where in haematopoiesis such changes may occur with preference to one lineage or another. In addition to this, the presence of mutant SLFN14 may present different co-localisation patterns of rRNA in haematopoietic cells, showing evidence of endoribonucleolytic activity and RNA degradation in haematopoiesis similar to Dami and HEK293T cell experiments by Fletcher et al. 2018. (Fletcher et al., 2018).

Recently Di Giandomenico et al identified a key physiological role of MKs in erythropoiesis. In the bone marrow MKs are one of the main sources of transforming growth factor β1 (TGFβ1), a major cytokine involved in haematopoietic stem cell fate, proliferation and differentiation (Blobe et al., 2000). Briefly, suppression of TGFβ1 in MKs has shown to

accelerate erythropoiesis through increased EPO production and the subsequent feedback loop accelerating erythropoiesis (Di Giandomenico et al., 2020). In an MK specific *TGFβ1* knockout mouse they show an increased expansion of erythroid progenitors, reduced apoptosis which under usual circumstances controls excess erythrocyte production and a final elevated erythrocyte count (Di Giandomenico et al., 2020 {Zhao, 2014 #221). In the context of this thesis it may be interesting to study the SLFN14 K208N mutation in cytokine regulation, specifically to investigate if SLFN14 or its mutations interfere with the MK-TGFβ1 axis and subsequently increases erythrocyte production in response to EPO signalling.

The *SLFN14PF4Cre* model will be useful in eliminating effects of SLFN14 in other haematopoietic lineages and pinpointing differences only present in the MK. Although platelet function was retained in these mice, SLFN14 activity in megakaryopoiesis and particularly the production of enlarged platelets will be more relevant to patient phenotypes.

Importantly, could this model be applicable as a therapeutic target? In patients with haematopoietic disorders such as polycythaemia vera or thrombocythaemia which have elevated erythrocyte and platelet counts respectively, it raises the question whether SLFN14 in RNA cleavage or degradation may be a positive mechanism for controlling the over-production of some cell types? Could lineage restriction or biases actually be beneficial in patients with heightened risk of thrombosis? If a sequence target for SLFN14 in haematopoiesis can be identified, it may be possible to reprogram the bone marrow in directing lineage preference to correct disorders of cell number without functional impairment. This would alleviate pressures of finding donor matched blood for transfusions with patients of rare blood types or those who have become alloimmunised.

This is very much a future perspective but bone marrow transplantation in *SLFN14*-K208N and *SLFN14 PF4Cre* mice will highlight if SLFN14 functions in an innate or acquired manner. Can SLFN14 function in haematopoiesis be corrected by bone marrow transplantation of

wild-types or is this an intrinsic response which can only be treated later in blood cell production?

### 7.3.1 *SLFN14* in megakaryopoiesis

Aims 3 and 4 of this thesis were to investigate platelet production and function in both *SLFN14*-K208N and *SLFN14 PF4Cre* mouse models. Circulating platelet counts were normal in K208N heterozygote mice although the immature platelet fraction was increased. Previous studies have suggested that immature platelets may be more reactive but this did not appear to be the case, and as such did not hold any functional relevance. In the *SLFN14 PF4Cre* model, mice showed macrothrombocytopenia although at this stage it has not been determined if this enlarged size is due to an elevated immature platelet fraction. *In vivo* platelet depletion and recovery assays (depleting using a GPIB antibody and lifespan labelling platelets with biotin) will reveal the rate of megakaryopoiesis and platelet production alongside platelet destruction and clearance. Given normal circulating levels in K208N mice it may be predicted that platelet clearance is normal but megakaryopoiesis may be accelerated hence premature release of immature platelets. This may be the opposite in *SLFN14 PF4Cre* mice whereby megakaryopoiesis is delayed or reduced in response to endoribonucleolytic activity of SLFN14 in transcription regulation or cytokine signalling in megakaryopoiesis. It would also be interesting to examine the differentiation and maturation process of *SLFN14 PF4Cre* MKs *in vitro,* using varying concentrations of cytokines to observe if this macrothrombocytopenia is mirrored in TPO deficient conditions, or can be corrected with additional TPO supplementation.

To mimic endoribonucleolytic properties of SLFN14 in megakaryopoiesis it may be possible to use CRISPR genome engineering in inducible pluripotent stem cells (iPSCs). Due to the difficulty in obtaining MKs from *SLFN14* patients, inducing mutations into these cell lines using CRISPR and *in vitro* forward programming techniques will allow investigation into SLFN14 activity with respect to human megakaryopoiesis. Platelet function in these patients

has been well characterised, but the question is now what the mechanism is for these and where do differences arise during megakaryopoiesis? Using iPSCs will also allow production of progenitors from other lineages and in particular explore the behaviour of cells within the erythroid lineage of *SLFN14* patient mutations.

### 7.3.2 *SLFN14* in erythropoiesis and anaemia

Aim 3 of this thesis was to address the role of *SLFN14*-K208N in the myeloid lineage of haematopoiesis. This arose due the unexpected erythrocyte defect observed in chapter 4 when investigating platelet function. It was at this point it became clear that SLFN14 was functioning during haematopoiesis and may affect multiple lineages.

One major factor with regard to the erythrocyte phenotype was severe anaemia. This was particularly surprising given the elevated circulating erythrocyte count with erythrocytes produced in both the bone marrow and spleen. The splenomegaly observed in *SLFN14* K208N heterozygotes was attributed partly to EMH but may also be as a result of increased erythrocyte clearance. Given normal proportions of progenitors in the bone marrow, the current working hypothesis is that the EMH in the spleen is in fact a stress response in order to compensate for anaemia by production of additional erythrocytes. However, haemolysis in the spleen is also upregulated, suggesting the balance between production and destruction of erythrocytes is disrupted. Biotinylation of erythrocytes in the circulation will allow investigation into erythrocyte clearance patterns and deduce whether the increased population of EryC cells in spleens are newly produced (from EryB progenitors) or if they are awaiting clearance. In addition, it may be interesting to investigate complete blood counts over a period of weeks beginning from the early postnatal stage. The kinetics of blood cell production undergoes various shifts from the early embryo into adulthood, particularly between the liver and spleen which may provide useful insight into the mechanism of SLFN14 and RNA interactions specific to erythropoiesis (Baron et al., 2013). No bone marrow scarring was observed by reticulin staining suggesting bone marrow function is

retained and EMH is a stress response to anaemia, potentially triggered by upregulated EPO production. This could be assessed by splenectomy; removal of the spleen may result in a reduced erythrocyte count and a subsequent defect in bone marrow erythropoiesis may be highlighted which is currently being covered by EMH compensation. Despite erythrocyte membranes appearing distorted, they do not express PS under resting conditions suggesting they are not circulating in an apoptotic state. However it is unclear if these are older cells and therefore not being cleared properly by the spleen or newly produced poikilocytes. SYTO13 staining for residual RNA will address immature reticulocyte fraction accompanied by biotinylation assays will highlight if erythrocyte clearance is normal.

Bone marrow erythroid progenitors are at normal levels in *SLFN14*-K208N mice identified by their cell receptors but it unknown if they have the correct RNA sequence and binding sites for transcription regulation or if they respond normally to EPO. This could be addressed by RNA sequencing of erythroid progenitors to show differences in cell signatures which may be occurring in response to altered levels of haematopoietic mRNAs. RNAs may be cleaved in early primitive erythropoiesis in the yolk sac resulting in defective haemoglobin development. This may cause embryonic lethality in homozygotes after E16.5 but survival in heterozygotes due to effective stress response in postnatal splenic EMH. *In vitro* differentiation using EPO at varying concentrations will give information with regard to potential reduced EPO response in a similar way to that suggested in section 7.3.1 for megakaryopoiesis.

At this stage it appears *SLFN14 PF4Cre* phenotype is restricted to the MK lineage but haematopoiesis and potential EMH will be investigated in the future.

## 7.4 Contribution of this thesis to wider research on endoribonucleases and haematopoietic regulation

These species differences, as well as differences between mouse models suggest *SLFN14* is a key mediator in haematopoiesis. In mice and humans, expression of SLFN14 is limited to the myeloid lineage which affecting normal differentiation and function of terminal circulating

cells. In humans, this occurs in MKs and platelets, although erythroid lineage investigation is ongoing. With the generation of iPSCs containing *SLFN14* patient mutations, this will allow us to use forward programming and *in vitro* differentiation to fully scrutinise the mechanism of RNA cleavage with respect to MK lineage which leads to macrothrombocytopenia and bleeding in these patients. In a mouse model of the same mutation, the phenotype very much occurs in the erythroid lineage while platelet function is retained. MKs and ProEs have a common progenitor, namely MEP. This suggests, in a species dependent manner, SLFN14 as an endoribonuclease is cleaving RNAs potentially at the MEP which ultimately alters lineage fate or function in subsequent progenitors (Figure 7.1). In the *SLFN14 PF4Cre* model, although platelet function is normal, there is discrepancy with platelet production which may be of the same mechanism leading to reduced platelet count in patients.

As a whole, endoribonucleases are very under-researched, with very little information of their involvement in disease. However, SLFNs or more precisely subgroup III SLFNs, are often described in studies of differentiation, proliferation and replication stressing their importance in control of cell production (Table 7.1). This thesis has expressed the importance of species-specific differences which can arise when comparing mouse to man and the considerations which need to be made when likening phenotypes across species. In addition, this thesis has highlighted that SLFN14 is a novel regulator in the myeloid lineage of haematopoiesis and is an important transcription regulator of disease progression in both humans and mice.

**Table 7.1: Publications describing Schlafen genes/proteins involved in cell differentiation, transcription and replication.**

| Title | Reference |
|---|---|
| Schlafen, a New Family of Growth Regulatory Genes that Affect Thymocyte development | (Schwarz et al., 1998) |
| Characterization of Novel Ribosome-Associated Endoribonuclease SLFN14 from Rabbit Reticulocytes | (Pisareva et al., 2015) |
| Expression and regulation of Schlafen (SLFN) family members in primary human monocytes, monocyte-derived dendritic cells and T cells | (Puck et al., 2015) |
| Non-human Primate Schlafen11 Inhibits Production of Both Host and Viral Proteins | (Stabell et al., 2016) |
| Schlafen14 (SLFN14) is a novel antiviral factor involved in the control of viral replication | (Seong et al., 2017) |
| Role of the novel endoribonuclease SLFN14 and its disease-causing mutations in ribosomal degradation | (Fletcher et al., 2018) |
| Structure of Schlafen13 reveals a new class of tRNA/rRNA-targeting RNase engaged in translational control | (Yang et al., 2018) |
| The Schlafen family: Complex roles in different cell types and virus replication | (Liu et al., 2018) |
| SLFN11 promotes stalled fork degradation that underlies the phenotype in Fanconi anaemia cells | (Okamoto et al., 2021) |

**References**


ABRAM, C. L., ROBERGE, G. L., HU, Y. & LOWELL, C. A. 2014. Comparative analysis of the efficiency and specificity of myeloid-Cre deleting strains using ROSA-EYFP reporter mice. *J Immunol Methods,* 408**,** 89-100.

ADLI, M. 2018. The CRISPR tool kit for genome editing and beyond. *Nature Communications,* 9**,** 1911.

ALAN, T. N. & PAQUITA, N. 2020. Inherited thrombocytopenias: history, advances and perspectives. *Haematologica,* 105**,** 2004-2019.

ALMAZNI, I., CHUDAKOU, P., DAWSON-MEADOWS, A., DOWNES, K., FRESON, K., MASON, J., PAGE, P., REAY, K., MYERS, B. & MORGAN, N. V. 2021. A novel RUNX1 exon 3 - 7 deletion causing a familial platelet disorder. *Platelets***,** 1-4.

ALMAZNI, I., STAPLEY, R. & MORGAN, N. V. 2019. Inherited Thrombocytopenia: Update on Genes and Genetic Variants Which may be Associated With Bleeding. *Frontiers in Cardiovascular Medicine,* 6.

ALMAZNI, I., STAPLEY, R. J., KHAN, A. O. & MORGAN, N. V. 2020. A comprehensive bioinformatic analysis of 126 patients with an inherited platelet disorder to identify both sequence and copy number genetic variants. *Hum Mutat*.

AMBROSIO, A. L., BOYLE, J. A. & DI PIETRO, S. M. 2012. Mechanism of platelet dense granule biogenesis: study of cargo transport and function of Rab32 and Rab38 in a model system. *Blood,* 120**,** 4072-81.

ANTONY-DEBRÉ, I., BLUTEAU, D., ITZYKSON, R., BACCINI, V., RENNEVILLE, A., BOEHLEN, F., MORABITO, M., DROIN, N., DESWARTE, C., CHANG, Y., LEVERGER, G., SOLARY, E., VAINCHENKER, W., FAVIER, R. & RASLOVA, H. 2012. MYH10 protein expression in platelets as a biomarker of RUNX1 and FLI1 alterations. *Blood,* 120**,** 2719-2722.

ARIENS, R. A. S. 2015. Contribution of Red Blood Cells and Clot Structure to Thrombosis. *Blood,* 126**,** SCI-15-SCI-15.

ATHANASIOU, M., MAVROTHALASSITIS, G., SUN-HOFFMAN, L. & BLAIR, D. G. 2000. FLI-1 is a suppressor of erythroid differentiation in human hematopoietic cells. *Leukemia,* 14**,** 439-45.

AVECILLA, S. T., HATTORI, K., HEISSIG, B., TEJADA, R., LIAO, F., SHIDO, K., JIN, D. K., DIAS, S., ZHANG, F., HARTMAN, T. E., HACKETT, N. R., CRYSTAL, R. G., WITTE, L., HICKLIN, D. J., BOHLEN, P., EATON, D., LYDEN, D., DE SAUVAGE, F. & RAFII, S. 2004. Chemokine-mediated interaction of hematopoietic progenitors with the bone marrow vascular niche is required for thrombopoiesis. *Nat Med,* 10**,** 64-71.

BALDUINI, C. L., PECCI, A. & SAVOIA, A. 2011. Recent advances in the understanding and management of MYH9-related inherited thrombocytopenias. *British Journal of Haematology,* 154**,** 161-174.

BARDAWIL, T., REBEIZ, A., CHAABOUNI, M., EL HALABI, J., KAMBRIS, Z., ABBAS, O., ABOU HASSAN, O., HAMIE, L., BITAR, F. & KIBBI, A. G. 2017. Mutations in the ABCG8 gene are associated with sitosterolaemia in the homozygous form and xanthelasmas in the heterozygous form. *European Journal of Dermatology,* 27**,** 519-523.

BARON, M. H., VACARU, A. & NIEVES, J. 2013. Erythroid development in the mammalian embryo. *Blood Cells Mol Dis,* 51**,** 213-9.
BARRANGOU, R., FREMAUX, C., DEVEAU, H., RICHARDS, M., BOYAVAL, P., MOINEAU, S., ROMERO, D. A. & HORVATH, P. 2007. CRISPR provides acquired resistance against viruses in prokaryotes. *Science,* 315**,** 1709-12.
BARSHTEIN, G., BEN-AMI, R. & YEDGAR, S. 2007. Role of red blood cell flow behavior in hemodynamics and hemostasis. *Expert Rev Cardiovasc Ther,* 5**,** 743-52.
BASTIDA, J. M., BENITO, R., JANUSZ, K., DÍEZ-CAMPELO, M., HERNÁNDEZ-SÁNCHEZ, J. M., MARCELLINI, S., GIRÓS, M., RIVERA, J., LOZANO, M. L., HORTAL, A., HERNÁNDEZ-RIVAS, J. M. & GONZÁLEZ-PORRAS, J. R. 2017. Two novel variants of the ABCG5 gene cause xanthelasmas and macrothrombocytopenia: a brief review of hematologic abnormalities of sitosterolemia. *Journal of Thrombosis and Haemostasis,* 15**,** 1859-1866.
BEHNKE, O. 1968. An electron microscope study of the megacaryocyte of the rat bone marrow. I. The development of the demarcation membrane system and the platelet surface coat. *J Ultrastruct Res,* 24**,** 412-33.
BICK, R. L. 2000. Recurrent miscarriage syndrome due to blood coagulation protein/platelet defects: prevalence, treatment and outcome results. DRW Metroplex Recurrent Miscarriage Syndrome Cooperative Group. *Clin Appl Thromb Hemost,* 6**,** 115-25.
BLOBE, G. C., SCHIEMANN, W. P. & LODISH, H. F. 2000. Role of transforming growth factor beta in human disease. *N Engl J Med,* 342**,** 1350-8.
BLUTEAU, D., BALDUINI, A., BALAYN, N., CURRAO, M., NURDEN, P., DESWARTE, C., LEVERGER, G., NORIS, P., PERROTTA, S., SOLARY, E., VAINCHENKER, W., DEBILI, N., FAVIER, R. & RASLOVA, H. 2014. Thrombocytopenia-associated mutations in the ANKRD26 regulatory region induce MAPK hyperactivation. *Journal of Clinical Investigation,* 124**,** 580-591.
BOULAFTALI, Y., HESS, P. R., KAHN, M. L. & BERGMEIER, W. 2014. Platelet immunoreceptor tyrosine-based activation motif (ITAM) signaling and vascular integrity. *Circulation research,* 114**,** 1174-1184.
BULT, C. J., BLAKE, J. A., SMITH, C. L., KADIN, J. A. & RICHARDSON, J. E. 2019. Mouse Genome Database (MGD) 2019. *Nucleic Acids Res,* 47**,** D801-d806.
BUNN, H. F., GU, J., HUANG, L. E., PARK, J. W. & ZHU, H. 1998. Erythropoietin: a model system for studying oxygen-dependent gene regulation. *J Exp Biol,* 201**,** 1197-201.
BURK, C., NEWMAN, P., LYMAN, S., GILL, J., COLLER, B. & PONCZ, M. 1991. A deletion in the gene for glycoprotein IIb associated with Glanzmann's thrombasthenia. *The Journal of clinical investigation,* 87**,** 270-276.
BUSTOS, O., NAIK, S., AYERS, G., CASOLA, C., PEREZ-LAMIGUEIRO, M. A., CHIPPINDALE, P. T., PRITHAM, E. J. & DE LA CASA-ESPERON, E. 2009. Evolution of the Schlafen genes, a gene family associated with embryonic lethality, meiotic drive, immune processes and orthopoxvirus virulence. *Gene,* 447**,** 1-11.
BYRNES, J. R. & WOLBERG, A. S. 2017. Red blood cells in thrombosis. *Blood,* 130**,** 1795-1799.
CALAMINUS, S. D., GUITART, A. V., SINCLAIR, A., SCHACHTNER, H., WATSON, S. P., HOLYOAKE, T. L., KRANC, K. R. & MACHESKY, L. M. 2012. Lineage

tracing of Pf4-Cre marks hematopoietic stem cells and their progeny. *PLoS One,* 7**,** e51361.
CAPECCHI, M. R. 1989. The new mouse genetics: altering the genome by gene targeting. *Trends Genet,* 5**,** 70-6.
CARVER-MOORE, K., BROXMEYER, H. E., LUOH, S. M., COOPER, S., PENG, J., BURSTEIN, S. A., MOORE, M. W. & DE SAUVAGE, F. J. 1996. Low levels of erythroid and myeloid progenitors in thrombopoietin-and c-mpl-deficient mice. *Blood,* 88**,** 803-8.
CHASIS, J., PRENANT, M., LEUNG, A. & MOHANDAS, N. 1989. Membrane assembly and remodeling during reticulocyte maturation. *Blood,* 74**,** 1112-1120.
CHEN, K., LIU, J., HECK, S., CHASIS, J. A., AN, X. & MOHANDAS, N. 2009. Resolving the distinct stages in erythroid differentiation based on dynamic changes in membrane protein expression during erythropoiesis. *Proceedings of the National Academy of Sciences,* 106**,** 17413-17418.
CHOI, E. S., NICHOL, J. L., HOKOM, M. M., HORNKOHL, A. C. & HUNT, P. 1995. Platelets generated in vitro from proplatelet-displaying human megakaryocytes are functional. *Blood,* 85**,** 402-13.
COONEY, K. A., NICHOLS, W. C., BRUCK, M. E., BAHOU, W. F., SHAPIRO, A. D., BOWIE, E. J. W., GRALNICK, H. R. & GINSBURG, D. 1991. The Molecular Defect in Type IIB von Willebrand Disease. *J. Clin. Invest.***,** 1227-1233.
DAVIS, B. H., ORNVOLD, K. & BIGELOW, N. C. 1995. Flow cytometric reticulocyte maturity index: a useful laboratory parameter of erythropoietic activity in anemia. *Cytometry,* 22**,** 35-9.
DEUTSCH, V. R. & TOMER, A. 2006. Megakaryocyte development and platelet production. *British Journal of Haematology,* 134**,** 453-466.
DI GIANDOMENICO, S., KERMANI, P., MOLLÉ, N., YABUT, M. M., ABU-ZEINAH, G., STEPHENS, T., MESSALI, N., SCHREINER, R., BRENET, F., RAFII, S. & SCANDURA, J. M. 2020. Megakaryocyte TGFβ1 partitions erythropoiesis into immature progenitor/stem cells and maturing precursors. *Blood,* 136**,** 1044-1054.
DORÉ, L. C., CHLON, T. M., BROWN, C. D., WHITE, K. P. & CRISPINO, J. D. 2012. Chromatin occupancy analysis reveals genome-wide GATA factor switching during hematopoiesis. *Blood,* 119**,** 3724-33.
DUNCKLEY, T. & PARKER, R. 2001. RNA Turnover. *In:* MALOY, S. & HUGHES, K. (eds.) *Brenner's Encyclopedia of Genetics (Second Edition).* San Diego: Academic Press.
ENSEMBL 2018. SLFN14 Gene: SLFN14 ENSMUSG00000082101. October 2018.
FLANAGAN, J. G. & LEDER, P. 1990. The kit ligand: a cell surface molecule altered in steel mutant fibroblasts. *Cell,* 63**,** 185-94.
FLETCHER, S. J., JOHNSON, B., LOWE, G. C., BEM, D., DRAKE, S., LORDKIPANIDZÉ, M., GUIÚ, I. S., DAWOOD, B., RIVERA, J., SIMPSON, M. A., DALY, M. E., MOTWANI, J., COLLINS, P. W., WATSON, S. P., MORGAN, N. V., ON BEHALF OF THE, U. K. G. & PHENOTYPING OF PLATELETS STUDY, G. 2015. SLFN14 mutations underlie thrombocytopenia with excessive bleeding and platelet secretion defects. *The Journal of Clinical Investigation,* 125**,** 3600-3605.

FLETCHER, S. J., PISAREVA, V. P., KHAN, A. O., TCHEREPANOV, A., MORGAN, N. V. & PISAREV, A. V. 2018. Role of the novel endoribonuclease SLFN14 and its disease-causing mutations in ribosomal degradation. *Rna,* 24**,** 939-949.

FRESON, K., WIJGAERTS, A. & GEET, C. V. 2017. GATA1 gene variants associated with thrombocytopenia and anemia.

FUJIWARA, Y., CHANG, A. N., WILLIAMS, A. M. & ORKIN, S. H. 2004. Functional overlap of GATA-1 and GATA-2 in primitive hematopoietic development. *Blood,* 103**,** 583-5.

FUTTERER, J., DALBY, A., LOWE, G. C., JOHNSON, B., SIMPSON, M. A., MOTWANI, J., WILLIAMS, M., WATSON, S. P. & MORGAN, N. V. 2018. Mutation in GNE is associated with severe congenital thrombocytopenia. *Blood,* 132**,** 1855-1858.

GAJ, T., GERSBACH, C. A. & BARBAS, C. F. 2013. ZFN, TALEN and CRISPR/Cas-based methods for genome engineering. *Trends Biotechnol,* 31**,** 397-405.

GEDDIS, A. E. 2010. Megakaryopoiesis. *Semin Hematol,* 47**,** 212-9.

GEER, M. J., VAN GEFFEN, J. P., GOPALASINGAM, P., VÖGTLE, T., SMITH, C. W., HEISING, S., KUIJPERS, M. J. E., TULLEMANS, B. M. E., JARVIS, G. E., EBLE, J. A., JEEVES, M., OVERDUIN, M., HEEMSKERK, J. W. M., MAZHARIAN, A. & SENIS, Y. A. 2018. Uncoupling ITIM receptor G6b-B from tyrosine phosphatases Shp1 and Shp2 disrupts murine platelet homeostasis. *Blood,* 132**,** 1413-1425.

GERMESHAUSEN, M., ANCLIFF, P., ESTRADA, J., METZLER, M., PONSTINGL, E., SCHWABE, D., SCOTT, R. H., UNAL, S., WAWER, A., ZELLER, B. & BALLMAIER, M. 2018. MECOM-associated syndrome: a heterogeneous inherited bone marrow failure syndrome with amegakaryocytic thrombocytopenia.

GESERICK, P., KAISER, F., KLEMM, U., KAUFMANN, S. H. E. & ZERRAHN, J. 2004. Modulation of T cell development and activation by novel members of the Schlafen (slfn) gene family harbouring an RNA helicase-like motif. *International Immunology,* 16**,** 1535-1548.

GOEL, M. S. & DIAMOND, S. L. 2002. Adhesion of normal erythrocytes at depressed venous shear rates to activated neutrophils, activated platelets, and fibrin polymerized from plasma. *Blood,* 100**,** 3797-3803.

GOLEBIEWSKA, E. M. & POOLE, A. W. 2015. Platelet secretion: From haemostasis to wound healing and beyond. *Blood Rev.*

GROVE, E. L., HVAS, A.-M. & KRISTENSEN, S. D. 2009. Immature platelets in patients with acute coronary syndromes. *Thrombosis and haemostasis,* 101**,** 151-153.

GUPTA, R. M. & MUSUNURU, K. 2014. Expanding the genetic editing tool kit: ZFNs, TALENs, and CRISPR-Cas9. *J Clin Invest,* 124**,** 4154-61.

GURNEY, A. L., CARVER-MOORE, K., DE SAUVAGE, F. J. & MOORE, M. W. 1994. Thrombocytopenia in c-mpl-deficient mice. *Science,* 265**,** 1445-7.

HAINING, E. J., CHERPOKOVA, D., WOLF, K., BECKER, I. C., BECK, S., EBLE, J. A., STEGNER, D., WATSON, S. P. & NIESWANDT, B. 2017. CLEC-2 contributes to hemostasis independently of classical hemITAM signaling in mice. *Blood,* 130**,** 2224-2228.

HANSON, P. I. & WHITEHEART, S. W. 2005. AAA+ proteins: have engine, will work. *Nature Reviews Molecular Cell Biology,* 6**,** 519.
HEIJNEN, H. F., DEBILI, N., VAINCHENCKER, W., BRETON-GORIUS, J., GEUZE, H. J. & SIXMA, J. J. 1998. Multivesicular bodies are an intermediate stage in the formation of platelet alpha-granules. *Blood,* 91**,** 2313-25.
HILLE, L., CEDERQVIST, M., HROMEK, J., STRATZ, C., TRENK, D. & NUHRENBERG, T. G. 2019. Evaluation of an Alternative Staining Method Using SYTO 13 to Determine Reticulated Platelets. *Thromb Haemost,* 119**,** 779-785.
HOFFMANN-FEZER, G., MASCHKE, H., ZEITLER, H. J., GAIS, P., HEGER, W., ELLWART, J. & THIERFELDER, S. 1991. Direct in vivo biotinylation of erythrocytes as an assay for red cell survival studies. *Annals of Hematology,* 63**,** 214-217.
HORVAT-SWITZER, R. D. & THOMPSON, A. A. 2006. HOXA11 mutation in amegakaryocytic thrombocytopenia with radio-ulnar synostosis syndrome inhibits megakaryocytic differentiation in vitro. *Blood Cells, Molecules, and Diseases,* 37**,** 55-63.
HOU, Y., CARRIM, N., WANG, Y., GALLANT, R. C., MARSHALL, A. & NI, H. 2015. Platelets in hemostasis and thrombosis: Novel mechanisms of fibrinogen-independent platelet aggregation and fibronectin-mediated protein wave of hemostasis. *J Biomed Res,* 29.
HURTADO, B., TRAKALA, M., XIMÉNEZ-EMBÚN, P., BAKKALI, A. E., PARTIDA, D., SANZ-CASTILLO, B., ÁLVAREZ-FERNÁNDEZ, M., MAROTO, M., SÁNCHEZ-MARTÍNEZ, R., MARTÍNEZ, L., MUÑOZ, J., DE FRUTOS, P. G. & MALUMBRES, M. 2018. Thrombocytopenia-associated mutations in Ser/Thr kinase MASTL deregulate actin cytoskeletal dynamics in platelets. *Journal of Clinical Investigation,* 128**,** 5351-5367.
IHARA, K., ISHII, E., EGUCHI, M., TAKADA, H., SUMINOE, A., GOOD ¶, R. A. & HARA, T. 1999. Identification of mutations in the c-mpl gene in congenital amegakaryocytic thrombocytopenia.
IKONOMI, P., RIVERA, C. E., RIORDAN, M., WASHINGTON, G., SCHECHTER, A. N. & NOGUCHI, C. T. 2000. Overexpression of GATA-2 inhibits erythroid and promotes megakaryocyte differentiation. *Experimental Hematology,* 28**,** 1423-1431.
IMAI, K., AOI, T., KITAI, H., ENDO, N., FUJINO, M. & ICHIDA, S. 2017. A case of perirenal extramedullary hematopoiesis in a patient with primary myelofibrosis. *CEN Case Rep,* 6**,** 194-199.
JACKSON, S. P. 2007. The growing complexity of platelet aggregation. *Blood,* 109**,** 5087-5095.
JANDROT-PERRUS, M., BUSFIELD, S., LAGRUE, A.-H., XIONG, X., DEBILI, N., CHICKERING, T., COUEDIC, J.-P. L., GOODEARL, A., DUSSAULT, B., FRASER, C., VAINCHENKER, W. & VILLEVAL, J.-L. 2000. Cloning, characterization, and functional studies of human and mouse glycoprotein VI: a platelet-specific collagen receptor from the immunoglobulin superfamily. *Blood,* 96**,** 1798-1807.
JANEWAY, C. A., JR. & MEDZHITOV, R. 2002. Innate immune recognition. *Annu Rev Immunol,* 20**,** 197-216.

JIN, L. F. & LI, J. S. 2016. Generation of genetically modified mice using CRISPR/Cas9 and haploid embryonic stem cell systems. *Dongwuxue Yanjiu,* 37**,** 205-13.
KAHR, W. H. A., HINCKLEY, J., LI, L., SCHWERTZ, H., CHRISTENSEN, H., ROWLEY, J. W., PLUTHERO, F. G., URBAN, D., FABBRO, S., NIXON, B., GADZINSKI, R., STORCK, M., WANG, K., RYU, G. Y., JOBE, S. M., SCHUTTE, B. C., MOSELEY, J., LOUGHRAN, N. B., PARKINSON, J., WEYRICH, A. S. & DI PAOLA, J. 2011. Mutations in NBEAL2, encoding a BEACH protein, cause gray platelet syndrome. *Nature Genetics,* 43**,** 738-740.
KAISER, F., ZERRAHN, J., GESERICK, P., KAUFMANN, S. H. E. & KLEMM, U. 2004. Modulation of T cell development and activation by novel members of the Schlafen (slfn) gene family harbouring an RNA helicase-like motif. *International Immunology,* 16**,** 1535-1548.
KAUSHANSKY, K. 2005. The molecular mechanisms that control thrombopoiesis. *J Clin Invest,* 115**,** 3339-47.
KAUSHANSKY, K. 2009. Determinants of platelet number and regulation of thrombopoiesis. *Hematology Am Soc Hematol Educ Program***,** 147-52.
KAUSHANSKY, K., BROUDY, V. C., LIN, N., JORGENSEN, M. J., MCCARTY, J., FOX, N., ZUCKER-FRANKLIN, D. & LOFTON-DAY, C. 1995. Thrombopoietin, the Mp1 ligand, is essential for full megakaryocyte development. *Proc Natl Acad Sci U S A,* 92**,** 3234-8.
KAWAMATA, M. & OCHIYA, T. 2010. Generation of genetically modified rats from embryonic stem cells. *Proceedings of the National Academy of Sciences,* 107**,** 14223-14228.
KAY, J. G. & GRINSTEIN, S. 2013. Phosphatidylserine-mediated cellular signaling. *Adv Exp Med Biol,* 991**,** 177-93.
KENDALL, R. G. 2001. Erythropoietin. *Clin Lab Haematol,* 23**,** 71-80.
KHAN, A. O., SLATER, A., MACLACHLAN, A., NICOLSON, P. L. R., PIKE, J. A., REYAT, J. S., YULE, J., STAPLEY, R., RAYES, J., THOMAS, S. G. & MORGAN, N. V. 2020a. Post-translational polymodification of β1-tubulin regulates motor protein localisation in platelet production and function. *Haematologica*.
KHAN, A. O., STAPLEY, R., PIKE, J. A., WIJESINGHE, S. N., REYAT, J. S., ALMAZNI, I., MACHLUS, K. R. & MORGAN, N. V. 2020b. Novel gene variants in patients with platelet-based bleeding using combined exome sequencing and RNAseq murine expression data. *J Thromb Haemost*.
KHAN, A. O., STAPLEY, R. J., PIKE, J. A., WIJESINGHE, S. N., REYAT, J. S., ALMAZNI, I., MACHLUS, K. R. & MORGAN, N. V. 2021. Novel gene variants in patients with platelet-based bleeding using combined exome sequencing and RNAseq murine expression data. *J Thromb Haemost,* 19**,** 262-268.
KLATT, C., KRÜGER, I., ZEY, S., KROTT, K.-J., SPELLEKEN, M., GOWERT, N. S., OBERHUBER, A., PFAFF, L., LÜCKSTÄDT, W., JURK, K., SCHALLER, M., AL-HASANI, H., SCHRADER, J., MASSBERG, S., STARK, K., SCHELZIG, H., KELM, M. & ELVERS, M. 2018. Platelet-RBC interaction mediated by FasL/FasR induces procoagulant activity important for thrombosis. *The Journal of Clinical Investigation,* 128**,** 3906-3925.
KOREN, A., KHAYAT, M., HAUSCHNER, H., PRETORIUS, E., ROSENBERG, N., ZALMAN, L., ELPELEG, O., SALAMA, I., SHALEV, S., SHENKMAN, B. &

LEVIN, C. 2015. Deleterious mutation in the FYB gene is associated with congenital autosomal recessive small-platelet thrombocytopenia. *Journal of Thrombosis and Haemostasis,* 13**,** 1285-1292.
KROLL, M. H., MICHAELIS, L. C. & VERSTOVSEK, S. 2015. Mechanisms of thrombogenesis in polycythemia vera. *Blood Rev,* 29**,** 215-21.
KUNISHIMA, S., KOBAYASHI, R., ITOH, T. J., HAMAGUCHI, M. & SAITO, H. 2009. Mutation of the 1-tubulin gene associated with congenital macrothrombocytopenia affecting microtubule assembly.
KUNISHIMA, S., OKUNO, Y., YOSHIDA, K., SHIRAISHI, Y., SANADA, M., MURAMATSU, H., CHIBA, K., TANAKA, H., MIYAZAKI, K., SAKAI, M., OHTAKE, M., KOBAYASHI, R., IGUCHI, A., NIIMI, G., OTSU, M., TAKAHASHI, Y., MIYANO, S., SAITO, H., KOJIMA, S. & OGAWA, S. 2013. ACTN1 mutations cause congenital macrothrombocytopenia. *American Journal of Human Genetics,* 92**,** 431-438.
LACRUZ, R. S. & FESKE, S. Diseases caused by mutations in ORAI1 and STIM1.
LENNARTSSON, J. & RÖNNSTRAND, L. 2012. Stem cell factor receptor/c-Kit: from basic science to clinical implications. *Physiol Rev,* 92**,** 1619-49.
LENTAIGNE, C., GREENE, D., SIVAPALARATNAM, S., FAVIER, R., SEYRES, D., THYS, C., GRASSI, L., MANGLES, S., SIBSON, K. & STUBBS, M. 2019. Germline mutations in the transcription factor IKZF5 cause thrombocytopenia. *Blood, The Journal of the American Society of Hematology,* 134**,** 2070-2081.
LEVY, G. G., NICHOLS[2], W. C., LIAN[3], E. C., FOROUD, T., MCCLINTICK, J. N., MCGEE, B. M., YANG, A. Y., SIEMIENIAK, D. R., STARK, K. R., GRUPPOK, R., SARODE, R., SHURIN, S. B., CHANDRASEKARANI, V., STABLER, S. P., SABIO[22], H., BOUHASSIRA[33], E. E., UPSHAW, J. D., GINSBURG, D. & TSAIKK, H.-M. 2001. Mutations in a member of the ADAMTS gene family cause thrombotic thrombocytopenic purpura.
LIU, F., ZHOU, P., WANG, Q., ZHANG, M. & LI, D. 2018. The Schlafen family: complex roles in different cell types and virus replication. *Cell Biology International,* 42**,** 2-8.
LOK, S., KAUSHANSKY, K., HOLLY, R. D., KUIJPER, J. L., LOFTON-DAY, C. E., OORT, P. J., GRANT, F. J., HEIPEL, M. D., BURKHEAD, S. K., KRAMER, J. M. & ET AL. 1994. Cloning and expression of murine thrombopoietin cDNA and stimulation of platelet production in vivo. *Nature,* 369**,** 565-8.
LOO, B. V. D. & MARTIN, J. F. 1999. A Role for Changes in Platelet Production in the Cause of Acute Coronary Syndromes. *Arteriosclerosis, Thrombosis, and Vascular Biology,* 19**,** 672-679.
LORDIER, L., JALIL, A., AURADE, F., LARBRET, F., LARGHERO, J., DEBILI, N., VAINCHENKER, W. & CHANG, Y. 2008. Megakaryocyte endomitosis is a failure of late cytokinesis related to defects in the contractile ring and Rho/Rock signaling. *Blood,* 112**,** 3164-74.
LOWE, G. C., FICKOWSKA, R., AL GHAITHI, R., MACLACHLAN, A., HARRISON, P., LESTER, W., WATSON, S. P., MYERS, B., CLARK, J. & MORGAN, N. V. 2019. Investigation of the contribution of an underlying platelet defect in women with unexplained heavy menstrual bleeding. *Platelets,* 30**,** 56-65.
LU, Y.-C., SANADA, C., XAVIER-FERRUCIO, J., WANG, L., ZHANG, P.-X., GRIMES, H. L., VENKATASUBRAMANIAN, M., CHETAL, K., ARONOW, B., SALOMONIS, N. & KRAUSE, D. S. 2018. The Molecular Signature of

Megakaryocyte-Erythroid Progenitors Reveals a Role for the Cell Cycle in Fate Specification. *Cell Reports,* 25**,** 2083-2093.e4.
LUK, A. D. W., YANG, X., ALCASABAS, A. P., HAO, R. C., CHAN, K. W., LEE, P. P., YANG, J., CHAN, G. C. F., SO, J. C. C. & YANG, W. 2020. NF-E2 mutation as a novel cause for inherited thrombocytopenia. *British Journal of Haematology,* 189**,** e41.
LUPAS, A. N. & MARTIN, J. 2002. AAA proteins. *Current Opinion in Structural Biology,* 12**,** 746-753.
MACHLUS, K. R. & ITALIANO, J. E. 2013. The incredible journey: From megakaryocyte development to platelet formation. *The Journal of Cell Biology,* 201**,** 785-796.
MACHLUS, K. R., THON, J. N. & ITALIANO, J. E., JR. 2014. Interpreting the developmental dance of the megakaryocyte: a review of the cellular and molecular processes mediating platelet formation. *Br J Haematol,* 165**,** 227-36.
MACLACHLAN, A., DOLAN, G., GRIMLEY, C., WATSON, S. P., MORGAN, N. V. & ON BEHALF OF THE UK GAPP STUDY, G. 2017. Whole exome sequencing identifies a mutation in thrombomodulin as the genetic cause of a suspected platelet disorder in a family with normal platelet function. *Platelets,* 28**,** 611-613.
MADEIRA, F., PARK, Y. M., LEE, J., BUSO, N., GUR, T., MADHUSOODANAN, N., BASUTKAR, P., TIVEY, A. R. N., POTTER, S. C., FINN, R. D. & LOPEZ, R. 2019. The EMBL-EBI search and sequence analysis tools APIs in 2019. *Nucleic acids research,* 47**,** W636-W641.
MAKITA, T., HERNANDEZ-HOYOS, G., CHEN, T. H., WU, H., ROTHENBERG, E. V. & SUCOV, H. M. 2001. A developmental transition in definitive erythropoiesis: erythropoietin expression is sequentially regulated by retinoic acid receptors and HNF4. *Genes Dev,* 15**,** 889-901.
MALLERET, B., XU, F., MOHANDAS, N., SUWANARUSK, R., CHU, C., LEITE, J. A., LOW, K., TURNER, C., SRIPRAWAT, K., ZHANG, R., BERTRAND, O., COLIN, Y., COSTA, F. T. M., ONG, C. N., NG, M. L., LIM, C. T., NOSTEN, F., RÉNIA, L. & RUSSELL, B. 2013. Significant Biochemical, Biophysical and Metabolic Diversity in Circulating Human Cord Blood Reticulocytes. *PLOS ONE,* 8**,** e76062.
MANCHEV, V. T., HILPERT, M., BERROU, E., ELAIB, Z., AOUBA, A., BOUKOUR, S., SOUQUERE, S., PIERRON, G., RAMEAU, P., ANDREWS, R., LANZA, F., BOBE, R., VAINCHENKER, W., ROSA, J.-P., BRYCKAERT, M., DEBILI, N., FAVIER, R. & RASLOVA, H. 2014. A new form of macrothrombocytopenia induced by a germ-line mutation in the PRKACG gene Key Points.
MANUKJAN, G., BÖSING, H., SCHMUGGE, M., STRAUß, G. & SCHULZE, H. 2017. Impact of genetic variants on haematopoiesis in patients with thrombocytopenia absent radii (TAR) syndrome. *British Journal of Haematology,* 179**,** 606-617.
MARCONI, C., DE ROCCO, D., PECCI, A., NORIS, P., PIPPUCCI, T., MELAZZINI, F., SAVOIA, A., LOFFREDO, G., GIANGREGORIO, T. & SERI, M. 2017. A new form of inherited thrombocytopenia due to monoallelic loss of function mutation in the thrombopoietin gene. *British Journal of Haematology,* 181**,** 698-701.

MARCONI, C., DI BUDUO, C. A., BAROZZI, S., PALOMBO, F., PARDINI, S., ZANINETTI, C., PIPPUCCI, T., NORIS, P., BALDUINI, A., SERI, M. & PECCI, A. 2016. SLFN14-related thrombocytopenia: identification within a large series of patients with inherited thrombocytopenia. *Thrombosis and haemostasis,* 115**,** 1076-1079.

MARKELLO, T., CHEN, D., KWAN, J. Y., HORKAYNE-SZAKALY, I., MORRISON, A., SIMAKOVA, O., MARIC, I., LOZIER, J., CULLINANE, A. R., KILO, T., MEISTER, L., PAKZAD, K., BONE, W., CHAINANI, S., LEE, E., LINKS, A., BOERKOEL, C., FISCHER, R., TORO, C., WHITE, J. G., GAHL, W. A. & GUNAY-AYGUN, M. 2015. York platelet syndrome is a CRAC channelopathy due to gain-of-function mutations in STIM1 HHS Public Access. *Mol Genet Metab,* 114**,** 474-482.

MASSAAD, M. J., RAMESH, N. & GEHA, R. S. 2013. Wiskott-Aldrich syndrome: A comprehensive review. *Annals of the New York Academy of Sciences,* 1285**,** 26-43.

MASTERS, A. & HARRISON, P. 2014. Platelet counting with the BD Accuri(TM) C6 flow cytometer. *Platelets,* 25**,** 175-80.

MATTIJSSEN, S., WELTING, T. J. M. & PRUIJN, G. J. M. 2010. RNase MRP and disease. *WIREs RNA,* 1**,** 102-116.

MAVROMMATIS, E., ARSLAN, A. D., SASSANO, A., HUA, Y., KROCZYNSKA, B. & PLATANIAS, L. C. 2013. Expression and regulatory effects of murine Schlafen (Slfn) genes in malignant melanoma and renal cell carcinoma. *J Biol Chem,* 288**,** 33006-15.

MAY, F., HAGEDORN, I., PLEINES, I., BENDER, M., VÖGTLE, T., EBLE, J., ELVERS, M. & NIESWANDT, B. 2009. CLEC-2 is an essential platelet-activating receptor in hemostasis and thrombosis. *Blood,* 114**,** 3464-3472.

MEI, Y., LIU, Y. & JI, P. 2021. Understanding terminal erythropoiesis: An update on chromatin condensation, enucleation, and reticulocyte maturation. *Blood Reviews,* 46**,** 100740.

MERIKA, M. & ORKIN, S. H. 1993. DNA-binding specificity of GATA family transcription factors. *Mol Cell Biol,* 13**,** 3999-4010.

MILLER, I. J. & BIEKER, J. J. 1993. A novel, erythroid cell-specific murine transcription factor that binds to the CACCC element and is related to the Krüppel family of nuclear proteins. *Mol Cell Biol,* 13**,** 2776-86.

MIWA, Y., HAYASHI, T., SUZUKI, S., ABE, S., ONISHI, I., KIRIMURA, S., KITAGAWA, M. & KURATA, M. 2013. Up-regulated expression of CXCL12 in human spleens with extramedullary haematopoiesis. *Pathology,* 45**,** 408-16.

MORGAN, N. V. & DALY, M. E. 2017. Gene of the issue: RUNX1 mutations and inherited bleeding. *Platelets,* 28**,** 208-210.

MÖRÖY, T., VASSEN, L., WILKES, B. & KHANDANPOUR, C. 2015. From cytopenia to leukemia: the role of Gfi1 and Gfi1b in blood formation. *Blood,* 126**,** 2561-9.

MUSTAFA, I., AL MARWANI, A., MAMDOUH NASR, K., ABDULLA KANO, N. & HADWAN, T. 2016. Time Dependent Assessment of Morphological Changes: Leukodepleted Packed Red Blood Cells Stored in SAGM. *Biomed Res Int,* 2016**,** 4529434.

NAGY, Z., VÖGTLE, T., GEER, M. J., MORI, J., HEISING, S., DI NUNZIO, G., GAREUS, R., TARAKHOVSKY, A., WEISS, A., NEEL, B. G., DESANTI, G. E.,

MAZHARIAN, A. & SENIS, Y. A. 2019. The Gp1ba-Cre transgenic mouse: a new model to delineate platelet and leukocyte functions. *Blood,* 133**,** 331-343.
NARLA, A. & EBERT, B. L. 2010. Ribosomopathies: human disorders of ribosome dysfunction. *Blood,* 115**,** 3196-205.
NEUMANN, B., ZHAO, L., MURPHY, K. & GONDA, T. J. 2008. Subcellular localization of the Schlafen protein family. *Biochemical and Biophysical Research Communications,* 370**,** 62-66.
NG, A. P., KAUPPI, M., METCALF, D., HYLAND, C. D., JOSEFSSON, E. C., LEBOIS, M., ZHANG, J.-G., BALDWIN, T. M., DI RAGO, L., HILTON, D. J. & ALEXANDER, W. S. 2014. Mpl expression on megakaryocytes and platelets is dispensable for thrombopoiesis but essential to prevent myeloproliferation. *Proceedings of the National Academy of Sciences,* 111**,** 5884-5889.
NOETZLI, L., LO, R. W., LEE-SHERICK, A. B., CALLAGHAN, M., NORIS, P., SAVOIA, A., RAJPURKAR, M., JONES, K., GOWAN, K., BALDUINI, C. L., PECCI, A., GNAN, C., DE ROCCO, D., DOUBEK, M., LI, L., LU, L., LEUNG, R., LANDOLT-MARTICORENA, C., HUNGER, S., HELLER, P., GUTIERREZ-HARTMANN, A., XIAYUAN, L., PLUTHERO, F. G., ROWLEY, J. W., WEYRICH, A. S., KAHR, W. H. A., PORTER, C. C. & DI PAOLA, J. 2015. Germline mutations in ETV6 are associated with thrombocytopenia, red cell macrocytosis and predisposition to lymphoblastic leukemia. *Nature Genetics,* 47**,** 535-538.
NURDEN, A. T., PILLOIS, X. & WILCOX, D. A. 2013. Glanzmann Thrombasthenia: State of the Art and Future Directions. *Seminars in thrombosis and hemostasis,* 39**,** 642-642.
NURDEN, P., DEBILI, N., COUPRY, I., BRYCKAERT, M., YOULYOUZ-MARFAK, I., SOLÉ, G., CILE PONS, A.-C., BERROU, E., RIC ADAM, F., KAUSKOT, A., DANIEL LAMAZIÈ RE, J.-M., RAMEAU, P., FERGELOT, P., ROORYCK, C., CAILLEY, D., ARVEILER, B., LACOMBE, D., VAINCHENKER, W., NURDEN, A. & GOIZET, C. 2011. Thrombocytopenia resulting from mutations in filamin A can be expressed as an isolated syndrome.
OGAWA, M. 1993. Differentiation and proliferation of hematopoietic stem cells. *Blood,* 81**,** 2844-53.
OKAMOTO, Y., ABE, M., MU, A., TEMPAKU, Y., ROGERS, C. B., MOCHIZUKI, A. L., KATSUKI, Y., KANEMAKI, M. T., TAKAORI-KONDO, A., SOBECK, A., BIELINSKY, A.-K. & TAKATA, M. 2021. SLFN11 promotes stalled fork degradation that underlies the phenotype in Fanconi anemia cells. *Blood,* 137**,** 336-348.
ONG, L., MORISON, I. M. & LEDGERWOOD, E. C. 2017. Megakaryocytes from CYCS mutation-associated thrombocytopenia release platelets by both proplatelet-dependent and -independent processes. *British Journal of Haematology,* 176**,** 268-279.
ORAZI, A. & CZADER, M. 2010. 15 - Spleen. *In:* GATTUSO, P., REDDY, V. B., DAVID, O., SPITZ, D. J. & HABER, M. H. (eds.) *Differential Diagnosis in Surgical Pathology (Second Edition).* Philadelphia: W.B. Saunders.
OTHMAN, M. & EMSLEY, J. 2017. Gene of the issue: GP1BA gene mutations associated with bleeding. *Platelets,* 28**,** 832-836.
PANTELEEV, M. A., KORIN, N., REESINK, K. D., BARK, D. L., COSEMANS, J. M. E. M., GARDINER, E. E. & MANGIN, P. H. 2021. Wall shear rates in human

and mouse arteries: Standardization of hemodynamics for in vitro blood flow assays: Communication from the ISTH SSC subcommittee on biorheology. *Journal of Thrombosis and Haemostasis,* 19**,** 588-595.
PARALKAR, V. R., MISHRA, T., LUAN, J., YAO, Y., KOSSENKOV, A. V., ANDERSON, S. M., DUNAGIN, M., PIMKIN, M., GORE, M., SUN, D., KONUTHULA, N., RAJ, A., AN, X., MOHANDAS, N., BODINE, D. M., HARDISON, R. C. & WEISS, M. J. 2014. Lineage and species-specific long noncoding RNAs during erythro-megakaryocytic development. *Blood,* 123**,** 1927-37.
PATEL, S. R., HARTWIG, J. H. & ITALIANO, J. E., JR. 2005. The biogenesis of platelets from megakaryocyte proplatelets. *J Clin Invest,* 115**,** 3348-54.
PAYNE, H., PONOMARYOV, T., WATSON, S. P. & BRILL, A. 2017. Mice with a deficiency in CLEC-2 are protected against deep vein thrombosis. *Blood,* 129**,** 2013-2020.
PERTUY, F., AGUILAR, A., STRASSEL, C., ECKLY, A., FREUND, J. N., DULUC, I., GACHET, C., LANZA, F. & LÉON, C. 2015. Broader expression of the mouse platelet factor 4-cre transgene beyond the megakaryocyte lineage. *J Thromb Haemost,* 13**,** 115-25.
PEVNY, L., SIMON, M. C., ROBERTSON, E., KLEIN, W. H., TSAI, S. F., D'AGATI, V., ORKIN, S. H. & COSTANTINI, F. 1991. Erythroid differentiation in chimaeric mice blocked by a targeted mutation in the gene for transcription factor GATA-1. *Nature,* 349**,** 257-60.
PIKKARAINEN, S., TOKOLA, H., KERKELÄ, R. & RUSKOAHO, H. 2004. GATA transcription factors in the developing and adult heart. *Cardiovasc Res,* 63**,** 196-207.
PIPPUCCI, T., SAVOIA, A., PERROTTA, S., PUJOL-MOIX, N., NORIS, P., CASTEGNARO, G., PECCI, A., GNAN, C., PUNZO, F., MARCONI, C., GHERARDI, S., LOFFREDO, G., DE ROCCO, D., SCIANGUETTA, S., BAROZZI, S., MAGINI, P., BOZZI, V., DEZZANI, L., DI STAZIO, M., FERRARO, M., PERINI, G., SERI, M. & BALDUINI, C. L. 2011. Mutations in the 5′ UTR of ANKRD26, the ankirin repeat domain 26 gene, cause an autosomal-dominant form of inherited thrombocytopenia, THC2. *American Journal of Human Genetics,* 88**,** 115-120.
PISAREVA, V. P., MUSLIMOV, I. A., TCHEREPANOV, A. & PISAREV, A. V. 2015. Characterization of Novel Ribosome-Associated Endoribonuclease SLFN14 from Rabbit Reticulocytes. *Biochemistry,* 54**,** 3286-301.
PLEINES, I., WOODS, J., CHAPPAZ, S., KEW, V., FOAD, N., BALLESTER-BELTRÁN, J., AURBACH, K., LINCETTO, C., LANE, R. M., SCHEVZOV, G., ALEXANDER, W. S., HILTON, D. J., ASTLE, W. J., DOWNES, K., NURDEN, P., WESTBURY, S. K., MUMFORD, A. D., OBAJI, S. G., COLLINS, P. W., DELERUE, F., ITTNER, L. M., BRYCE, N. S., HOLLIDAY, M., LUCAS, C. A., HARDEMAN, E. C., OUWEHAND, W. H., GUNNING, P. W., TURRO, E., TIJSSEN, M. R. & KILE, B. T. 2017. Mutations in tropomyosin 4 underlie a rare form of human macrothrombocytopenia. *Journal of Clinical Investigation,* 127**,** 814-829.
PLUTHERO, F. G., DI PAOLA, J., CARCAO, M. D. & KAHR, W. H. A. 2018. NBEAL2 mutations and bleeding in patients with gray platelet syndrome.

PSAILA, B., BARKAS, N., ISKANDER, D., ROY, A., ANDERSON, S., ASHLEY, N., CAPUTO, V. S., LICHTENBERG, J., LOAIZA, S., BODINE, D. M., KARADIMITRIS, A., MEAD, A. J. & ROBERTS, I. 2016. Single-cell profiling of human megakaryocyte-erythroid progenitors identifies distinct megakaryocyte and erythroid differentiation pathways. *Genome Biol,* 17**,** 83.

PSAILA, B., WANG, G., RODRIGUEZ-MEIRA, A., LI, R., HEUSTON, E. F., MURPHY, L., YEE, D., HITCHCOCK, I. S., SOUSOS, N., O'SULLIVAN, J., ANDERSON, S., SENIS, Y. A., WEINBERG, O. K., CALICCHIO, M. L., ISKANDER, D., ROYSTON, D., MILOJKOVIC, D., ROBERTS, I., BODINE, D. M., THONGJUEA, S. & MEAD, A. J. 2020. Single-Cell Analyses Reveal Megakaryocyte-Biased Hematopoiesis in Myelofibrosis and Identify Mutant Clone-Specific Targets. *Mol Cell,* 78**,** 477-492.e8.

PUCK, A., AIGNER, R., MODAK, M., CEJKA, P., BLAAS, D. & STÖCKL, J. 2015. Expression and regulation of Schlafen (SLFN) family members in primary human monocytes, monocyte-derived dendritic cells and T cells. *Results Immunol,* 5**,** 23-32.

RACCUGLIA, G. 1971. Gray platelet syndrome: a variety of qualitative platelet disorder. *The American journal of medicine,* 51**,** 818-828.

REDDY, E. C. & RAND, M. L. 2020. Procoagulant Phosphatidylserine-Exposing Platelets in vitro and in vivo. *Frontiers in Cardiovascular Medicine,* 7.

REININGER, A. J. 2008. Function of von Willebrand factor in haemostasis and thrombosis. *Haemophilia,* 14**,** 11-26.

REVEL-VILK, S., SHAI, E., TURRO, E., JAHSHAN, N., HI-AM, E., SPECTRE, G., DAUM, H., KALISH, Y., ALTHAUS, K., GREINACHER, A., KAPLINSKY, C., IZRAELI, S., MAPETA, R., DEEVI, S. V. V., JAROCHA, D., OUWEHAND, W. H., DOWNES, K., PONCZ, M., VARON, D. & LAMBERT, M. P. 2018. GNE variants causing autosomal recessive macrothrombocytopenia without associated muscle wasting. American Society of Hematology.

RICCIARDI, S., MILUZIO, A., BRINA, D., CLARKE, K., BONOMO, M., AIOLFI, R., GUIDOTTI, L. G., FALCIANI, F. & BIFFO, S. 2015. Eukaryotic translation initiation factor 6 is a novel regulator of reactive oxygen species-dependent megakaryocyte maturation. *Journal of Thrombosis and Haemostasis,* 13**,** 2108-2118.

ROWLEY, J. W., SCHWERTZ, H. & WEYRICH, A. S. 2012. Platelet mRNA: the meaning behind the message. *Curr Opin Hematol,* 19**,** 385-91.

SAES, J. L., SIMONS, A., DE MUNNIK, S. A., NIJZIEL, M. R., BLIJLEVENS, N. M. A., JONGMANS, M. C., VAN DER REIJDEN, B. A., SMIT, Y., BRONS, P. P., VAN HEERDE, W. L. & SCHOLS, S. E. M. 2019. Whole exome sequencing in the diagnostic workup of patients with a bleeding diathesis. *Haemophilia,* 25**,** 127-135.

SANKARAN, V. G. & ORKIN, S. H. 2013. The switch from fetal to adult hemoglobin. *Cold Spring Harb Perspect Med,* 3**,** a011643.

SCHLITT, H. J., SCHÄFERS, S., DEIWICK, A., ECKARDT, K. U., PIETSCH, T., EBELL, W., NASHAN, B., RINGE, B., WONIGEIT, K. & PICHLMAYR, R. 1995. Extramedullary erythropoiesis in human liver grafts. *Hepatology,* 21**,** 689-96.

SCHWARZ, D. A., KATAYAMA, C. D. & HEDRICK, S. M. 1998. Schlafen, a new family of growth regulatory genes that affect thymocyte development. *Immunity,* 9**,** 657-68.

SEMENZA, G. L., NEJFELT, M. K., CHI, S. M. & ANTONARAKIS, S. E. 1991. Hypoxia-inducible nuclear factors bind to an enhancer element located 3' to the human erythropoietin gene. *Proc Natl Acad Sci U S A,* 88**,** 5680-4.

SEO, A., GULSUNER, S., PIERCE, S., BEN-HAROSH, M., SHALEV, H., WALSH, T., KRASNOV, T., DGANY, O., DOULATOV, S., TAMARY, H., SHIMAMURA, A. & KING, M. C. 2019. Inherited thrombocytopenia associated with mutation of UDP-galactose-4-epimerase (GALE). *Human molecular genetics,* 28**,** 133-142.

SEONG, R. K., SEO, S. W., KIM, J. A., FLETCHER, S. J., MORGAN, N. V., KUMAR, M., CHOI, Y. K. & SHIN, O. S. 2017. Schlafen 14 (SLFN14) is a novel antiviral factor involved in the control of viral replication. *Immunobiology,* 222**,** 979-988.

SHAHRIZAILA, N., GAFFNEY, P. M., NESIN, V., ONG, E. C., TSIOKAS, L., NICHOLL, D. J., KOUSI, M., LEHMANN, T., WILEY, G., SURI, M., KATSANIS, N. & WIERENGA, K. J. 2014. Activating mutations in STIM1 and ORAI1 cause overlapping syndromes of tubular myopathy and congenital miosis. *Proceedings of the National Academy of Sciences,* 111**,** 4197-4202.

SHI, G., FIELD, D. J., KO, K. A., TURE, S., SRIVASTAVA, K., LEVY, S., KOWALSKA, M. A., PONCZ, M., FOWELL, D. J. & MORRELL, C. N. 2014. Platelet factor 4 limits Th17 differentiation and cardiac allograft rejection. *J Clin Invest,* 124**,** 543-52.

SHIDE, K., SHIMODA, H. K., KUMANO, T., KARUBE, K., KAMEDA, T., TAKENAKA, K., OKU, S., ABE, H., KATAYOSE, K. S., KUBUKI, Y., KUSUMOTO, K., HASUIKE, S., TAHARA, Y., NAGATA, K., MATSUDA, T., OHSHIMA, K., HARADA, M. & SHIMODA, K. 2008. Development of ET, primary myelofibrosis and PV in mice expressing JAK2 V617F. *Leukemia,* 22**,** 87-95.

SHIN, Y. & MORITA, T. 1998. Rhodocytin, a Functional Novel Platelet Agonist Belonging to the Heterodimeric C-Type Lectin Family, Induces Platelet Aggregation Independently of Glycoprotein Ib. *Biochemical and Biophysical Research Communications,* 245**,** 741-745.

SHIVDASANI, R. A. 2001. Molecular and Transcriptional Regulation of Megakaryocyte Differentiation. *STEM CELLS,* 19**,** 397-407.

SILVAIN, J., COLLET, J. P., NAGASWAMI, C., BEYGUI, F., EDMONDSON, K. E., BELLEMAIN-APPAIX, A., CAYLA, G., PENA, A., BRUGIER, D., BARTHELEMY, O., MONTALESCOT, G. & WEISEL, J. W. 2011. Composition of coronary thrombus in acute myocardial infarction. *J Am Coll Cardiol,* 57**,** 1359-67.

SIVAPALARATNAM, S., WESTBURY, S. K., STEPHENS, J. C., GREENE, D., DOWNES, K., KELLY, A. M., LENTAIGNE, C., ASTLE, W. J., HUIZINGA, E. G., NURDEN, P., PAPADIA, S., PEERLINCK, K., PENKETT, C. J., PERRY, D. J., ROUGHLEY, C., SIMEONI, I., STIRRUPS, K., HART, D. P., CAMPBELL TAIT, R., MUMFORD, A. D., BIORESOURCE, N., LAFFAN, M. A., FRESON, K., OUWEHAND, W. H., KUNISHIMA, S. & TURRO, E. 2017. Brief Report Rare variants in GP1BB are responsible for autosomal dominant macrothrombocytopenia.

SOCOLOVSKY, M., FALLON, A. E., WANG, S., BRUGNARA, C. & LODISH, H. F. 1999. Fetal anemia and apoptosis of red cell progenitors in Stat5a-/-5b-/- mice: a direct role for Stat5 in Bcl-X(L) induction. *Cell,* 98**,** 181-91.
SOHAWON, D., LAU, K. K., LAU, T. & BOWDEN, D. K. 2012. Extra-medullary haematopoiesis: a pictorial review of its typical and atypical locations. *J Med Imaging Radiat Oncol,* 56**,** 538-44.
SONG, M. K., PARK, B. B. & UHM, J. E. 2018. Understanding Splenomegaly in Myelofibrosis: Association with Molecular Pathogenesis. *Int J Mol Sci,* 19.
SPINELLI, S. L., O'BRIEN, J. J., BANCOS, S., LEHMANN, G. M., SPRINGER, D. L., BLUMBERG, N., FRANCIS, C. W., TAUBMAN, M. B. & PHIPPS, R. P. 2008. The PPAR-Platelet Connection: Modulators of Inflammation and Potential Cardiovascular Effects. *PPAR Research,* 2008**,** 328172.
STABELL, A. C., HAWKINS, J., LI, M., GAO, X., DAVID, M., PRESS, W. H. & SAWYER, S. L. 2016. Non-human Primate Schlafen11 Inhibits Production of Both Host and Viral Proteins. *PLoS pathogens,* 12**,** e1006066-e1006066.
STAPLEY, R. J., PISAREVA, V. P., PISAREV, A. V. & MORGAN, N. V. 2020. SLFN14 gene mutations associated with bleeding. *Platelets,* 31**,** 407-410.
STAPLEY, R. J., SMITH, C. W., HAINING, E. J., BACON, A., LAX, S., PISAREVA, V. P., PISAREV, A. V., WATSON, S. P., KHAN, A. O. & MORGAN, N. V. 2021. Heterozygous mutation SLFN14 K208N in mice mediates species-specific differences in platelet and erythroid lineage commitment. *Blood Advances,* 5**,** 377-390.
STEVENSON, W. S., MOREL-KOPP, M.-C., CHEN, Q., LIANG, H. P., BROMHEAD, C. J., WRIGHT, S., TURAKULOV, R., NG, A. P., ROBERTS, A. W., BAHLO, M. & WARD, C. M. 2013a. GFI1B mutation causes a bleeding disorder with abnormal platelet function. *Journal of Thrombosis and Haemostasis,* 11**,** 2039-2047.
STEVENSON, W. S., MOREL-KOPP, M. C., CHEN, Q., LIANG, H. P., BROMHEAD, C. J., WRIGHT, S., TURAKULOV, R., NG, A. P., ROBERTS, A. W., BAHLO, M. & WARD, C. M. 2013b. GFI1B mutation causes a bleeding disorder with abnormal platelet function. *Journal of Thrombosis and Haemostasis,* 11**,** 2039-2047.
STEVENSON, W. S., RABBOLINI, D. J., BEUTLER, L., CHEN, Q., GABRIELLI, S., MACKAY, J. P., BRIGHTON, T. A., WARD, C. M. & MOREL-KOPP, M.-C. 2015. Paris-Trousseau thrombocytopenia is phenocopied by the autosomal recessive inheritance of a DNA-binding domain mutation in FLI1. *Blood,* 126**,** 2027-2030.
STRASSEL, C., GACHET, C. & LANZA, F. 2018. On the Way to in vitro Platelet Production. *Frontiers in Medicine,* 5.
STRITT, S., NURDEN, P., FAVIER, R., FAVIER, M., FERIOLI, S., GOTRU, S. K., M VAN EEUWIJK, J. M., SCHULZE, H., NURDEN, A. T., LAMBERT, M. P., TURRO, E., BURGER-STRITT, S., MATSUSHITA, M., MITTERMEIER, L., BALLERINI, P., ZIERLER, S., LAFFAN, M. A., CHUBANOV, V., GUDERMANN, T., NIESWANDT, B. & BRAUN, A. 2016a. Defects in TRPM7 channel function deregulate thrombopoiesis through altered cellular Mg2+ homeostasis and cytoskeletal architecture. *Nature Communications,* 7.
STRITT, S., NURDEN, P., TURRO, E., GREENE, D., JANSEN, S. B., WESTBURY, S. K., PETERSEN, R., ASTLE, W. J., MARLIN, S. & BARIANA, T. K. 2016b. A

gain-of-function variant in DIAPH1 causes dominant macrothrombocytopenia and hearing loss. *Blood,* 127**,** 2903-2914.
SUCCAR, J., MUSALLAM, K. M. & TAHER, A. T. 2011. Thalassemia and venous thromboembolism. *Mediterr J Hematol Infect Dis,* 3**,** e2011025.
TAVASSOLI, M. 1991. Embryonic and fetal hemopoiesis: an overview. *Blood Cells,* 17**,** 269-81; discussion 282-6.
TECHNOLOGIES, T. 2012. *CRISPR Genome Editing* [Online]. transomic.com. Available: http://www.transomic.com/Products/CRISPR-Genome-Editing.aspx [Accessed 03/10/2018 2018].
THON, J. N. & ITALIANO, J. E. 2010. Platelet formation. *Semin Hematol,* 47**,** 220-6.
THON, J. N., PETERS, C. G., MACHLUS, K. R., ASLAM, R., ROWLEY, J., MACLEOD, H., DEVINE, M. T., FUCHS, T. A., WEYRICH, A. S., SEMPLE, J. W., FLAUMENHAFT, R. & ITALIANO, J. E., JR. 2012. T granules in human platelets function in TLR9 organization and signaling. *J Cell Biol,* 198**,** 561-74.
TIEDT, R., SCHOMBER, T., HAO-SHEN, H. & SKODA, R. C. 2007. Pf4-Cre transgenic mice allow the generation of lineage-restricted gene knockouts for studying megakaryocyte and platelet function in vivo. *Blood,* 109**,** 1503.
TOMECKI, R. & DZIEMBOWSKI, A. 2010. Novel endoribonucleases as central players in various pathways of eukaryotic RNA metabolism. *RNA (New York, N.Y.),* 16**,** 1692-1724.
TSAI, S. F., STRAUSS, E. & ORKIN, S. H. 1991. Functional analysis and in vivo footprinting implicate the erythroid transcription factor GATA-1 as a positive regulator of its own promoter. *Genes Dev,* 5**,** 919-31.
TSANG, A. P., VISVADER, J. E., TURNER, C. A., FUJIWARA, Y., YU, C., WEISS, M. J., CROSSLEY, M. & ORKIN, S. H. 1997. FOG, a multitype zinc finger protein, acts as a cofactor for transcription factor GATA-1 in erythroid and megakaryocytic differentiation. *Cell,* 90**,** 109-19.
TUCKER, K. L., SAGE, T. & GIBBINS, J. M. 2012. Clot retraction. *Methods Mol Biol,* 788**,** 101-7.
TURITTO, V. T. & BAUMGARTNER, H. R. 1975. Platelet interaction with subendothelium in a perfusion system: Physical role of red blood cells. *Microvascular Research,* 9**,** 335-344.
TURITTO, V. T. & WEISS, H. J. 1980. Red blood cells: their dual role in thrombus formation. *Science (New York, N.Y.),* 207**,** 541-543.
TURRO, E., GREENE, D., WIJGAERTS, A., THYS, C., LENTAIGNE, C., BARIANA, T. K., WESTBURY, S. K., KELLY, A. M., SELLESLAG, D., STEPHENS, J. C., PAPADIA, S., SIMEONI, I., PENKETT, C. J., ASHFORD, S., ATTWOOD, A., AUSTIN, S., BAKCHOUL, T., COLLINS, P., DEEVI, S. V. V., FAVIER, R., KOSTADIMA, M., LAMBERT, M. P., MATHIAS, M., MILLAR, C. M., PEERLINCK, K., PERRY, D. J., SCHULMAN, S., WHITEHORN, D., WITTEVRONGEL, C., DE MAEYER, M., RENDON, A., GOMEZ, K., ERBER, W. N., MUMFORD, A. D., NURDEN, P., STIRRUPS, K., BRADLEY, J. R., RAYMOND, F. L., LAFFAN, M. A., VAN GEET, C., RICHARDSON, S., FRESON, K. & OUWEHAND, H. 2016. A dominant gain-of-function mutation in universal tyrosine kinase SRC causes thrombocytopenia, myelofibrosis, bleeding, and bone pathologies. *Science Translational Medicine,* 8**,** 328-358.

UNDAS, A. & ARIËNS, R. A. 2011. Fibrin clot structure and function: a role in the pathophysiology of arterial and venous thromboembolic diseases. *Arterioscler Thromb Vasc Biol,* 31**,** e88-99.
VANDAMME, T. F. 2014. Use of rodents as models of human diseases. *J Pharm Bioallied Sci,* 6**,** 2-9.
VELTEN, L., HAAS, S. F., RAFFEL, S., BLASZKIEWICZ, S., ISLAM, S., HENNIG, B. P., HIRCHE, C., LUTZ, C., BUSS, E. C., NOWAK, D., BOCH, T., HOFMANN, W. K., HO, A. D., HUBER, W., TRUMPP, A., ESSERS, M. A. & STEINMETZ, L. M. 2017. Human haematopoietic stem cell lineage commitment is a continuous process. *Nat Cell Biol,* 19**,** 271-281.
VYAS, P., AULT, K., JACKSON, C. W., ORKIN, S. H. & SHIVDASANI, R. A. 1999. Consequences of GATA-1 deficiency in megakaryocytes and platelets. *Blood,* 93**,** 2867-75.
WATOWICH, S. S., XIE, X., KLINGMULLER, U., KERE, J., LINDLOF, M., BERGLUND, S. & DE LA CHAPELLE, A. 1999. Erythropoietin Receptor Mutations Associated With Familial Erythrocytosis Cause Hypersensitivity to Erythropoietin in the Heterozygous State. *Blood,* 94**,** 2530-2532.
WATSON, S. P. 2009. Platelet activation by extracellular matrix proteins in haemostasis and thrombosis. *Curr Pharm Des,* 15**,** 1358-72.
WATSON, S. P., LOWE, G. C., LORDKIPANIDZE, M. & MORGAN, N. V. 2013. Genotyping and phenotyping of platelet function disorders. *J Thromb Haemost,* 11 Suppl 1**,** 351-63.
WEISS, M. J., KELLER, G. & ORKIN, S. H. 1994. Novel insights into erythroid development revealed through in vitro differentiation of GATA-1 embryonic stem cells. *Genes Dev,* 8**,** 1184-97.
WEN, R. & WANG, D. 2019. PTPRJ: a novel inherited thrombocytopenia gene. *Blood,* 133**,** 1272-1274.
WHELIHAN, M. F. & MANN, K. G. 2013. The role of the red cell membrane in thrombin generation. *Thrombosis Research,* 131**,** 377-382.
WHELIHAN, M. F., ZACHARY, V., ORFEO, T. & MANN, K. G. 2012. Prothrombin activation in blood coagulation: the erythrocyte contribution to thrombin generation. *Blood,* 120**,** 3837-45.
WILLIAMS, D. E., EISENMAN, J., BAIRD, A., RAUCH, C., VAN NESS, K., MARCH, C. J., PARK, L. S., MARTIN, U., MOCHIZUKI, D. Y., BOSWELL, H. S. & ET AL. 1990. Identification of a ligand for the c-kit proto-oncogene. *Cell,* 63**,** 167-74.
WOLF, B. C. & NEIMAN, R. S. 1987. Hypothesis: splenic filtration and the pathogenesis of extramedullary hematopoiesis in agnogenic myeloid metaplasia. *Hematol Pathol,* 1**,** 77-80.
WOLLMANN, M., GERZSON, B. M. C., SCHWERT, V., FIGUERA, R. W. & RITZEL, G. D. O. 2014. Reticulocyte maturity indices in iron deficiency anemia. *Revista brasileira de hematologia e hemoterapia,* 36**,** 25-28.
WRIGHT, S. D., MICHAELIDES, K., JOHNSON, D., WEST, N. C. & TUDDENHAM, E. 1993. Double heterozygosity for mutations in the platelet glycoprotein IX gene in three siblings with Bernard-Soulier syndrome.
WU, H., LIU, X., JAENISCH, R. & LODISH, H. F. 1995. Generation of committed erythroid BFU-E and CFU-E progenitors does not require erythropoietin or the erythropoietin receptor. *Cell,* 83**,** 59-67.

XAVIER-FERRUCIO, J., SCANLON, V., LI, X., ZHANG, P. X., LOZOVATSKY, L., AYALA-LOPEZ, N., TEBALDI, T., HALENE, S., CAO, C., FLEMING, M. D., FINBERG, K. E. & KRAUSE, D. S. 2019. Low iron promotes megakaryocytic commitment of megakaryocytic-erythroid progenitors in humans and mice. *Blood,* 134**,** 1547-1557.

XU, M., LI, J., NEVES, M. A. D., ZHU, G., CARRIM, N., YU, R., GUPTA, S., MARSHALL, J., ROTSTEIN, O., PENG, J., HOU, M., KUNISHIMA, S., WARE, J., BRANCH, D. R., LAZARUS, A. H., RUGGERI, Z. M., FREEDMAN, J. & NI, H. 2018. GPIbα is required for platelet-mediated hepatic thrombopoietin generation. *Blood,* 132**,** 622-634.

YAMAMOTO, K., MIWA, Y., ABE-SUZUKI, S., ABE, S., KIRIMURA, S., ONISHI, I., KITAGAWA, M. & KURATA, M. 2016. Extramedullary hematopoiesis: Elucidating the function of the hematopoietic stem cell niche (Review). *Mol Med Rep,* 13**,** 587-91.

YANG, J.-Y., DENG, X.-Y., LI, Y.-S., MA, X.-C., FENG, J.-X., YU, B., CHEN, Y., LUO, Y.-L., WANG, X., CHEN, M.-L., FANG, Z.-X., ZHENG, F.-X., LI, Y.-P., ZHONG, Q., KANG, T.-B., SONG, L.-B., XU, R.-H., ZENG, M.-S., CHEN, W., ZHANG, H., XIE, W. & GAO, S. 2018. Structure of Schlafen13 reveals a new class of tRNA/rRNA- targeting RNase engaged in translational control. *Nature Communications,* 9**,** 1165.

ZANG, C., LUYTEN, A., CHEN, J., LIU, X. S. & SHIVDASANI, R. A. 2016. NF-E2, FLI1 and RUNX1 collaborate at areas of dynamic chromatin to activate transcription in mature mouse megakaryocytes. *Scientific Reports,* 6**,** 30255.

ZARPELLON, A., KANAJI, T., KANAJI, S., MORODOMI, Y. & RUGGERI, Z. M. 2017. Expression of Functional Human Proteinase Activated Receptor (PAR)-1 on Mouse Platelets. *Blood,* 130**,** 451-451.

ZEIGLER, F. C., DE SAUVAGE, F., WIDMER, H. R., KELLER, G. A., DONAHUE, C., SCHREIBER, R. D., MALLOY, B., HASS, P., EATON, D. & MATTHEWS, W. 1994. In vitro megakaryocytopoietic and thrombopoietic activity of c-mpl ligand (TPO) on purified murine hematopoietic stem cells. *Blood,* 84**,** 4045-52.

ZHANG, Y., GAO, S., XIA, J. & LIU, F. 2018. Hematopoietic Hierarchy – An Updated Roadmap. *Trends in Cell Biology,* 28**,** 976-986.

ZHU, J. & EMERSON, S. G. 2002. Hematopoietic cytokines, transcription factors and lineage commitment. *Oncogene,* 21**,** 3295-3313.

ZSEBO, K. M., WILLIAMS, D. A., GEISSLER, E. N., BROUDY, V. C., MARTIN, F. H., ATKINS, H. L., HSU, R. Y., BIRKETT, N. C., OKINO, K. H., MURDOCK, D. C. & ET AL. 1990. Stem cell factor is encoded at the Sl locus of the mouse and is the ligand for the c-kit tyrosine kinase receptor. *Cell,* 63**,** 213-24.

**Appendix:** Heterozygous mutation SLFN14 K208N in mice mediates species-specific differences in platelet and erythroid lineage commitment. Blood Advances. 2021;5(2):377-390. (Stapley et al., 2021)

REGULAR ARTICLE

blood advances

Check for updates

# Heterozygous mutation SLFN14 K208N in mice mediates species-specific differences in platelet and erythroid lineage commitment

Rachel J. Stapley,[1] Christopher W. Smith,[1] Elizabeth J. Haining,[1] Andrea Bacon,[2] Sian Lax,[3] Vera P. Pisareva,[4] Andrey V. Pisarev,[4] Steve P. Watson,[1,5] Abdullah O. Khan,[1] and Neil V. Morgan[1]

[1]Institute of Cardiovascular Sciences, College of Medical and Dental Sciences, [2]MRC Centre for Immune Regulation, Transgenics Facility, and [3]Institute of Cancer and Genomic Sciences, College of Medical and Dental Sciences, University of Birmingham, Edgbaston, United Kingdom; [4]Department of Cell Biology, SUNY Downstate Health Sciences University, Brooklyn, NY; and [5]Centre of Membrane Proteins and Receptors, Universities of Birmingham and Nottingham, Midlands, United Kingdom



**Key Points**

- Heterozygous mutations in the SLFN14 AAA domain cause species-specific differences in platelet and erythroid lineage commitment.
- SLFN14$^{K208N/1}$ mice display pronounced microcytic erythrocytosis and anemia resulting from defective red blood cell formation.

Schlafen 14 (SLFN14) has recently been identified as an endoribonuclease responsible for cleaving RNA to regulate and inhibit protein synthesis. Early studies revealed that members of the SLFN family are capable of altering lineage commitment during T-cell differentiation by using cell-cycle arrest as a means of translational control by RNase activity. SLFN14 has been reported as a novel gene causing an inherited macrothrombocytopenia and bleeding in human patients; however, the role of this endoribonuclease in megakaryopoiesis and thrombopoiesis remains unknown. To investigate this, we report a CRISPR knock-in mouse model of SLFN14 K208N homologous to the K219N mutation observed in our previous patient studies. We used hematological analysis, in vitro and in vivo studies of platelet and erythrocyte function, and analysis of spleen and bone marrow progenitors. Mice homozygous for this mutation do not survive to weaning age, whereas heterozygotes exhibit microcytic erythrocytosis, hemolytic anemia, splenomegaly, and abnormal thrombus formation, as revealed by intravital microscopy, although platelet function and morphology remain unchanged. We also show that there are differences in erythroid progenitors in the spleens and bone marrow of these mice, indicative of an upregulation of erythropoiesis. This SLFN14 mutation presents distinct species-specific phenotypes, with a platelet defect reported in humans and a severe microcytic erythrocytosis in mice. Thus, we conclude that SLFN14 is a key regulator in mammalian hematopoiesis and a species-specific mediator of platelet and erythroid lineage commitment.

## Introduction

Endoribonucleases are a family of proteins responsible for cleaving RNA to regulate and inhibit protein synthesis.[1] The Schlafen (SLFN) family of proteins/genes is made up of 10 mouse and 6 human SLFN genes, all of which possess a characteristic AAA domain coding for DNA helicases, transcription regulators, protein folding regions, and a distinctive SLFN box of unknown function.[2] SLFN proteins are divided into 3 subgroups and are highly homologous, classified based on their increasing length. Subgroups II and III contain the aforementioned regions and a SWADL region, whereas subgroup III also possesses an additional helicase region ; 400 aa.[2-5]

Reported roles for the SLFN family of proteins include translational control by RNase activity (SLFN14), transfer RNA cleavage as part of the DNA damage response in tumor cells, and T-cell lineage and commitment (SLFN1).[6] Recently, SLFN14 mutations have been reported in 5 unrelated families worldwide who present with macrothrombocytopenia and associated excessive bleeding.[7-11] Patients

Submitted 20 May 2020; accepted 1 December 2020; published online 19 January 2021. DOI 10.1182/bloodadvances.2020002404.

Data sharing requests should be sent to Neil V. Morgan (n.v.morgan@bham.ac.uk).

The full-text version of this article contains a data supplement.

with these mutations have a platelet function defect in response to adenosine diphosphate, collagen, and PAR1-peptide and decreased platelet adenosine triphosphate secretion.[7] Further investigation discovered that SLFN14 colocalizes with ribosomes and causes endoribonucleolytic degradation of ribosomal RNA in cells.[12] These data, coupled with expression data from several databases, suggest that *SLFN14* is responsible for cleavage and regulation of critical RNAs in megakaryocytic and erythroid differentiation. Regulatory RNAs are thought to be critical in hematopoietic lineage commitment, with unique RNA signatures reported in multipotent and bipotent progenitors.[13-15] Pisareva et al revealed that SLFN14 is associated with cleaving RNA and ribosome-bound messenger RNA (mRNA) in an $Mg^{2+}$-dependent and nucleotide triphosphate (NTP)–independent manner.[16] Recent evidence in primary human cells from platelet and erythroid lineages suggests that SLFN14 may function in a similar way in cleaving RNA from the ribosomal unit prior to splitting, influencing hemoglobin production during blood cell development.[17]

Despite these insights, the mechanistic role of *SLFN14* in megakaryocyte (MK) development and hemostasis is unknown. To address this, we generated a global CRISPR-mediated knock-in (KI) mouse model of the patient mutation K219N missense substitution (mouse K208N homolog), which is known to cause thrombocytopenia, and investigated its overall role in hematopoiesis and platelet function. Homozygous KI mice for this mutation ($SLFN14^{K208N/K208N}$) did not survive to weaning and, similarly, *SLFN14* mutations identified in humans are all of a heterozygous nature; therefore, heterozygous mice were used in all experiments compared with litter-matched wild-type controls ($SLFN14^{K208N/+}$ and $SLFN14^{+/+}$, respectively). We investigated the *SLFN14 K208N* mutation through hematological analysis, platelet activation, function, and its overall role in hematopoiesis. $SLFN14^{K208N/+}$ mice showed significant differences from $SLFN14^{+/+}$ mice in gross hematological analyses. However, unlike the human variants, these mice demonstrate a major defect in erythropoiesis but not megakaryopoiesis or thrombopoiesis.

Differences in the consequences of this missense mutation suggest that *SLFN14* is a species-specific regulator of platelet and erythroid lineage commitment. In humans, the mutation causes a defect in thrombopoiesis, whereas a homologous missense mutation in mice causes a significant defect in erythropoiesis. $SLFN14^{K208N/+}$ mice present with pronounced microerythrocytosis, hemolytic anemia, splenomegaly, and abnormal thrombus formation in vivo.

## Materials and methods

### Mice

A *SLFN14 K208N*–KI mouse was generated in-house using CRISPR-Cas9 gene editing. All mice were generated on a C57BL/6J background and were bred in heterozygote/wild-type pairs. Animal care and welfare were in accordance with United Kingdom Home Office regulations and the use of Animals (Scientific Procedures) Act 1986. Animals were housed at the Biomedical Services Unit at the University of Birmingham.

### Genotyping

All mice were genotyped in-house using DNA extraction from mouse ear clips (DNeasy Blood & Tissue Kits; Qiagen, Manchester, United Kingdom). Polymerase chain reaction (PCR) and Sanger sequencing were used to identify *SLFN14 K208N*–KI mice following the procedure and conditions outlined in supplemental Tables 1 and 2.

### Flow cytometry

Flow cytometry was performed on a BD Accuri C6 flow cytometer, and results were analyzed using BD Accuri C6 software. Flow cytometry antibodies are listed in supplemental Tables 4.

### Platelet preparation

Mice were exsanguinated under terminal anesthesia by isoflurane/$O_2$ (5%) gas. Blood was drawn from the inferior vena cava, using a 25-gauge needle, into 1:10 (volume-to-volume ratio) acid citrate dextrose anticoagulant. Washed platelets were prepared as described in supplemental Material.

### Light transmission aggregometry

Washed platelet counts were normalized to $2 \times 10^8$/mL with Tyrode's-HEPES buffer. Aggregation in 300 μL of platelets was measured using a lumi-aggregometer (Chrono-Log, Havertown, PA) at 37°C under stirring conditions (1200 rpm) for 6 minutes post–agonist addition.

### Platelet spreading

Washed platelets at $2 \times 10^7$/mL were incubated for 45 minutes on collagen-coated (10 μg/mL) and fibrinogen-coated (100 μg/mL) coverslips under resting or preactivated conditions (0.1 U/mL thrombin). Adhered cells were fixed with 10% formalin, permeabilized, and stained with Alexa Fluor 488–conjugated phalloidin. Images were captured on a Zeiss Epifluorescence microscope and analyzed using a semiautomated machine learning–based workflow.[18,19]

### Hemostasis assay

All experiments were double blinded and conducted on 20 to 29g $SLFN14^{K208N/+}$ and litter-matched wild-type mice. Mice were anesthetized using isoflurane/$O_2$ (5%) gas, and 2 to 3 mm of tail tip was excised using a sterile razor blade and placed in prewarmed saline (37°C). Time until first cessation of bleeding was recorded.

### Clot retraction

Platelet-rich plasma (PRP) from $SLFN14^{K208N/+}$ and $SLFN14^{+/+}$ mice was adjusted to a final concentration of $2 \times 10^8$/mL using platelet-poor plasma and Tyrode's-HEPES buffer supplemented with 2mM $CaCl_2$, as previously described.[20] Erythrocytes were added for visualization, and clot formation was stimulated by 1 U/mL thrombin. Clots were monitored every 30 minutes for 2 hours, and clot weight and volume were calculated.

### In vivo thrombosis assays

Laser-induced injury of cremaster arterioles and $FeCl_3$-induced injury of carotid arteries were performed and analyzed as previously described.[21]

### Histological analysis

Spleens and decalcified bones were embedded in paraffin wax and sectioned at 5 μm prior to staining with hematoxylin and eosin (H&E) and Perls Prussian blue. Sections were scanned using a Zeiss Axio ScanZ1 slide scanner (Carl Zeiss Ltd., Cambridge, UK). The number of MKs was counted in 10 fields of view taken

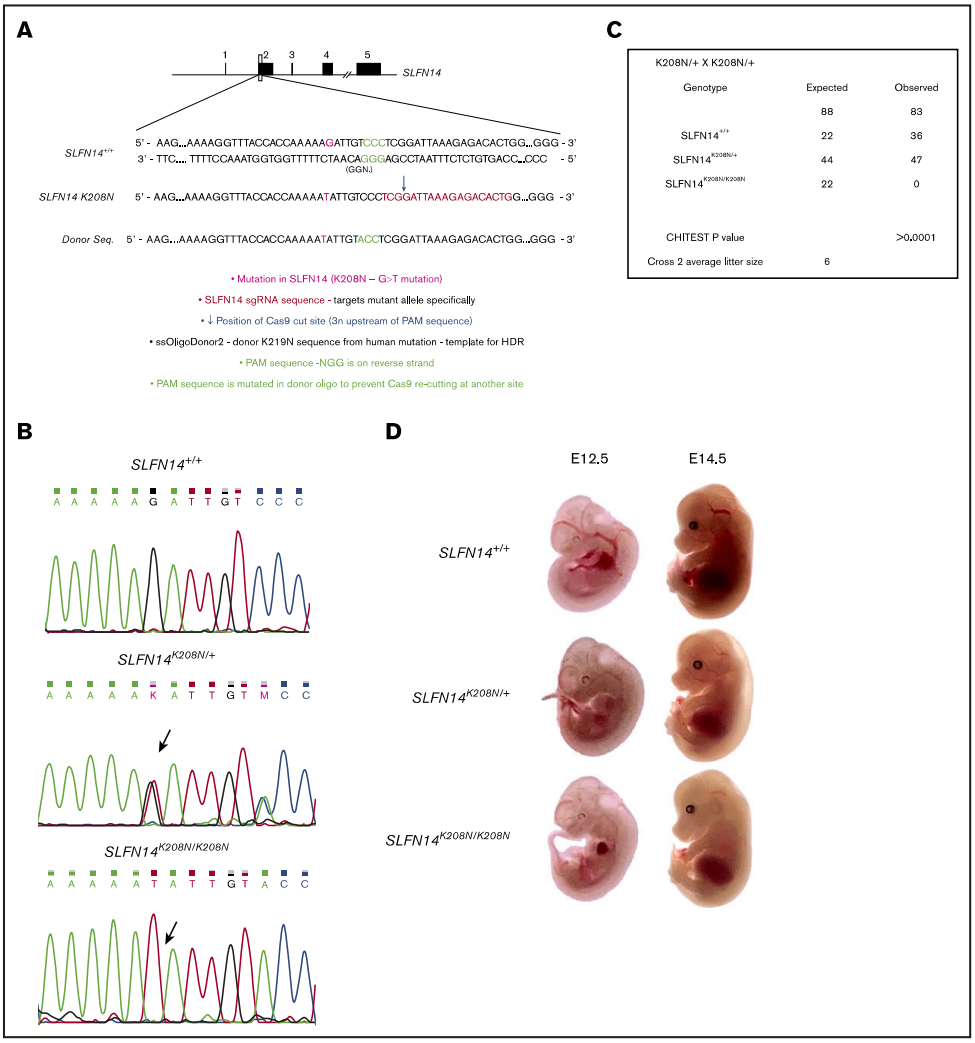


**Figure 1. Generation of *SLFN14 K208N* mice using CRISPR-Cas9 gene editing and embryo development.** (A) Schematic diagram of CRISPR-Cas9 gene-editing mechanism using human K219N donor oligonucleotide. (B) Wild-type, $SLFN14^{K208N/+}$, and $SLFN14^{K208N/K208N}$ traces showing successful KI of G>T missense mutation (arrow). (C) Non-Mendelian inheritance pattern of *SLFN14 K208N* mice. $\chi^2$ square analysis shows significant deviation from Mendelian inheritance and prewean loss of homozygotes ($P < .0001$). Data are taken from 15 litters of heterozygote/heterozygote (cross 2) breeding pairs. (D) Representative images of backlit embryos taken at E12.5 and E14.5 (original magnification ×3). n = 3 to 9 embryos per genotype.

from 2 femur sections and 1 spleen section per mouse. Sectioning and image analysis were performed double blinded.

### Spleen and bone marrow progenitor flow cytometry

Spleens were homogenized and whole bone marrow was flushed from mouse femurs and tibias in 1% fetal bovine serum and 2 mM EDTA in phosphate-buffered saline. Cells were filtered through a 70-μm cell strainer and stained with antibodies as per supplemental Table 4. A total of 50 000 events was collected using a BD Accuri C6 flow cytometer and gated to eliminate dead and cell doublets. Cells were imaged on poly-L-lysine coated coverslips using a Zeiss LSM880 confocal microscope.

### Statistical analysis

Data are presented as mean ± standard error of the mean (SEM), unless stated otherwise. A Student *t*-test and 2-way analysis of

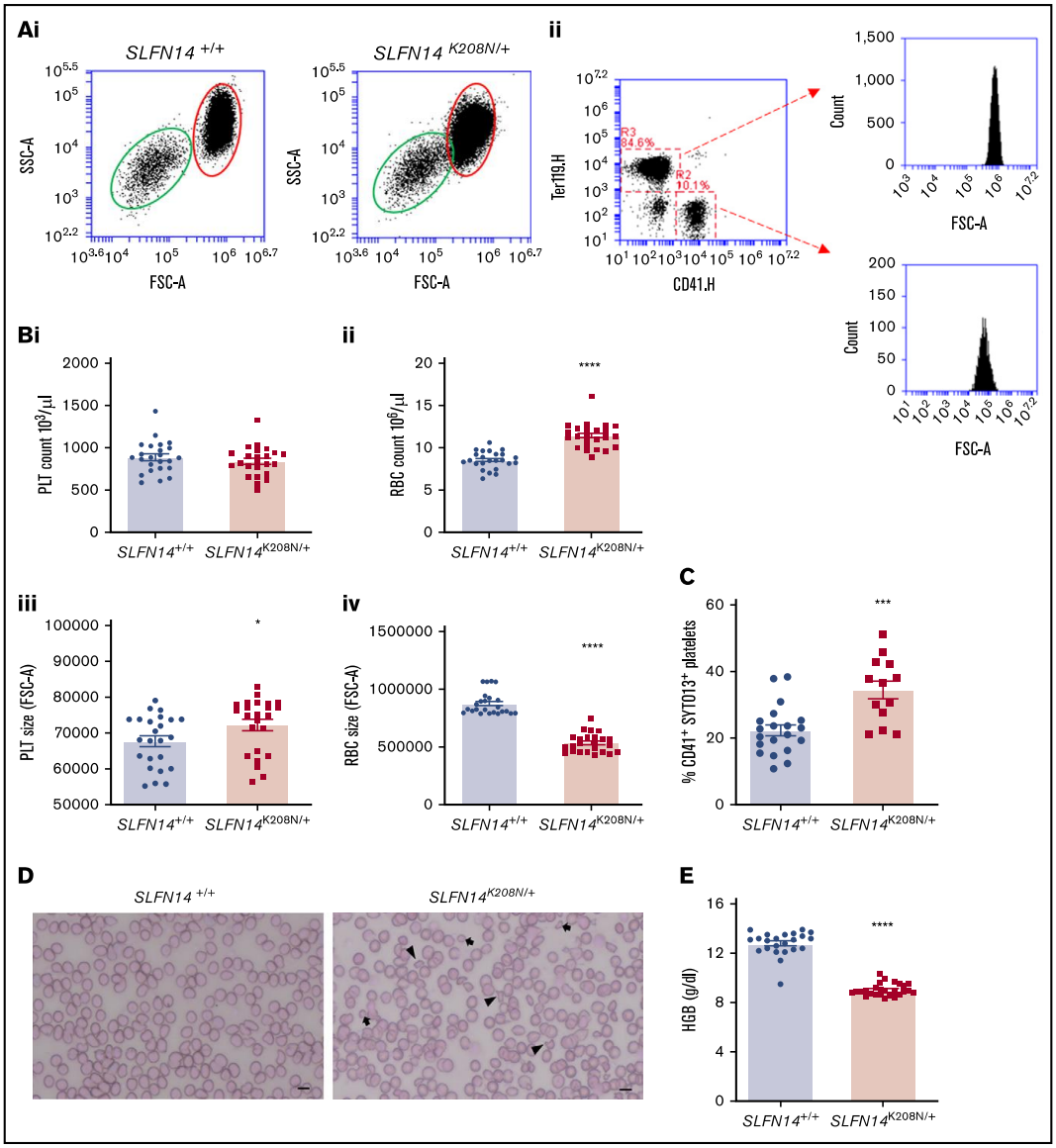


**Figure 2. Hematological analysis of *SLFN14*$^{K208N/+}$ mice.** (A) Flow cytometry–based counting of platelets and erythrocytes. (Ai) Flow cytometry forward scatter (FSC) and side scatter (SSC) plots showing size overlap of erythrocyte (red oval) and platelet (green oval) populations. (Aii) Gating method shown for double stain using CD41 (R2) and Ter119 (R3). Representative plots of n = 18 mice per genotype. (B) Platelet (PLT) (i) and erythrocyte (RBC) (ii) count and platelet (iii) and erythrocyte (iv) size from flow cytometry–based counting. Data are mean ± standard error of the mean (SEM); n = 18 mice per genotype. (C) Immature platelet fraction in *SLFN14*$^{K208N/+}$ mice. CD41$^{+}$ platelets were gated, and the immature platelet population was assessed by SYTO13 staining. Data are mean ± SEM; n = 13 to 20 mice per genotype. (D) Whole blood smears from wild-type and *SLFN14*$^{K208N/+}$ mice. Blood smears were stained with H&E histological stain to view blood cell size and morphology. Poikilocytes (irregularly shaped cells; arrowheads) and microcytes (arrows) are shown. Representative images of n = 6 or 7 mice per genotype. Scale bar, 10 µm. (E) *SLFN14*$^{K208N/+}$ mice are anemic. Hemoglobin levels were measured by an automated hematology analyzer in *SLFN14*$^{K208N/+}$ mice and wild-type controls. Data are mean ± SEM; n = 23 to 26 mice per genotype. *$P < .05$, ***$P < .001$, ****$P < .0001$.

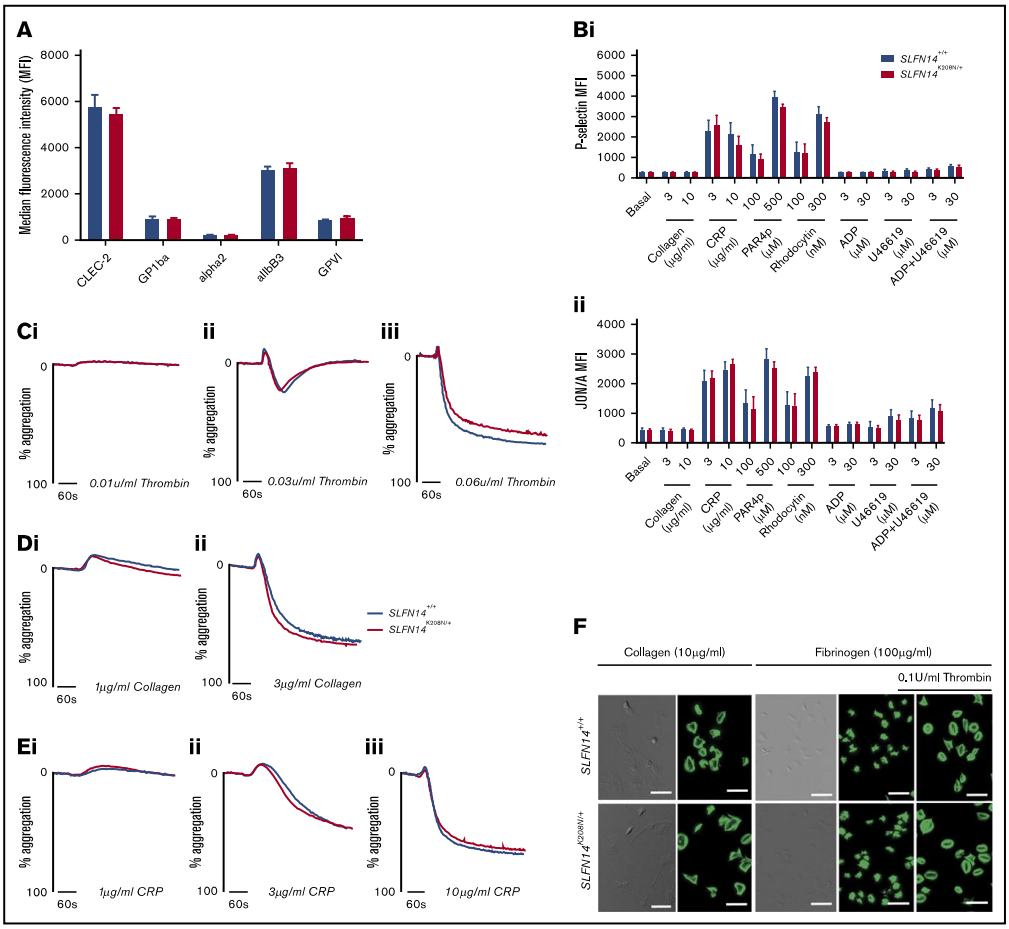


**Figure 3. In vitro assessment of platelet function in *SLFN14*$^{K208N/+}$ mice.** (A) Resting platelet surface glycoprotein expression levels. GP1ba$^{+}$ platelets were costained for the indicated surface receptors in whole blood. Median fluorescence intensity (MFI) from 4 to 6 mice per genotype. Data are mean ± standard error of the mean (SEM); significance was assessed using Welch's *t* test for multiple comparisons. (B) P-selectin (i) and activated αIIbβ3 (JON/A) (ii) expression on *SLFN14*$^{K208N/+}$ mouse platelets in response to the indicated agonist stimulation. Data are MFI (mean ± SEM) for 9 mice per genotype per condition. Significance was assessed by Sidak's 2-way analysis of variance. (C) Platelet reactivity in washed platelets in response to 0.01 U/mL (i), 0.03 u/mL (ii), or 0.06 U/mL (iii) thrombin. (D) Platelet reactivity in washed platelets in response to 1 μg/mL (i) or 3 μg/mL (ii) collagen. (E) Platelet reactivity in washed platelets in response 1 μg/mL (i), 3 μg/mL (ii), or 10 μg/mL (iii) collagen-related peptide. Representative traces of 3 to 6 mice per genotype per condition are shown. (F) Platelet spreading and adhesion in *SLFN14*$^{K208N/+}$ mice. *SLFN14*$^{K208N/+}$ platelets spread on collagen or fibrinogen under resting and thrombin-preactivated conditions (0.1 U/mL thrombin). Representative differential interference contrast and fluorescent phalloidin–stained images are shown from 3 mice per genotype/condition. Scale bar, 10 μm.

variance were used for platelet activation, and a Mann-Whitney *U* test was used for in vivo analysis, with $P < .05$ deemed significant. All analyses were conducted using GraphPad Prism software (v8.4).

Animal care and welfare were in accordance with United Kingdom Home Office regulations and the use of Animals in Scientific Procedures Act 1986 under Project License number P53D52513 (to N.V.M.).

## Results

### *SLFN14 K208N* homozygotes do not survive to weaning because of severe anemia

An in-house CRISPR-KI model was developed using homology directed repair (HDR). Human oligonucleotide donor templates of the K219N mutation were coinjected with single guide RNA as per the CRISPR-Cas9 mechanism (Figure 1A). This resulted in the

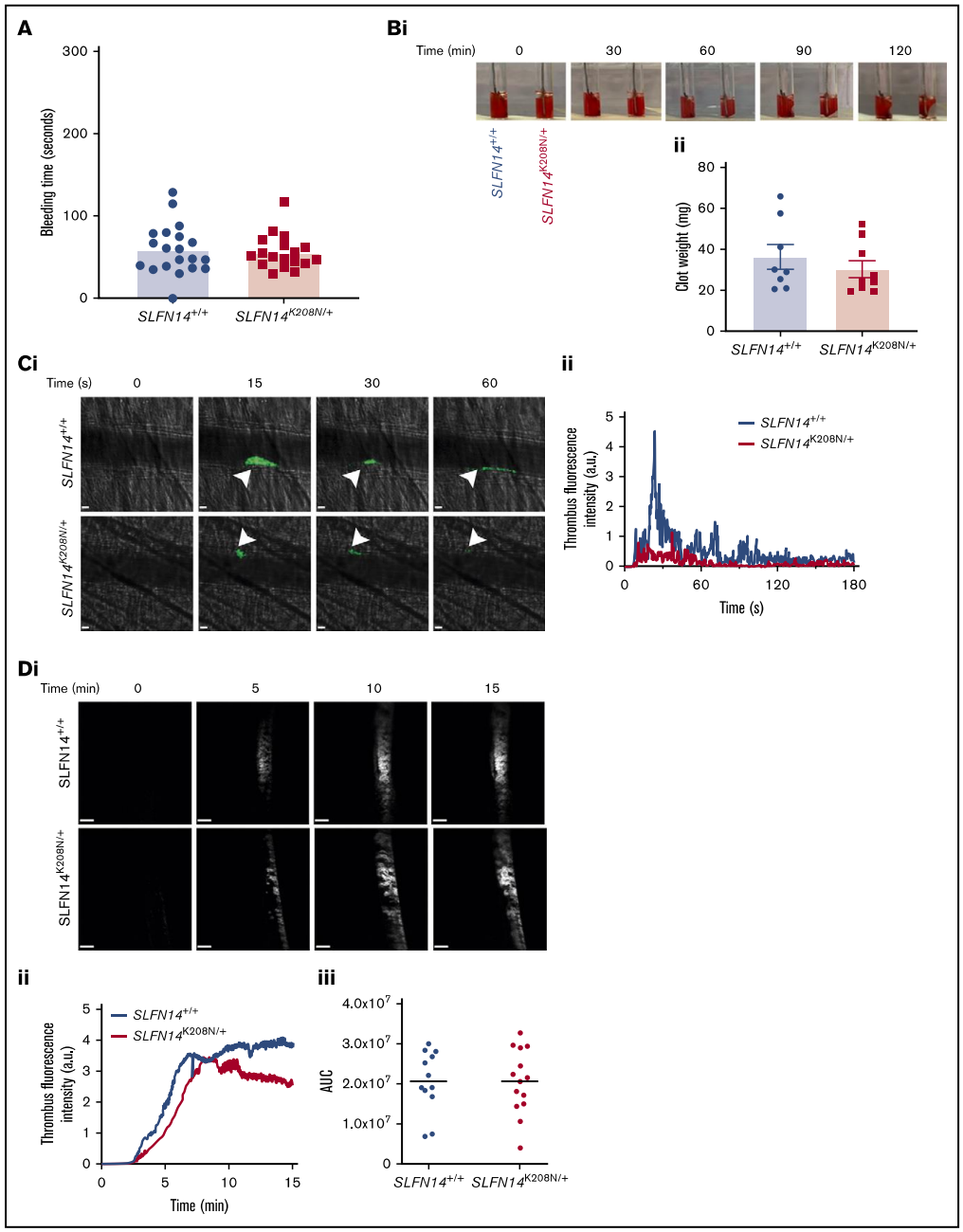


Figure 4.

G>T substitution and subsequent K208N amino acid change. Sanger sequencing was used to genotype mice, with Figure 1B showing successful KI of the mutation. A $\chi^2$ analysis of heterozygote/heterozygote breeding pairs shows significant deviation from Mendelian inheritance, with ~25% of offspring lost preweaning ($P < .0001$; Figure 1C). The average prewean loss was 25% across 15 litters, the same proportion of expected homozygote offspring according to Mendel's law (supplemental Table 3). To assess embryonic lethality, embryos were gathered for observation and genotyping at 12.5 and 14.5 days post–vaginal plug. At embryonic day 12.5 (E12.5), *SLFN14*$^{K208N/+}$ mice were not different from wild-type littermates. However, *SLFN14*$^{K208N/K208N}$ embryos were significantly paler, with less-defined vasculature (Figure 1D). E14.5 *SLFN14*$^{K208N/K208N}$ embryos were much more pale, with substantially less vascular definition than that seen in the other genotypes (Figure 1D). No *SLFN14*$^{K208N/K208N}$ mice survived to weaning for genotyping; therefore, we can deduce that if *SLFN14*$^{K208N/K208N}$ pups do survive beyond the critical fetal liver stage at day 14.5, they die shortly after birth. Therefore, in parallel with K219N heterozygous patients, *SLFN14 K208N* heterozygotes were used in analyses.

### *SLFN14*$^{K208N/+}$ mice have microcytic erythrocytosis, poikilocytosis, and anemia

*SLFN14*$^{K219N/+}$ patients exhibit macrothrombocytopenia; however, we did not observe any difference in platelet count in homologous *SLFN14*$^{K208N/+}$ mice, but we did detect an increase in size using a flow cytometry counting assay and single positive events of CD41 and Ter119–stained cells (Figure 2A,Bi-ii; $P < .0001$). Contrary to the patient mutation, for which no effect on erythrocyte production or function was reported, *SLFN14*$^{K208N/+}$ mice exhibit microcytic erythrocytosis, an increase in erythrocyte count accompanied by a reduction in size (Figure 2Biii-iv). We did not observe any difference in leukocyte counts between genotypes (data not shown).

*SLFN14*$^{K219N/+}$ patients have a high immature platelet fraction (IPF).[7] We assessed IPF in *SLFN14*$^{K208N/+}$ mice using a flow cytometry method and nucleic acid stain SYTO13, which was recently reported to be a more specific marker than its predecessor, Thiazole orange.[22] A 15% increase in the proportion of CD41$^+$ SYTO13$^+$ cells was observed in *SLFN14*$^{K208N/+}$ mice compared with *SLFN14*$^{+/+}$ controls (Figure 2C; $P = .0003$). Combined with the observed increase in platelet size, these data indicate an increase in the proportion of immature platelets in *SLFN14*$^{K208N/+}$ mice.

Whole blood smears from *SLFN14*$^{K208N/+}$ mice show irregularly shaped smaller erythrocytes (poikilocytes and microcytes) compared with the characteristic plump-shaped cells observed in wild-type controls (Figure 2D). This microcytosis is accompanied by lower hemoglobin levels in *SLFN14*$^{K208N/+}$ mice (Figure 2E).

These results and previous work in T-cell lineage commitment studies identify *SLFNs* as key drivers in species-dependent hematopoietic lineage commitment. In this case, we observe *SLFN14* mutations causing distinct differences in platelet and erythrocyte production and morphology.[3,6]

### *SLFN14*$^{K208N/+}$ mice exhibit normal platelet function in response to major agonists

No alteration in major glycoprotein receptor levels was observed in *SLFN14*$^{K208N/+}$ platelets (Figure 3A). Platelet activation was assessed by flow cytometry, and both genotypes displayed similar α-granule secretion (P-selectin) and integrin αIIbβ3 activation (JON/A) in response to agonists at varying doses (Figure 3B). Platelet function in *SLFN14*$^{K208N/+}$ mice was assessed using light transmission aggregometry. *SLFN14*$^{K208N/+}$ mice display normal platelet function compared with their wild-type littermates in response to the agonists thrombin, collagen, and collagen-related peptide (Figure 3C-E), which are mediated by G protein–coupled receptors and ITAM/receptor tyrosine kinase, and are the 2 main types of activation receptors in platelets.

We next investigated platelet adhesion and spreading on collagen- or fibrinogen-coated surfaces. Under resting and preactivated conditions, no difference in adhesion or cytoskeletal remodeling was observed in *SLFN14*$^{K208N/+}$ platelets (Figure 3F).[18,19]

### Hemostasis and thrombosis in *SLFN14*$^{K208N}$ mice

*SLFN14* patients were recruited to studies based on their bleeding phenotypes. To establish whether *SLFN14* transgenic mice had a bleeding phenotype, 2 to 3 mm of tail tip was excised, and time to bleeding cessation in prewarmed (37°C) saline was measured. No difference was observed in either genotype, indicating that platelets retain normal function, and abnormal erythrocytes do not impact hemostasis in this model (Figure 4A).

Clot retraction was also investigated in PRP to assess αIIbβ3-mediated platelet function. No visual difference was observed during the time course, and final mean clot weight of 36.0 mg and 30.0 mg for *SLFN14*$^{+/+}$ and *SLFN14*$^{K208N/+}$ mice, respectively, was not significantly different (Figure 4B). This supports our findings that platelet function is maintained and that the *SLFN14 K208N* mutation in mice does not lead to platelet function defects.

Thrombus formation was assessed in vivo by laser- and $FeCl_3$-induced injury models. Following laser injury, *SLFN14*$^{K208N/+}$ mice



**Figure 4. Functional role of *SLFN14* in thrombosis.** (A) Tail bleeding time assay. Two to 3 millimeters of tail was removed, and bleeding time until first stop was measured. Each data point represents 1 animal; n = 18 to 20 mice per genotype. (B) Clot retraction of *SLFN14*$^{K208N/+}$ mouse platelets in PRP. Clots were formed by stimulating $2 \times 10^8$ platelets per milliliter with 0.1 U/mL thrombin; monitoring took place for 2 hours. Representative images (Bi) and final clot weight (Bii). Data are mean ± SEM; n = 8 or 9 mice per genotype. (C) Laser-induced thrombus formation in vivo. (Ci) Representative composite brightfield and fluorescence images of thrombus formation. Mice were injected with anti-GPIbβ DyLight488 (0.1 μg/g body weight). Arterioles of the cremaster muscle were subsequently injured by laser (arrowheads) and thrombi fluorescence was measured. Scale bars, 10 μm. (Cii) Graph showing median integrated thrombus formation fluorescence intensity in arbitrary units (a.u.) for 31 or 32 injuries in 4 mice per genotype. (D) $FeCl_3$-induced thrombus formation. Mice were injected with DyLight488-conjugated anti-GPIbβ antibody (0.1 μg/g body weight), and the carotid artery was subsequently injured with 10% $FeCl_3$ solution for 3 minutes. (Di) Representative fluorescence images of platelets (GPIbβ). Scale bars, 200 μm. (Dii) Graph showing median integrated thrombus fluorescence. (Diii) Area under the curve (AUC) of the integrated fluorescence density (in a.u). Data are mean; n = 11 or 12 mice per genotype. See supplemental Videos 3 and 4 for wild-type and mutants, respectively.

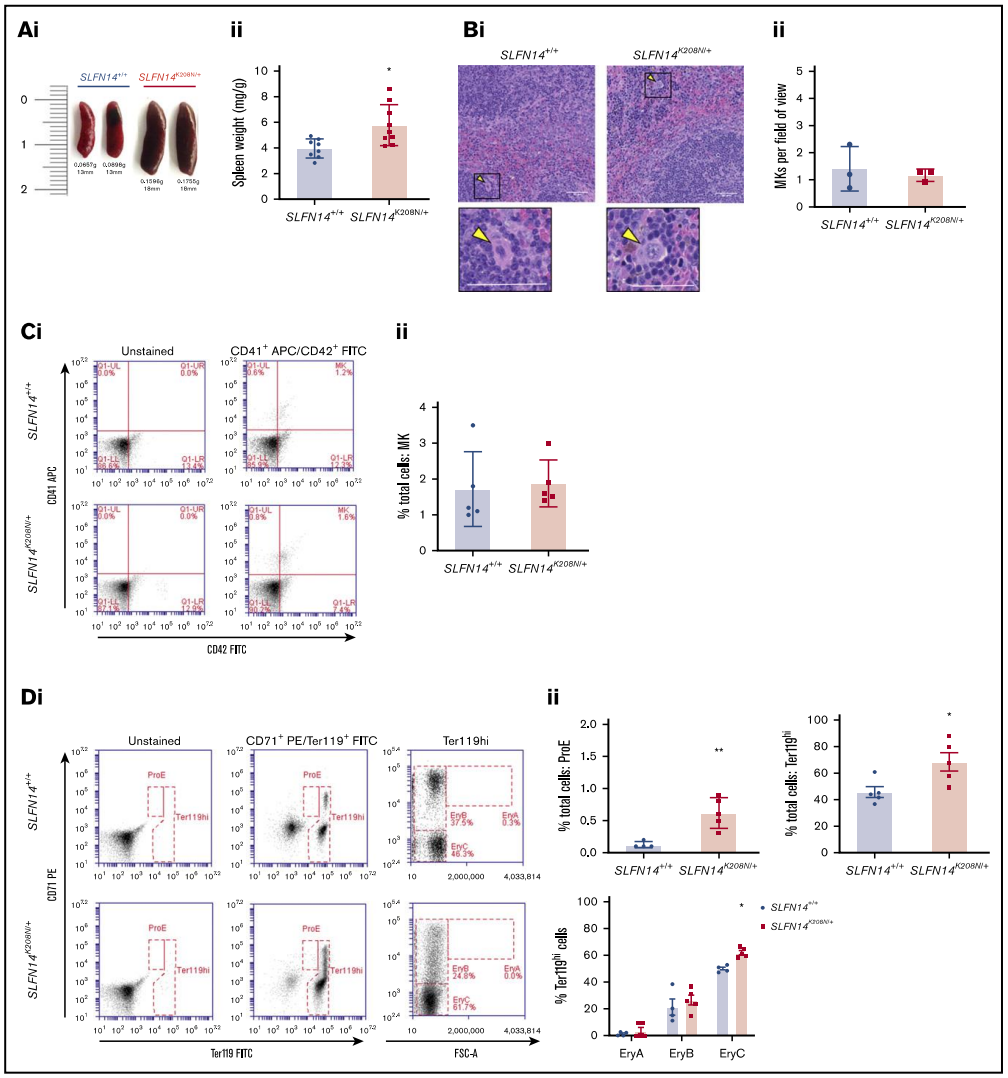


**Figure 5. *SLFN14*$^{K208N/+}$ mice exhibit splenomegaly and extramedullary erythropoiesis.** (Ai) Representative images of spleens from *SLFN14*$^{K208N/+}$ and *SLFN14*$^{+/+}$ mice. (Aii) Normalized spleen weight. Spleen weight/body weight (mg/g) from 8 or 9 mice per genotype. (Bi) Representative images of H&E-stained spleen sections from *SLFN14*$^{K208N/+}$ and wild-type controls. Arrowheads indicate MKs. Scale bars, 50 μm. (Bii) Quantification of MK number per field of view. n = 3 mice per genotype, 10 or 11 fields of view per tissue sample. Analysis was conducted blind. (C) Quantification of MKs in spleen. (Ci) MK staining: MKs were identified by CD41 (αIIb) allophycocyanin (APC) and CD42 (GPIb) fluorescein isothiocyanate (FITC) double staining. (Cii) Proportion of MKs in spleen flow cytometry. (D) Quantification of erythroid progenitors in spleen. (Di) ProE staining: ProEs were identified as double-positive CD71 (transferrin receptor 1) phycoerythrin (PE) and Ter119 FITC cells (ProE gate). (Dii) Quantification of ProEs, increased Ter119$^{+}$ cell population in *SLFN14*$^{K208N/+}$ mice, and profile of Ter119$^{hi}$ cells by EryA, EryB, and EryC gates. (E) Quantification of MK-EB–primed MEPs in the spleen: MEPs were identified as a small population positive for CD71 (transferrin receptor 1) PE and CD41 (αIIb) APC (MEP). (Ei) Flow cytometry plots show a slight, but insignificant, increase in MEP cell numbers in *SLFN14 K208N* mice compared with wild-type. (Eii) MEP quantification. All spleen flow cytometry data and quantification are representative of 4 or 5 mice per genotype/staining condition. (F) Representative images of hemosiderin deposits in spleen sections of wild-type and *SLFN14*$^{K208N/+}$ mice highlighted by Perls Prussian blue staining. Scale bars, 50 μm. n = 3 mice per genotype. *$P < .05$, **$P < .01$, Student *t* test.

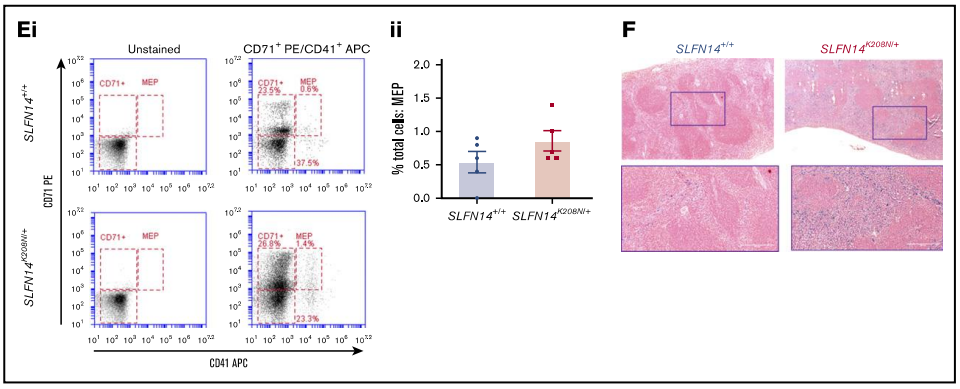


**Figure 5. (Continued).**

form thrombi at a similar rate to *SLFN14*$^{+/+}$ controls, although they are smaller, with fewer platelets recruited, and embolize more quickly than do those in littermate controls (Figure 4C; supplemental Videos 1 and 2, respectively). $FeCl_3$ injury to the carotid artery resulted in occlusive thrombus formation in both genotypes (Figure 4D; supplemental Videos 3 and 4). Monitoring the accumulation of fluorescently labeled platelets shows that *SLFN14*$^{K208N/+}$ mice form thrombi at a slightly slower rate and have a tendency for reduced stability, although these were not statistically different from littermate controls (Figure 4Dii-iii). Ultimately, thrombus formation and stability defects in *SLFN14*$^{K208N/+}$ mice are driven by the involvement of other blood cells; together with in vitro platelet function studies, these findings suggest that *SLFN14 K208N* has only a minor role in mouse platelets.

## Splenomegaly in *SLFN14*$^{K208N/+}$ mice is due to extramedullary erythropoiesis, the accumulation of mature erythrocytes, and hemolytic anemia

The spleen acts as a major site for filtering and clearance of blood from the circulation. In classical findings of clearance, platelets undergo phagocytosis controlled by their immunoglobulin G–coated surfaces, rendering Fc receptor–directed clearance by macrophages in the spleen.[23] The spleen can also act as an additional site of hematopoiesis in the event of myelofibrosis or bone marrow scarring in certain pathologies.[24] We investigated the spleen to assess differences in blood cell production and clearance. After controlling for body weight, spleens of *SLFN14*$^{K208N/+}$ mice were significantly larger with regard to weight and size compared with those from *SLFN14*$^{+/+}$ littermates (Figure 5A). MK counts from histology sections in the spleen were normal, and the proportion of MKs was unchanged between genotypes by flow cytometry analysis (Figure 5B-C).

Using a similar gating strategy to Koulnis et al, we used CD71 (early erythroid progenitor marker) and Ter119 (mature erythroid marker) to detect erythroid cells and categorized Ter119$^{hi}$ cells according to size (Figure 5Di).[25] There was a significant increase in the proportion of proerythroblasts (ProEs) in heterozygotes (CD71$^{+}$/Ter119$^{+}$; Figure 5Dii). In these spleens, we did not detect any EryA progenitors in either genotype (Figure 5D). However, despite fairly consistent proportions of Ter119$^{hi}$ cells between genotypes, we observed a difference in the distribution and greater spread of CD71$^{+}$ cells within the EryB gate and an increase in EryCs (most mature erythroid cells) in heterozygotes that was suggestive of erythroid maturation from the intermediate progenitor within the spleen (Figure 5D). Gating strategy for spleen flow cytometry is detailed in supplemental Figure 1.

Our flow cytometry progenitor panel aimed to detect megakaryocyte-erythroid progenitors (MEPs). Consistent with previous findings by Psaila et al, we identified 2 subpopulations by differential expression of CD71 and a small MEP population by coexpression of CD41,[26] CD71$^{+}$/CD41$^{+}$ cells were rare in these samples, consistent with previous findings, although we did detect an almost threefold increase in MEPs in *SLFN14*$^{K208N/+}$ mice than in wild-types[26] (Figure 5E). In addition, we observed a greater spread of cells within our CD71$^{+}$ population in contrast to the more clustered appearance in controls.

We discovered substantial hemosiderin staining in lysed erythrocytes. These hemoglobin deposits occur naturally as a result of macrophage-mediated clearance of erythrocytes. Using Perls Prussian blue staining, we see a substantial increase in sites of free heme staining, as indicated by the blue areas in Figure 5F. Interestingly, we see staining in the red and white pulp of *SLFN14*$^{K208N/+}$ mice but only red pulp where macrophage clearance occurs in controls. This is also supported by the color difference in heterozygous spleens, which appear significantly darker than *SLFN14*$^{+/+}$ spleens (Figure 5Ai). Here, we hypothesize that erythropoiesis is accelerated to compensate for reduced hemoglobin levels. We suggest that *SLFN14*$^{K208N/+}$ erythrocytes are more prone to hemolysis and that the spleen acts as a secondary site of hematopoiesis, specifically upregulating erythropoiesis. The spleen also acts in cell clearance; as such, it may be unable to recognize the need for these additional erythrocytes in oxygen transport which, in the case of *SLFN14*$^{K208N/+}$ mice, may also be the cause of accelerated hemolysis.

## Bone marrow profiles showed significant alterations in erythroid progenitors in *SLFN14*$^{K208N/+}$ mice

The main site of hematopoiesis is the bone marrow; therefore, to assess discrepancies in hematopoiesis or altered progenitor levels

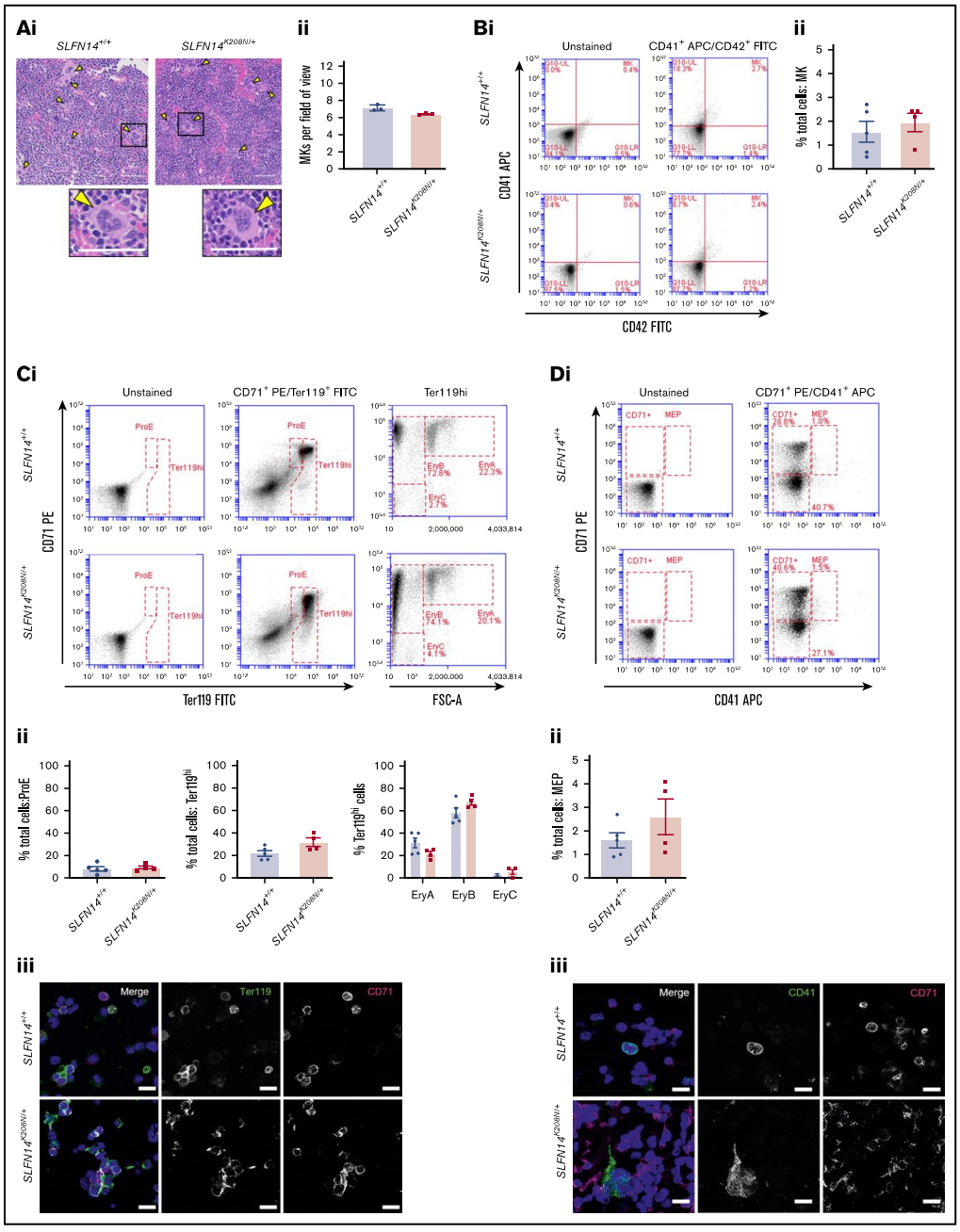


Figure 6.

leading to differences in platelet and erythrocyte counts, we examined bone marrow sections and flow cytometry panels, staining for progenitors. Double-blinded evaluation of bone marrow histology sections revealed that MKs were highly populated within the bone marrow, with morphology, including the characteristic polyploid nuclei, consistent across the 2 genotypes (Figure 6A). We analyzed progenitor levels in flushed whole bone marrow from mouse femurs and tibias by flow cytometry. Live single cells were selected based on size and forward scatter to detect progenitor cells and subsequent double-positive populations (determined by antibody staining) gated for analysis (supplemental Figure 2). MKs were highlighted by $CD41^+/CD42^+$ events (MK quadrant); no difference in the percentage of MKs was observed between genotypes (Figure 6B).

Using CD71 and Ter119 as before, there was no significant difference in the proportion of ProEs in the bone marrow (Figure 6Ci-ii). The percentage of $Ter119^{hi}$ cells was consistent between $SLFN14^{K208N/+}$ and wild-type mice; within this population, EryA, EryB, and EryC populations were also unchanged between genotypes (Figure 6Ci-ii). As in spleens, we observed the similar "spread distribution" of variable CD71 expression within the EryB gate; however, in contrast, mature erythrocytes (EryC) were rare. Confocal imaging of this staining pattern is shown in Figure 6Cii.

The predecessor to MKs and ProEs is the MEP. Given the differences that we observed in erythroid cell distribution (Figure 6C) and evidence suggestive of a platelet defect in our patient data, we detected megakaryocyte-erythroblast (MK-EB)–primed MEPs using CD71 and CD41, as before. These double-positive primed MEPs are often difficult to detect in situ within the bone marrow (Figure 6Di).[26] We did not observe any difference in the proportion of $CD71^+/CD41^+$ cells in $SLFN14^{K208N/+}$ mice (Figure 6Dii). Confocal imaging supports an increase in cellular events in the double-positive channel of heterozygotes and more $CD71^+$ single-stained events (Figure 6Diii). The reason for this shift in the MEP population is yet to be determined; however, we hypothesize that it results from $SLFN14^{K208N/+}$ MK-EB MEPs being more primed in the erythroid direction, consistent with higher single CD71 positivity in this staining panel ($CD71^+$; Figure 6Di). Increased $CD71^+$ staining may be expansion of the MEP with preference towards the erythroid lineage, as well as due to increased erythroid progenitors after this stage.

### *SLFN14*$^{K208N}$ reduces GATA1 and SLFN14 mRNA levels in hematopoietic cells

To examine whether the K208N mutation led to aberrant expression in hematopoietic cells of $SLFN14^{K208N/+}$ mice, we measured the abundance of *SLFN14* mRNA in whole bone marrow by real-time quantitative PCR. Compared with RNA from wild-type controls, *SLFN14* mRNA levels were reduced significantly (by ~50%) in $SLFN14^{K208N/+}$ mice ($P < .01$; supplemental Figure 3).

Furthermore, we considered whether levels of the master transcription factor GATA1 were altered as a result of the K208N mutation. Real-time quantitative PCR was performed to measure *GATA1* mRNA levels using cDNA-specific primers for *GATA1* and *GAPDH* as the endogenous control housekeeping gene. *GATA1* levels were reduced substantially in RNA from $SLFN14^{K208N/+}$ mice compared with litter-matched controls ($P < .05$; supplemental Figure 3). All primers are given in supplemental Table 5.

## Discussion

*SLFN14* is a poorly studied endoribonuclease with suspected roles in cleaving RNA that may contribute to a reported thrombocytopenia and clinical bleeding in multiple unrelated patients/families. Here, we present a CRISPR KI mutation of K208N in mice and establish the role of *SLFN14* as a key player in the lineage-commitment pathway, giving rise to species-specific phenotypes in hematopoiesis. In this study, we analyzed heterozygous mutants, because homozygous mutants did not survive to weaning and showed significant deviation from Mendelian inheritance patterns. This suggests that *SLFN14* has a critical role in mouse embryogenesis and, particularly, erythropoiesis. *SLFN14 K208N* is likely to be particularly relevant in future studies of gene-expression profiling in erythrocytes and anemia. E12.5 and E14.5 homozygous embryos were paler than their littermates, showed less distinct vasculature, and did not survive to weaning. These are most likely due to homozygotes' more severe anemia and hemolysis that results in death shortly after birth.[27]

The *K208N* mutation in mice presents with a different phenotype than in its homologous human version, suggesting that it plays a critical role at the MEP junction in lineage fate decisions. Previous studies found that endoribonuclease function is critical in RNA regulation in various bacterial species; however, to our knowledge,

**Figure 6. Bone marrow progenitor profile of *SLFN14*$^{K208N/+}$ mice.** (Ai) Representative images of H&E-stained femur sections from $SLFN14^{K208N/+}$ and $SLFN14^{+/+}$ mice. Femurs were fixed in 4% formaldehyde and decalcified before sectioning, staining and quantification of MK number per field of view. MKs are indicated by arrowheads. Scale bars, 50 μm. (Aii) Quantification of MK number per field of view from 3 mice per genotype. Two femurs per mouse were sectioned, and 10 to 13 fields of view per section were quantified blind. Students *t* test was used to assess significance. (B) Quantification of MKs in bone marrow. (Bi) MK staining: MKs were identified by CD41 (αIIb) allophycocyanin (APC) and CD42 (GPIb) fluorescein isothiocyanate (FITC) double staining. (Bii) Quantification of MKs in whole bone marrow by flow cytometry. (C) Quantification of erythroid progenitors in bone marrow. (Ci) ProE staining: ProEs were identified as double-positive CD71 (transferrin receptor 1) phycoerythrin (PE) and Ter119 FITC cells (ProE gate). Maturation of ProEs to mature erythrocytes can be monitored by $Ter119^{hi}$ expression and loss of CD71 expression (EryB and EryC gates). Note the spread of intermediate cells in EryBs, supporting evidence for an altered EryB fate in heterozygotes. (Cii) Quantification of erythroid progenitors in the bone marrow. (Ciii) Confocal images of flow cytometry samples show a double-positive ProE population. Ter119 Alexa Fluor 488 and CD71 Alexa Fluor 647 and DAPI counterstain. Scale bars, 50 μm. (D) Quantification of MEPs in bone marrow. (Di) MK-EB–primed MEPs: MEPs were identified as a small population positive for CD71 (transferrin receptor 1) PE and CD41 (αIIb) APC (MEP). Flow cytometry plots show a slight, but insignificant, increase in MEP cell numbers in SLFN14 K208N mice compared with wild-types. (Dii) MEP quantification in the bone marrow. Staining for these markers highlights MEP cells preferential to the MK or EB lineage. (Diii) Representative images of CD41 Alexa Fluor 488 and CD71 Alexa Fluor 647 stained bone marrow cells imaged by confocal microscopy and using DAPI counterstain. Scale bars, 50 μm. All bone marrow flow cytometry data and quantifications are representative of 4 to 6 mice per genotype/staining condition.

this is the first discovery of endoribonuclease-mediated species differences in mammals.[28,29]

*SLFN14*$^{K219N}$ patients have a high IPF, suggesting that thrombopoiesis is not sufficient to maintain steady levels of platelet production or that platelet clearance is accelerated. Platelets contain residual RNA from their predecessors, MKs, which form beaded extensions into the lumen of bone marrow sinusoids (proplatelets) and subsequent shear forces of the bloodstream that cause release of preplatelets and platelets into the blood.[30] RNA content can be used to estimate the rate of thrombopoiesis and platelet turnover by measuring the proportion of reticulated platelets within the circulation. An elevated platelet RNA content signifies newer platelets in the circulation that was previously shown to increase platelet reactivity in cardiovascular events and mortality.[31] In the case of *SLFN14*$^{K208N/+}$ mice, we infer that the slight increase in platelet size is due to their immaturity (determined by SYTO13 staining), but this is not accompanied by increased platelet reactivity, as shown in our in vitro and in vivo experiments.

Although no platelet defects were observed in in vitro functional studies, *SLFN14*$^{K208N/+}$ mice exhibited reduced thrombus formation in vivo. These defects in the formation and stability of in vivo thrombi are likely attributable to the abnormal erythrocytes in these mice. Erythrocytes are the primary determinant of blood rheology and promote platelet margination, increasing their concentration near endothelium to enable rapid formation of thrombi in response to vessel damage.[32-34] Indeed, previous studies have shown reduced thrombus formation and extended bleeding times in anemic mice.[35] Although we did not observe altered hemostasis in *SLFN14*$^{K208N/+}$ mice, changes in the size and number of erythrocytes may explain thrombosis findings. Erythrocyte contribution to platelet activation and thrombin generation should also be taken into consideration, together with their unusual role supporting platelet adhesion in the $FeCl_3$ model.[35-37] Although *SLFN14* patients display excessive bleeding phenotypes, we do not report these similarities in mice.[7] Bleeding in *SLFN14* patients has been characterized and explained by defects in platelet aggregation, but little to no effect on platelet function was found in *SLFN14*$^{K208N/+}$ mice. We believe that this work precedes what is to become extensive research into platelet-erythrocyte interactions in health and disease and reveals potential novel mechanisms in hemolysis and anemia.

In *SLFN14*$^{K208N/+}$ mice, we understand that the spleen acts as a secondary site for erythropoiesis. Here, intermediate progenitors (EryBs) differentiate into mature erythrocytes (EryCs), which are highly populated within the spleen. Loss of CD71 expression is indicative of erythrocyte maturation, and the "spread" appearance of EryB cells in heterozygotes clearly shows this maturation phase. This enhanced erythropoiesis is likely due to severe anemia and hemolysis in these mice attempting to compensate for lower hemoglobin levels. The following questions then arise: at what stage in hematopoiesis do *SLFN14* and its mutations cause a shift in lineage commitment to platelet or erythroid directions and how, as an endoribonuclease, does *SLFN14* mediate this transition? Our bone marrow flow cytometry data did not show any difference in bone marrow MK, ProE, or MEP numbers, but there are discrepancies within progenitors of the erythroid lineage suggesting that, in hematopoiesis, *SLFN14*$^{K208N/+}$ leads to altered erythropoiesis and defects in erythroid cells. In the bone marrow, *SLFN14*$^{K208N/+}$ Ter119$^{hi}$ cells expressing CD71 also showed variable expression within the EryB gate, whereas wild-type cells present a more clustered distribution. Platelets and erythrocytes originate from a common progenitor; therefore, pinpointing the exact location of this shift is notoriously difficult. However, we believe that using RNA-sequencing of *SLFN14* progenitors (MKs, ProEs, and MK/EB-MEPs) will reveal discrepancies in RNA expression profiles to support our preliminary findings that a reduction in *GATA1* mRNA is specifically involved in erythroid development. Future work will establish the mechanistic effects of these mutations on human and murine RNA signatures that are critical in lineage commitment. This will uncover novel insights into *SLFN14*'s ability to cleave RNAs which perturb RNA metabolism and protein synthesis in MK and erythroid lineages in a species-dependent manner.

## Acknowledgments

The authors thank all technicians and staff at Biomedical Services Unit at the University of Birmingham for housing and husbandry of animals used in this study. They also acknowledge Pip Nicolson for expertise in whole blood smear analysis.

Work in the authors' laboratories is supported by grants from the British Heart Foundation (PG/16/103/32650, FS/18/11/33443) (N.V.M.) and National Institutes of Health, National Institute of General Medical Sciences grant GM097014 (A.V.P.) and National Heart, Lung, and Blood Institute grant HL146544 (A.V.P. and N.V.M.).

## Authorship

Contribution: R.J.S., C.W.S., A.O.K., and N.V.M. designed the study, designed and performed experiments, and wrote the manuscript; A.B. generated CRISPR mouse colonies; E.J.H. and S.L. contributed to mouse colony maintenance and experiments; V.P.P., A.V.P., and S.P.W contributed intellectually to the study; and all authors reviewed the manuscript.

Conflict-of-interest disclosure: The authors declare no competing financial interests.

ORCID profiles: R.J.S., 0000-0002-0027-9158; S.L., 0000-0002-0248-8973; S.P.W., 0000-0002-7846-7423; A.O.K., 0000-0003-0825-3179; N.V.M., 0000-0001-6433-5692.

Correspondence: Neil V. Morgan, Institute of Cardiovascular Sciences, College of Medical and Dental Sciences, University of Birmingham, Edgbaston B15 2TT, United Kingdom; e-mail: n.v.morgan@bham.ac.uk.

## References

1. Yang J-Y, Deng X-Y, Li Y-S, et al. Structure of Schlafen13 reveals a new class of tRNA/rRNA- targeting RNase engaged in translational control. *Nat Commun*. 2018;9(1):1165.

2. Stapley RJ, Pisareva VP, Pisarev AV, Morgan NV. *SLFN14* gene mutations associated with bleeding. *Platelets*. 2020;31(3):407-410.

3. Geserick P, Kaiser F, Klemm U, Kaufmann SHE, Zerrahn J. Modulation of T cell development and activation by novel members of the Schlafen (slfn) gene family harbouring an RNA helicase-like motif. *Int Immunol*. 2004;16(10):1535-1548.
4. Neumann B, Zhao L, Murphy K, Gonda TJ. Subcellular localization of the Schlafen protein family. *Biochem Biophys Res Commun*. 2008;370(1):62-66.
5. Bustos O, Naik S, Ayers G, et al. Evolution of the Schlafen genes, a gene family associated with embryonic lethality, meiotic drive, immune processes and orthopoxvirus virulence. *Gene*. 2009;447(1):1-11.
6. Schwarz DA, Katayama CD, Hedrick SM. Schlafen, a new family of growth regulatory genes that affect thymocyte development. *Immunity*. 1998;9(5): 657-668.
7. Fletcher SJ, Johnson B, Lowe GC, et al; UK Genotyping and Phenotyping of Platelets study group. SLFN14 mutations underlie thrombocytopenia with excessive bleeding and platelet secretion defects. *J Clin Invest*. 2015;125(9):3600-3605.
8. Marconi C, Di Buduo CA, Barozzi S, et al. SLFN14-related thrombocytopenia: identification within a large series of patients with inherited thrombocytopenia. *Thromb Haemost*. 2016;115(5):1076-1079.
9. Saes JL, Simons A, de Munnik SA, et al. Whole exome sequencing in the diagnostic workup of patients with a bleeding diathesis. *Haemophilia*. 2019; 25(1):127-135.
10. Almazni I, Stapley RJ, Khan AO, Morgan NV. A comprehensive bioinformatic analysis of 126 patients with an inherited platelet disorder to identify both sequence and copy number genetic variants. *Hum Mutat*. 2020;41(11):1848-1865.
11. Khan AO, Stapley RJ, Pike JA, et al; UK GAPP Study Group. Novel gene variants in patients with platelet-based bleeding using combined exome sequencing and RNAseq murine expression data. *J Thromb Haemost*. 2021;19(1):262-268.
12. Fletcher SJ, Pisareva VP, Khan AO, Tcherepanov A, Morgan NV, Pisarev AV. Role of the novel endoribonuclease SLFN14 and its disease-causing mutations in ribosomal degradation. *RNA*. 2018;24(7):939-949.
13. Magella B, Adam M, Potter AS, et al. Cross-platform single cell analysis of kidney development shows stromal cells express Gdnf. *Dev Biol*. 2018;434(1): 36-47.
14. Olsson A, Venkatasubramanian M, Chaudhri VK, et al. Single-cell analysis of mixed-lineage states leading to a binary cell fate choice [published correction appears in *Nature*. 2019;569(7715):E3]. *Nature*. 2016;537(7622):698-702.
15. Lu YC, Sanada C, Xavier-Ferrucio J, et al. The molecular signature of megakaryocyte-erythroid progenitors reveals a role for the cell cycle in fate specification[published correction appears in *Cell Rep*. 2018;25(11):3229]. *Cell Rep*. 2018;25(8):2083-2093.e4.
16. Pisareva VP, Muslimov IA, Tcherepanov A, Pisarev AV. Characterization of novel ribosome-associated endoribonuclease SLFN14 from rabbit reticulocytes. *Biochemistry*. 2015;54(21):3286-3301.
17. Mills EW, Wangen J, Green R, Ingolia NT. Dynamic regulation of a ribosome rescue pathway in erythroid cells and platelets. *Cell Rep*. 2016;17(1):1-10.
18. Khan AO, Maclachlan A, Lowe GC, et al. High-throughput platelet spreading analysis: a tool for the diagnosis of platelet- based bleeding disorders. *Haematologica*. 2020;105(3):e124-e128.
19. Pike JA, Simms VA, Smith CW, et al. An adaptable analysis workflow for characterization of platelet spreading and morphology. *Platelets*. 2020;Apr 23: 1-5.
20. Tucker KL, Sage T, Gibbins JM. Clot retraction. *Methods Mol Biol*. 2012;788:101-107.
21. Smith CW, Raslan Z, Parfitt L, et al. TREM-like transcript 1: a more sensitive marker of platelet activation than P-selectin in humans and mice. *Blood Adv*. 2018;2(16):2072-2078.
22. Hille L, Cederqvist M, Hromek J, Stratz C, Trenk D, Nührenberg TG. Evaluation of an alternative staining method using SYTO 13 to determine reticulated platelets. *Thromb Haemost*. 2019;119(5):779-785.
23. Crow AR, Lazarus AH. Role of Fcgamma receptors in the pathogenesis and treatment of idiopathic thrombocytopenic purpura. *J Pediatr Hematol Oncol*. 2003;25(suppl 1):S14-S18.
24. Mori J, Nagy Z, Di Nunzio G, et al. Maintenance of murine platelet homeostasis by the kinase Csk and phosphatase CD148. *Blood*. 2018;131(10): 1122-1144.
25. Koulnis M, Pop R, Porpiglia E, Shearstone JR, Hidalgo D, Socolovsky M. Identification and analysis of mouse erythroid progenitors using the CD71/ TER119 flow-cytometric assay. *J Vis Exp*. 2011;(54):2809.
26. Psaila B, Barkas N, Iskander D, et al. Single-cell profiling of human megakaryocyte-erythroid progenitors identifies distinct megakaryocyte and erythroid differentiation pathways. *Genome Biol*. 2016;17(1):83.
27. Baron MH, Vacaru A, Nieves J. Erythroid development in the mammalian embryo. *Blood Cells Mol Dis*. 2013;51(4):213-219.
28. Trinquier A, Durand S, Braun F, Condon C. Regulation of RNA processing and degradation in bacteria. *Biochim Biophys Acta Gene Regul Mech*. 2020; 1863(5):194505.
29. Mardle CE, Shakespeare TJ, Butt LE, et al. A structural and biochemical comparison of Ribonuclease E homologues from pathogenic bacteria highlights species-specific properties. *Sci Rep*. 2019;9(1):7952.
30. Machlus KR, Italiano JE Jr.. The incredible journey: from megakaryocyte development to platelet formation. *J Cell Biol*. 2013;201(6):785-796.
31. Grove EL, Hvas A-M, Kristensen SD. Immature platelets in patients with acute coronary syndromes. *Thromb Haemost*. 2009;101(01):151-153.
32. Byrnes JR, Wolberg AS. Red blood cells in thrombosis. *Blood*. 2017;130(16):1795-1799.
33. Turitto VT, Baumgartner HR. Platelet interaction with subendothelium in a perfusion system: physical role of red blood cells. *Microvasc Res*. 1975;9(3): 335-344.

34. Turitto VT, Weiss HJ. Red blood cells: their dual role in thrombus formation. *Science*. 1980;207(4430):541-543.

35. Klatt C, Krüger I, Zey S, et al. Platelet-RBC interaction mediated by FasL/FasR induces procoagulant activity important for thrombosis. *J Clin Invest*. 2018;128(9):3906-3925.

36. Barr JD, Chauhan AK, Schaeffer GV, Hansen JK, Motto DG. Red blood cells mediate the onset of thrombosis in the ferric chloride murine model. *Blood*. 2013;121(18):3733-3741.

37. Woollard KJ, Sturgeon S, Chin-Dusting JP, Salem HH, Jackson SP. Erythrocyte hemolysis and hemoglobin oxidation promote ferric chloride-induced vascular injury. *J Biol Chem*. 2009;284(19):13110-13118.